DYNAMIC RESPONSE OF HULL DUE TO BOTTOM SLAMMING AND DECK WETNESS

BENAMEUR HAMOUDI, B.Eng.

SUBMITTED AS THESIS
FOR THE DEGREE OF DOCTOR OF PHILOSOPHY
IN ENGINEERING

DEPARTMENT OF NAVAL ARCHITECTURE AND OCEAN ENGINEERING
UNIVERSITY OF GLASGOW

ProQuest LLC.
789 East Eisenhower Parkway
P.O. Box 1346
Ann Arbor, MI 48106 – 1346

DEDICATION

To my dearest mother Kheira and my father Boualem,
to my brothers Abderahim, Mohamed and his wife Kheira,
to my sisters Fatima and her family, Fadhela (Djemaia) and Souad (Zohra),
to my friend Khaled,
this work is dedicated.

TABLE OF CONTENT Page no.

NOMENCLATURE

A : sectional area

A_{ij} : added mass coefficients

$\overline{A}_H$: heave amplitude ratio

$A_R = 0.06 L_{cr} B$, impact reference area [in^2]

a_{2n-1} : conformal mapping parameter

a_1 : the first conformal mapping parameter

a_3 : the second conformal mapping parameter

a_5 : the third conformal mapping parameter

a_{cg} : design vertical acceleration

B : total ship breadth

B_{ij} : damping coefficients

$B(x)$: sectional breadth or deck beam at x

$\frac{B}{2}$: half breadth of a section

$b_{1/10}$: breadth at one tenth of the design draught

C : structure impedance ratio

C_0 : speed of sound for pure liquid

C_{air} : speed of sound in air=1125 [fps]

C_{ij} : hydrostatic restoring coefficients

C_s : swell-up coefficient

$d_{1/10}$: one tenth of the design draught

$Error_i$: error for each test

F : force in the longitudinal direction

$F_{\frac{1}{3}}$: significant force (load)

$\overline{F}$: complex amplitude of the total exciting force

F_a : amplitude of the total exciting force

F_i : exciting force and moment

F_{zc} : the cosine part of the total exciting force

F_{zs} : the sine part of the total exciting force

F_{zc}^{FK} : cosine part of Froude-Krylov force component

F_{zs}^{FK} : the sine part of Froude-Krylov force component

F_{zc}^{d} : the cosine part of the diffraction force component

F_{zs}^{d} : the sine part of the diffraction force component

Fr : Froude number

$F(x,t)$: transient force

f	:	freeboard
g	:	acceleration of gravity
I_y	:	moment of inertia
H	:	ship draught at station where the slamming may occur
H_0	:	ratio of the half breadth to the draught
H_c	:	vertical distance from waterline to load point
K	:	dimensional constant depending upon section shape
K_4	:	free surface coefficient of added mass
k	:	wave number $= \frac{\omega^2}{g}$
k_1	:	pressure coefficient for slamming pressure (nondimensional K-value)
k_t	:	longitudinal pressure distribution factor
k	:	dispersion coefficient (factor)
L	:	ship length
L_{cr}	:	length of cross structure [inch]
$\overline{M}$	:	complex amplitude of the total exciting moment
M_a	:	amplitude of the total exciting moment
M_{ij}	:	generalised mass
M_H	:	sectional added mass
$[M_H]$	:	added mass per unit length for the end part
M_s	:	mass of ship
$M_{\theta c}$	:	real part (cosine part) of the total exciting moment
$M_{\theta s}$	:	imaginary part (sine part) of the total exciting moment
$M_{\theta c}^{d}$	:	the cosine part of the diffraction moment component
$M_{\theta s}^{d}$	:	the sine part of the diffraction moment component
$M_{\theta c}^{FK}$	:	cosine part of Froude-Krylov moment component
$M_{\theta s}^{FK}$	:	the sine part of Froude-Krylov moment component
$\frac{M}{d_{1/10}}, \frac{M}{d}$	:	contraction factor
Mean	:	average of n values
Mean error	:	mean value of the errors obtained from the n tests
$m(x,t)$	:	instantaneous added mass
N_H	:	sectional damping coefficient
$[N_H]$	:	damping coefficient per unit length for the end part
N_z	:	impact load factor or maximum amplitude vertical acceleration
n	:	number of tests
p_1	:	absolute ambient pressure
p_2	:	absolute impact pressure

$p(\theta_m)$	:	distribution of the pressure over the girth
p_{keel}	:	impact pressure at keel [psi]
p_{max}	:	maximum impact pressure [psi]
R_r	:	twice variance of relative motion
$R_{\dot{r}}$	:	twice variance of relative velocity
r	:	vertical relative motion
r_a	:	amplitude of the vertical relative motion
$\dot{r} = \frac{dr}{dt}$	:	vertical relative velocity obtained from the first derivative of the vertical relative motion with respect to time
r(x,t)	:	relative motion for a given location at given time
$S(\omega_e)$	:	wave spectrum encountered by the ship
S(x,t)	:	instantaneous submerged area of the hull section as it re-enters the water
s	:	absolute motion
s_B	:	bow vertical displacement
s_s	:	stern vertical displacement
T, d	:	service draught
T_1	:	characteristic wave period
t	:	time in general
U	:	the forward speed of the ship
V	:	impact velocity at time 't'
V_0	:	relative velocity at impact
$V_1 = \frac{p_1}{\rho_0 C_0}$		
V_m	:	amplitude of vertical relative velocity
$V_r(t)$	:	vertical relative velocity
V_{cr}	:	threshold velocity (critical velocity)
x	:	distance between LEDs = 2.125 [metres]
W_L	:	gross weight of the vehicle [lbs]
$y(\theta_m)$	:	coordinate for conformal mapping
Z(x)	:	longitudinal wave shape function
$\bar{z}$	:	heave complex amplitude
z_a	:	heave amplitude
z	:	heave displacement
$\dot{z}$	:	heave velocity
$\ddot{z}$	:	heave acceleration
α	:	Buttock angle
β	:	deadrise angle

β_{eh} : Angle on wave surface measured from forward longitudinal direction to the plane normal to wave surface and impact surface on hull bottom at a considered point

β_{ev} : Angle on transverse plane normal to wave surface and measured from impact surface on hull bottom to wave surface

Δ : fully loaded displacement [tonnes]

δ : heave phase angle

δ_r : relative motion phase angle

ε : pitch phase angle

$\Phi(x,y,z;t)$: the total velocity potential

ϕ_I : incident wave potential

ϕ_D : diffraction potential

ϕ_j : radiation contribution

ω_e : frequency of encounter

ζ : wave elevation

$\zeta_{1/3}$: significant wave height

ζ_w, ζ_a : wave amplitude of incident wave

ξ : the distance from the location of the centre of gravity of the body to the station in consideration

∇ : volume of water

η_j : (j=1, 2 . . . 6) are the amplitudes of the oscillations of rigid body in six degrees of freedom

θ : pitch angular displacement

$\dot{\theta}$: pitch velocity

$\ddot{\theta}$: pitch acceleration

$\bar{\theta}$: pitch complex amplitude

θ_a : pitch amplitude

θ_m : the conformal mapping angle

θ_w : Wave slope

σ : sectional area coefficient

ρ : fluid density

ρ_0 : mass density for pure liquid

δ_v : liquid-air mixture volumetric impedance ratio (=0.0236)

ω : wave frequency

ω_e : frequency of encounter

χ : the angle of the incident wave

τ : Trim angle

LIST OF FIGURES

CHAPTER 2 Page

CHAPTER 3

CHAPTER 4

CHAPTER 5

CHAPTER 6

LIST OF TABLES

CHAPTER 3

CHAPTER 4

CHAPTER 5

CHAPTER 6

ACKNOWLEDGEMENTS

The author wishes to express his gratitude to Professor D. Faulkner, head of the Department of Naval Architecture and Ocean Engineering, for his interest, valuable help and continuous encouragement throughout this research.

The author would like to express his gratitude to Dr. K.S. Varyani, the Deputy Superintendent of the Hydrodynamics Laboratory, and Supervisor for this research work, for his qualitative guidance, valuable advice, lasting encouragement and rich discussion.

The author also would like to thank Dr. A. Incecik, Superintendent of the Hydrodynamics Laboratory, for his kind assistance, advice and valuable discussion throughout this research.

The author would like to extend his gratitude to the technical staff at the Hydrodynamics Laboratory for their assistance during the experimental work.

Special thanks are made to Dr. D.H. Derouich for his excellent friendship and nice years spent sharing the same house and office, to Mr. A. McLeary for his valued friendship, and to the researchers and staff of the Department for their warm friendship.

Finally, the author is greatly indebted to the Algerian Ministry of High Education, the British Council and Glasgow University for the financial support to carry out this research.

DECLARATION

Except where reference is made, this thesis is believed to be original.

SUMMARY

When a marine vehicle navigates in rough weather and at high speed, it experiences large motions; these large motions induce heavy responses, such as deck wetness, bottom slamming, rolling, vertical and transverse accelerations. Therefore, in extremely heavy seaways, the ship would generally slow down and/or change the heading angle against the waves to avoid critical conditions arising from such heavy responses. This is confirmed from operation and from experiments where bottom slamming and deck wetness (classified as secondary loads) are found to be severe in head seas at high speed. There is therefore a penalty paid by decreasing the performance and the effectiveness of the marine vehicle.

The thesis presents an investigation of two secondary loads applied on a marine vehicle; namely, bottom slamming loads below the waterline structure and deck wetness loads on the above waterline structure, on the deck in particular. At present, these two loads are receiving considerable theoretical and experimental attention (model experiments as well as full scale trial) because of their major influence on local structural design.

The first chapter presents an introduction and history of slamming and deck wetness. Bottom slamming and deck wetness events are defined and classified in the range of secondary loads. This chapter also summarizes the considerable work which has been investigated in previous studies carried out on similar subjects by other researchers.

The second chapter is concerned with the motion response prediction for a monohull. Full details, of the development of the New Strip Method (NSM), where the end effect of the ship is taken into consideration, is given. The hydrodynamic coefficients are calculated using the Multipole Expansion Method. The excitation forces and moments (Froude Krylov component and diffraction force component) in the right hand side of the equations of motion are presented. The coupled heave and pitch motion equations are solved in the frequency domain. The vertical relative motion is calculated and derived with respect to time to obtain the relative vertical velocity of the wave surface with respect to the mobile ship. This velocity is compared with the threshold value beyond which slamming occurs and prediction of impact pressures due to bottom slamming can be made.

In the third chapter, major attention is given to the prediction of pressure due to bottom slamming. Different techniques for the determination of the pressure coefficient such as the conformal mapping technique, deadrise angle prediction technique and experimental prediction technique are detailed and discussed. The use of the two and three parameter pressure coefficient prediction technique is studied and compared with other prediction methods. The occurrence of the bottom slamming phenomenon based on the vertical relative velocity exceeding its threshold value is discussed.

Chapter 4 presents an experimental analysis of bottom slamming. A high speed monohull marine vehicle (S175 container ship) was chosen for the experimental investigation of bottom slamming. The ship model was run in regular waves for different forward speeds and wave frequencies which have been carefully chosen to avoid tank wall interference. The instrumentation set-up, calibration of measuring devices and test procedures are presented in this chapter.

Theoretical and experimental comparisons of impact pressures due to bottom slamming are presented in chapter 5. Correlation of slamming pressure predictions by theoretical and experimental methods is made to show the validity and the accuracy of the prediction. Spectrum analysis is used to predict the motion behaviour in irregular waves. Moreover, the wave statistical approach is used to predict probability of slamming occurrence, the number of impacts and the extreme loads due to impact pressures which are required for fatigue and ultimate strength design. Other slamming pressure predictions are presented.

In chapter 6 theoretical and experimental investigations of the deck wetness phenomenon, on the above waterline structure, namely, the deck structure, are presented. For the first time, a theoretical prediction of the horizontal impact loads, applied to vertical deck-mounted equipment, is formulated and developed. Experimentally, load cells and a catch tank technique are used to quantify load and shipment of water due to the deck wetness event. The statistical wave approach is used to predict the probability of occurrence of deck wetness and the frequency of occurrence in different sea states. Comparison of experimentally obtained data with previous researchers' works is presented.

In the last chapter the major findings and conclusions from the research are drawn. Recommendations for future work are made.

CHAPTER 1

INTRODUCTION

CHAPTER 1

INTRODUCTION

1.1 GENERAL

Marine vehicles are always experiencing heavy responses such as slamming, deck wetness, rolling, vertical and transverse accelerations, especially at high forward speed in stormy weather.

This investigation shows a major concern on bottom slamming and deck wetness. These two phenomena have been known for long time in marine vehicle operation and design, and they are classified in the range of secondary loads which can be cited as follows:

- Slamming loads
- Green sea loads (deck wetness)
- Inertia loads
- Berthing
- Docking
- Ice loads
- Grounding
- Collision

The first two loads, known as slamming and green sea (deck wetness) loads have a significant influence on local structural design. However, it is still not possible to make a best choice between the load prediction methods given in the rules of the classification societies, which partially cover these complicated loads, more investigations, such as model tests and full scale measurements, have been recommended to be carried out in the field of slamming and deck wetness.

1.2 REVIEW OF THE SLAMMING PHENOMENON

Slamming is one of the areas of major concern in seaway loads, this phenomenon is associated with extreme motions of marine vehicles in waves. At certain forward speeds in rough seas the fore-foot of a vessel emerges from the water as a result of combination of large pitching and heaving motions. As the fore-foot re-enters at high vertical relative velocity between the hull and the local wave profile, transient and large impulsive loadings applied on a relatively small reference area of the bottom of the hull occur. These transient and large impulsive loadings consist of the potential energy transmitted by the local wave to the bottom of the structure receiving the shock at the instant of the impact. This energy is absorbed by a local area which can be damaged by peak impact pressure.

Slamming can be classified as the most significant secondary load and considered to be imposed on local structure resulting in plastic deformation of the bottom part of a vessel. Faulkner et al (1993) suggested that such a phenomenon, which is wave induced, is a constant source of hull cracking in the forward void spaces of fast multi-hull vessels.

The phenomenon of slamming is one of the heaviest responses which tends to inevitably become more severe by decreasing the draught and maintaining high forward speed in heavy weather and head seas in particular. With regards to the effect of draught, vessels in the loaded condition do not slam with the same persistence and impact pressure magnitude as in the ballast draught conditions. Moreover, reduction in forward speed of a marine vehicle always plays an important part in reducing or eliminating the impact pressures due to slamming of the bottom hull structure. In order to reduce or avoid slamming damage, captains may reduce speed or alter course so that waves are not encountered head on. Captains have to use their judgment to reduce the forward speed when it is required. As a result of reducing speed, there will be a loss of operation time and effectiveness but damage of the structure is avoided. The speed reduction should be based on rational criteria, in the sense that the speed should not be reduced to certain levels which will cause steering problems or vice versa.

Response behaviour to slamming varies according to the type and the purpose of the vessel. High speed marine vehicles such as warships and container ships, are also subjected to structural damage due to slamming phenomenon. The bottom shape of the vessel also plays a significant role in response to the load due to bottom slamming. For example the V-shaped bottom experiences a smaller load than the U-shaped bottom.

Furthermore, ship slamming is significantly influenced by the ship's loading condition, i.e as the draught increases it is less likely for slamming to occur. This can be explained by reduced vertical relative motion at the bow which influences the emergence of the fore-foot.

The slamming phenomenon occurs at random intervals and the impact slam is transient. It rises to a very high impulsive pressures for a very short duration of time, which is in the order of milliseconds. Such an impact pressure is experienced in the centre of the slam reference area and decreases away from the centre of the load. This type of impact load may cause a local effect on the local structure and global effect on the entire ship structure. The local effect, concentrated in the slam reference area, may result in plastic deformation of the bottom structure and the global effect may cause the entire hull to vibrate (whipping).

The drop test results of Chuang (1973) are used to derive the magnitude of the impact pressure as a function of the body shape, water surface (calm water and/or waves) and the relative speed between the body and water surface (drop height). In the experimental investigation of Chuang (1970) a set of equations for estimating the maximum impact pressure for different deadrise angles (from flat bottom to 18 degrees) of a wedge penetrating a fresh water surface is provided. He also discussed the effect of air cushioning in reducing the severity of an impact. The quantity of air trapped between the falling body and the water surface has an important role in reducing the impact. Khattab (1986) stated that the air layer reduces the maximum impact pressure to about a tenth of the acoustic pressure. Furthermore, Lewison (1970 a) concluded from his investigation that the peak pressure could be reduced if an artificial air layer was ejected from a hole in the forefoot when the bow emerged from the water. Such a suggestion is costly to install and it needs an accurate technique to eject the air when slamming is imminent. Such equipment to eject air can be installed for the whole life of the ship but it does serve only when slamming is imminent, but this latter does not occur often.

Miyamoto et al (1985) found that for 1 degree wedge the air cushioning effects start to appear when the drop velocity is higher than 0.4 m/s, but in another investigation Yamamoto et al (1984) found that the air cushioning effect has to be neglected if the deadrise angle is more than 3 degrees, but no reference was made about the drop velocity which is important in such cases.

One can learn from these investigations that the air layer underneath the ship hull plays a role of a damper. The effect of this air layer depends on the shape of the bottom of the ship subjected to slamming phenomenon.

On the basis of the results of a set of experiments, which consist of dropping a flat-plate model from various elevated positions, Chuang(1966) presented an expression to predict the maximum impact pressure of a rigid flat-bottom body, given as:

$$p_{max} = 0.0021 \rho_{fluid} C_{air} V_0 \tag{1.1}$$

and the pressure time history can approximated as follows:

$$p(t) = 2 p_{max} e^{-1.4t/T} \sin \pi \frac{t}{T} \tag{1.2}$$

with

$$T = 4L / C_{air} \tag{1.3}$$

where:

C_{air}	:	speed of sound in air=1125 fps,
V_0	:	impact velocity (fps),
ρ_{fluid}	:	mass density of fluid (fresh water)=1.94 lb-sec^2/ft^4
p_{max}	:	maximum impact pressure (psi),
T	:	duration of positive pulse,
t	:	time in general and
L	:	half-width of plate.

Chuang mentioned that the given expression in equation (1.1) is valid only for flat plates, and for wedge-shaped bodies with small deadrise angle penetrating a water surface the impact pressure at the keel, if the vertical acceleration is neglected, as given by Chuang (1967) is as follows:

$$p_{keel} = \frac{1}{2} \rho V_0^2 \frac{\pi}{\tan \beta} \tag{1.4}$$

where:

β : deadrise angle,
V_0 : vertical velocity at instant of impact and
ρ : density of fluid.

From a physical point of view, equation (1.4) is valid only at the instant of impact. Furthermore, on the basis of experimental investigations, a number of empirical formulae were derived for the calculation of the impact pressure at the keel and away from the keel for different deadrise angles up to 18 degrees. From theoretical investigations on slamming of cone-shaped bodies, Chuang (1969) derived an expression to evaluate the pressure distribution on a cone penetrating the water surface. It was found that the maximum impact pressure of a wedge-shaped body is higher than that of a cone-shaped body by about 25 percent.

Verhagen (1967) found the maximum impact pressure is directly proportional to the drop heights and it is independent of the mass of the falling body. This is also found by Chuang (1970) concluding that most of his data show that the maximum impact pressures at the keel are independent of drop weight, but this is not generally agreed from model tests. Further, Verhagen found that the time duration of an impact for different drop heights was found to be around 5 milliseconds. This is in good agreement with the duration time of 5.5 milliseconds obtained after the analysis of the experimental data on the model of the S175 container ship tested by Hamoudi (1993) at the Hydrodynamics Laboratory of the University of Glasgow.

The main purpose in relating drop tests to the slamming phenomenon is to provide more information and clarify the understanding of the impact of the body with the water surface. Such investigations provide the designer with information on the severity of impact, the distribution of the impact pressure, the relationship between load exerted and shape of the area subjected to the impact, such as deadrise angle.

From Chuang's (1969) previous investigations there is a good correlation between the impact pressure measured from drop tests and the pressure calculated theoretically by taking into account the shape of the falling body. However, in reality some discrepancies always occur between measured and calculated impact pressure for a

high speed marine vehicles (Container ships) experiencing slamming.

Nagai and Chuang (1977) concluded that sea conditions and ship speed are the prime cause of slamming occurrence. The master has to reduce the ship speed and/or to change the heading in order to control the severity of slamming response. The ship speed is an important factor and plays an important role in reducing slamming severity.

Stavovy and Chuang (1976) determined analytically the impact pressure due to slamming in waves for high speed vehicles up to 100 knots. They divided the total pressure acting normal to the slamming area into two components, namely the impact pressure and the planing pressure. The agreement between analysis and experimental results is good and the planing pressure was found to be small and insignificant compared with the impact pressure.

A recent investigation on slamming from forced oscillating wedges at forward speed was carried out by Radev and Beukelman (1992) where peak pressures and rise times were determined for four metal wedges with different deadrise angles. It has been confirmed and clarified from this set of experiments that the measured peak pressures show a clear proportionality to the squared amplitudes of the vertical relative velocities at the instant of impact. Furthermore, the forward speed has a significant effect on the measured peak pressures. The rise times of the peak pressures decrease significantly with trim angle, vertical and forward velocity. This contradicts with duration time found by Verhagen (1967) and Hamoudi (1993).

Lewison (1970 b) summarised in his work that the pressure due to slamming measured on the bottom of ship models can be related to the relative velocity component at impact and to the shape of the bottom portion. He mentioned that the air trapped between the bottom of the ship and the water surface reduces the peak pressure but did not mention that the slowing down of the forward speed of ship reduces the impact pressure.

On the basis of an experimental investigation on two merchant ship V and U-shaped hull forms, model tests were carried out by Ochi (1958) on bottom slamming in regular waves. The conclusions from this investigation are listed as follows:

- Slamming damages occur mostly at light draught
- The shape of the bottom portion is important in slamming, that means V-form is superior to the U-form as far as slamming pressure reduction is concerned

- The ship which has the same pitching period as the wave period responds well to slamming
- The forward part of ship is the location which is affected and suffers from ship slamming
- The forward speed of ship is an important factor in the occurrence of slamming

Another conclusion can be added to those listed above, i.e:

- The vertical relative velocity can be taken from seakeeping theory.

Regarding the huge amount of investigation which has been done recently and in the past, there is still a need for further research in this field, with emphasis on full scale measurements.

Considerable work has been done to estimate the maximum slamming pressure theoretically and empirically. The present study does not investigate the problems arising from slamming associated with damage of shell plating and local structure response which are categorized as hydroelastic problems, but it concentrates on the impact pressure (the pressure at the initial contact of the bottom of a ship with a wave) exerted on local panels of the structure where the impact occurs, namely the impact load.

Bishop and Price (1979) described the magnitude of slam in two ways, i.e by evaluation of the forces at the instant the hull strikes the free surface of the waves (this slam is for a short duration), and from the effect of the pressure variations around the hull surface as it penetrates the moving fluid after initial entry.

Verhagen (1967) analysed the impact of a flat plate on a water surface theoretically and experimentally. He noticed that the layer of air between the falling body and the water surface had to be taken into account in order to accurately explain the phenomenon. His experiments showed that there is a difference between the maximum impact pressure measured experimentally and the the theoretical prediction without taking the entrapped air into account. Another explanation that can be given to this phenomenon is that the air which lies between the falling body and the water surface decreases the impact pressure.

Watanabe (1987) derived an expression for the impact pressure distribution on the flat bottom ship making slamming motion by the matched asymptotic expansion. A 3-D flat plate formulation is utilised for the solution in the outer region and 2-D planing plate flow for the inner region. Both methods are matched asymptotically. Good correlation is achieved between calculated and experimental results.

Lloyd (1989) described slamming as a re-entry of the keel after emergence which may cause damage to the hull, and create vibrations known as whipping (few cycles per second) and the fatigue occurring at this stage decreases the life of the hull.

The work of Mansour and de Oliviera (1975) presented details of the development of a mathematical formulation of the vibratory bending moments due to bottom slamming in regular waves. The overall response of the ships to bottom slamming forms a part of their work. They also developed a procedure of computation to predict the midship bending moment in the time domain. They divided the slamming problem into two categories; the first one deals with the local response of the ship hull to slamming (called the micro-problem) and the second one deals with the overall response of the ship hull to slamming (called the macro-problem).

Ferro and Mansour (1985) presented a new theory to combine the slamming and wave-induced responses of a ship hull moving in irregular seas by considering the slamming and wave-induced responses as a stochastic process. Several studies have been carried out in order to define the slamming statistics to develop a probalistic method which combines slamming stresses with other stresses, in particular with low frequency wave induced stresses.

Tick (1958) gave a procedure for computing the average submergence time of the bow and the average number of slams. An alternative representation of PIERSON's random process model of the sea surface and Korvin-Kroukovsky's equations of the response of a ship hull to a regular sea is given. The computational procedure developed in this paper was illustrated through an example based on the series 60 model.

Ulbright (1985) described the loading on a ship hull due to slamming as follows: the pressure due to bottom slamming of a ship is in general greater than that due to the side slamming and the short duration of the slamming forces induce transient dynamic

stresses due to global vibrations of the hull. He used a strip method for the motions calculation based on slender body theory . The vertical motion and the coupled roll and pitch motions were taken into consideration. These are important in slamming calculations. He deduced that for sharper-fore-body forms the slamming pressure is reduced by more than half.

The entire time history of the slam has to be taken into consideration and to be analysed. The peak pressure is important for local panel response, whereas the longer time history (sometimes referred to as "momentum phase") is necessary for global hydroelastic response.

Belik et al (1979 a) evaluated the steady state responses and the transient responses due to slamming in regular head sea. Part of their work was the impulsive fluid loading forces associated with slamming and comparison of the absolute magnitude of steady state and transient responses. In another work, Belik et al (1982) presented a time simulation of the responses such as displacement, shear force and bending moment based on the unified dynamic theory of ship response. They evaluated the transient excitation and responses due to slamming. It was found that the transient responses just after the slam depend on many factors and the important one is the spatial distribution of the transient excitation along the length of the hull. They found that the transient excitation depends on the wave amplitude, and the response to a slam depends possibly on the previous slamming if the time between two slams is short .

The main aim in carrying this present research is to investigate bottom slamming phenomenon and to generate experimental data from model tests. These data are used to show the validity and the accuracy of slamming pressure predictions by theoretical and experimental methods.

1.3 REVIEW OF THE DECK WETNESS PHENOMENON

Among the seakeeping characteristics which the ship designer has to consider during the design stage, is deck wetness (green seas). Investigations into wave loading on vessels have strongly emphasized the below water-line structure; for the simple reason that the above water-line structure are not subjected to regular significant loads as is the case for the below water-line.

During the operation time in heavy seas, high speed vessels are subjected to some penalties, among them is green seas (shipping water on deck or deck wetness). This problem has been dealt by several investigations on the theoretical and experimental aspect. However, there is much to be done to solve the above problem. The design stage requires more information gathered from many investigations to satisfy a good performance of vessel navigating in rough weather without being subjected to such phenomenon.

Many researchers investigated the deck wetness phenomenon by theoretical and experimental techniques. Lloyd et al (1982) investigated the effect of bow shape on deck wetness on the narrow beam LEANDER frigate which was equipped with nine different above water bow forms. The model was run in irregular head waves with a nominal Pierson-Moskowitz spectrum and significant wave height (for ship) of 5.0 metres. The wetness impact forces were measured during each run by using nine square plates which consist of load cells mounted in array over the deck at station 3 from the FP. He concluded from his experimental tests the following points:

- High freeboard is desirable and can reduce the frequency and the severity of wetness
- High overhang decreases the frequency of wetness
- Heavy flare increases the frequency of wetness at high forward speed.

The qualitative and quantitative data collected by Lloyd are very useful for the given ship (the narrow beam LEANDER), but the deck wetness is a common event for other ships and in particular the high speed vessels. Beside these, other conditions for ship navigation also have to be taken into account.

Bales (1979) introduced in his work a design procedure which yielded minimum freeboard. The freeboards required to operate in the wave environment and other cases were determined.

Measured impact pressure acting on a water breaker and numerical simulation on a model of S-175 container ship in regular head waves were carried out by Mizoguchi (1988) in order to investigate the complex phenomenon of shipping water on deck. The impact pressure acting on a water breaker is predicted using the empirical equation for impact pressure due water jet and the effect of deck form is investigated. It was

concluded from the measured wave height contours, at the beginning of shipping water, that the water flows into deck just like a dam break water, and if the wave height is high the water is concentrated at the forepart of fore castle deck and it crashes against the aft water breaker, but in the case of lower wave height, the water is also concentrated at the forepart of fore castle deck and it spreads to every direction. It was found also that the wave height and the deck area are the most important items in the shipping water on deck.

A technique to evaluate the duration of threshold crossing of a random process was applied for the first time to the shipping of green water by Oliver (1981). This technique predicts the probability of occurrence of a deck wetness event. Unlike Mizoguchi, Oliver has taken into account the relative motion of the vessel relative to the sea surface when it exceeds the freeboard. The amplitude of threshold crossing was evaluated by a Rayleigh distribution. Furthermore, the volume of shipping water on deck and total pressure on the deck were also calculated.

Edward and Todd (1938-39) reported that deck wetness is one of the factors which determines seakindliness or seaworthiness. Three models were tested with forwards freeboard of 11.75 ft, 8.5 ft and 11.75 ft respectively and with different forwards, amidships and aft draughts. The tests in regular waves showed the importance of sufficient forward freeboard. The second model sank, whilst the first and the third remained nearly dry, and no mention was made of the speed at which the models were run. In the above research no reference was made to deck wetness occurrence caused by relative motion exceeding freeboard.

Description of model experiments is given by Lloyd et al (1986) in order to study the deck wetness process and investigation on the effects of systematic variations in above water bow form. Measurements of relative bow motion and deck wetness frequency have been investigated. The results of the experiments confirmed that additional freeboard reduced deck wetness frequency and severity.

Experimental and theoretical investigation carried out by Tasai (1969) has shown the effect of dynamic swell-up on deck wetness. The problem has been tackled using two full ship forms. N-ship and R-ship were adopted for such investigation. The after parts of these two hull forms are the same but the difference is in the fore parts. Experimental work has been carried out for two conditions of displacement, i.e full load condition and ballast condition with 55% displacement of full load condition. The main parameter

which differs between the two forms is the draught at the fore perpendicular, midship and at aft perpendicular. As a final conclusion, it was found that the calculated values differ from the experiment, if the dynamic swell-up is not taken into consideration. On the other hand, if it is taken into account, the calculation and experiments show satisfactory agreement.

Newton (1960) has suggested that there are three degrees of wetness, namely, dry, wet and very wet corresponding to dry, heavy spray and green sea conditions. From his experimental results on the occurrence of wetness, the freeboard coefficient should increase up to a critical length of ship and decrease for ships of greater length. Moreover, the effect of increased flare, obtained by incorporating a knuckle below the forecastle, is also treated as an equivalent increase in freeboard.

The effect of forebody on deck wetness has been investigated by Swaan and Vossers (1961). Experiments have been carried out with a series of six models which had the same principal dimensions and displacement, but differed in section shape in the forebody and in prismatic coefficient. They concluded that U-shaped sections are advantageous as regards deck wetness. It has been also observed from experiments that a decrease in midship coefficient leads to unfavourable deck wetness.

Shipping water phenomena were studied by Goda et al (1978) by means of two-dimensional ship model tests. Behaviours of shipping water, pressures on deck and relative motions surface were investigated. Based on results of this investigation, a method for the calculation of volume of shipping water on the deck was established. A good agreement between the measured volume of shipping water and the calculated one was found.

A model test was carried out by Watanabe et al (1989) for a container ship with two kinds of bow flare forms and identical hull form. The main conclusion drawn from such an investigation occurs in the relative motion of the bow which can be influenced by the shape of the flare. The increased bow form experiences smaller relative motion. Deck wetness is related to flare form, and the increased flare form has more frequent deck wetness occurrence. However, ship motions measured by Lloyd (1983) in his experimental investigation is independent of the above water bow form if swell-up is not taken into account. From the same experimental investigation, Lloyd concluded that a high freeboard reduces severity of deck wetness and it was shown that a large overhang and moderate flare angle are found to be beneficial.

A time simulation technique for predicting the nonlinear ship motion and water shipping problems in head waves has been developed by Fang et al (1993). An experimental setup for a 3 metres Series 60 ship model is also designed for the test to confirm the theoretical results. Some conclusions drawn from this investigation are:

- The nonlinear effect of the large motion has to be taken into account
- The radiation and diffraction terms play important roles in the water shipping analysis.

It has also been found that while the wave amplitude is small, the results obtained by the time-domain analysis will be similar to those obtained by the frequency-domain analysis, in other words, the method approaches linear analysis.

Model experiments in regular waves and probability theory have been used by Goodrich (1964) in order to predict the probability of occurrence of wetness at the fore end. His calculations made for ships of different fullness suggest that the frequency of occurrence of wetness varies with block coefficient as well as with length for a given freeboard ratio. The results show that for equal probability of occurrence the freeboard ratio decreases with increasing ship length. He also found from his results that for C_B of 0.6 and 0.8 ships are similar but his analysis shows that for C_B of 0.7 the ships require a greater freeboard.

The effect of bow shape on spray is known as a difficult task to predict, moreover, the calculation of depth of water on deck may be equally complex. O'Dea et al (1984) investigated deck wetness phenomenon by measuring the depth of water on deck and they found that it varies with wave steepness. An adequate analytical prediction of deck wetness will require a time domain calculation. This will allow the incorporation of other physical phenomenon involved in the occurrence of the event.

O'Dea et al's work has dealt with regular wave problem and for one particular speed only. Hence it is also important to take into consideration several other factors like realistic sea state, irregular waves and the worst possible scenario.

From the structural and navigational seaworthiness point of view, the problem of shipping green seas is extremely important. Hence more investigation needs to be done

for deep draught (low freeboard) and high forward speed in rough seas in particular.

To date, knowledge of the deck wetness phenomenon is limited, and one may not be certain of how to tackle the practical problems of predicting deck wetness, or reducing its severity. Hence the initial aim of the present research is to generate experimental data on ship motions and deck wetness from model tests.

1.4 OBJECTIVES OF STUDY

As explained earlier slamming and deck wetness are one of the events which ship designer has to give a careful attention to at the initial design stage.

The overall aim of this research is to study the dynamic response of ship due to bottom slamming and deck wetness phenomenon and to provide the designer with the tools that could be of use at the design stage of ship. In studying the bottom slamming event, a computer program based on the new strip method, where the end effect is taken into account, is developed. Program results for frequency dependent motion equations are presented. Particular attention is given to the high vertical relative velocity, when the bottom of the ship hits the wave surface, which is derived from the vertical relative motion and when it exceeds to the threshold value. Impact pressures due to bottom slamming are measured experimentally from model tests, for different Froude numbers and calculated by using the new strip method for the high speed S175 container ship. Different techniques to predict the impact pressure and its coefficient are given. Moreover, the deck wetness phenomenon is investigated experimentally. The force in the longitudinal direction is measured for different Froude numbers. Vertical relative motion exceeding the freeboard is discussed. Formulation of the impact force and a new method to predict this force is detailed. Some statistical analysis for deck wetness occurrence are also incorporated.

CHAPTER 2

NEW STRIP METHOD

CHAPTER 2

NEW STRIP METHOD

2.1 INTRODUCTION

The naval architect needs to assess seakeeping at an early stage for the design of a new ship and this is often achieved with two-dimensional approximate calculation by means of the strip method computer programs as Lloyd (1989 a) mentioned in his paper. In this chapter the motion response of marine vehicle under environmental wave loading is predicted through frequency domain modelling. Here the New Strip Method, abbreviated as NSM and which incorporates the end effect terms is used for numerical computation. The NSM is a modified version of Korvin-Kroukovsky's Ordinary Strip Method. The end part of a ship affects the motion response of marine vehicle and this effect has to be taken into account in motion response calculations.

Predictions of seakeeping performance of marine vehicle rest primarily on accurate prediction of the motions experienced in different seaways. Furthermore, the required ship strength depends mainly on severity of different loads applied on the ship hull.

Most of theoretical prediction methods have been developed in order to quantify the motions and loads, but their accuracy has not yet been fully established because of the nonlinearities.

Severe responses, as defined in chapter 1, are often caused by large amplitude motions in rough seas. Slamming and deck wetness are results of the relative motion exceeding the draught and freeboard respectively. It is, therefore, important that the designer should understand the ship behaviour and weather conditions that produce slamming and deck wetness events and the precautions which must be taken in the design stage to eliminate, or at least to minimise the damage on the structure of a marine vehicle.

Large amplitude motions of heave and pitch in head seas in particular are the cause for slamming and deck wetness. These motions increase if the roughness of the weather increases (wave height) and the forward speed is maintained. The speed of

marine vehicle plays an important part in the occurrence of slamming and deck wetness.

Kent (1948-49) defined in his paper the known facts connected with slamming and that particular motion of the ship which may cause slamming. There may not be any slamming occurrence if the period of encounter with the waves is synchronised with the pitching period or if the pitch angle is large. Furthermore, if heave period is synchronised with the period of encounter of the waves and if a large heave motion takes place, then slamming will occur. However, in full scale trail the condition of synchronism cannot be satisfied easily.

In another paper, Kent (1949-50) reported that it is not possible to design a cargo vessel that will not ship seawater under any weather conditions, but it is possible to incorporate some improvements. In rough weather, when ship meets the waves head on, water is sometimes shipped forward and amidships and this may flood the decks. This water is randomly distributed on deck and freed by scuttles as the ship continues her pitch and roll motions.

Analytically calculated or experimentally measured ship motions are required to predict bow submergence which may result in slamming and shipping of water. Therefore, in the following sections of this chapter formulation of the problem followed by a conformal mapping technique is given. The equation of motions with solutions are also discussed.

2.2 FORMULATION OF NEW STRIP METHOD

The ship is assumed to be a long slender body, and the fluid flow around the ship will be decided by 2D cross-section. It is assumed that there will be no variations in the longitudinal direction, and strip method will be appropriate for establishing the motions of a ship. This was first applied by Korvin-Kroukovsky (1955).

It is convenient to refer the ship motion to various types of moving coordinate systems as well as a fixed coordinate system. The space fixed coordinates $O_0 - X_1Y_1Z_1$ is considered. The wave is assumed to propagate in the O_0x_1 direction. The ship is moving at an angle χ from the propagating wave in the O_0X_1 axis direction, as shown in Fig. 2.1. $O_0 - XYZ$ is new space fixed coordinate and $O - xyz$ are space coordinates moving in O_0X direction with the velocity U of the ship and O is on the calm water

surface. Body fixed coordinates $\bar{O}-\bar{x}\bar{y}\bar{z}$ is also considered. $\bar{O}$ will coincide with O when the ship is not oscillating. The centre of gravity of the ship is as shown in Fig. 2.1 is below the free surface.

Using the relations between the different coordinates considered above a relation is established and which is used to calculate the radiation potential, and the pressure due to the radiation potential. It is also possible to represent the line integral results of the radiation potential by 2D theory in terms of added mass and damping coefficients. To calculate the added mass and damping coefficient, in the present research a stream function approach is adopted. The advantage of using this method in conjunction with the multipole expansion method is to increase the accuracy of the solution as the stream function is orthogonal of the velocity potential. The accuracy of the coefficients involved in the calculation of the stream function can be checked by the well known relation of Ursell. To increase the accuracy in the estimation of the hydrodynamic coefficients a least square method is adopted in order to obtain the coefficients of the stream function. Having calculated these coefficients, these values are then input in the equation of De Jong (1973) of added mass and damping coefficient in order to obtain the hydrodynamic quantities required for input into the linear equations of motion. An alternative method for further increasing the output results of hydrodynamic calculation is by taking the least of the least square method, but for all practical purposes in the present research emphasis was paid only to the least square method for the evaluation of the hydrodynamic coefficient.

2.3 CONFORMAL MAPPING TECHNIQUE

The objective of conformal mapping technique is to map a complicated geometry into a simpler one. Therefore, in the present study, the ship is assumed to be moving with constant forward speed, and the fluid flow around the ship will be decided by 2D cross-section. The section of a ship can be mapped into a unit semi circle by using conformal mapping parameters which can be calculated by employing Lewis transformation method. In the present research information of the mapped coefficient at every station is used as an input to calculate the added mass and damping coefficient. The detail at steps involved in the present calculation is referred to in detail in the Appendix.

The mapping can be determined by several coefficients called conformal mapping parameters. It is possible to map a simple ship section using a two or three parameter mapping technique to a unit semi-circle if the following input data are known, i.e:

- Ship breadth
- Ship draught
- Sectional area
- Location of vertical centre of gravity

A complicated section can be mapped by increasing the number of parameters.

In the present study the conformal mapping problem is applied to one part of the underwater ship transverse section due to the conventional port starboard symmetry. The relations in which the transformations are possible, are given in the Seakeeping Symposium of the Society of Naval Architect of Japan (1969) and used by Hamoudi (1992) by the following expression:

$$z = x + iy = R\, e^{i(\frac{\pi}{2}-\varphi)} \tag{2.1}$$

$$\zeta = \xi + i\eta = r\, e^{i(\frac{\pi}{2}-\theta)} \tag{2.2}$$

for a symmetrical shape we can write:

$$z = M[\zeta + \sum_{n=1}^{N} a_{2n-1}\zeta^{-(2n-1)}] \tag{2.3}$$

from this relation one can calculate x and y coordinates by taking into account the value of x equals to the real part and the value of y equals to the imaginary part:

$$x = M[r\sin\theta + \sum_{n=1}^{N}(-1)^{n+1}a_{2n-1}\frac{\sin(2n-1)\theta}{r^{2n-1}}] \tag{2.4}$$

$$y = M[r\cos\theta + \sum_{n=1}^{N}(-1)^{n}a_{2n-1}\frac{\cos(2n-1)\theta}{r^{2n-1}}] \tag{2.5}$$

where:

a_{2n-1} : conformal mapping parameter
r : radius of the cylinder

θ : mapping angle

the coefficients 'M' and 'a' are functions of breadth, draught, sectional area and centre of gravity. They are calculated by taking the integral for θ from 0 to $\frac{\pi}{2}$.

In practice the appropriate way to calculate the coordinates x and y is to truncate the transformation series to two or three terms as follows:

1- Two parameters fit

Approaching the same problem with the coordinates shown in Fig.A.2.1 in the Appendix, one can write the coordinates as:

$$x = M[(1 + a_1)\sin\theta - a_3\sin 3\theta] \tag{2.6}$$

$$y = M[(1 - a_1)\cos\theta + a_3\cos 3\theta] \tag{2.7}$$

where the radius of the cylinder is set to the unit, r=1.

The coefficients can be calculated from the following conditions:

1. θ equals to $\frac{\pi}{2}$:

$$\frac{B}{2} = M[1 + a_1 + a_3] \tag{2.8}$$

where:

$\frac{B}{2}$: half breadth of a section
a_1 : the first conformal mapping parameter
a_3 : the second conformal mapping parameter

2. θ equals to 0:

$$d = M[1 - a_1 + a_3] \tag{2.9}$$

where:

d : draught of a section

3. the ratio of the half breadth to the draught

$$H_0 = \frac{B}{2d} = \frac{1 + a_1 + a_3}{1 - a_1 + a_3} \tag{2.10}$$

where:

H_0 : ratio of the half breadth to the draught

4. the sectional area

$$\sigma = \frac{A}{Bd} = \frac{\pi}{4} H_0 \frac{1 - a_1^2 - 3a_3^2}{(1 + a_1 + a_3)^2} \tag{2.11}$$

where:

A : sectional area
σ : sectional area coefficient

the two parameters a_1 and a_3 can be calculated by the following equations:

$$a_1 = \frac{H_0 - 1}{2(\frac{M}{d})} \tag{2.12}$$

$$a_3 = \frac{H_0 + 1}{2(\frac{M}{d})} - 1 \tag{2.13}$$

where:

$\frac{M}{d}$: contraction factor

$$a_1^2 = \frac{(H_0 - 1)^2}{4(\frac{M}{d})^2},\ a_3^2 = \frac{(H_0 + 1)^2}{4(\frac{M}{d})^2} - \frac{H_0 + 1}{(\frac{M}{d})} + 1$$

$$1 - a_1^2 - 3a_3^2 = 1 - \frac{(H_0 - 1)^2}{4(\frac{M}{d})^2} - 3[\frac{(H_0 + 1)^2}{4(\frac{M}{d})^2} - \frac{H_0 + 1}{(\frac{M}{d})} + 1]$$

put $\frac{M}{d} = m$,

$$1 - a_1^2 - 3a_3^2 = \frac{1}{4m^2}[4m^2 - (H_0 - 1)^2 - 3(H_0 + 1)^2 + 12m(H_0 + 1) - 12m^2]$$
$$= \frac{1}{m^2}[-2m^2 + 3m(H_0 + 1) - (H_0^2 + H_0 + 1)] \qquad (2.14)$$

$$\frac{4\sigma}{\pi} = \frac{H_0 \frac{1}{m^2}[-2m^2 + 3m(H_0 + 1) - (H_0^2 + H_0 + 1)]}{\frac{H_0^2}{m^2}} \qquad (2.15)$$

$$\frac{4\sigma}{\pi} = \frac{1}{H_0}[-2m^2 + 3m(H_0 + 1) - (H_0 + 1)^2] + 1 \qquad (2.16)$$

$$H_0(\frac{4\sigma}{\pi} - 1) = -2m^2 + 3m(H_0 + 1) - (H_0 + 1)^2 \qquad (2.17)$$

i.e.

$$2m^2 - 3m(H_0 + 1) + (H_0 + 1)^2 - H_0(1 - \frac{4\sigma}{\pi}) = 0 \qquad (2.18)$$

$$m = \frac{1}{4}[3(H_0 + 1) \pm \sqrt{9(H_0 + 1)^2 - 8(H_0 + 1)^2 + 8H_0(1 - \frac{4\sigma}{\pi})}] \qquad (2.19)$$

therefore

$$\frac{M}{d} = \frac{1}{4}[3(H_0 + 1) \pm \sqrt{(H_0 + 1)^2 + 8H_0(1 - \frac{4\sigma}{\pi})}] \qquad (2.20)$$

when a vertical flat plate is considered:

$$B = 0,\ H_0 = 0$$

if the coefficient $a_1 = -1$ then $a_3 = 0$

therefore

$$d = 2M,\ \frac{M}{d} = \frac{1}{2} \tag{2.21}$$

$$\frac{M}{d} = \frac{1}{4}[3 \pm \sqrt{1+0}] = \frac{1}{4}[3 \pm 1] \tag{2.22}$$

the minus sign has to be taken to satisfy the previous condition. Finally the contraction factor can be written as follows:

$$\frac{M}{d} = \frac{1}{4}[3(H_0 + 1) - \sqrt{(H_0 + 1)^2 + 8H_0(1 - \frac{4\sigma}{\pi})}] \tag{2.23}$$

Having calculated the contraction factor the conformal mapping coefficients can be determined.

The comparison of mapped sections to the real geometry of ship sections is shown in Figs. 2.2 to 2.10. Though this method satisfies the boundary conditions, however near the corner of the section in the case of fine section the mapped coordinates take a fuller form, to compensate for the change in sectional area. The mapped sections behave well in the case of full form section in the region of the parallel middle body. In the case of section 1 and 9 more parameters need to be taken into account for the transformation process. If a section is more complicated, the error in mapping increases.

2- Three parameters fit

Approaching the same problem with different coordinates as shown in Fig. A.2.2 in the Appendix, one can write the coordinates as:

$$z = x + iy = R\, e^{i\varphi}$$

$$\zeta = \xi + i\eta = r\, e^{i\theta}$$

therefore

$$x = M[(1 + a_1)\cos\theta + a_3\cos 3\theta + a_5\cos 5\theta] \tag{2.24}$$

$$y = M[(1 - a_1)\sin\theta - a_3\sin 3\theta - a_5\sin 5\theta] \tag{2.25}$$

where:

a_5 : the third conformal mapping parameter

The conditions for the calculation of the coefficients are given:

1. θ equals to 0:

$$\frac{B}{2} = M[1 + a_1 + a_3 + a_5] \tag{2.26}$$

2. θ equals to $\frac{\pi}{2}$:

$$d = M[1 - a_1 + a_3 - a_5] \tag{2.27}$$

3. The sectional area is given by:

$$A = \frac{\pi}{2} M^2[1 - a_1^2 - 3a_3^2 - 5a_5^2] \tag{2.28}$$

or it can be calculated by the following integral:

$$A = 2\int_0^d x\,dy \tag{2.29}$$

the following ratios are given by the relations:

$$H_0 = \frac{\frac{B}{2}}{d} = \frac{1 + a_1 + a_3 + a_5}{1 - a_1 + a_3 - a_5} \tag{2.30}$$

$$\sigma = \frac{A}{Bd} = \frac{\pi}{4} H_0 \frac{1 - a_1^2 - 3a_3^2 - 5a_5^2}{(1 + a_1 + a_3 + a_5)^2} \tag{2.31}$$

The coefficients a_1 and a_3 are function of the coefficient a_5 and $\frac{M}{d}$ according to the following equations:

$$a_1 = \frac{H_0 - 1}{2(\frac{M}{d})} - a_5 \tag{2.32}$$

and

$$a_3 = \frac{H_0 + 1}{2(\frac{M}{d})} - 1 \tag{2.33}$$

with

$$\frac{M}{d} = \frac{3(H_0 + 1) + a_5(H_0 - 1)}{4(1 + 3a_5^2)} - \frac{\sqrt{(H_0 + 1)^2 + 8H_0(1 - \frac{4\sigma}{\pi}) - a_5^2[23H_0^2 + 2H_0(13 + 48\frac{\sigma}{\pi}) + 23] + 6a_5(H_0^2 - 1)}}{4(1 + 3a_5^2)} \tag{2.34}$$

The contraction coefficient $\frac{M}{d}$ is also function of H_0, σ and a_5. The value of a_5 is assumed as known and calculated by iteration. A computer program called ITER, developed in FORTRAN 77, calculates the coefficient a_5 which lies between the values of -0.2 and 0.2. If the value of a_5 is found between -0.2 and 0.2, another iteration has to be done between the upper and the lower value of a_5. The selected then needs to satisfy the following conditions:

$$\frac{dy}{d\theta_{\theta=0}} \geq 0 \qquad 1 - a_1 - 3a_3 - 5a_5 \geq 0 \tag{2.35}$$

$$\left.\frac{dx}{d\theta}\right|_{\theta=\frac{\pi}{2}} \le 0 \qquad 1+a_1-3a_3+5a_5 \ge 0 \tag{2.36}$$

$$\left.\frac{dx}{d\theta}\right|_{r=1} = 0 \qquad 25a_5^2-5a_1a_5-1-3a_3 \le 0 \tag{2.37}$$

having found many values by the present method and which satisfies the previous conditions, the right value is the one which satisfies the condition of the centre of gravity given by the following formula:

$$\frac{OG}{d} = \frac{2}{\pi}\frac{\overline{m}_x}{(1-a_1^2-3a_3^2-5a_5^2)(1-a_1+a_3-a_5)} \tag{2.38}$$

where OG is the centre of gravity and $\overline{m}_x$ is given by:

$$\begin{aligned}\overline{m}_x = [&\frac{2}{3}(1-a_1)^2(1+a_1)+\frac{2}{3}a_3^3+\frac{2}{3}a_5^3+\frac{2}{15}(1-a_1)(5a_1a_3-a_3)\\ &-\frac{2}{105}(1-a_1)(3a_5-7a_1a_5)+\frac{18}{35}(7a_1-5)a_3^2+\frac{50}{99}(11a_1-9)a_5^2\\ &+\frac{10}{63}(14-18a_1)a_3a_5+\frac{18}{5}a_3^2a_5+\frac{50}{21}a_3a_5^2]\end{aligned} \tag{2.39}$$

The comparisons using the third parameter a_5 is shown in Figs. 2.11 to 2.19. The mapped sections match well at the boundaries with the geometry of the real sections. For precise mapping of the sections more parameters are required to be incorporated in equations (2.24) to (2.25).

2.4 EQUATION OF MOTIONS

According to Newton's second law, at any instant all vertical forces on the ship are in equilibrium, or the sum of all the forces acting on a body at any instant is equal to the product of the body mass and its acceleration.

The equations of motion are presented in this section for ship advancing at constant mean forward speed with arbitrary heading in regular sinusoidal waves. Under the assumptions that the responses are linear and harmonic, the six linear coupled differential equations of motion, as given by Salvesen et al (1970), are written as follows:

$$\sum_{j=1}^{6}[(M_{ij}+A_{ij})\ddot{\eta}_j + B_{ij}\dot{\eta}_j + C_{ij}\eta_j] = F_i e^{i\omega_e t} \qquad (2.40)$$

where:

i and *j* are subscript (i, j=1, 2 . . . 6) correspond to the mode and direction, respectively. η_j is the displacement (j=1,2 ...6 refer to surge, sway, heave, roll, pitch and yaw respectively), and

A_{ij} : added mass coefficients
B_{ij} : damping coefficients
C_{ij} : : hydrostatic restoring coefficients
F_i : exciting force and moment
M_{ij} : generalised mass
η_j : displacement.

If one assumes that the ship has a long slender hull, the hydrodynamic coefficients (added mass and damping coefficients) in the equations of motion will be determined by longitudinal integrals over the length of the ship of two-dimensional transverse sections. Furthermore, the slender body theory is the basis of strip method.

The vertical ship motions are of importance for slamming and deck wetness investigations. According to Ulbright (1985), these vertical motions are combination of heave and pitch motions and sometimes roll motions.

In the present study, heave and pitch motions are assumed to be the main degrees of freedom which may be the cause of slamming. Therefore, emphasis is given to the coupled heave and pitch motions.

2.4.1 Coupled Heave and Pitch Motion Equations

To begin with, the motions of heave and pitch may be coupled because one motion normally affects the other as the ship responds to wave excitation. As the ship moves with forward speed, the problem becomes complicated. To simplify these complications, the ship motions in surge, sway, yaw, and roll are neglected. The vertical motion of each transverse segment (strip) is assumed to be composed of the combined

heave and pitch motions. The total ship response can be found by integrating the strips along the ship's length. If the strip is disturbed by a passing wave train, the fluctuating water level causes a disturbing force known as the exciting force.

The linearised equations in heave and pitch motions affected by each other are written as follows:

$$(M_s + A_{33})\ddot{z} + B_{33}\dot{z} + C_{33}z + A_{53}\ddot{\theta} + B_{53}\dot{\theta} + C_{53}\theta = (F_{zc} + iF_{zs})e^{i\omega_e t} \tag{2.41}$$

$$(I_y + A_{55})\ddot{\theta} + B_{55}\dot{\theta} + C_{55}\theta + A_{35}\ddot{z} + B_{35}\dot{z} + C_{35}z = (M_{\theta c} + iM_{\theta s})e^{i\omega_e t} \tag{2.42}$$

where:

F_{zc} : real part (cosine part) of the exciting force
F_{zs} : imaginary part (sine part) of the exciting force
M_s : mass of ship
$M_{\theta c}$: real part (cosine part) of the exciting moment
$M_{\theta s}$: imaginary part (sine part) of the exciting moment
I_y : moment of inertia
z : heave displacement
$\dot{z}$: heave velocity
$\ddot{z}$: heave acceleration
θ : pitch angular displacement
$\dot{\theta}$: pitch velocity
$\ddot{\theta}$: pitch acceleration

2.4.2 Heave and Pitch Hydrodynamic Coefficients and Coupling Terms

The hydrodynamic coefficients and the coupling terms for heave motion by including the end effect using New Strip Method (NSM) are given in the following equations:

$$A_{33} = \int_L M_H dx \tag{2.43}$$

$$B_{33} = \int_L N_H dx - U[M_H] \tag{2.44}$$

$$C_{33} = \rho g \int_L B(x)dx - U[N_H] \tag{2.45}$$

$$A_{53} = -\int_L xM_H dx - \frac{U}{\omega_e^2}\int_L N_H dx \tag{2.46}$$

$$B_{53} = -\int_L xN_H dx + U\int_L M_H dx + U[xM_H] + \frac{U^2}{\omega_e^2}[N_H] \tag{2.47}$$

$$C_{53} = -\rho g \int_L xB(x)dx + U[xN_H] - U^2[M_H] \tag{2.48}$$

The hydrodynamic coefficients and the coupling terms for pitch motion by including the end effect using NSM are given in the following equations:

$$A_{55} = \int_L x^2 M_H dx + \frac{U^2}{\omega_e^2}\int_L M_H dx \tag{2.49}$$

$$B_{55} = \int_L x^2 N_H dx + \frac{U^2}{\omega_e^2}\int_L N_H dx - U[x^2 M_H] - \frac{U^2}{\omega_e^2}[xN_H] \tag{2.50}$$

$$C_{55} = \rho g \int_L x^2 B(x)dx - U[x^2 N_H] + U^2[xM_H] \tag{2.51}$$

$$A_{35} = -\int_L xM_H dx + \frac{U}{\omega_e^2}\int_L N_H dx \tag{2.52}$$

$$B_{35} = -\int_L xN_H dx - U\int_L M_H dx + U[xM_H] \tag{2.53}$$

$$C_{35} = -\rho g \int_L xB(x)dx + U[xN_H] \tag{2.54}$$

where:

$B(x)$	:	sectional breadth
g	:	acceleration of gravity
M_H	:	sectional added mass

$[M_H]$: added mass per unit length for the end part
N_H : sectional damping coefficient
$[N_H]$: damping coefficient per unit length for the end part
U : ship speed
ρ : water density.

the first subscript corresponds to the oscillation mode and the second one represents the direction.

2.5 EXCITATION FORCE AND MOMENT DUE TO WAVES FROM ARBITRARY DIRECTION

Wave excitation forces are derived from the hydrodynamic pressure due to incident and diffraction wave potentials. Hence two-dimensional exciting forces are obtained by diffraction force due to wave diffracted from the body and Froude-Krylov force due to the incident wave. The summation of these two forces gives the total force acting on a cross-section which can be integrated over the length of the hull, to obtain the excitation forces acting on the ship.

2.5.1 Froude-Krylov force and moment components

The excitation force on the right hand side of the equation due to the incident wave is represented by the cosine part and the sine part. The cosine part of Froude-Krylov force and moment components in heave and pitch directions are written as:

$$F_{zc}^{FK} = 2\rho g\zeta_a \int_L Cosk^*x \int_0^{B/2} e^{-kz} Cos(kySin\chi)dy.dx \qquad (2.55)$$

$$M_{\theta c}^{FK} = -2\rho g\zeta_a \int_L xCosk^*x \int_0^{B/2} e^{-kz} Cos(kySin\chi)dy.dx \qquad (2.56)$$

where:

F_{zc}^{FK} : cosine part of Froude-Krylov force component
$M_{\theta c}^{FK}$: cosine part of Froude-Krylov moment component
k : wave number
ζ_a : wave amplitude

χ : wave direction.

and the sine part of Froude-Krylov force and moment components are given by the following equations:

$$F_{zs}^{FK} = -2\rho g\zeta_a \int_L \mathrm{Sink^*x} \int_0^{B/2} e^{-kz}\mathrm{Cos(kySin}\chi)\mathrm{dy.dx} \tag{2.57}$$

$$M_{\theta s}^{FK} = 2\rho g\zeta_a \int_L \mathrm{xSink^*x} \int_0^{B/2} e^{-kz}\mathrm{Cos(kySin}\chi)\mathrm{dy.dx} \tag{2.58}$$

where:

F_{zs}^{FK} : the sine part of Froude-Krylov force component
$M_{\theta s}^{FK}$: the sine part of Froude-Krylov moment component

here the cosine part and the sine part of Froude-Krylov forces are given in heave and pitch directions only.

2.5.2 Diffraction force and moment components

The cosine part of diffraction force and moment components in heave and pitch directions are written as:

$$F_{zc}^{d} = \zeta_a \omega e^{-kT_m}\{\int_L N_H \mathrm{Sink^*xdx} - \omega_e \int_L M_H \mathrm{Cosk^*xdx} - U[M_H \mathrm{Sink^*x}] - \frac{U}{\omega_e}[N_H \mathrm{Cosk^*x}]\} \tag{2.59}$$

$$M_{\theta c}^{d} = \zeta_a \omega e^{-kT_m}\{-\int_L \mathrm{x}N_H \mathrm{Sink^*xdx} + \omega_e \int_L \mathrm{x}M_H \mathrm{Cosk^*xdx} - U\int_L M_H \mathrm{Sink^*xdx} - \frac{U}{\omega_e}\int_L N_H \mathrm{Cosk^*xdx} + U[\mathrm{x}M_H \mathrm{Sink^*x}] + \frac{U}{\omega_e}[\mathrm{x}N_H \mathrm{Cosk^*x}]\} \tag{2.60}$$

where:

F^d_{zc} : the cosine part of the diffraction force component

$M^d_{\theta c}$: the cosine part of the diffraction moment component

The sine part of the diffraction force and moment components in heave and pitch directions can be given by:

$$F^d_{zs} = \zeta_a \omega e^{-kT_m}\{\int_L N_H \mathrm{Cosk}^* x dx + \omega_e \int_L M_H \mathrm{Sink}^* x dx - U[M_H \mathrm{Cosk}^* x] + \frac{U}{\omega_e}[N_H \mathrm{Sink}^* x]\} \quad (2.61)$$

$$M^d_{\theta s} = \zeta_a \omega e^{-kT_m}\{-\int_L x N_H \mathrm{Cosk}^* x dx - \omega_e \int_L x M_H \mathrm{Sink}^* x dx - U\int_L M_H \mathrm{Cosk}^* x dx + \frac{U}{\omega_e}\int_L N_H \mathrm{Sink}^* x dx + U[x M_H \mathrm{Cosk}^* x] - \frac{U}{\omega_e}[x N_H \mathrm{Sink}^* x]\} \quad (2.62)$$

where:

F^d_{zs} : sine part of the diffraction force component

$M^d_{\theta s}$: sine part of the diffraction moment component

Hence the total force which is superposition of Froude-Krylov and diffraction force is written as:

$$F_{zc} = F^d_{zc} + F^{Fk}_{zc} \quad (2.63)$$

or

$$F_{zc} = \zeta_a \omega e^{-kT_m}\{\int_L N_H \mathrm{Sink}^* x dx - \omega_e \int_L M_H \mathrm{Cosk}^* x dx - U[M_H \mathrm{Sink}^* x] - \frac{U}{\omega_e}[N_H \mathrm{Cosk}^* x]\} + 2\rho g \zeta_a \int_L \mathrm{Cosk}^* x \int_0^{B/2} e^{-kz} \mathrm{Cos}(ky \mathrm{Sin}\chi) dy.dx \quad (2.64)$$

where:

F_{zc} : the cosine part of the total exciting force

and the sine part of the total exciting force is written as:

$$F_{zs} = F_{zs}^{d} + F_{zs}^{Fk} \tag{2.65}$$

or

$$\begin{aligned} F_{zs} = \zeta_a \omega e^{-kT_m} \{ & \int_L N_H \mathrm{Cosk}^* x dx + \omega_e \int_L M_H \mathrm{Sink}^* x dx \\ & - U[M_H \mathrm{Cosk}^* x] + \frac{U}{\omega_e}[N_H \mathrm{Sink}^* x]\} \\ & - 2\rho g \zeta_a \int_L \mathrm{Sink}^* x \int_0^{B/2} e^{-kz} \mathrm{Cos}(ky\mathrm{Sin}\chi) dy.dx \end{aligned} \tag{2.66}$$

where:

F_{zs} : the sine part of the total exciting force

and the wave number is written as:

$$k^* = k\mathrm{Cos}\chi \tag{2.67}$$

The cosine part of the exciting moment is written as:

$$M_{\theta c} = M_{\theta c}^{d} + M_{\theta c}^{Fk} \tag{2.68}$$

or

$$\begin{aligned} M_{\theta c} = \zeta_a \omega e^{-kT_m} \{ & -\int_L x N_H \mathrm{Sink}^* x dx + \omega_e \int_L x M_H \mathrm{Cosk}^* x dx \\ & - U \int_L M_H \mathrm{Sink}^* x dx - \frac{U}{\omega_e} \int_L N_H \mathrm{Cosk}^* x dx \\ & + U[x M_H \mathrm{Sink}^* x] + \frac{U}{\omega_e}[x N_H \mathrm{Cosk}^* x]\} \\ & - 2\rho g \zeta_a \int_L x \mathrm{Cosk}^* x \int_0^{B/2} e^{-kz} \mathrm{Cos}(ky\mathrm{Sin}\chi) dy.dx \end{aligned} \tag{2.69}$$

where:

$M_{\theta c}$: the cosine part of the total exciting moment

The sine part of the exciting moment is written as:

$$M_{\theta s} = M^{d}_{\theta s} + M^{Fk}_{\theta s} \tag{2.70}$$

or

$$\begin{aligned} M_{\theta s} = \zeta_a \omega e^{-kT_m} \{ & -\int_L x N_H \mathrm{Cosk}^* x dx - \omega_e \int_L x M_H \mathrm{Sink}^* x dx \\ & -U \int_L M_H \mathrm{Cosk}^* x dx + \frac{U}{\omega_e} \int_L N_H \mathrm{Sink}^* x dx \\ & + U[x M_H \mathrm{Cosk}^* x] - \frac{U}{\omega_e}[x N_H \mathrm{Sink}^* x]\} \\ & + 2\rho g \zeta_a \int_L x \mathrm{Sink}^* x \int_0^{B/2} e^{-kz} \mathrm{Cos}(ky \mathrm{Sin}\chi) dy.dx \end{aligned} \tag{2.71}$$

where:

$M_{\theta s}$: the sine part of the total exciting moment

The procedure for mathematical calculation of the sectional added mass M_H and damping coefficients N_H, which are functions of the free surface coefficient of added mass K_4 and heave amplitude ratio $\overline{A}_H$, are detailed in the Appendix.

Predicted numerical computation results of non-dimensionalised free surface coefficients K_4 are given in Figs. 2.20 to 2.30 for each station along the ship. As shown in these results there is good correlation between the present method and that of Tasai (1959) and Bishop and Price (1979). There are some discrepancies in the case of fine section shape but in general the correlation is good for full section shapes. Some discrepancies take place place because of the difference in the input data for the present sections and those data obtained from the geometries given by Tasai (1959) and Bishop and Price (1979).

For heave amplitude ratio $\overline{A}_H$, numerical computation of non-dimensionalised results are shown in Figs. 2.31 to 2.41 for each station along the ship. Comparison of the present results, with those given by the geometries of Tasai (195) and Bishop and Price (1979), are found to be in good agreement except of the small difference which are due to the difference in the input data.

2.6 SOLUTION OF MOTION EQUATION

The exciting forces and moments in equations (2.63), (2.65), (2.68) and (2.70) can be expressed in complex form in order to facilitate the algebraic solution. The exciting functions are harmonic, hence the solution for the equations (2.41) and (2.42) can be assumed harmonic according to Korvin-Kroukovsky (1955) and to be of the form:

$$z = \bar{z}e^{i\omega_e t} \tag{2.72}$$

$$\theta = \bar{\theta}e^{i\omega_e t} \tag{2.73}$$

where $\bar{z}$ and $\bar{\theta}$ are complex amplitudes given by the following equations:

$$\bar{z} = z_a e^{i\delta} \tag{2.74}$$

$$\bar{\theta} = \theta_a e^{i\varepsilon} \tag{2.75}$$

where:

$\bar{z}$: heave complex amplitude
z_a : heave amplitude
$\bar{\theta}$: pitch complex amplitude
θ_a : pitch amplitude
δ : heave phase angle
ε : pitch phase angle.

The forcing function is given in complex form as follows:

$$\bar{F} = F_a e^{i\sigma} \tag{2.76}$$

$$\overline{M} = M_a e^{i\tau} \tag{2.77}$$

where:

$\overline{F}$: complex amplitude of the total exciting force
F_a : amplitude of the total exciting force
$\overline{M}$: complex amplitude of the total exciting moment
M_a : amplitude of the total exciting moment
σ : phase angle of the total exciting force
τ : phase angle of the total exciting moment

The amplitude of the exciting force, which is superposition of Froude-Krylov and diffraction force, is written as follows:

$$F_a = \sqrt{F_{zc}^2 + F_{zs}^2} \tag{2.78}$$

and σ the phase angle of the exciting force is written as:

$$\sigma = \arctan(\frac{F_{zs}}{F_{zc}}) \tag{2.79}$$

The amplitude of the exciting moment is given by:

$$M_a = \sqrt{M_{\theta c}^2 + M_{\theta s}^2} \tag{2.80}$$

and τ the phase angle of the exciting moment is written as:

$$\tau = \arctan(\frac{M_{\theta s}}{M_{\theta c}}) \tag{2.81}$$

From equation (2.41) and (2.42), one can introduce the complex forms by the coefficients:

$$P = -(M_s + A_{33})\omega_e^2 + iB_{33}\omega_e + C_{33} \tag{2.82}$$

$$Q = -A_{53}\omega_e^2 + iB_{53}\omega_e + C_{53} \tag{2.83}$$

$$S = -(I_y + A_{55})\omega_e^2 + iB_{55}\omega_e + C_{55} \tag{2.84}$$

$$R = -A_{35}\omega_e^2 + iB_{35}\omega_e + C_{35} \tag{2.85}$$

'i' represents the complex quantity $\sqrt{-1}$.

Hence if we insert in the equations (2.41) and (2.42) the quantities given in equation (2.74) to (2.77) and (2.82) to (2.85), the equations of motions become as follows:

$$P\bar{z} + Q\bar{\theta} = \bar{F} \tag{2.86}$$

$$S\bar{\theta} + R\bar{z} = \bar{M} \tag{2.87}$$

Solving each equation for $\bar{z}$ and $\bar{\theta}$, we arrive at the solution for complex heave and pitch:

$$\bar{z} = \frac{\bar{M}Q - \bar{F}S}{QR - PS} \tag{2.88}$$

$$\bar{\theta} = \frac{\bar{F}R - \bar{M}P}{QR - PS} \tag{2.89}$$

This is the final solution of the motion equations. Having found amplitudes and phase angles for heave and pitch motions, we can express the two motions in their final forms as:

$$\bar{z} = z_a e^{i\delta} = z_a(\cos\delta + i\sin\delta) \tag{2.90}$$

$$\bar{\theta} = \theta_a e^{i\varepsilon} = \theta_a(\cos\varepsilon + i\sin\varepsilon) \tag{2.91}$$

The steps, which have been taken for the calculation of coupled heave and pitch motions, are summarised as follows:

- divide the ship into a finite number of sections to represent the hull form.
- derive the hydrodynamic coefficients by using new strip method which takes the end effect into account and integrate this coefficients along the ship length.
- calculate the exciting force and moment from Froude-Krylov and diffraction

components.

- use the complex solution to calculate heave and pitch response for a given seaway.

Fig. 2.42 shows a comparison of non-dimensionalised heave amplitude results obtained from New Strip Method calculation with those obtained from Ship Motion software package SHIPMO-PC (1992). For Froude number 0.275, the comparison is in good agreement. The effect of the end term is noticeable where a shift in the peak is taking place in the frequency range of $1.5 \leq \omega\sqrt{L/g} \leq 2.0$. For the same Froude number, non-dimensionalised pitch amplitude results are also compared, as shown in Fig. 2.43, with those results obtained from the same program.

As a double check, results of heave and pitch motions in Figs. 2.46 and 2.47 respectively are compared with those obtained from the Ship Motion software package by neglecting the effect of the end term. The comparison is in good agreement except for slight differences.

2.7 VERTICAL RELATIVE MOTION

Seakeeping studies often require assessments of motions experienced at some particular point of the marine vehicle, such as the vertical relative motion exceeding its threshold value in slamming or deck wetness events. These two events are mainly dependent on the quantity of the vertical relative motion. Moreover, if this quantity exceeds the local draught, slamming is imminent and if it exceeds the freeboard deck wetness may occur. The severity of slamming and deck wetness depends mainly on the vertical relative motion.

The vertical relative motion is given by Lloyd (1989 b) as the superposition of the absolute motion and the wave elevation, that is to say:

$$r = s - \zeta \tag{2.92}$$

where:

r : vertical relative motion
s : absolute motion

ζ : wave elevation

's' the absolute motion is a combination of heave and pitch motions at different positions along the ship's hull and is given as:

$$s = z + \xi\theta \tag{2.93}$$

where:

ξ : the distance from the location of the centre of gravity of the body to the station in consideration.

'ζ' is the wave elevation which is defined by:

$$\zeta = \zeta_a \sin(k\xi - \omega_e t)e^{-kz} \tag{2.94}$$

The final equation of the vertical relative motion, given in terms of heave, pitch and wave elevation, is given as:

$$r = z + \xi\theta - \zeta \tag{2.95}$$

and it is also expressed as:

$$r(t) = r_a \cos(\omega_e t + \delta_r) \tag{2.96}$$

r_a : amplitude of the vertical relative motion
δ_r : relative motion phase angle

According to Price et al (1974) the relative motion is the quantity which may define the occurrence of the event of slamming and deck wetness. This vertical relative motion increases if the distance between the centre of gravity and the station considered increases.

Fig. 2.44 shows non-dimensionalised vertical relative motion for Froude number 0.275 at station 8 1/2. This vertical relative motion is larger in the range of $2.0 \leq \omega\sqrt{L/g} \leq 2.5$ and that is where slamming may occur.

2.8 VERTICAL RELATIVE VELOCITY

Among the conditions related to slamming occurrence are bow emergence and a certain magnitude of the vertical relative velocity which is referred to as threshold the velocity. As detailed by Bishop et al (1974), this threshold velocity has been established by Ochi from model tests as 12.0 ft/s for a 520 ft ship. Ochi et al (1973) suggested the following Froude scaling law for the threshold velocity:

$$V_{cr} = 0.093\sqrt{gL} \tag{2.97}$$

where:

V_{cr} : threshold vertical velocity (critical velocity)
g : acceleration of gravity
L : length of ship

In reality, the meaning of threshold velocity is still obscure and more investigations need to be carried out in this field to clarify this obscurity.

The vertical relative velocity is the first derivative of the vertical relative motion with respect to time, i.e:

$$V_r(t) = \frac{dr}{dt} \tag{2.98}$$

or

$$V_r(t) = \omega_e r(t) \tag{2.99}$$

where:

$V_r(t)$: vertical relative velocity

and the amplitude of the vertical relative velocity is expressed as:

$$V_{ra} = \omega_e r_a \tag{2.100}$$

where:

V_m : amplitude of vertical relative velocity

Since slamming pressure is approximately proportional to the square of the relative velocity at the moment of impact, it is meaningful to approximate the impact relative velocity by the amplitude of relative velocity. As the amplitude of the relative velocity is somewhat larger than the impact velocity, it does not influence the prediction of the impact pressure and that is why, to a certain extent, in most of the cases the predicted value of pressure due to slamming is greater than the magnitude of the measured value.

The computed vertical relative velocity is given in Fig. 2.45 for Froude number 0.275. In the frequency range of $2.0 \leq \omega\sqrt{L/g} \leq 2.5$, Ochi's condition is satisfied and if the vertical relative velocity exceeds its threshold value, as given in equation (2.97), bottom slamming is imminent.

2.9 CONCLUSIONS

In the present investigation it is appropriate to calculate the hydrodynamic coefficients by using the conformal mapping parameter in the multipole expansion method. To get reasonable and accurate prediction of the hydrodynamic coefficients for input into the equations of motions, it is usual to truncate the mapped section to two parameters only from the point of numerical accuracy. The end effect terms play an important role in the prediction of ship motions.

For numerical prediction of the coefficient a least square method is adopted and these results are compared with those of Tasai (1959) and Bishop and Price (1979). For nearly the same conditions, one can notice that the present method, Tasai's (1959) and Bishop and Price's (1979) methods match very well as in Figs. 2.20 to 2.41. However some differences took place in the free surface coefficient of added mass and amplitude ratio which are due to the difference in the input data.

Using this analogy the results of the motions obtained by the present method, New Strip Method, and by SHIPMO package are as in Figs. 2.42 to 2.43. Especially for the lower frequency range one can notice the shift in the peak and an increase in the magnitude of the heave motion which results in large motions of the ship and which in

turn may cause slamming and/or deck wetness. As a double check, results of heave and pitch motions are compared with those obtained from the SHIPMO package by neglecting the effect of the end term.

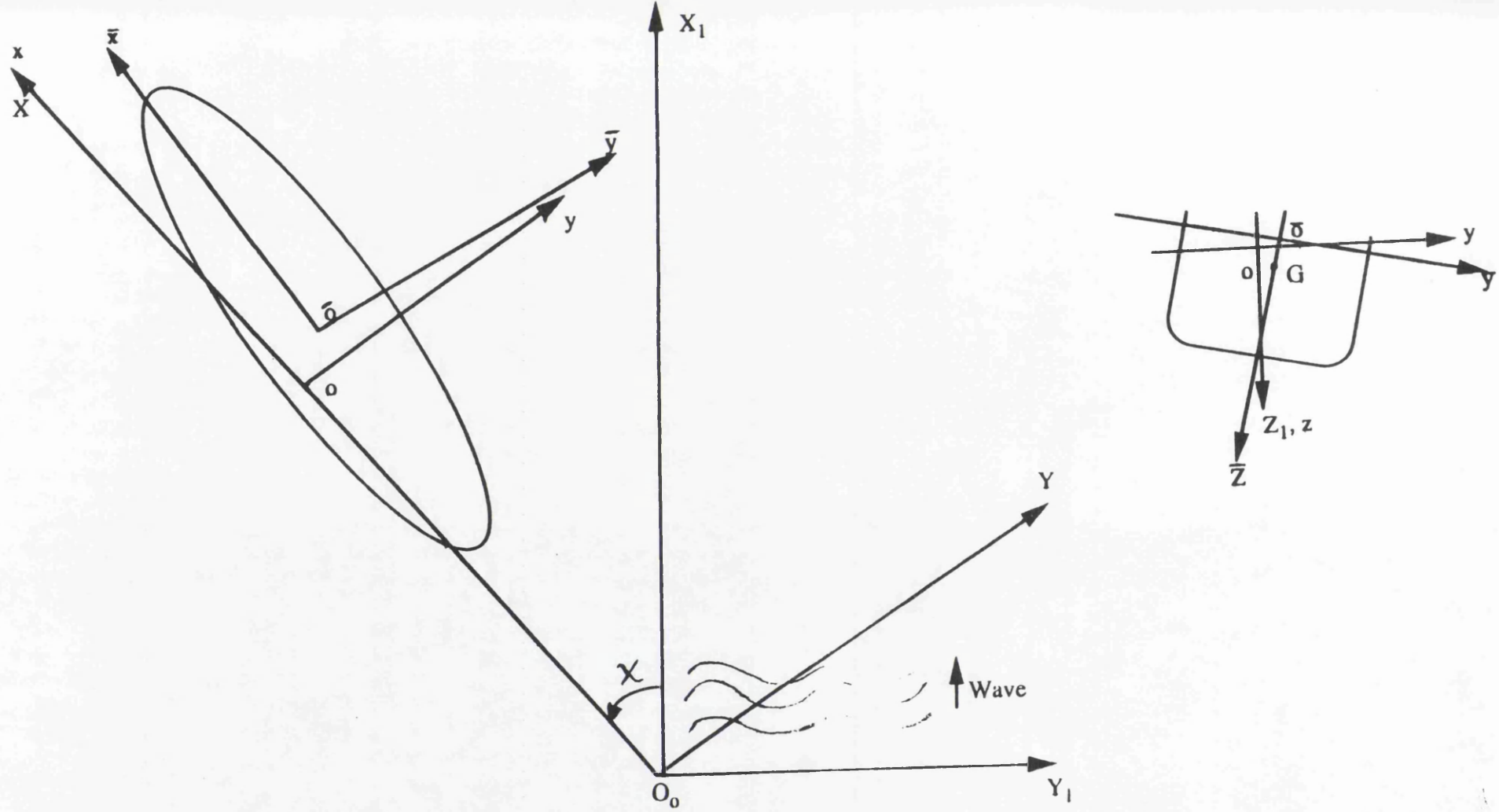

Fig. 2.1 Coordinate system

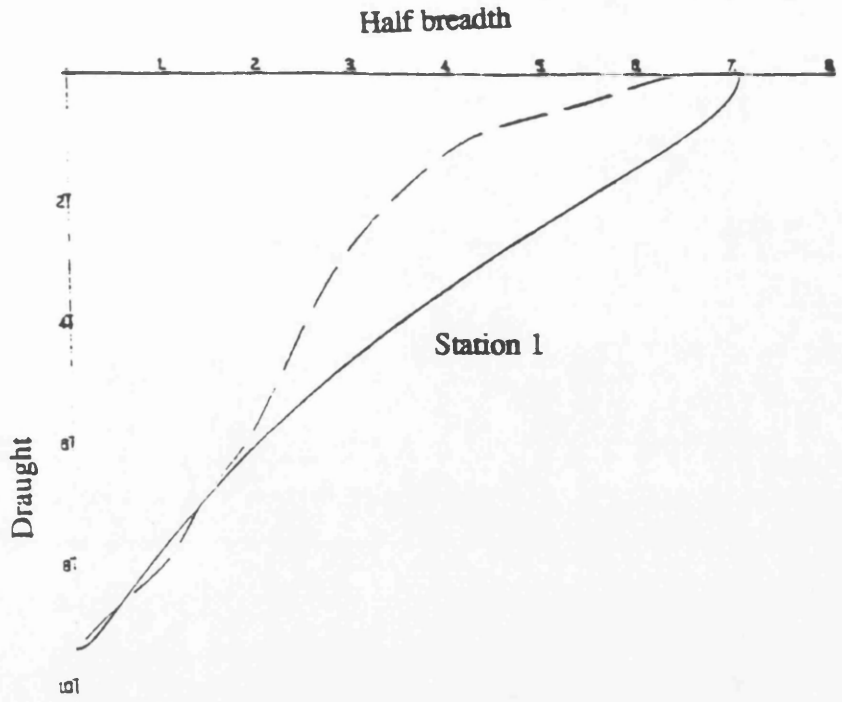

Fig. 2.2 Comparison of mapped section 1 to the real geometry of ship section 1 using two parameter

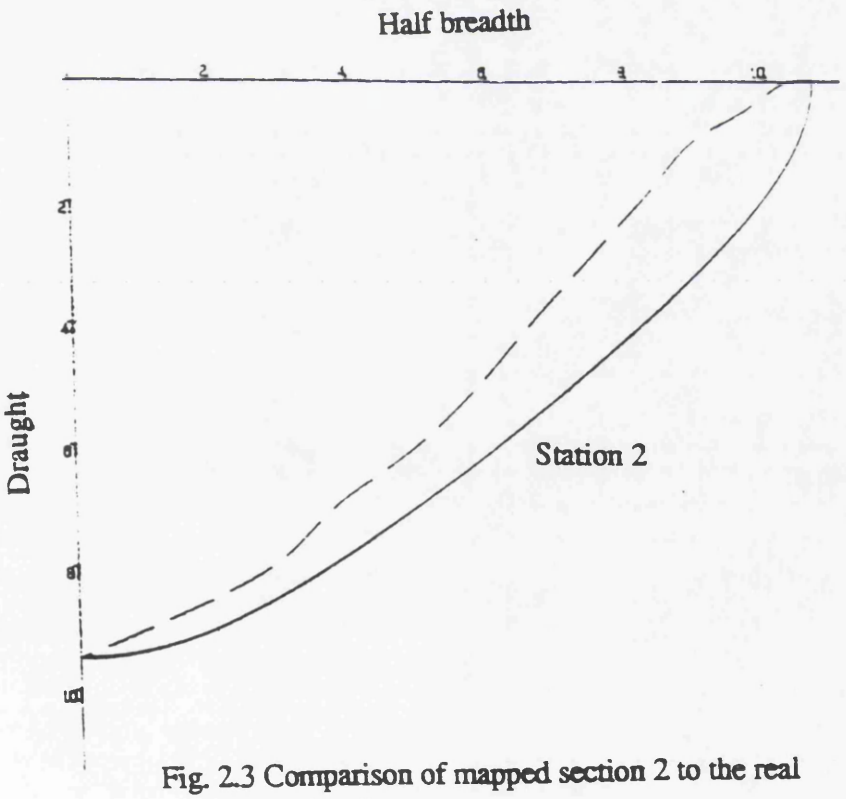

Fig. 2.3 Comparison of mapped section 2 to the real geometry of ship section 2 using two parameter

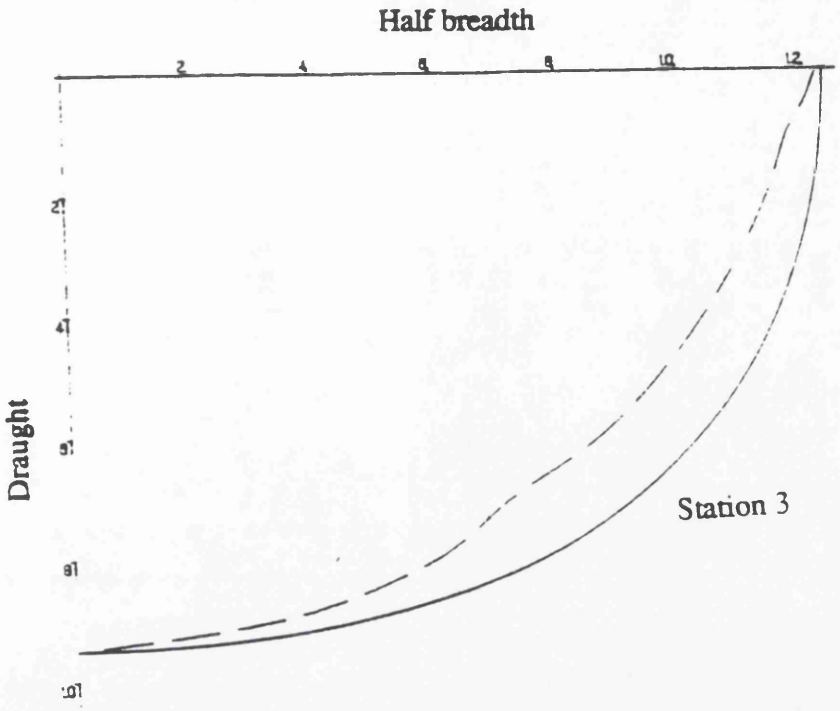

Fig. 2.4 Comparison of mapped section 3 to the real geometry of ship section 3 using two parameter

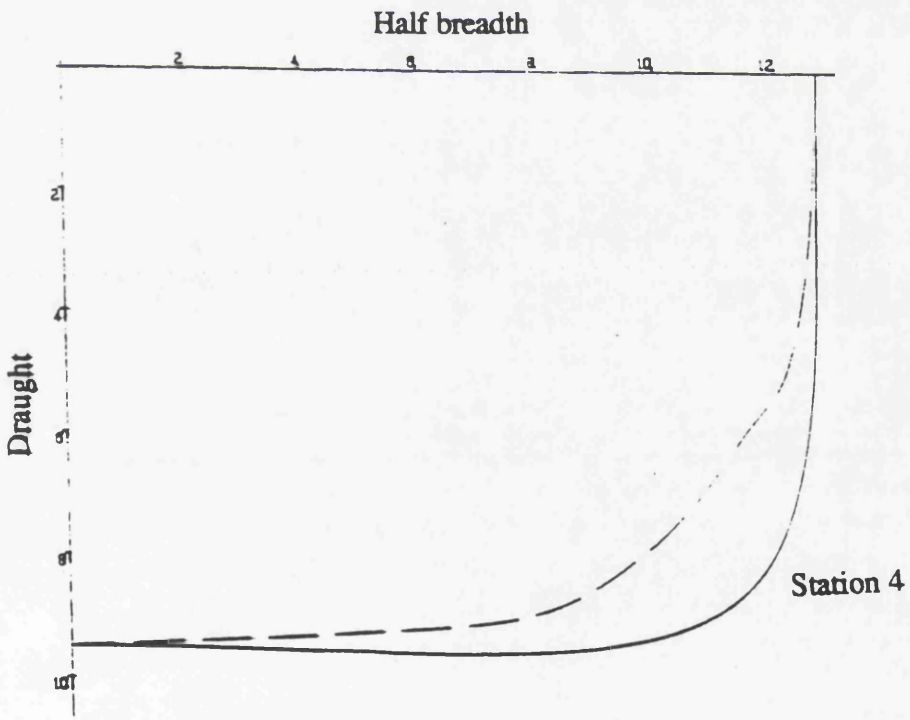

Fig. 2.5 Comparison of mapped section 4 to the real geometry of ship section 4 using two parameter

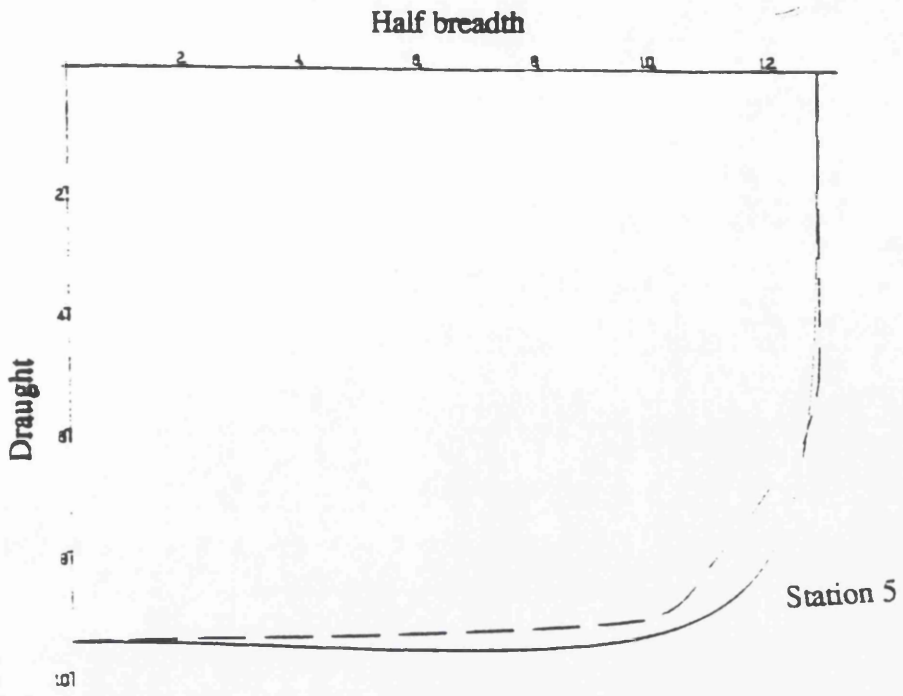

Fig. 2.6 Comparison of mapped section 5 to the real geometry of ship section 5 using two parameter

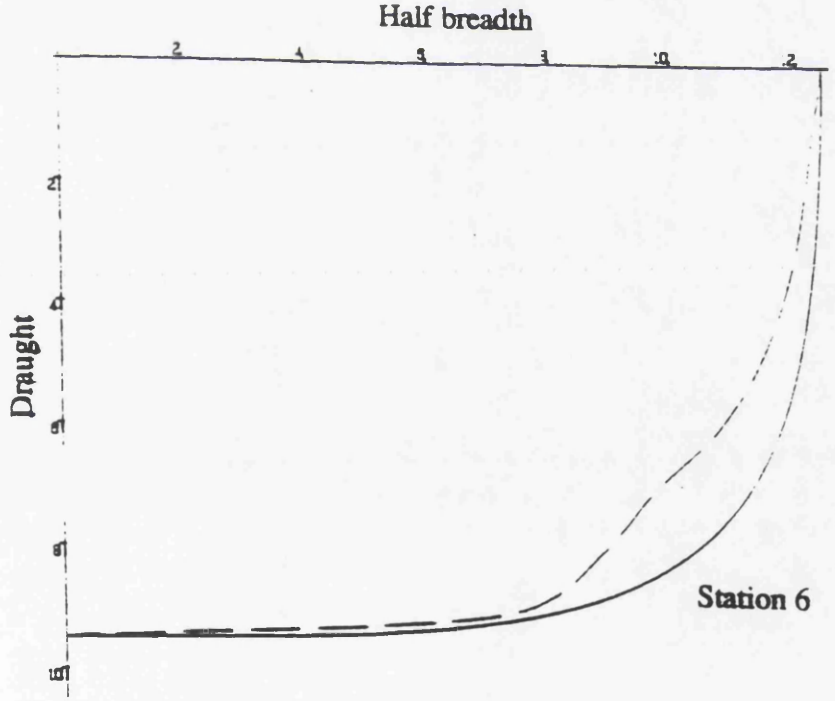

Fig. 2.7 Comparison of mapped section 6 to the real geometry of ship section 6 using two parameter

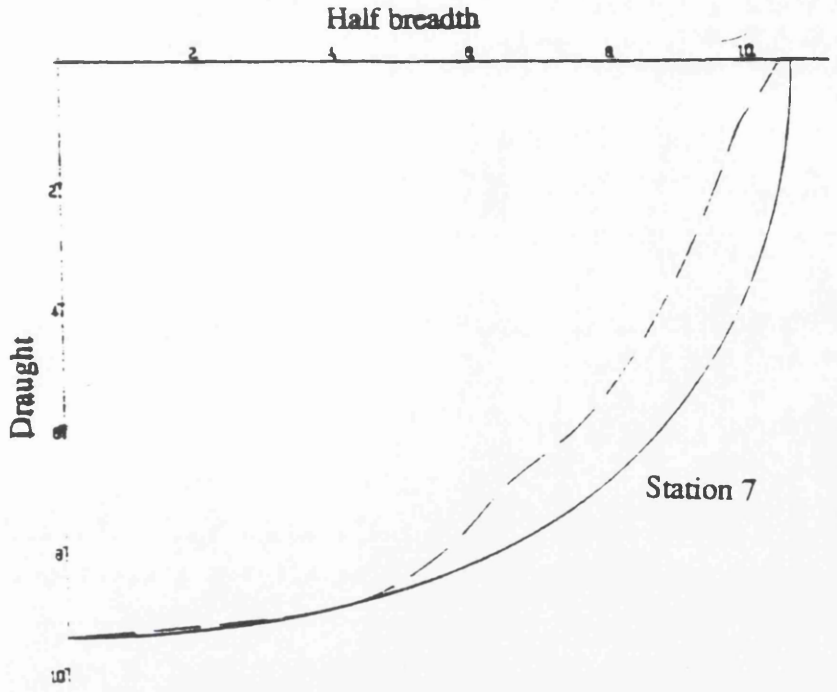

Fig. 2.8 Comparison of mapped section 7 to the real geometry of ship section 7 using two parameter

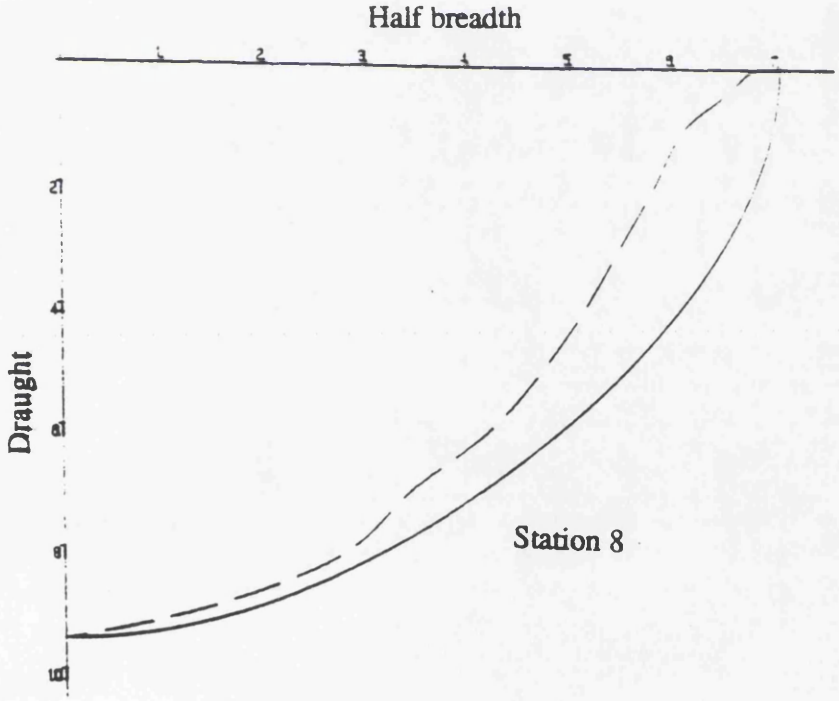

Fig. 2.9 Comparison of mapped section 8 to the real geometry of ship section 8 using two parameter

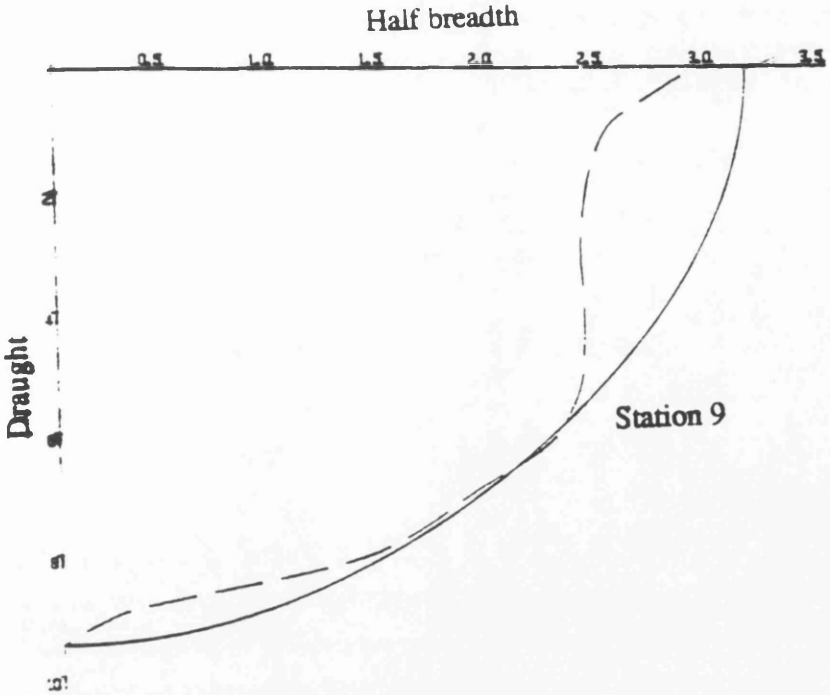

Fig. 2.10 Comparison of mapped section 9 to the real geometry of ship section 9 using two parameter

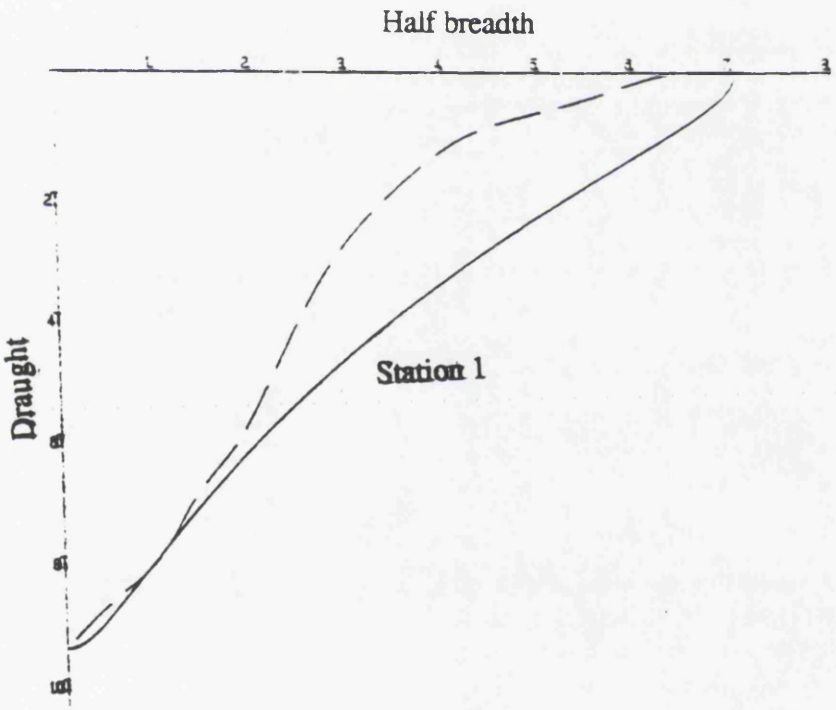

Fig. 2.11 Comparison of mapped section 1 to the real geometry of ship section 1 using three parameter

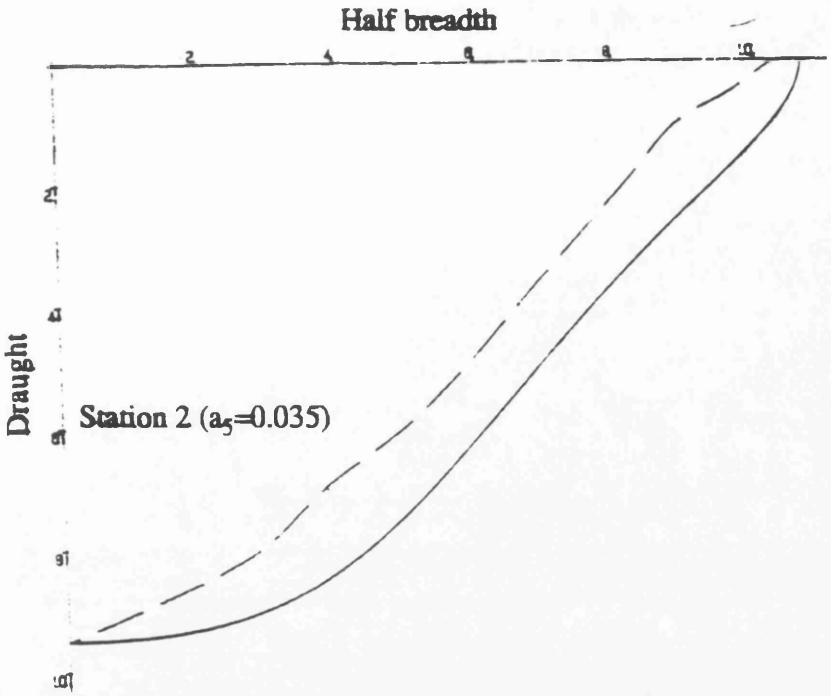

Fig. 2.12 Comparison of mapped section 2 to the real geometry of ship section 2 using three parameter

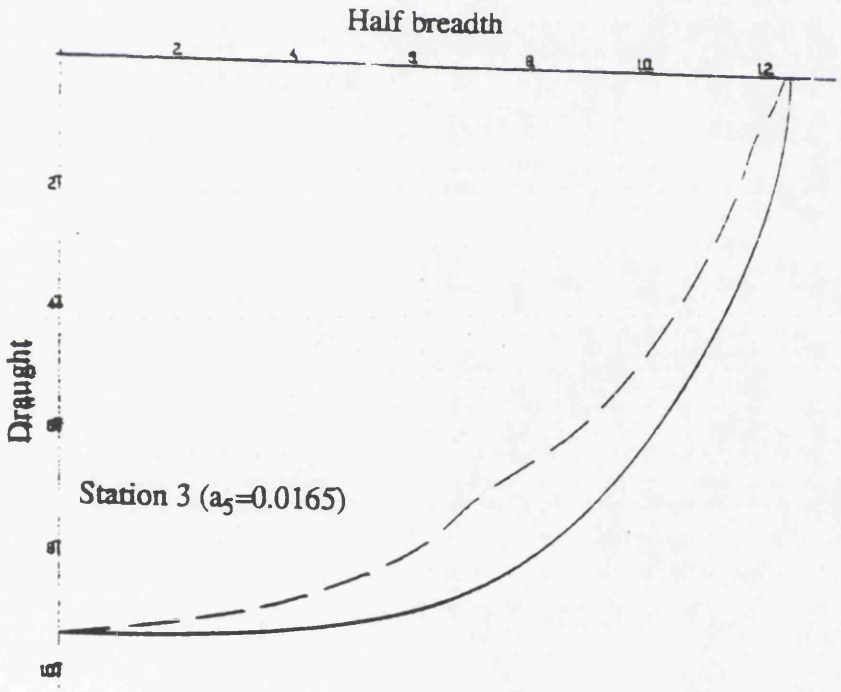

Fig. 2.13 Comparison of mapped section 3 to the real geometry of ship section 3 using three parameter

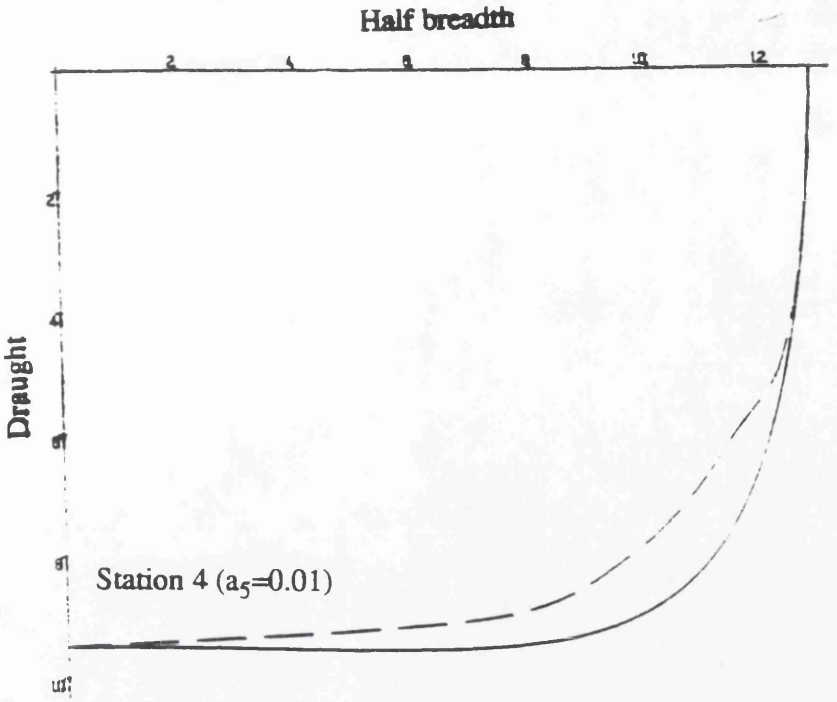

Fig. 2.14 Comparison of mapped section 4 to the real geometry of ship section 4 using three parameter

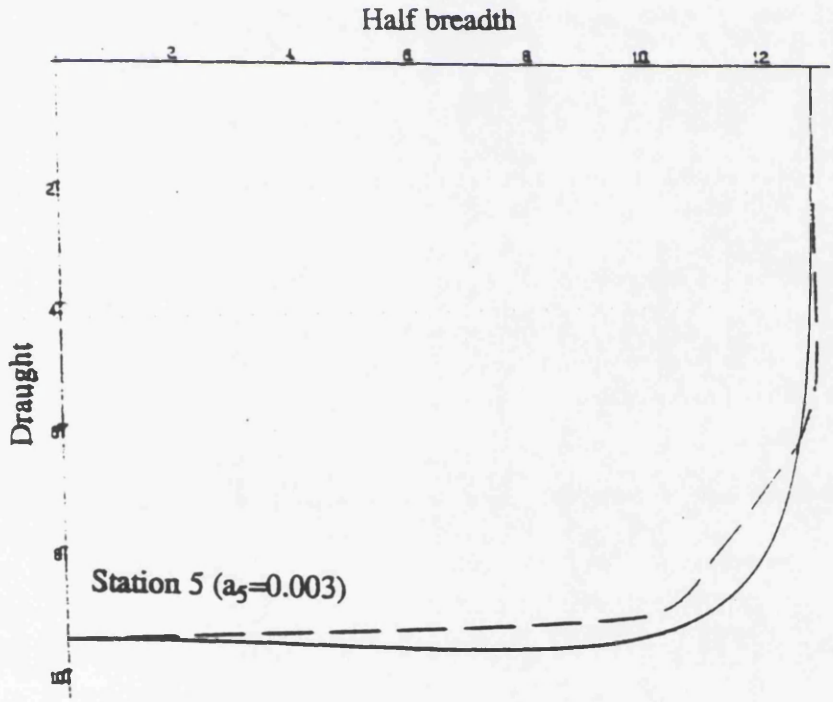

Fig. 2.15 Comparison of mapped section 5 to the real geometry of ship section 5 using three parameter

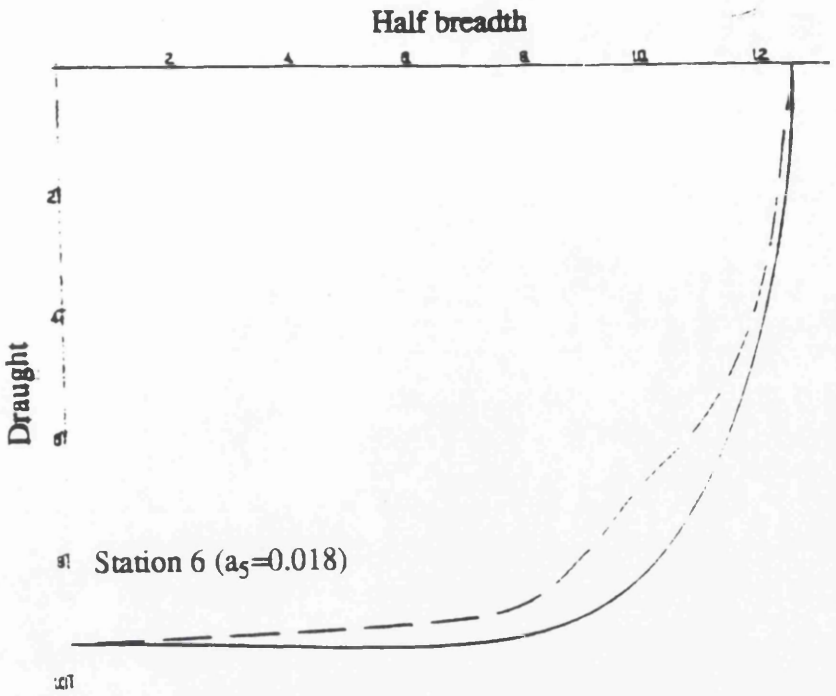

Fig. 2.16 Comparison of mapped section 6 to the real geometry of ship section 6 using three parameter

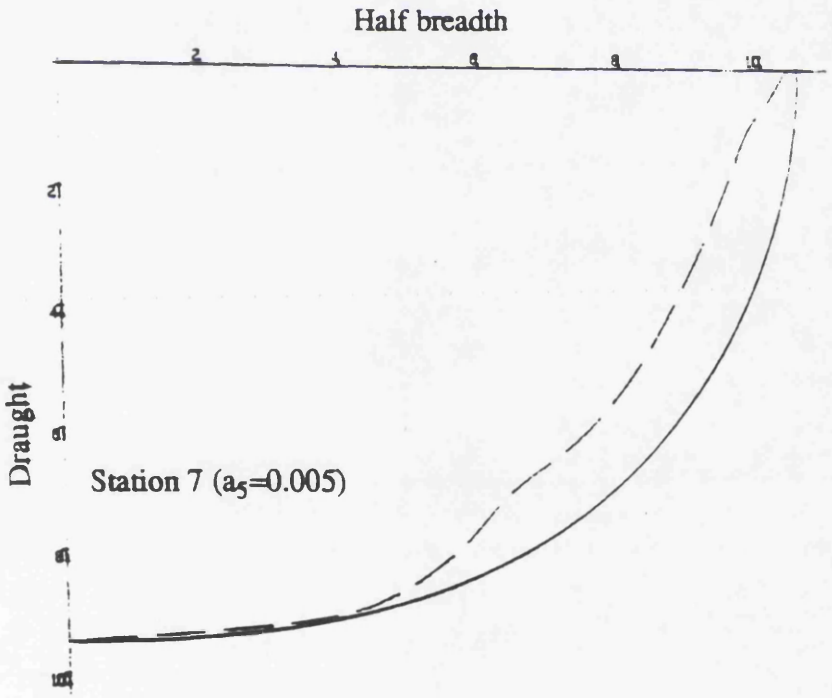

Fig. 2.17 Comparison of mapped section 7 to the real geometry of ship section 7 using three parameter

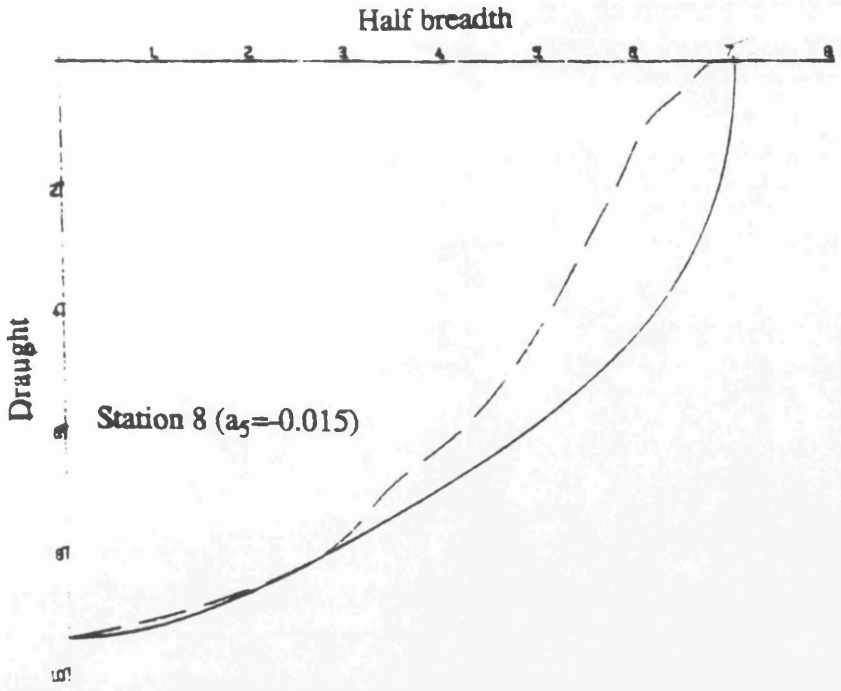

Fig. 2.18 Comparison of mapped section 8 to the real geometry of ship section 8 using three parameter

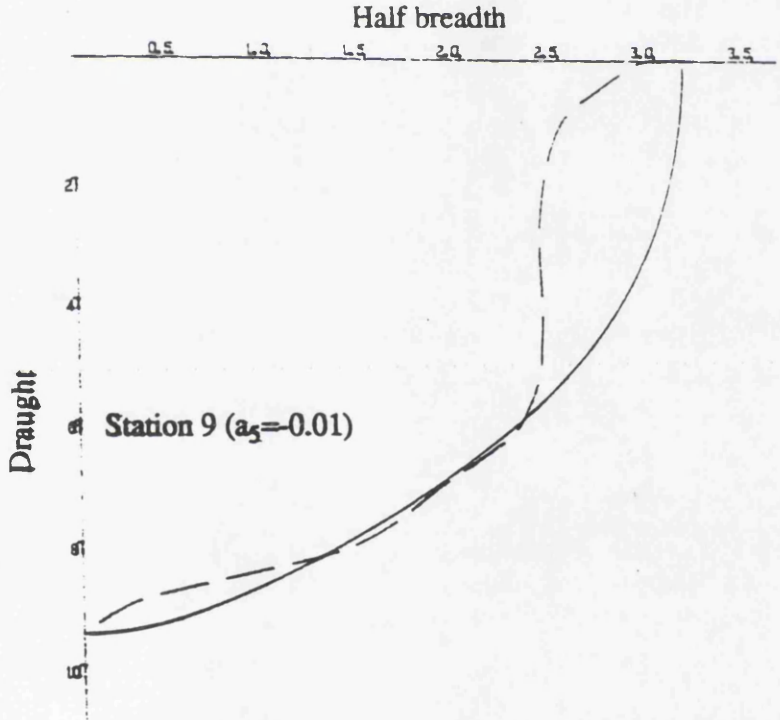

Fig. 2.19 Comparison of mapped section 9 to the real geometry of ship section 9 using three parameter

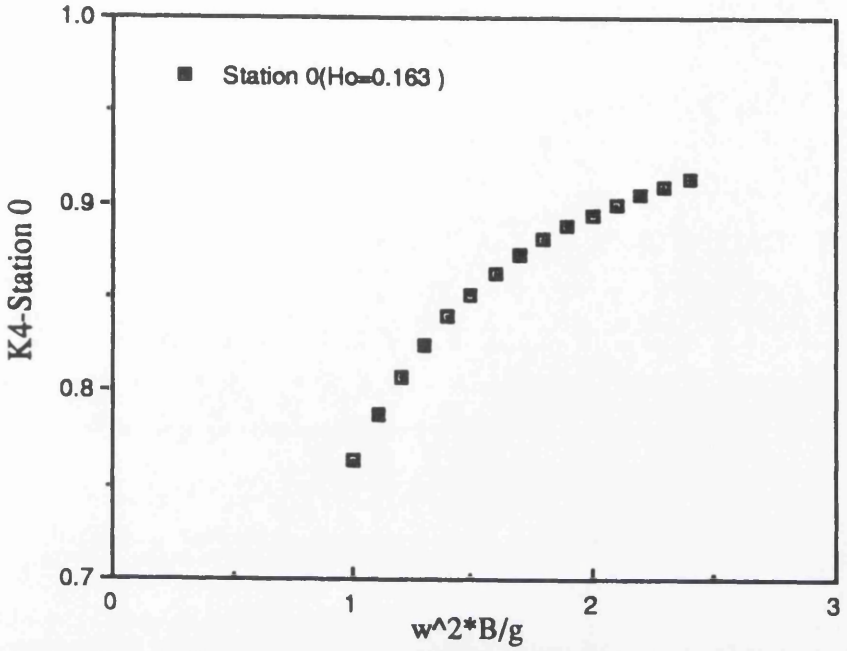

Fig. 2.20 Free surface coefficient of added mass for station 0

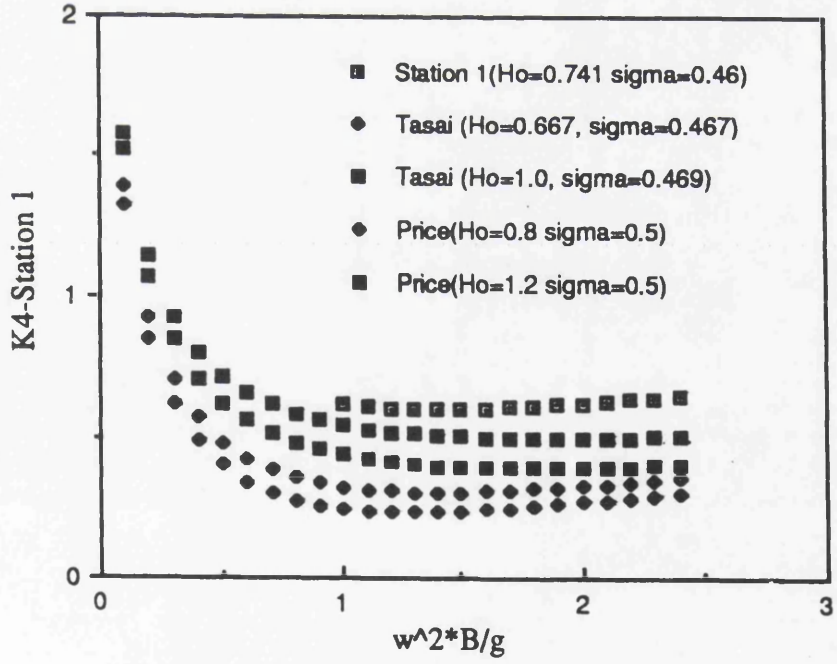

Fig. 2.21 Free surface coefficient of added mass for station 1

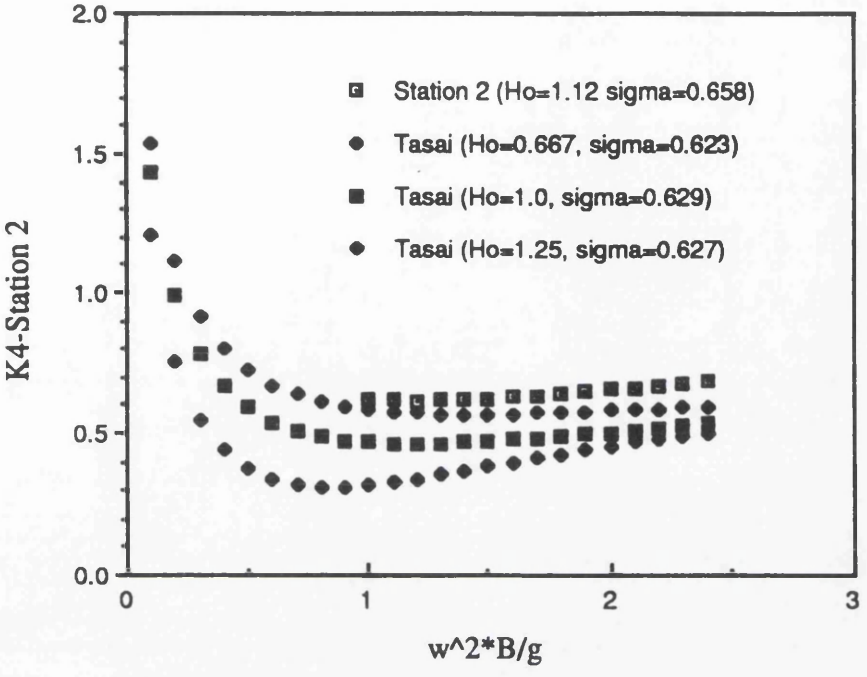

Fig. 2.22 Free surface coefficient of added mass for station 2

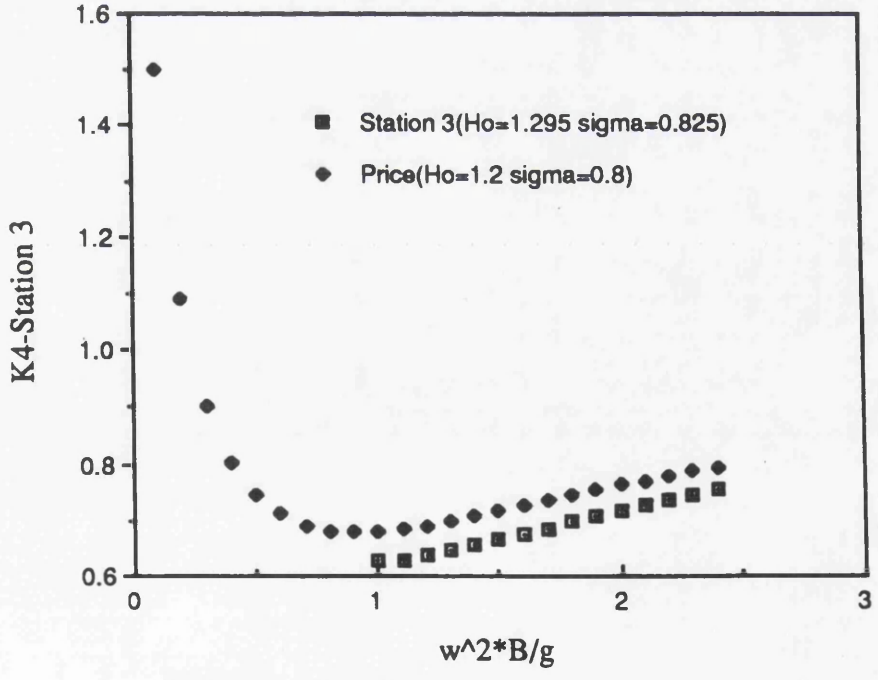

Fig. 2.23 Free surface coefficient of added mass for station 3

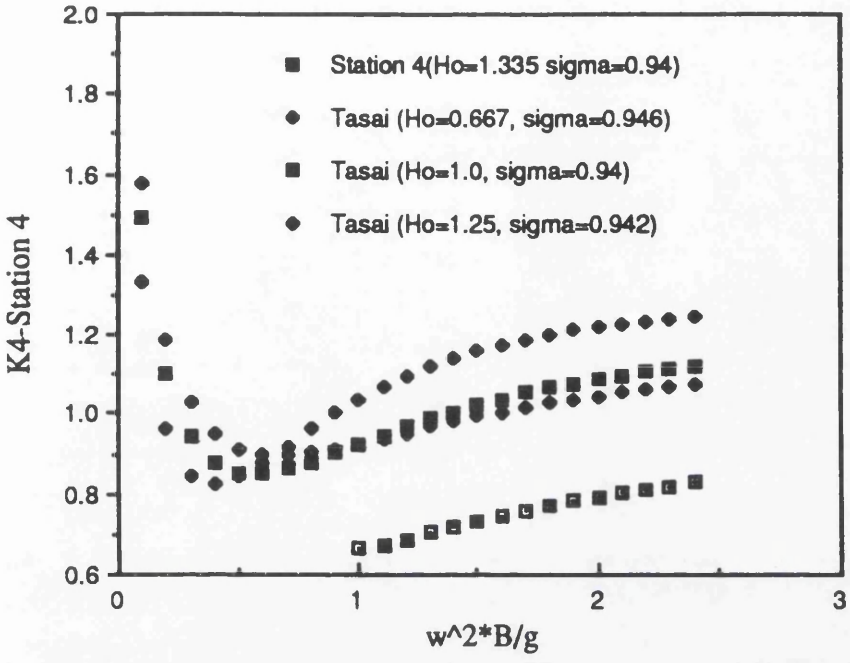

Fig. 2.24 Free surface coefficient of added mass for station 4

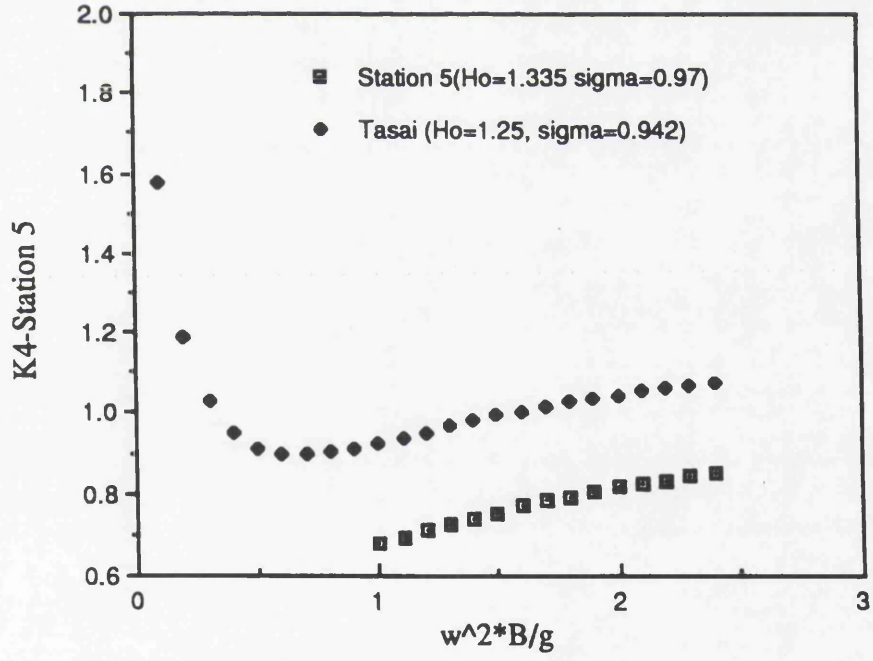

Fig. 2.25 Free surface coefficient for added mass for station 5

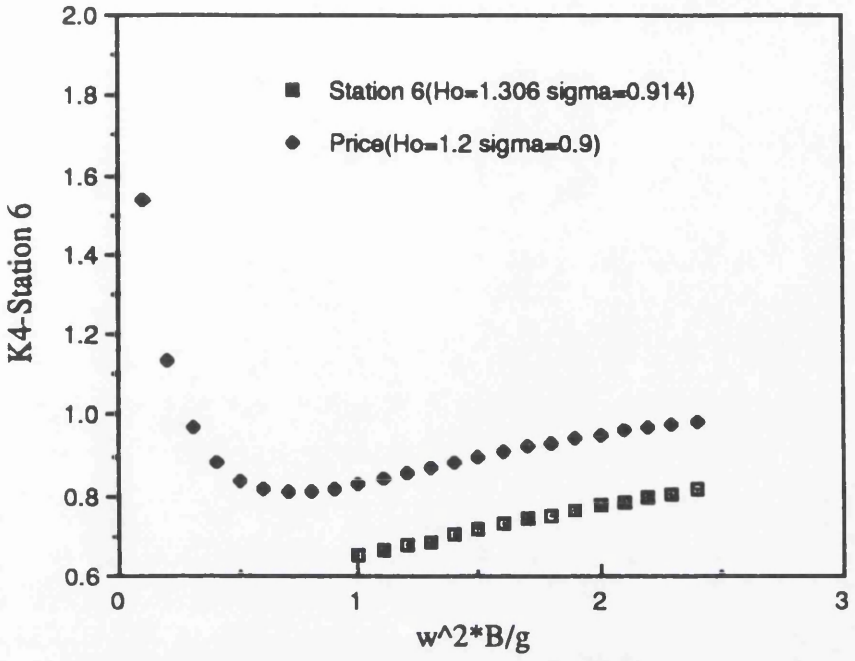

Fig. 2.26 Free surface coefficient for added mass for station 6

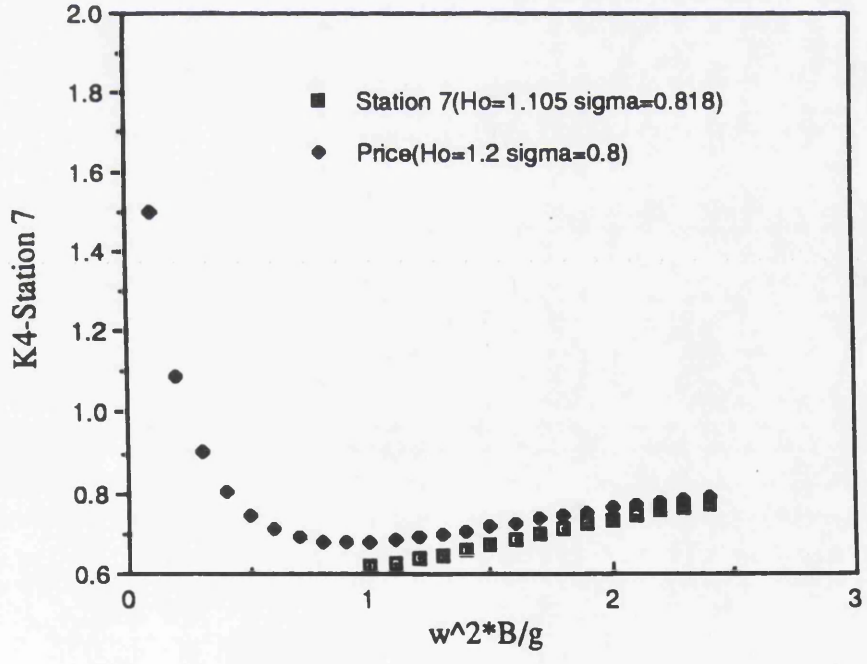

Fig. 2.27 Free surface coefficient of added mass for station 7

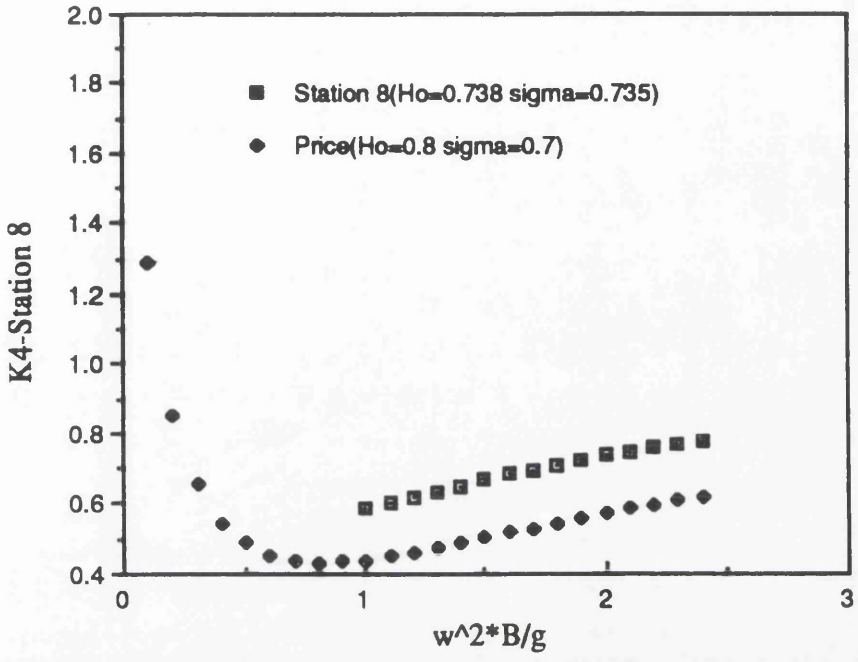

Fig. 2.28 Free surface coefficient of added mass for station 8

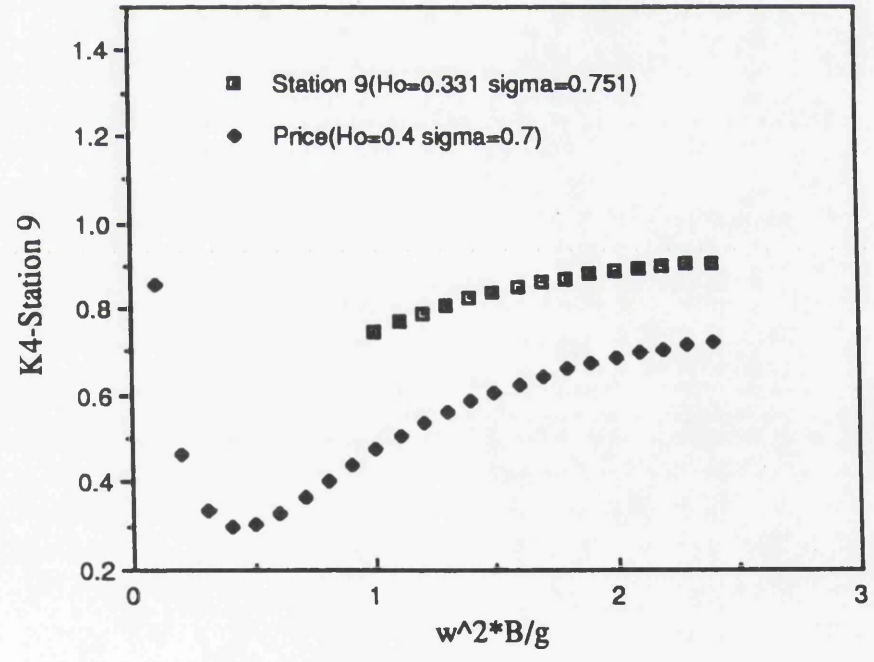

Fig. 2.29 Free surface coefficient of added mass for station 9

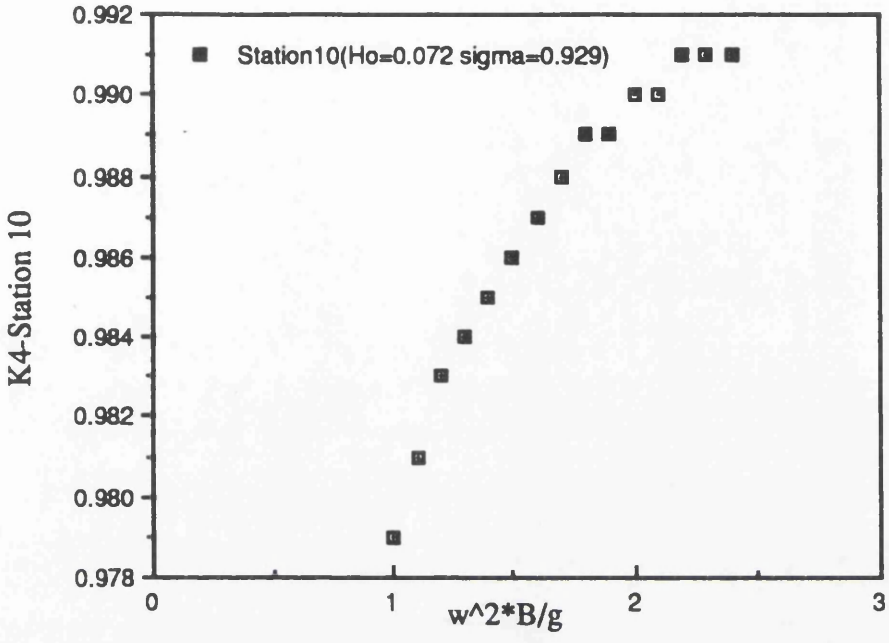

Fig. 2.30 Free surface coefficient of added mass for station 10

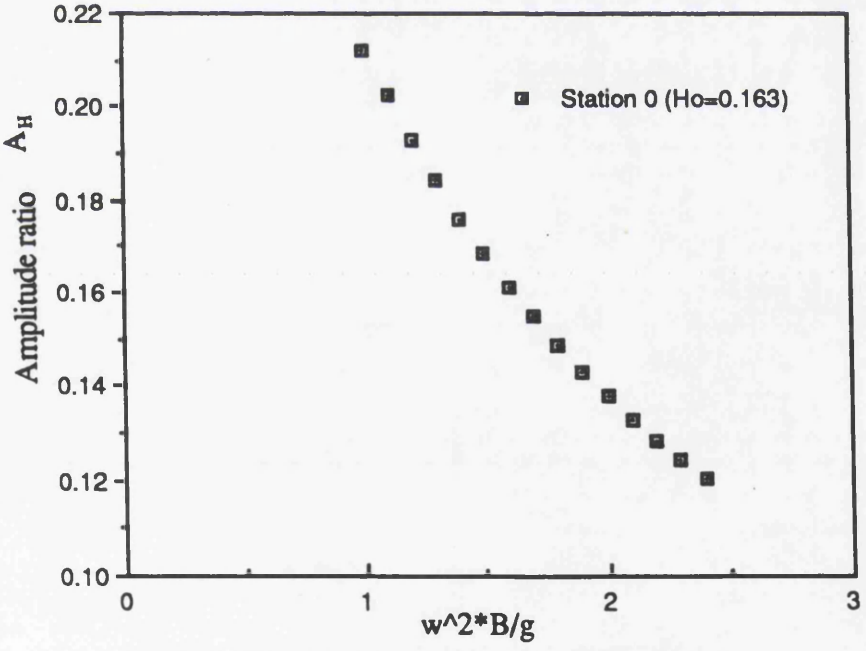

Fig. 2.31 Amplitude ratio for station 0

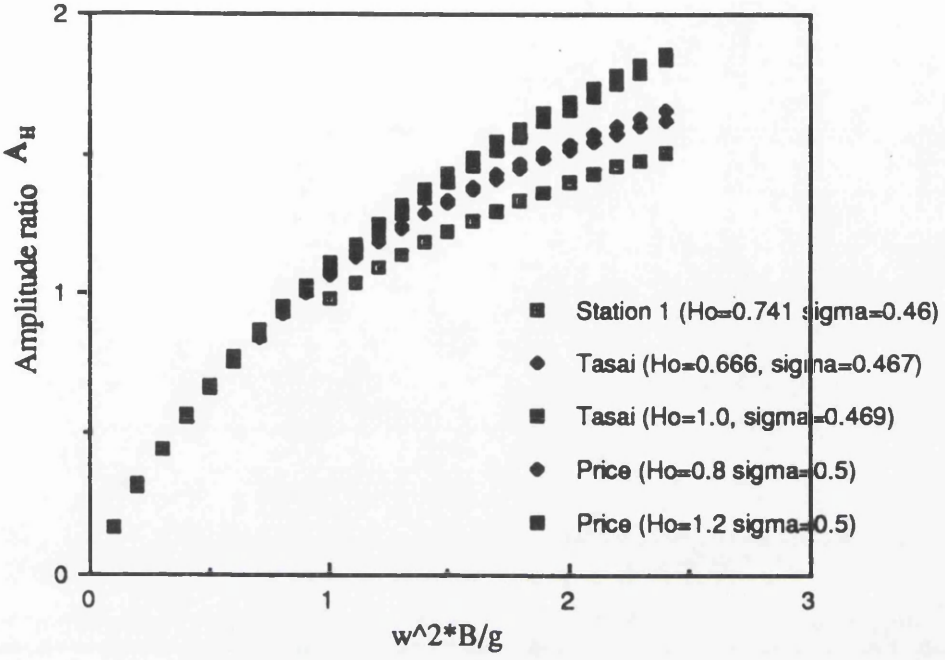

Fig. 2.32 Amplitude ratio for station 1

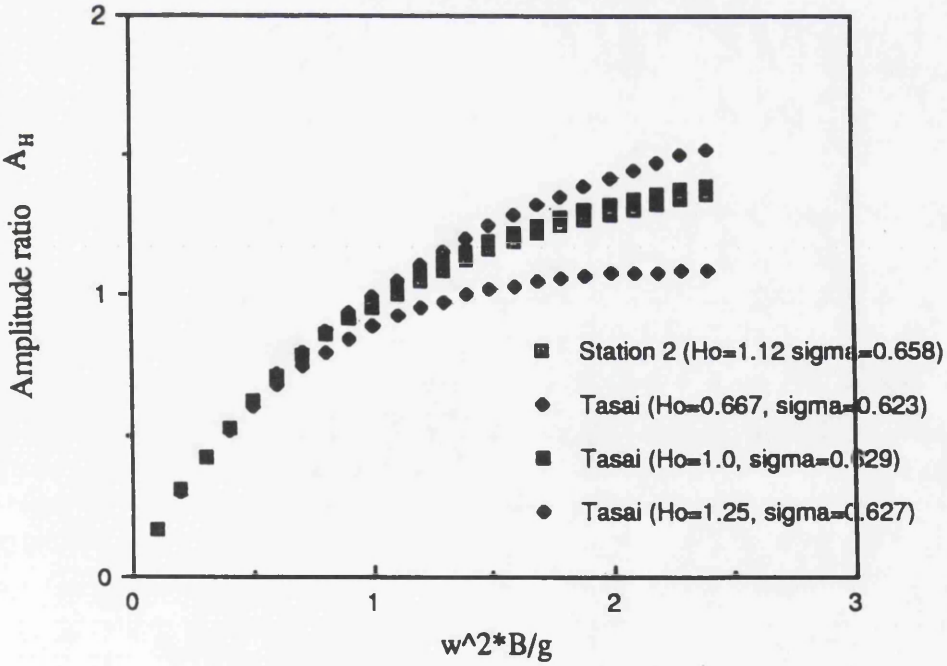

Fig. 2.33 Amplitude ratio for station 2

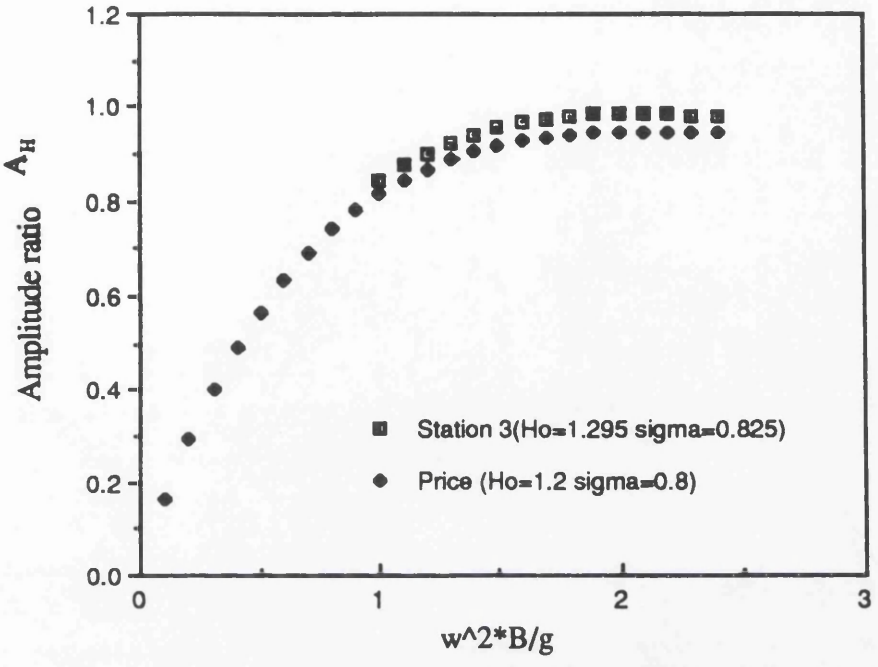

Fig. 2.34 Amplitude ratio for station 3

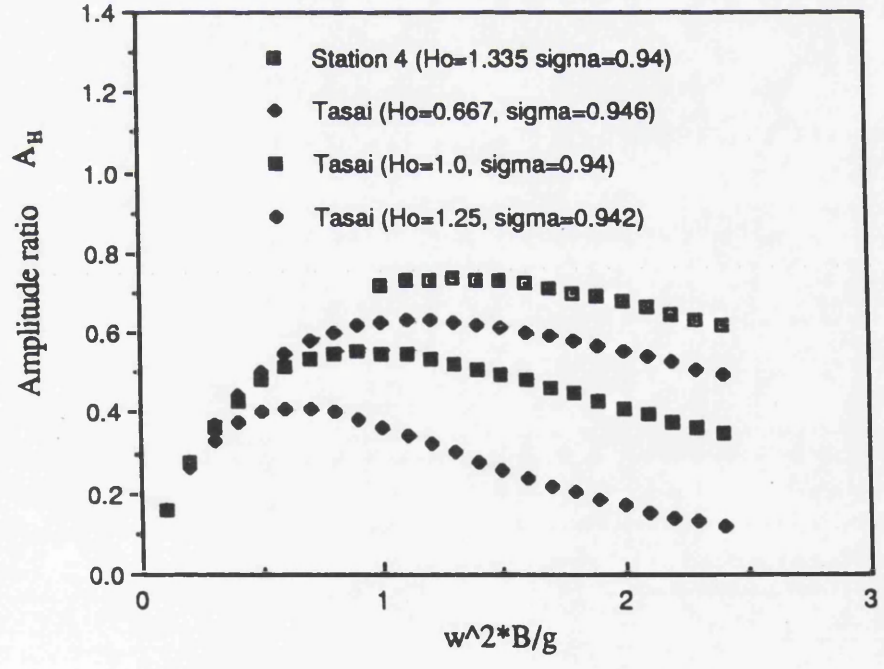

Fig. 2.35 Amplitude ratio for station 4

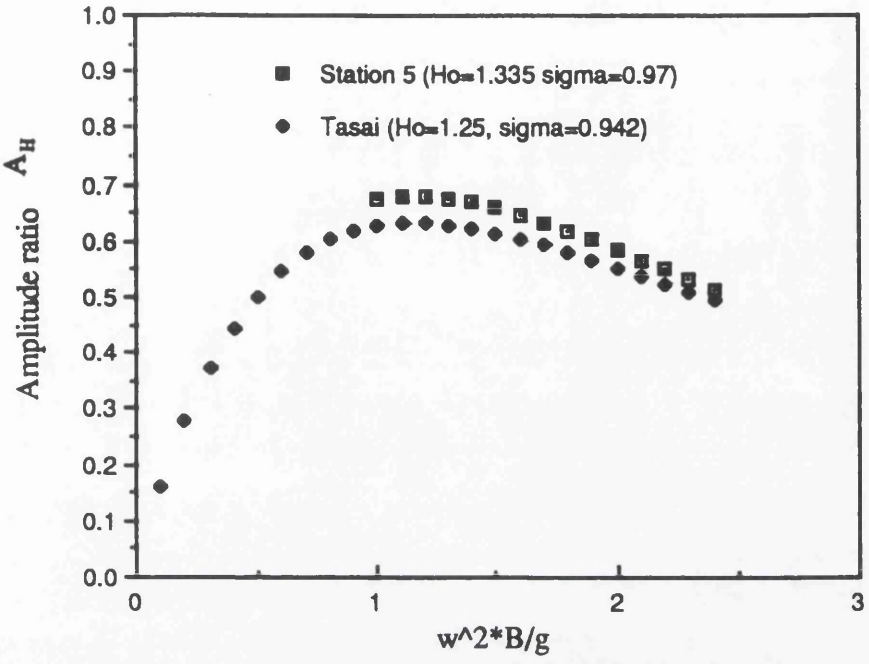

Fig. 2.36 Amplitude ratio for station 5

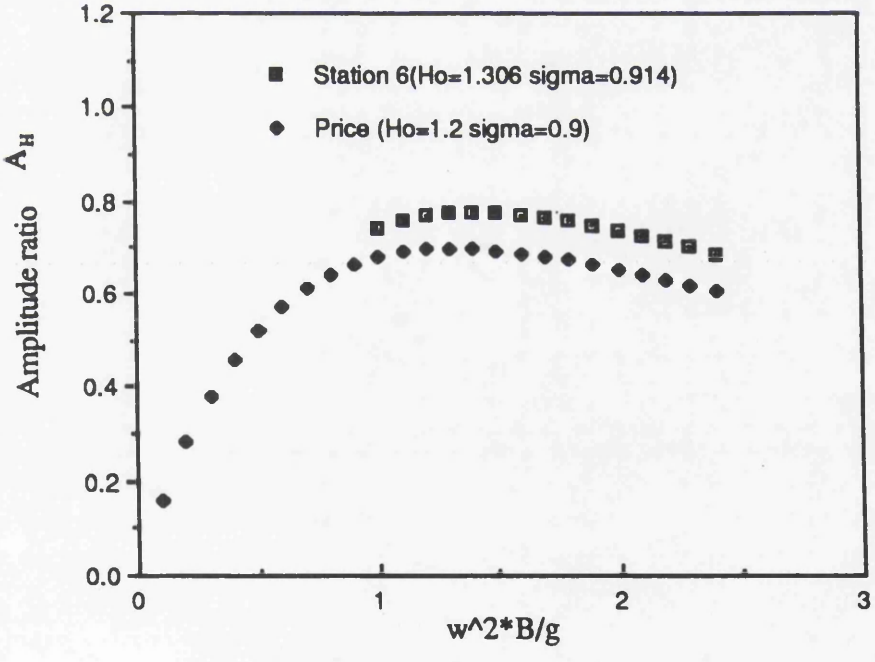

Fig. 2.37 Amplitude ratio for station 6

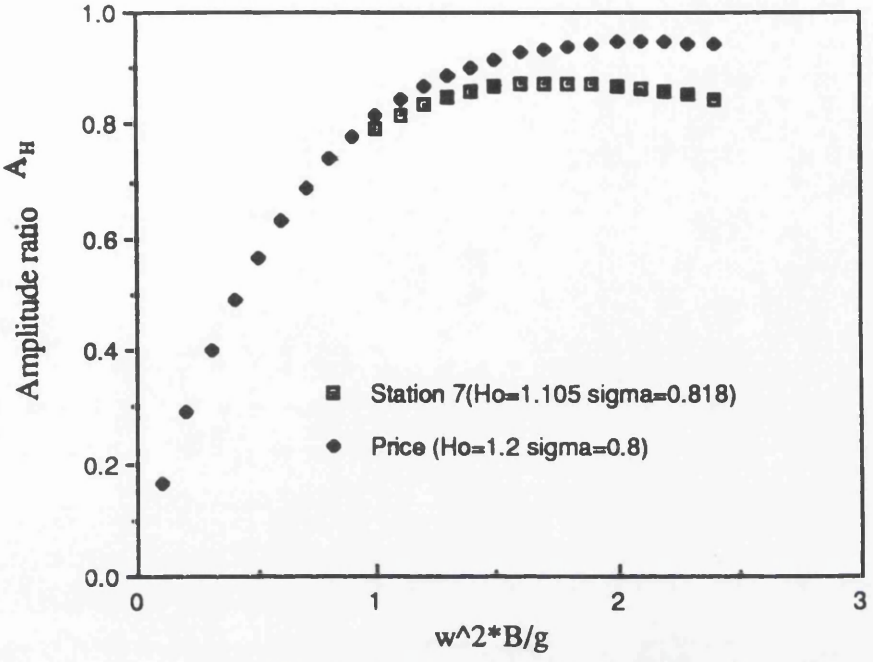

Fig. 2.38 Amplitude ratio for station 7

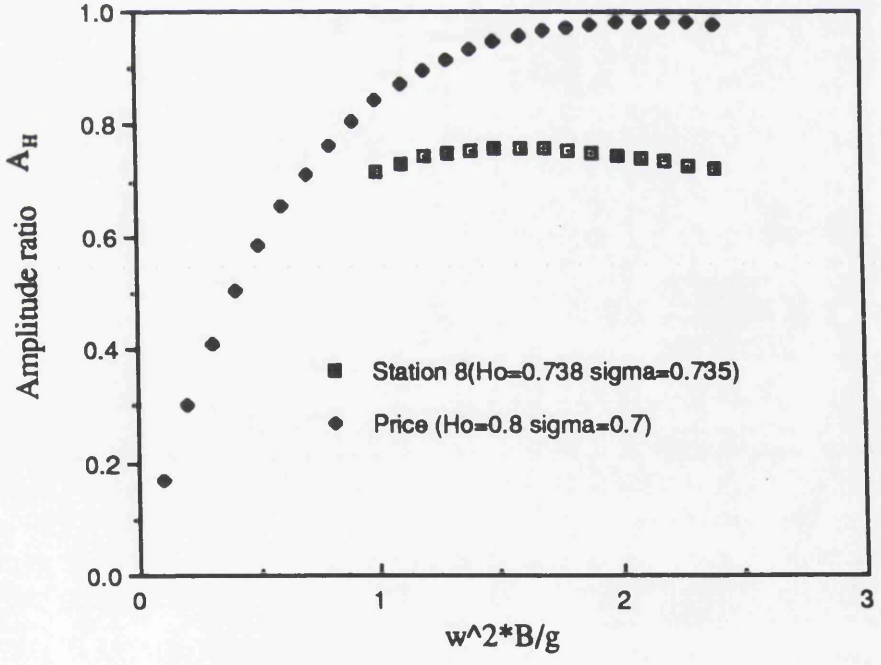

Fig. 2.39 Amplitude ratio for station 8

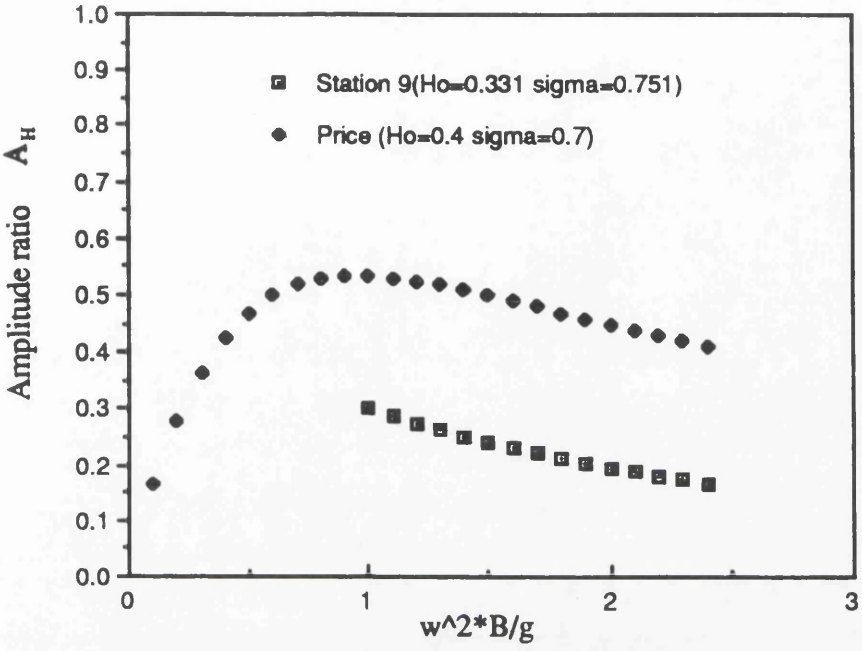

Fig. 2.40 Amplitude ratio for station 9

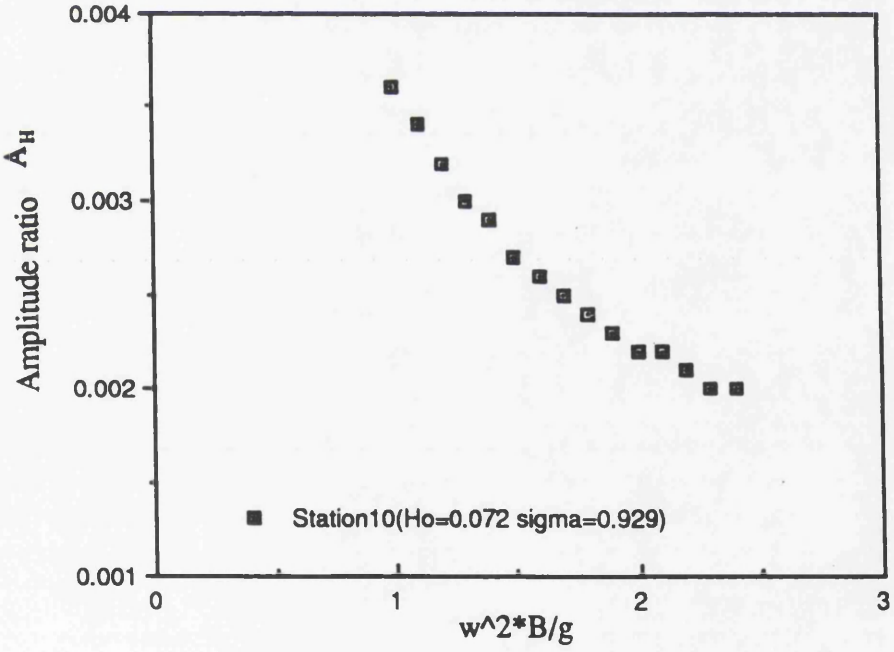

Fig. 2.41 Amplitude ratio for station 10

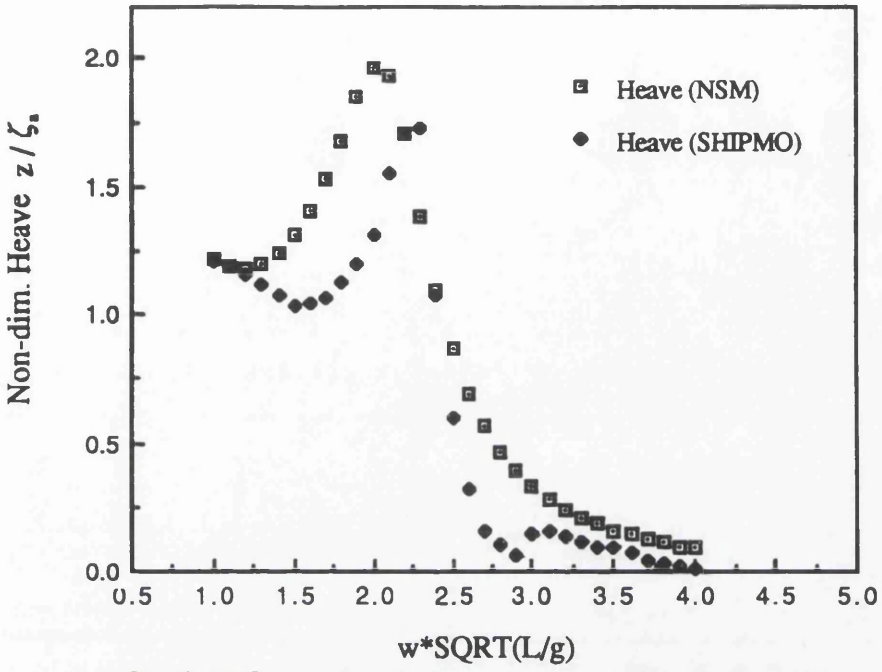

Fig. 2.42 Comparison between heave amplitude obtained from NSM and Ship Motion package for Fr=0.275

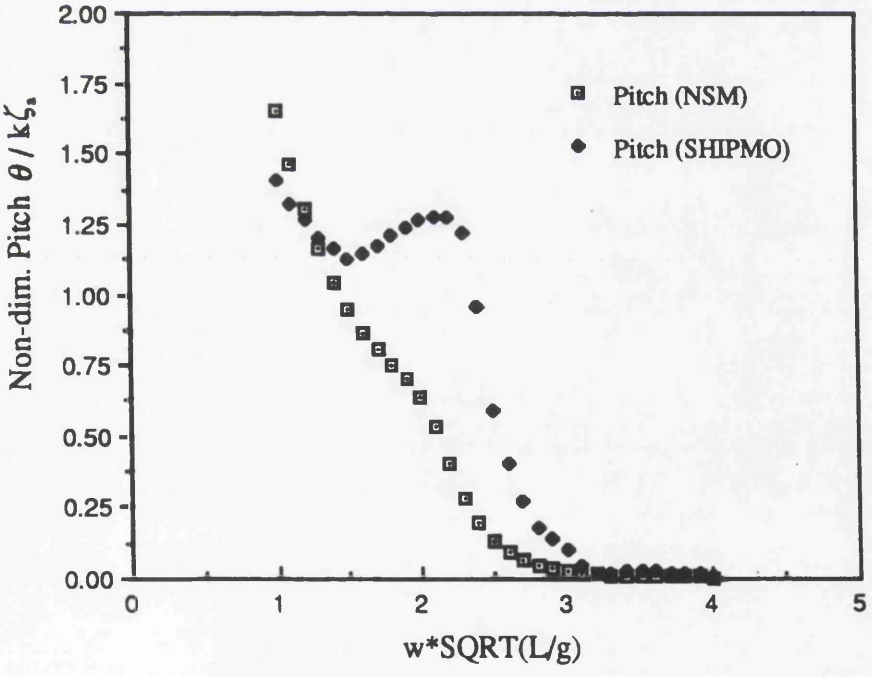

Fig. 2.43 Comparison between pitch amplitude obtained form NSM and Ship Motion package for Fr=0.275

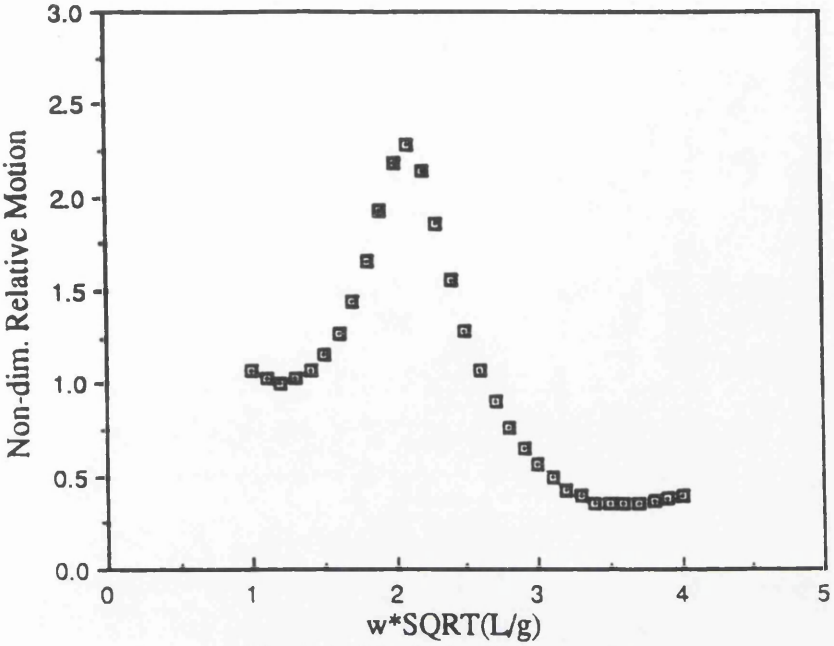

Fig. 2.44 Vertical relative motion
for Fr=0.275 at station 8 1/2

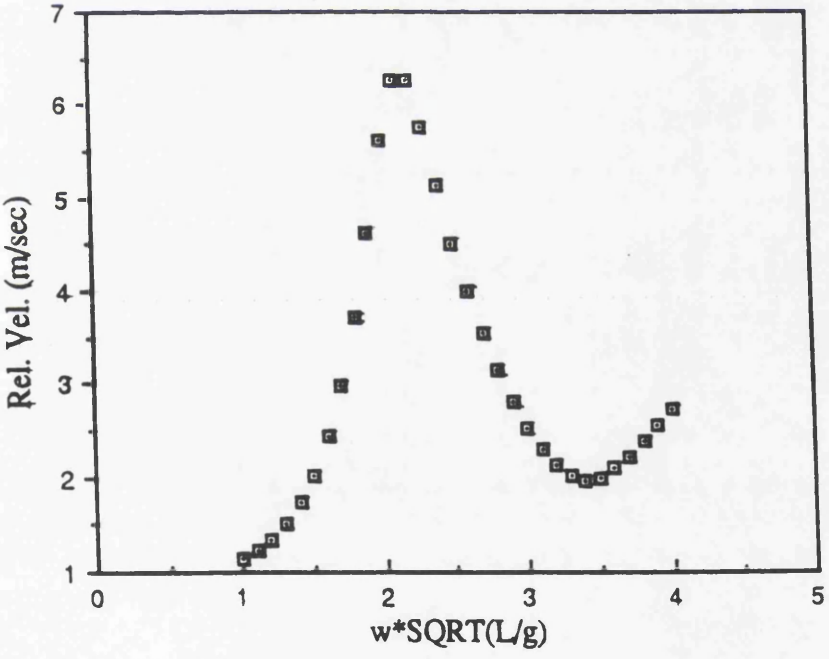

Fig. 2.45 Vertical relative velocity
for Fr=0.275 at station 8 1/2

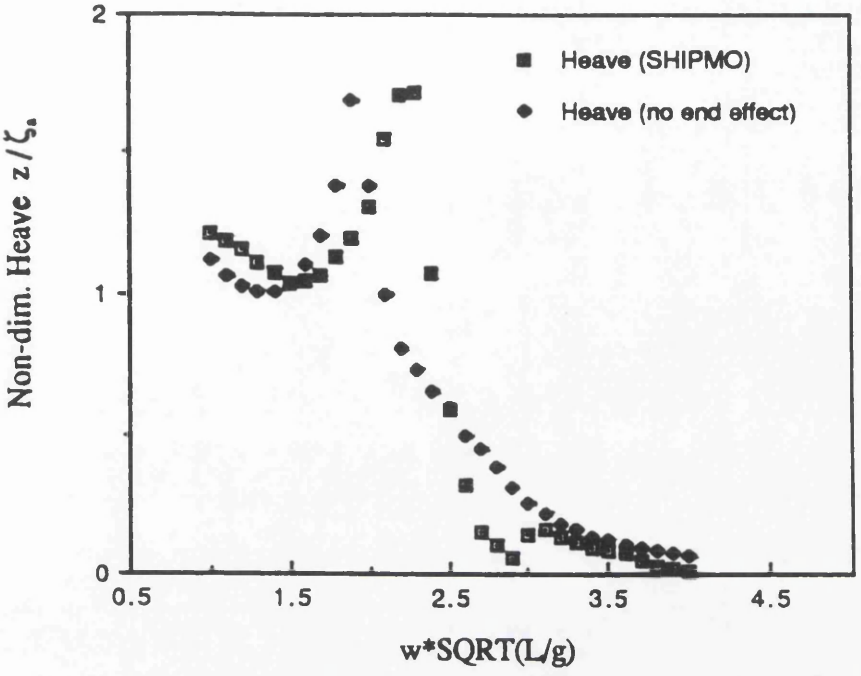

Fig. 2.46 Comparison of heave amplitude obtained by NSM (no end effect) and Ship Motion package for Fr=0.275

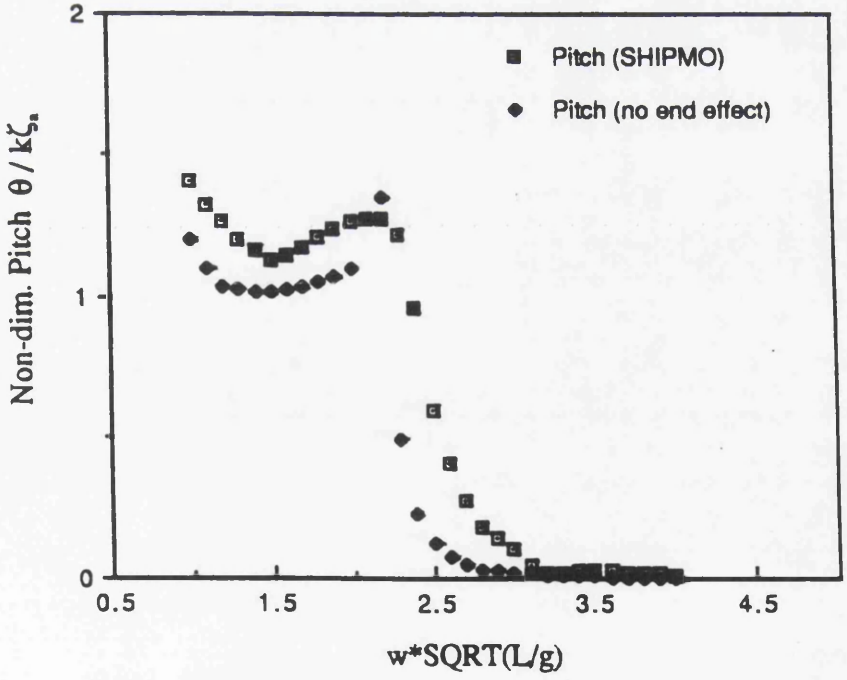

Fig. 2.47 Comparison of pitch amplitude obtained from NSM (no end effect) and Ship Motion package for Fr=0.275

CHAPTER 3

BOTTOM SLAMMING

CHAPTER 3

BOTTOM SLAMMING

3.1 INTRODUCTION

Bottom slamming phenomenon is an event associated with extreme motions of ship in waves. At certain speeds in rough seas the fore-foot of a ship emerges from the water. As the fore-foot re-enters the water surface with a high vertical velocity between ship and local wave profile, a large impact load occurs, it is called impact pressure due to bottom slamming.

Investigation of this repeated dynamic load, caused by bottom slamming, is very important, and is a major problem which fine ships, such as warships and container ships are subjected to, in rough weather, if the forward speed is maintained. The response behaviour of a hull varies according to the type of ship.

The physical understanding of response to a slam is located in the energy absorbed by a local area which can be damaged by the peak pressure of very short duration.

3.2 PREDICTION OF IMPACT PRESSURE DUE TO BOTTOM SLAMMING

Impulse loads with high pressure peaks occur during impact between two bodies; in the case of marine vehicles the impact takes place between the marine vehicle body and the water. Specifically, the phenomenon is known as slamming when the body hits the water surface with a high velocity. The impact pressure due to slamming can be found by two methods, experimentally and theoretically. Theoretically, there are two approaches to predict the magnitude of a given slam. The first approach is called 'Impact Slamming' or 'Wagner' theory, it evaluates the magnitude of a slam at the instant when the hull strikes the wave profile for a short duration and the impact pressure depends on the vertical relative velocity at the instant of re-entry. The second approach is called 'Momentum Slamming' or 'Von Karman' theory; it describes the variation of the pressure after initial entry as the hull penetrates the water. Aertssen (1978) mentioned that this theory is

adequate for description of flare slamming.

It was Von Karman (1929) who first proceeded to calculate the impact pressure (force) by application of the momentum theorem. He derived the impact formula by considering a horizontal cylindrical body with wedge-shaped as it strikes a horizontal surface of water from momentum changes caused by entry of a seaplane into the water, which is a related problem. Details of the calculations are also given by Faltinsen (1990). Bishop et al (1978) concluded that the time history of the transient force is related to the rate of change of momentum of the surrounding fluid and the instantaneous buoyancy, that is to say:

$$F(x,t) = -[\frac{d}{dt}\{m(x,t)\frac{d}{dt}r(x,t)\} - \rho g S(x,t)] \qquad (3.1)$$

where:

$F(x,t)$	:	transient force
$m(x,t)$	:	instantaneous added mass
$r(x,t)$	:	relative motion for a given location at given time
ρ	:	fluid density
g	:	acceleration of gravity
$S(x,t)$	:	instantaneous submerged area of the hull section as it re-enters the water.

As mentioned earlier, Aertssen (1978) suggested that the momentum slamming theory would be more convenient for bow-flare slamming of a medium or fully-loaded ship.

The main difference between bow-flare slamming and bottom slamming is that the first process takes much longer duration than the second one. Bottom slamming, as it is defined earlier, occurs when the emerged ship bottom strikes the water surface, however the process of bow-flare slamming, according to Hwang et al (1983), takes place when the bow-flare submerges in the water. When a ship is going in the water and the wave is going upward, there is a rapid change in momentum of added mass and the bow-flare impact forces can be obtained from the changes in the momentum of added mass.

As defined by Belik et al (1987), a slam produces a continuously varying action on the hull, i.e as the bow re-enters the wave, the slam is described by three different stages which are listed as follows:

- an impact slam at the first instant of contact between body and water surface
- immersion of each slamming section from keel to still water draught allowing for rate of change of fluid momentum
- immersion of a bow section/deck as it plunges and re-emerges from the wave until still water draught is reached and/or the steady state components begin to dominate the fluid action. This involves contributions of fluid momentum and buoyancy.

The first and second points are classified as bottom slamming, but the third one is known as bow-flare slamming.

Belik et al (1979) assumed that the total transient loading during a slam, is the sum of two loadings known as transient impact loading which will be detailed in this chapter and transient momentum loading given in equation (3.1). It was also mentioned that the total loading varies with time and depends on the relative velocity and acceleration as well as the submerged volume of the ship.

3.2.1 Empirical Prediction of Impact Pressure due to Bottom Slamming

For design purposes the main parameter in determining the local scantlings as given by Jones (1976), Fukasawa (1980) and Allen et al (1977) is the maximum pressure arising from bottom slamming. Hence the emphasis is on the prediction of pressure due to bottom slamming and Wagner theory will be used through the investigation.

Slamming pressure can be predicted by semi-empirical formulae. The flow-chart, presented in Fig. 3.1, explains the occurrence of a slam when the vertical relative motion exceeds a certain level. This causes the vertical relative velocity to exceed its threshold value, and this is an indication that bottom slamming is taking place.

A complete prediction of a slamming event is a complex task which is beyond the scope of any existing theory. The sea conditions with associated ship motions and ship hull form are prime factors to be considered for information needed to evaluate slamming

pressure at the initial stage of ship design. However, from a number of experiments slamming pressure is assumed by Ochi (1973) to be proportional to the square of the vertical relative velocity between the hull and wave at the instant of impact. In other words, the pressure is expressed by:

$$p_{max} = KV_r^2 \tag{3.2}$$

or

$$p_{max} = \frac{1}{2}\rho k_1 V_r^2 \tag{3.3}$$

where:

ρ : density of water

K : dimensional constant depending upon section shape

k_1 : nondimensional K-value.

V_r : $\dot{r} = \frac{dr}{dt}$ is the vertical relative velocity obtained from the first derivative of the vertical relative motion with respect to time as it is given in equation (2.98).

Here the nondimensional constant k_1 represents the factor of the ship hull form which can be determined from experimental tests such as model test and drop test or can be obtained from theoretical investigation such as conformal mapping method. Moreover, the vertical relative velocity V_r is result of superposition of ship motions associated with sea conditions.

It is important to note that the vertical relative velocity V_r in equation (3.2) or (3.3) is at the moment of impact. This impact velocity is approximated by the amplitude of the vertical relative velocity and can be obtained by applying the threshold crossing problem. Hamoudi et al (1992 b) mentioned that as the vertical relative velocity is a sinusoidal function and in order to obtain the maximum vertical relative velocity it is appropriate to take the amplitude of the relative velocity for the pressure prediction due to bottom slamming. This is also the reason for the predicted impact pressure to be greater than the measured value.)

Lloyd (1989) described that the amplitude of the vertical relative velocity can be obtained from equation (2.100) by multiplying the vertical relative motion amplitude by the encounter frequency. In the same equation the amplitude of the vertical relative motion can be calculated from theory or measured from model tests.

Stavovy and Chuang (1976) stated that slamming of a ship at high speed results in pressures acting normal to the hull bottom in the slamming area, may be separated into two components:

- The impact pressure due to the normal component to wave surface of the relative velocity between the impact surface and the wave.
- The planing pressure due to tangential component to wave surface of the relative velocity between the impact surface and the wave.

They concluded that the planing pressures obtained from tangential velocities are small and less than one percent when compared with impact pressures.

3.2.2 Pressure Coefficient

As stated in earlier sections, the pressure coefficient k_1 depends on the shape of the bottom of the partial emerged keel of the hull. This constant can be determined by several methods, namely drop tests of two or three-dimensional models, full seakeeping experiments as stated by Chan et al (1992) and also by conformal mapping parameter as stated by Hamoudi et al (1992 b). All these methods show significant variations in the value of k_1. From the majority of the methods presented, the method which is widely used to determine value of this constant is the one determined by Ochi and Motter (1973) and (1971).

3.2.2.1 Conformal Mapping Prediction Technique for Pressure Coefficient

The pressure coefficient or the form coefficient of slamming pressure is one of the important factors to be used for evaluating the impact pressure due to slamming besides the vertical relative velocity. This constant nondimensional factor called k_1 depends on the shape of section's bottom. The value of k_1 is function of the hull section shape only, and particularly for the region below one tenth of the design draught as used by Ochi et al (1971).

From a set of seakeeping tests, it was revealed that the critical portion of the impact process is over when the bottom of the section has submerged to a depth of one tenth of the local draught, and if the bottom section is below or above the base line, the distance between water line and the bottom is substituted by the draught.

Multiple regression analysis is performed by Ochi and Motter (1971) to establish the best regression equation for the form coefficient for slamming pressure on the variables called conformal mapping parameters. At an early stage of ship design, it is convenient to evaluate the pressure coefficient using two or three parameters even if some discrepancies are involved in the evaluation. Furthermore, Ochi and Motter prepared a chart which gives a quick estimation of the pressure coefficient value with reasonable accuracy as in Fig. 3.2. In this figure results are given for three different series of lines together with parameters necessary for evaluation, such as breadth to draught ratio, sectional area at one tenth of the design draught.

3.2.2.2 Three Parameter Pressure Coefficient Prediction Technique

As mentioned earlier, the pressure coefficient k_1 can be determined by the conformal mapping parameter (ship lines) for the bottom portion below one tenth of the design draught. The expression by which the pressure coefficient can be estimated is widely used and is given by Ochi et al (1971) as follows:

$$k_1 = \exp(1.377 + 2.419a_1 - 0.873a_3 + 9.624a_5) \tag{3.4}$$

as said earlier, the conformal mapping parameter a_1, a_3 and a_5 are calculated by using the transformation method by mapping a section of ship to unit semi-circle. These parameters are function of the breadth, draught, sectional area and centre of gravity of the sectional area. The coefficients a_1 and a_3 are given in equation (2.32) and (2.33) respectively and are as follows:

$$a_1 = \frac{H_0 - 1}{2(\frac{M}{d_{1/10}})} - a_5 \tag{3.5}$$

and

$$a_3 = \frac{H_0 + 1}{2(\frac{M}{d_{1/10}})} - 1 \qquad (3.6)$$

The coefficients H_o and $\frac{M}{d_{1/10}}$ are function of breadth, draught and sectional area as it was used by Hamoudi et al (1992 b), whereas the coefficient a_5 is assumed as some value and thereafter determined by iteration. The value of a_5, iterated by a computer program developed for this purpose must satisfy the conditions given in equations (2.35), (2.36) and (2.37). Having found many values by this method and having satisfied the previous conditions, the correct value is the one which satisfies the condition of the centre of gravity given in equation (2.38).

This method can be adopted for any arbitrary section where bottom slamming may occur. Two computer programs were used for this purpose. The first program is Ochi's (1971) which requires as an input data of half breadth at one tenth of the design draught, design draught, eleven offsets read at equal intervals starting on and continuing below one tenth of the design draught, equal spacing between the intervals and half breadth of ship. The second computer program requires the area at one tenth of the design draught, centre of gravity of this area, half breadth and the draught at one tenth of the design draught. This computer program is developed in FORTRAN 77 and consists of the calculation of the area, moment of the area and centre of gravity of the area for the section under consideration. It also iterates the a_5 value and the parameters a_1 and a_3 can be determined by satisfying the conditions listed above. The final step is to calculate the pressure coefficient k_1 for station 8 1/2 of the container ship, using the regression equation.

Table 3.1 gives a comparison of the computed pressure coefficient by two methods and a good agreement can be seen from the results obtained. Comparison of the pressure coefficient values in Table 3.1 with the experimental results published by Kawakami et al (1980) as shown in Fig. 3.9 show good agreement at station 8 1/2.

3.2.2.3 Two Parameter Pressure Coefficient Prediction Technique

The two parameter pressure coefficient prediction technique is used for a quick and simple method for the estimation of the pressure coefficient by Hamoudi et al (1992 a). This method can be used if the input data for a given station lacks in the

information of the centre of gravity of the station under consideration. This is an important parameter to be used in the three parameter prediction technique. The third parameter a_5 explains only 0.63 per cent of the variance according to Hamoudi et al (1992 a). Hence a use of two parameter a_1 and a_3 is required. This method is a useful tool for the initial stage design prediction of slamming pressure, and it is rather convenient to evaluate.

By equating the third parameter a_5 to zero, the equation (3.4) becomes as follows:

$$k_1 = \exp(1.377 + 2.419a_1 - 0.873a_3) \tag{3.7}$$

The two parameter method shows some discrepancies when it is employed as in Table 3.2, and this means that incorporation of the third constant a_5 is important as it has a valuable contribution for the prediction of the slamming pressure.

Table 3.2 represents a value of the pressure coefficient k_1 calculated by two and three parameter. The two parameter method is 24.1% lower than the three parameter method.

3.2.2.4 Deadrise Angle Prediction Technique for Pressure Coefficient

Another method used for the pressure coefficient prediction is the deadrise angle. Lewison (1970 b) predicted an expression to evaluate the value of k_1 by the effective deadrise angle of the bottom of the section. This relationship has been confirmed by number of experiments, and it is given as follows:

$$k_1 = 1 + \frac{\pi^2}{4}\cot^2\beta \tag{3.8}$$

where:

β : deadrise angle.

The form factor of the impact pressure due to bottom slamming estimated using equation (3.8) is likely to be too high if no account is being taken of the effect of the air trapped

between the keel and the water surface during the impact.

In the case when the bottom of the ship is flat and the deadrise angle β is zero, the form factor of the impact pressure is infinitely large and which is not true in practice if equation (3.8) is used. Fig. 3.3 explains clearly the variation of the pressure coefficient with deadrise angle by using the above equation.

From a number of experiments, it has been been realised that the air layer between the body and the water surface plays an important role in determining the peak pressure which occurs during flat impact. More investigations conducted by Chuang (1966) and Lewison (1968) have shown that air escape from under the flat bottom is not complete and therefore a large bubble provides a cushion to the impact.

From a set of drop tests on slamming of wedge-shaped rigid bodies, Chuang (1967) obtained a linear relationship between deadrise angle and pressure due impact, these relationships are summarised here as follows:

1. For flat bottom at keel and away from keel:

$$p_{max} = 4.5V_o \tag{3.9}$$

2. Deadrise angle β =1 degree

a) at keel:

$$p_{keel} = 3.15V_o^{1.4} \tag{3.10}$$

b) away from keel

$$p_{max} = 3.15V^{1.4} \tag{3.11}$$

3. Deadrise angle β =3 degree

a) at keel:

$$p_{keel} = 1.04V_o^{1.6} \tag{3.12}$$

b) away from keel:

$$p_{max} = 4.11V^{1.6}$$

4. Deadrise angle β =6 degree

a) at keel:

$$p_{keel} = \frac{1}{2}\rho V^2 \frac{\pi}{\beta} \tag{3.13}$$

b) away from keel:

$$p_{max} = 0.87V^2 \tag{3.14}$$

5. Deadrise angle β =10 degree

a) at keel:

$$p_{keel} = \frac{1}{2}\rho V^2 \frac{\pi}{\beta} \tag{3.15}$$

b) away from keel:

$$p_{max} = 0.42V^2 \tag{3.16}$$

6. Deadrise angle β =15 degree

a) at keel:

$$p_{keel} = \frac{1}{2}\rho V^2 \frac{\pi}{\beta} \tag{3.17}$$

b) away from keel:

$$p_{max} = 0.24V^2 \tag{3.18}$$

7. Deadrise angle β =18 degree and above

a) at keel:

$$p_{keel} = \frac{1}{2}\rho V^2 \frac{\pi}{\beta} \tag{3.19}$$

b) away from keel

$$p_{max} = \frac{1}{2}\rho V^2 [1 + \frac{\pi^2}{4\beta^2}] \tag{3.20}$$

where:

V_o : impact velocity at instant of impact [fps]
V : impact velocity at time 't' [fps]
p_{keel} : impact pressure at keel [psi]
p_{max} : maximum impact pressure [psi]
ρ : mass density of fluid [lb-sec^2/ft^4].

in equations (3.13), (3.15), (3.17), (3.19) and (3.20) the deadrise angle β is in radians. For sea water slamming problem, a correction factor which is the ratio of the mass density of sea water to the one of fresh water is taken. V_o in the above equation is used to calculate the maximum pressure at the instant of impact, and V is used for the impact at any time 't'.

3.2.2.5 Impact Angle Prediction Technique for Pressure Coefficient

The pressure coefficient k_1 is also approximated, using the impact angle called ξ. This angle is called effective impact angle on a plane normal to wave surface and impact surface on hull bottom measured from wave surface to impact surface of hull bottom as explained by Stavovy and Chuang (1976). The relationship between the pressure coefficient and different impact angle is presented by Chuang (1967) and modified Stavovy and Chuang (1976) and Chuang (1973), as:

1. For $0 \le \xi < 2.2$ degrees :

$$k_1 = 0.37\xi / 2.2 + 0.5 \tag{3.21}$$

2. For $2.2 \le \xi < 11$ degrees:

$$k_1 = 2.1820894 - 0.9451815\xi + 0.2037541\xi^2 - 0.0233896\xi^3 + 0.0013578\xi^4 - 0.00003132\xi^5 \tag{3.22}$$

3. For $11 \le \xi < 20$ degrees:

$$k_1 = 4.748742 - 1.3450284\xi + 0.1576516\xi^2 - 0.0092976\xi^3 + 0.0002735\xi^4 - 0.0000319864\xi^5 \tag{3.23}$$

4. For $20\,\text{degree} \le \xi$:

$$k_1 = (1 + 2.4674 / \tan^2 \xi) 0.76856471 / 288 \tag{3.24.a}$$

Equation (3.24.a) has been modified slightly by Umeda et al (1993) and is rewritten as:

$$k_1 = (1 + 2.4674 / \tan^2 \xi) \cos^4 \xi / 288 \tag{3.24.b}$$

the impact angle takes the form :

$$\tan \xi = \cos\beta_{eh} \tan(\tau + \alpha - \theta_w) + \sin\beta_{eh} \tan\beta_{ev} \tag{3.25}$$

where:

α : Buttock angle

β_{eh} : Angle on wave surface measured from forward longitudinal direction to the plane normal to wave surface and impact surface on hull bottom at a considered point

β_{ev} : Angle on transverse plane normal to wave surface and measured from impact surface on hull bottom to wave surface

θ_w : Wave slope

τ : Trim angle.

the angle β_{eh} and β_{ev} can be calculated by the following equations:

$$\tan\beta_{eh} = \frac{\tan\beta}{\sin(\tau-\theta_w)+\tan\alpha\cos(\tau-\theta_w)} \tag{3.26}$$

$$\tan\beta_{ev} = \frac{\tan\beta}{\cos(\tau-\theta_w)-\tan\alpha\sin(\tau-\theta_w)} \tag{3.27}$$

where:

β : deadrise angle.

θ_w the wave slope can be calculated by multiplying the wave amplitude by the wave number, that is to say:

$$\theta_w(t) = \zeta_a k\sin(kx+\omega_e t) \tag{3.28}$$

where:

ζ_a : wave amplitude
k : wave number
x : longitudinal location of station considered from centre of gravity
ω_e : frequency of encounter.

3.2.2.6 Pressure Coefficient Prediction Technique Employing Breadth and Draught

Prediction of pressure coefficient using breadth and draught at one tenth of the design draught is simple and a straight method which does not require any complications, as according to Kawakami et al (1980) the mapping coefficient can be generally expressed as a_1 equals to 10 a_3 and 20 times a_5. Hence the main influencing parameter can be said to be the coefficient a_1. Kawakami et al (1980) obtained an estimation of slamming impact pressure coefficient by using only the breadth and the draught at one tenth of the design draught. This method is used by Hamoudi et al (1993) and takes the following form:

$$k_1 = \exp(1.26 + 3.375\gamma) \tag{3.29}$$

where:

$$\gamma = \frac{\frac{b_{1/10}}{d_{1/10}} - 1}{\frac{b_{1/10}}{d_{1/10}} + 1} \tag{3.30}$$

where:

$b_{1/10}$: breadth at one tenth of the design draught
$d_{1/10}$: draught at one tenth of the design draught.

'$b_{1/10}$' and '$d_{1/10}$' are presented in Fig. 3.4 showing a bottom of a section at one tenth of the design draught.

The nondimensional coefficient k_1 in equation (3.29) increases if the section's bottom is flat and vice versa. Fig. 3.5 shows variation of the pressure coefficient along the fore region of the S175 container ship. The method given above is in good agreement with the three parameter prediction technique given by Ochi in equation (3.4).

3.2.2.7 Experimental Prediction Technique for Pressure Coefficient

The pressure coefficient k_1 depends mainly on the bottom portion of the ship section as mentioned earlier, starting and continuing below one tenth of the design draught (the design draught taken from the loaded water line to the bottom of the section, because for some sections the bottom is above or below the base line). The constant k_1 can be obtained from seakeeping tests by measuring the pressure and the amplitude of the relative velocity at the instant of impact, obtained from the measured relative motion. From the following equation the pressure coefficient can be calculated as:

$$k_1 = \frac{p_{max}}{\frac{1}{2}\rho V_r^2} \tag{3.31}$$

where:

p_{max} : the maximum impact pressure
V_r : vertical relative velocity
ρ : mass density of fluid.

It is convenient to average the value of the pressure coefficient if it is obtained from seakeeping tests in order to minimise the error accumulated from the experiment and the nonlinearities, such as air cushioning.

3.2.3 Distribution of Slamming Pressure over the Section's Bottom

Bishop et al (1978) assumed that the pressure due to bottom slamming varies over the girth of the section at one tenth of the design draught. This pressure is zero at one tenth of the design draught and is a maximum at the keel. Fig. 3.6 shows the distribution of the slamming pressure over the region of one tenth of the design draught. This means at and above the region of one tenth there is no pressure due to slamming, and there is only the so-called dynamic pressure. This statement requires more investigation by placing a number of pressure transducers over the girth at equal intervals and to carry out a seakeeping test for validation purposes. The distribution of the slamming pressure is given by the following equation:

$$p(\theta_m) = p_{max}\left(\frac{y(\theta_m)}{d_{1/10}}\right) \tag{3.32}$$

where:

$d_{1/10}$: one tenth of the design draught
$p(\theta_m)$: distribution of the pressure over the girth
p_{max} : measured or calculated slamming pressure at the keel
$y(\theta_m)$: y coordinate for conformal mapping
θ_m : conformal mapping angle

From the values in Fig. 3.6, obtained from equation (3.32) one may conclude that the distribution of slamming pressure is uniform. In reality there are also other variations that take place during impact, such as cushioning of air between the body and water surface, shape of the bottom section and interference rolling motion, when slamming is imminent.

3.2.4 The Entrapped Air Between Body and Wave Surface during Impact

As mentioned in the 9th International Ship Structure Congress (1985), the phenomenon of air trapped between a body and wave surface is a well known problem in the field of slamming. This is a major factor from the point of view of impact of flat with low deadrise bottoms. In most of the research carried out in the past by various researchers, the effect of the presence of air was ignored. Chuang (1965) took high speed motion pictures of his experiment and his photographs indicate what is apparently air trapped in the top of water below the falling body just after contact between water and body takes place. In another investigation by Chuang (1967), an electronic detection method was used in an experimental attempt to detect the air trapped between a falling impact surface of a flat bottom model and the water surface. It was concluded that at the instant of impact of a flat bottom and 1 degree wedge trap a considerable amount of air between the falling body and the water surface.

This brings the matter to the effect of deadrise angle in connection with the trapped air. As said earlier, the impact pressure becomes very large for small deadrise angles according to equation (3.8) for the pressure coefficient prediction. Chuang observed (1970) in his experimental investigation that most of the air has not been trapped at the instant of impact with a deadrise angle of 3 degrees and higher. The trapped air phenomenon can be described as unstable with respect to the bottom shape (deadrise angle) and time duration. He concluded that during the impact of a wedge with deadrise angle of 3 degrees or greater, most of the air is pushed aside by the wedge before the keel pierces the water surface.

Sellars (1976) concluded from his work that restricting air flow to two rather than three dimensional condition reduces value of peak impact pressure and the pressure reduction is greater for larger model.

Actually, the air bubbles in the water lead to reductions in pressures during the impact, therefore one may conclude that the existing air between the hull and the water surface plays a role of an amortisseur which reduces the severity of the peak pressure. Furthermore, Lewison (1970 a) investigated in a set of experiments the reduction of slamming pressure by reinforcing (ejecting) artificial air when slamming is imminent or preventing the air which already exists from escaping by mean of flanges. Air ejection reduced impact pressure by three times as given in Fig. 3.7. Hamoudi et al (1992 b)

stated that this operation is costly to install in the ship. Equipment for injecting artificial air in the bottom of ship needs an accurate technique for its use, moreover the flanges increase the resistance.

Sellars (1976) stated in his investigation that air entrapment is one of the phenomena not included in the scaling laws and may cause errors when extrapolating model results of initial impact pressure to full scale. The reason proposed for such an effect is that, since air escape is controlled by the speed of sound in air and this speed is the same in model and ship scale, air entrapment will not scale. One may conclude from this statement that the trapped air is expected to play an important role and that model experiments will tend to overestimate impact pressure.

3.2.5 Threshold Velocity

The definition of threshold is the crossing phase for a certain state to change to another/different state. In this context, threshold velocity can be defined as the value beyond which slamming occurs and prediction of impact pressures due to bottom slamming can be made. In other words it is the magnitude of vertical relative velocity required for slamming impact to take place.

The phenomenon of slamming is associated with two conditions, according to Price et al (1974), which can be listed as follows:

- the bow emerges
- a certain magnitude of the relative velocity between ship and wave measured at bow, called threshold velocity, is exceeded.

these two conditions are sufficient for slamming to occur, therefore not every bow emergence leads to slamming occurrence.

The magnitude of the threshold velocity was examined for five models having different hull forms by Ochi (1964), and the results showed that the magnitude is nearly constant for all form; this magnitude was evaluated by 12 fps (3.65 m/sec) for a 520 ft vessel. Threshold velocity obtained empirically, as in equation (2.97) in chapter 2, obeys Froude scaling and is given as:

$$V_{cr} = 0.093\sqrt{gL} \qquad (3.33)$$

where:

V_{cr} : threshold velocity (critical velocity)
g : acceleration of gravity
L : length of ship

Fig. 3.8 shows the threshold velocity predicted by Ochi (1973), Tasai and Ferdinande. According to Wilson (1992), the value of threshold velocity is still under discussion as no physical explanation has yet been established. The problem with threshold velocity can be fully explained by carrying out well designed experiments.

3.2.6 Vertical Acceleration

The relevance of vertical acceleration was considered to be important in describing the severity of slamming phenomenon. Lewison (1970 b) reported that the slamming event is observed when the vertical acceleration was of the order of 8.8 m/sec^2 (double amplitude) for the cargo ships 'Lukuga' and 'Jordaens'. Aertssen (1969) proposed that events causing the double amplitude, of the deceleration of the bow of the order of 8.8 m/sec^2 should be called slams.

However, in the case of slamming occurring with bow emergence the relative vertical velocity is important. When this exceeds a threshold value, slamming occurrs and the pressures arising are proportional to vertical relative velocity. The vertical acceleration has only a minor influence in this event.

3.3 CONCLUSIONS

Prediction of pressure due to bottom slamming is detailed and bottom slamming is investigated by using the impact theory (Wagner theory).

The pressure due to bottom slamming is proportional to the square of the vertical relative velocity and the constant of proportionality is obtained from the pressure coefficient or factor of ship hull which depends mainly on the shape of the bottom portion of the section under consideration.

Pressure coefficient is investigated in this chapter and can be determined by several methods, such as conformal mapping parameter (two or three parameter prediction techniques), deadrise angle, impact angle, breadth and draught (at one tenth of the design draught) prediction technique and experimental method. Comparison of the predicted coefficient by different methods is given here and good correlation is found between these methods. For example the pressure coefficient predicted by the three parameter technique using an iteration program is 15.1 for station 8 1/2 for the S175 container ship and 15.35 using Ochi's (1971) prediction technique. The method for predicting the pressure coefficient by two parameter does not fully agree with that of the three parameter, but it gives reliable results and for the same station the pressure coefficient is found to be 11.46. Though various methods have been discussed in this chapter on the pressure coefficient, emphasis has been placed on obtaining the pressure coefficient by conformal mapping and breadth and draught formulae. Depending on the amount of input data available one may need to adopt either of these methods. The accuracy however varies, as for the case of two parameter conformal mapping technique the variation is 24% when compared with the three parameter mapping technique. There is also good agreement with the experimental pressure coefficient at station 8 1/2 obtained by Kawakami et al (1980).

There are hardly any papers which give a detailed procedure for calculating the third parameter a_5 as even Kawakami et al (1980) used the relation that a_1 equals 10 times a_3 and a_1 also equals 20 times a_5 for his calculation of slamming pressure coefficient. The present prediction technique which incorporates the third parameter a_5 due to additional information of the centre of gravity of the station under consideration will benefit designers to obtain similar pressure coefficient without having to make approximations.

Distribution of the pressure due bottom slamming over the girth is given, it is maximum at the centre of the girth and zero at one tenth of the design draught. Hence if the maximum impact pressure is obtained through experiments or calculations, the distribution can be obtained. This distribution will be explained in the next chapter.

Also one may conclude that the trapped air is expected to play an important role in reducing the pressure due bottom slamming. But air entrapment is not included in the scaling laws and may cause errors when extrapolating model results of initial impact

pressure to full scale.

The meaning of the threshold velocity is still vague as not enough investigations have been carried out to interpret its physical meaning. Hence a wide use of Ochi's (1964) postulation for the threshold velocity is employed.

Table 3.1 Comparison of pressure coefficient using iteration program and Ochi's program

	Iteration program	Ochi's program
Pressure coefficient	15.1	15.35

Table 3.2 Comparison of pressure coefficient using two and three parameter prediction

	Two parameter	Iteration program
Pressure coefficient	11.46	15.1

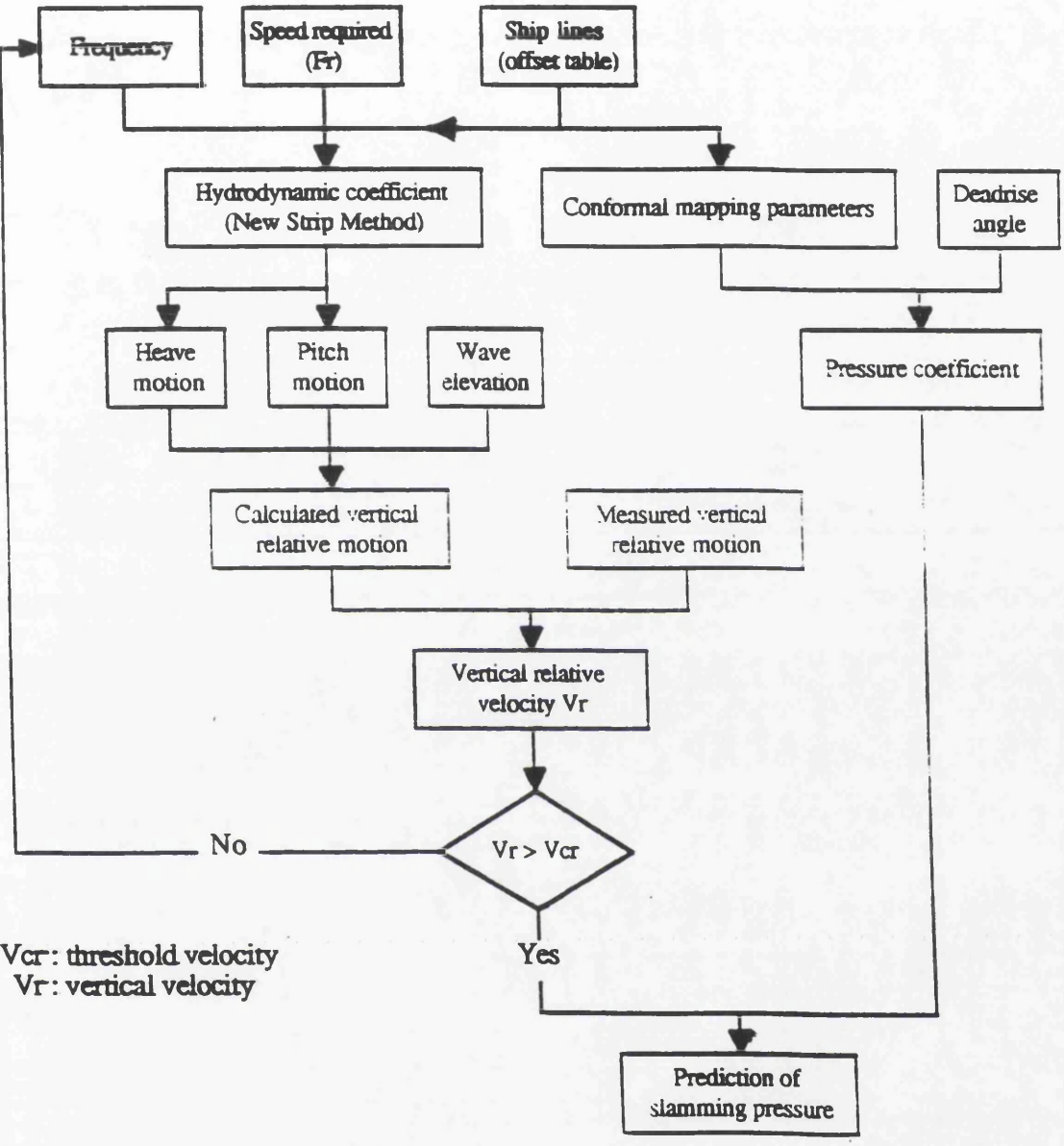

Fig. 3.1 Flow-chart : Slamming pressure prediction

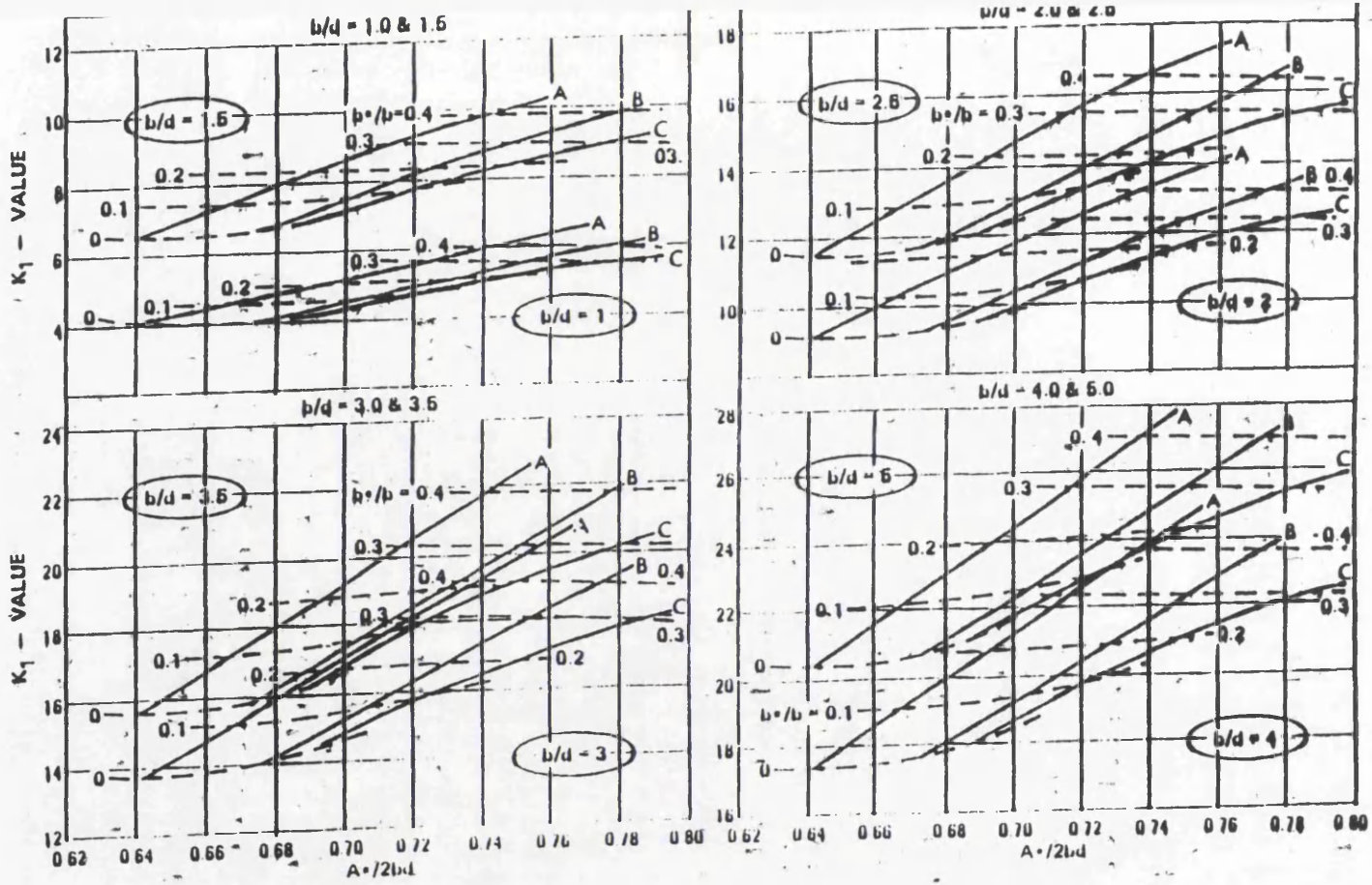

Fig. 3.2 Estimation chart of K_1-value by Ochi et al (1973)

A, B and C are three series of lines

A* is the sectional area below 1/10 of design draught

b/d is the ratio between half width and draught at 1/10 of design draught

b* is the width of flat bottom

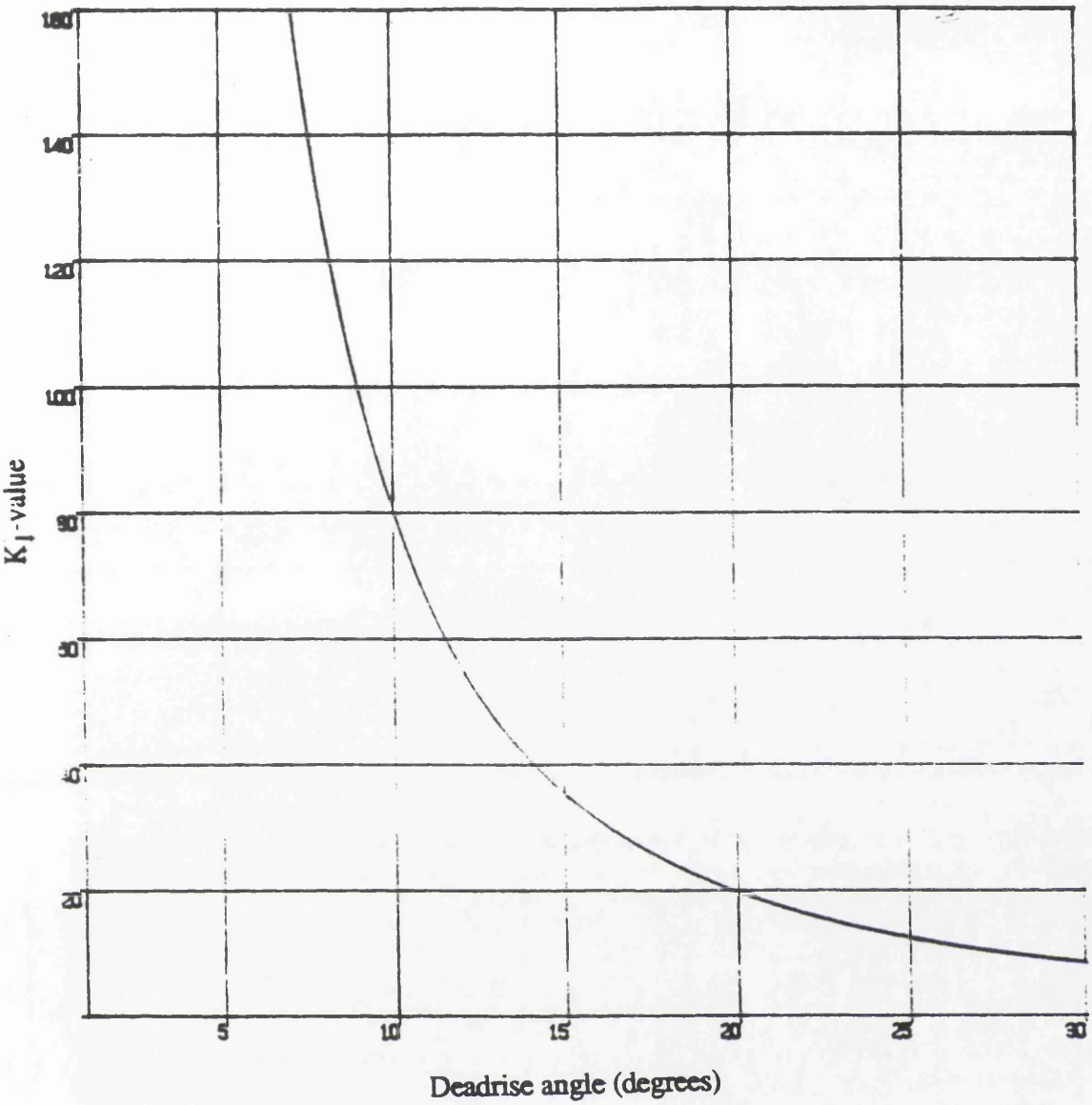

Fig. 3.3 Pressure coefficient function of the deadrise angle

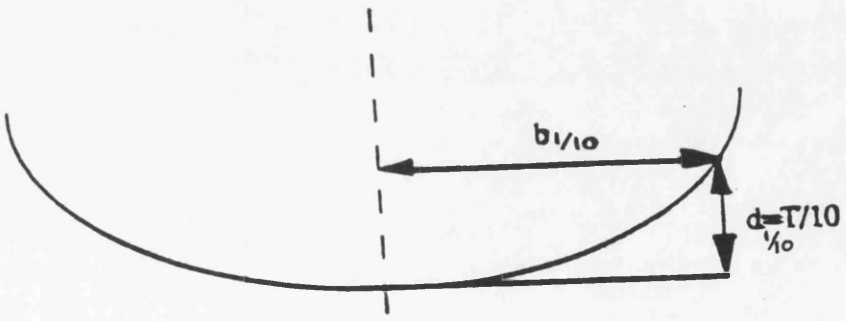

Fig. 3.4 Example of a section at one tenth of the design draught

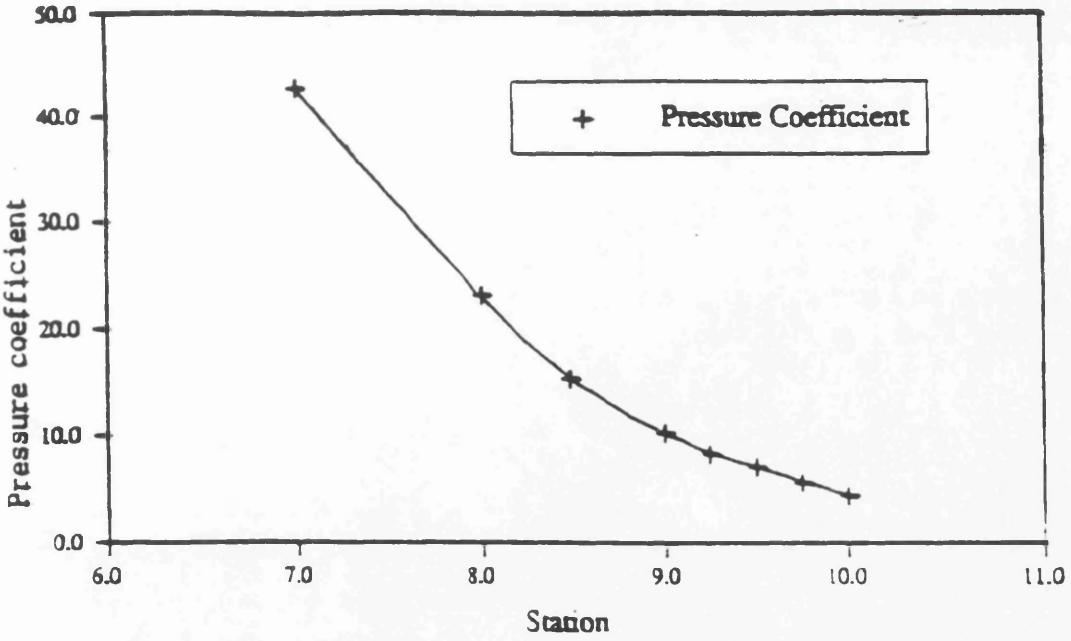

Fig. 3.5 Variation of the pressure coefficient along the fore part

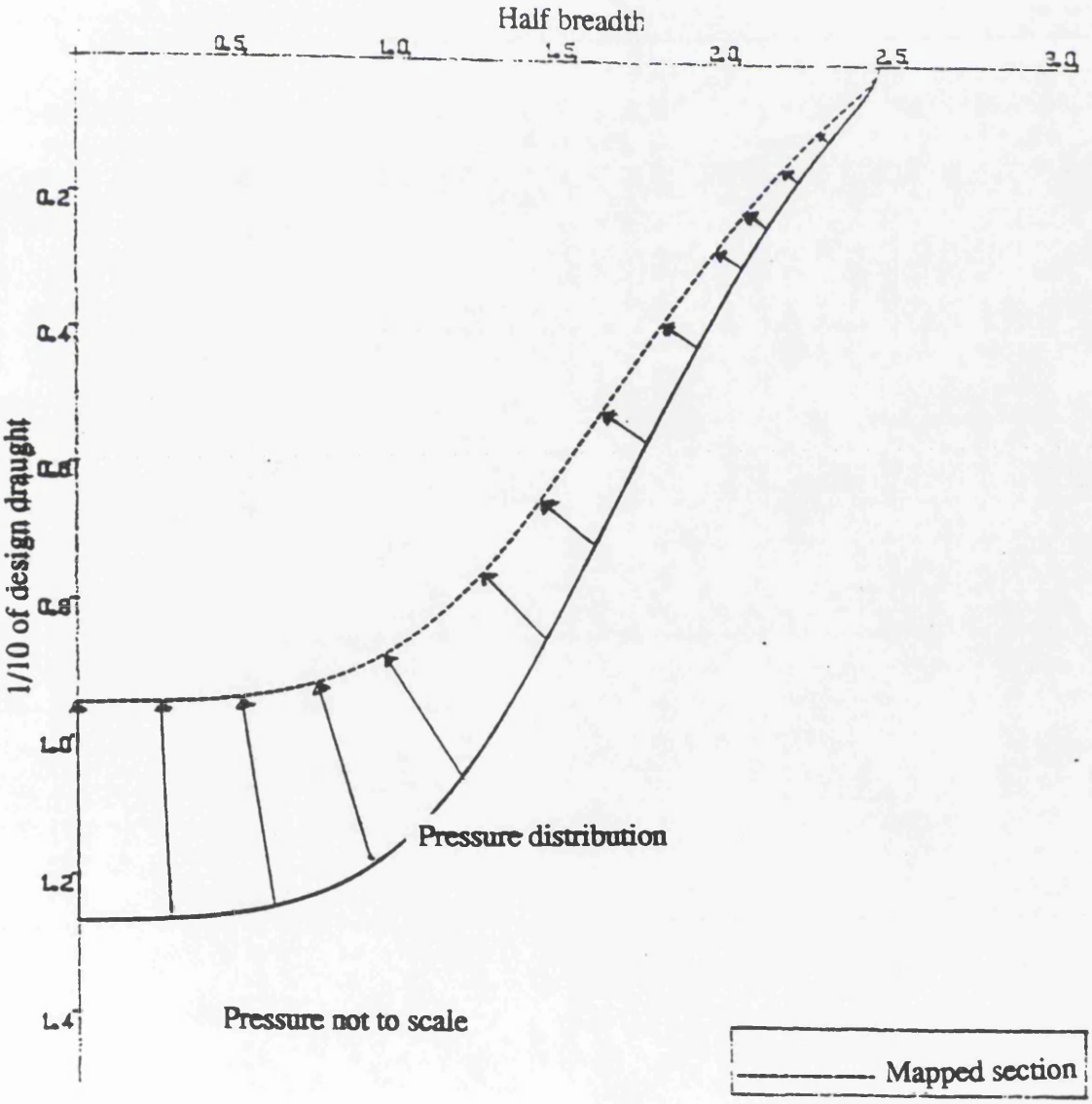

Fig. 3.6 Distribution of slamming pressure over the section's bottom

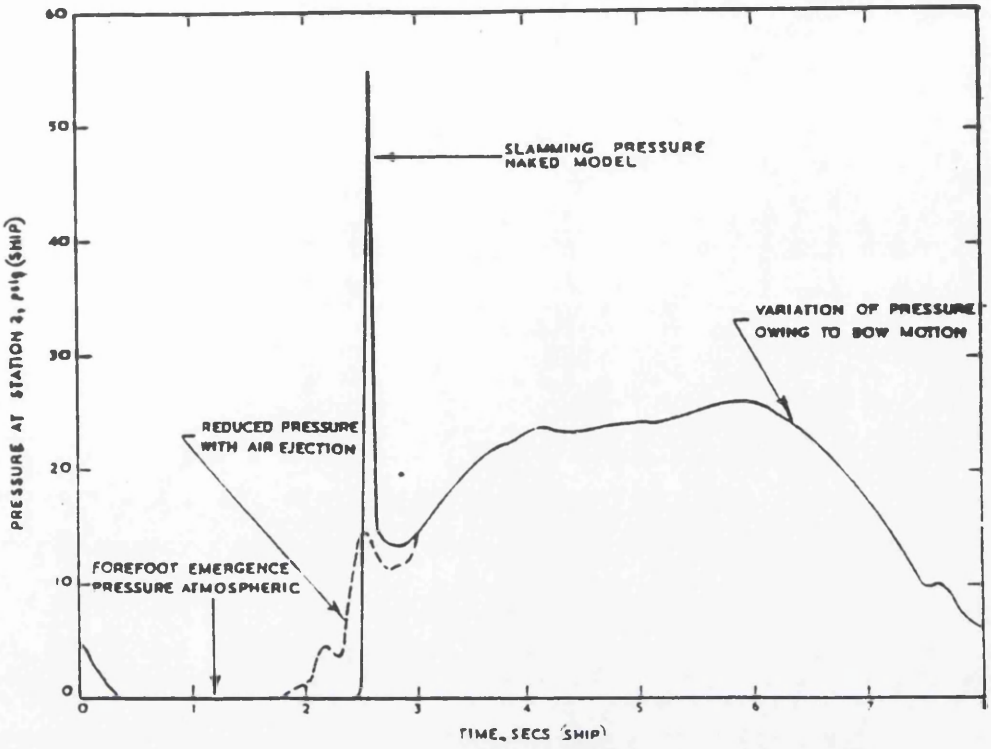

Fig. 3.7 Reduction of slamming pressure with air ejection from Lewison (1970)

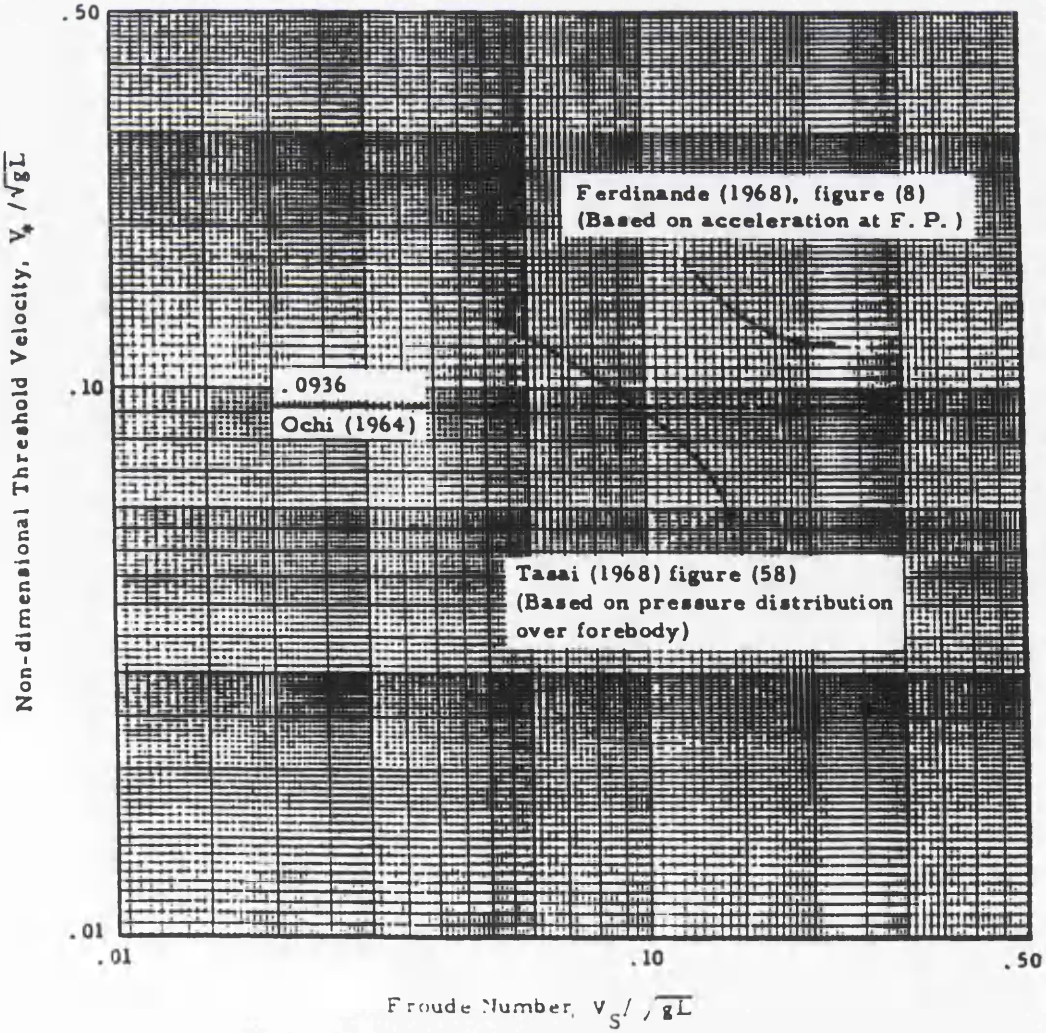

Fig. 3.8 Experimental values of threshold velocity for ship slamming from Ochi et al (1973)

	Experiment	Ochi's Method	Present Method
Container Ship	—o—	—— · ——	X
General Cargo	—△—	—— ·· ——	not investigated
Ore Carrier	—□—	··· —— —	not investigated

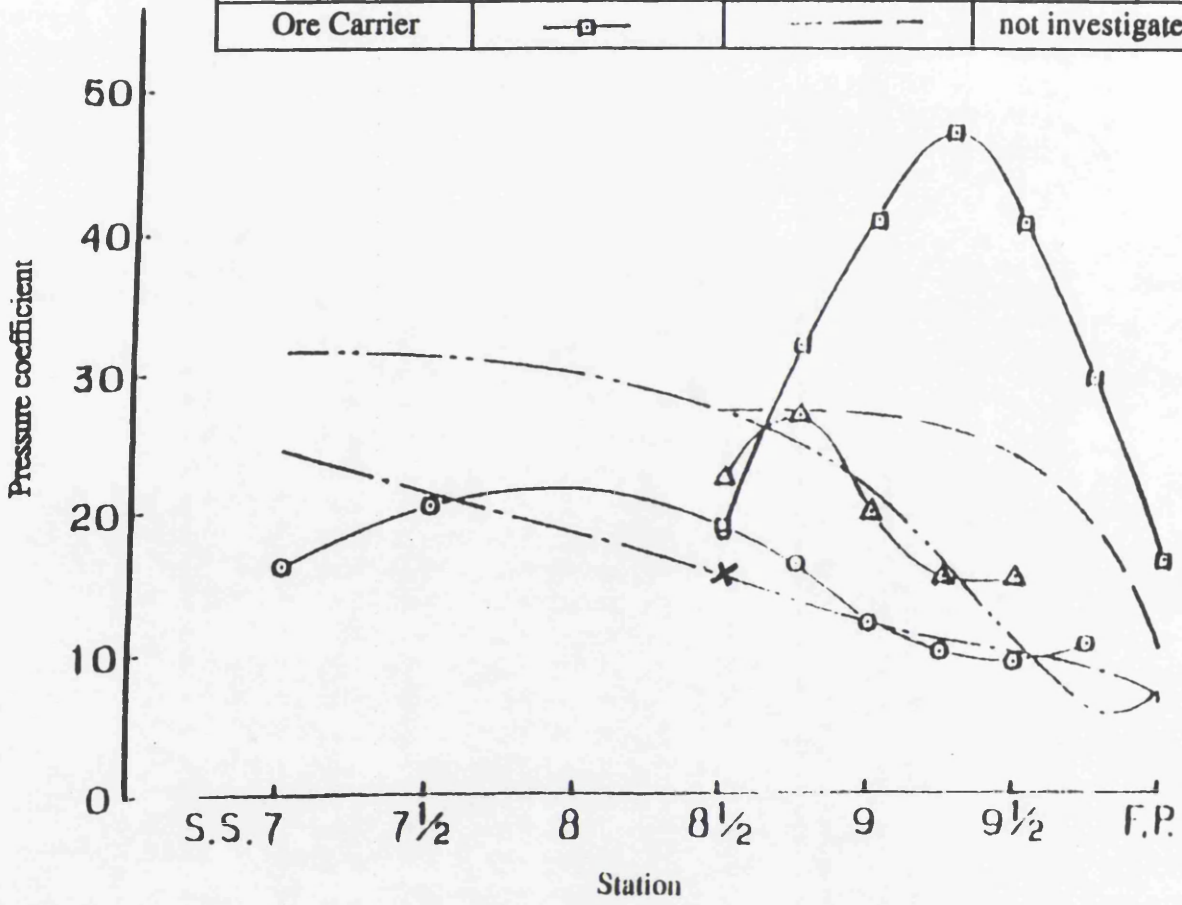

Fig. 3.9 Pressure coefficient for container ship, ore carrier and general cargo by Kawakami et al (1980)

CHAPTER 4

EXPERIMENT ANALYSIS OF BOTTOM SLAMMING

CHAPTER 4

EXPERIMENTAL ANALYSIS OF BOTTOM SLAMMING

4.1 INTRODUCTION

Experimental investigation is a verification of the effectiveness of the theoretical prediction. Faulkner (1994) mentioned in his public lecture, any behaviour can be understood and clarified through this process.

In some cases there are discrepancies between theoretical and experimental results and which are due to the assumptions incorporated in the theoretical method and also due to the nonlinearities which are not included in the modelling.

In order to investigate a semi-theoretical approach on bottom slamming using the impact theory, experiments were conducted on a monohull container ship model S175.

4.2 CHOICE OF MODEL

As introduced earlier, bottom slamming is a major problem which fine ship forms, such as container ships and warships, are subjected to, in rough weather if the forward speed is maintained. The response of the hull to a repeated dynamic load caused by bottom slamming varies according to the type of the ship.

Nakamura (1980) mentioned that the main characteristics of a container ship are high speed and large size. For these two important reasons the container ship S175 has been chosen for experimental investigation of bottom slamming as it is most likely to occur at high speed and in rough weather. Investigation on this type of ship is recommended by the seakeeping committee of the International Towing tank Conference (1978). A comparative study has been made for this ship for ship motion and loads between different towing tanks.

Full details of the hull form and the specification of the ship are given from Murdey's paper (1978). Table 4.1 presents principal particulars of the S175 container ship, Table 4.2 gives the parameters of the sections and Table 4.3 shows the offset table

of the hull.

Over a period of years, container ships have been subjected to a number of investigations carried out by many researchers in the field, including towing tank model experiments, structural model tests and finite element analysis. For example, on the structural side, Elbatouti et al (1976) performed a finite element static analysis of a model of container ship and compared it with test results. Stiansen et al (1979) also presented their results on an extensive correlation study for the SL-7 container ship in which the total structural responses due to hull girder and local loads measured at sea were compared with analytically predicted values.

In the classic paper of Boylston et al (1974) description of the performance of SL-7 container ships in the combined fields of hydrodynamics, hull structure and vibration were presented.

Fukasawa and Yamamoto (1980) proposed, in their investigations, guides for bow-form design and ship handling in rough seas by taking into consideration bow form and handling of fast cargo/container ships from the viewpoint of slamming.

In particular, the S175 container ship was subjected to many hydrodynamic investigations over a period of years. Son et al (1981) studied the coupled motion of steering and rolling of a high speed container ship. Fukuda et al (1983) investigated the speed loss of a container ship on different routes in the north pacific ocean in winter. Furthermore, Yoshifumi et al (1971) studied, theoretically and experimentally, the motions of a high speed container ship with a single screw and in oblique waves.

The container ship S175 represents a modern type of ship and is appropriate for relatively higher speed. Also as these ships have a large bow flare, they encounter severe slamming problems. Hence from the view point of design such aspects should be taken into consideration.

4.2.1 Calculation of Ballast Draught

The effect of draught is significant on the occurrence of slamming. Slamming is more severe in the ballast condition than in the loaded condition. Ochi (1958) concluded that increasing the draught of a ship generally leads to a decrease in slamming pressure.

Also an increase in draught (decrease of freeboard) leads to a decrease in slamming pressure, and this in turn gives rise to deck wetness as it is most likely to take place at low freeboard. This event of deck wetness will be treated in a later chapter.

Ballast draught is one of the important parameters to be determined in order to quantify the occurrence of slamming events and the magnitude of impact pressure variation. The full displacement of the ship is given along with the design loaded draught in Table 4.1. This displacement is a summation of the light ship mass and the deadweight. Once the light ship mass is determined the ballast draught can be determined. The light ship mass is composed of the steel mass, outfit mass and mass of the engine plant as given by Chatterjee (1982). Using this method of calculation, the ballast draught is found to be 3.15 metres.

4.2.2 Model Preparation and Blockage Phenomenon

The model of the high speed container ship S175 has been built in the workshop of the Hydrodynamic Laboratory of the University of Glasgow. As described by Hamoudi (1992 a), the model was made of glass reinforced plastic (GRP) to a ratio of 1/70. This ratio has been chosen with respect to the dimensions of the towing tank. Four layers of glass reinforced plastic were used for model construction in order to withstand any extreme load which may result from slamming impact.

Fig. 4.1, given in Murdey's report (1978), represents the body plan for the S175 container ship below the water line as well as the shape of the above water line part.

Full care of the choice of the model ratio has been taken in order to run the test, at the frequency and speed required, without creating any blockage phenomenon. Hence a computer program called FREQ was developed to calculate the frequency at which the tank wall interference is avoided according to the 15th ITTC (1978) report (Seakeeping Committee). Fig. 4.2 shows the blockage phenomenon, the horizontal axis represents the breadth of the tank divided by the model length and the vertical axis represents Froude number (the forward speed) times the maximum frequency (at which tank wall interference may occur) times the square root of the ratio of the model length divided by the acceleration of gravity.

The question of the choice of the model along with the speed and the range of the frequencies depends mainly on the dimensions of the towing tank and the instruments

available to perform a standard test and minimise the errors which may result from an unexpected source.

4.3 THE TOWING TANK

The tank in the Hydrodynamics Laboratory is 77 metres long, 4.6 metres wide and 2.7 metres deep. The tank is equipped with an electro-hydraulic plunger type wave-maker fitted across the width at one end of the tank which generates regular waves of frequency 0.4-1.4 Hz. The maximum wave height which can be generated in the towing tank is in the order of 22 cm as given in Table 4.4. At the other end of the tank, an inclined mesh beach is fitted to absorb the energy of the oncoming waves. The tank is also equipped with an electronically controlled towing carriage with observation platform which enables any towed model to travel with a speed up to 6.4 m/sec.

4.4 INSTRUMENTATION SETUP

As the slamming phenomenon occurs in the fore region of the ships, therefore most of the measuring devices are placed in the fore region. Fig. 4.3 represents the set up of the equipment on the model in order to investigate the slamming phenomenon.

4.4.1 Wave Probes and Calibration Procedure

In order to measure the undisturbed wave heights, three resistance type wave probes fixed to a bridge were placed across the tank width at a distance of about 5 metres in front of the wave-maker and the spreading of the wave probes were B/2, B/3 and B/4 from the tank side wall, and in this case B is the tank width. These wave probes induce electrical signals whose strength varies with the varying wave height. These signals are recorded in a chart recorder for wave height measurements purpose. From the calibration process, taken every morning before the tests, the wave height was determined by multiplying the measured value in the chart recorder by the calibration factor. The calibration factor was obtained by lifting the wave probes bridge by 5 cm and recording the corresponding analogue signal in the chart recorder. In order to avoid any uncertainties in the measurement procedure, three values of the wave height were measured from the three wave probes and the average value was taken.

Other resistance wave probes of the same type were fixed to the model at station 8 1/2 port and starboard in order to measure the motion response (vertical relative motion) due to excitation forces and moments. The wave induced electric signals are amplified and recorded in the wave monitoring systems which include amplifiers and filters. Fang (1994) found that there are some disadvantages in using these resistance type wave probes. As the model is running in medium or high forward speeds (Froude number) the wave probe will be bent significantly in the wave direction by the water current load and this may lead to an error in the measurement of the wave height. As this error is assumed to be small it is neglected during the analysis of the experiments.

4.4.2 Selspot System and Light-Emitting Diodes

The selspot system is a new method for measure the coordinates of multiple points. Small light-emitting diodes are used to identify the selected points. A versatile optoelectronic camera detects the position of the diodes for registration and analysis of static as well as dynamic processes in real time as described by the Selspot System (1977). This device is a specially developed photodetector with four electrodes, and when the infrared light from a light-emitting diode (LED) is focused on the detector surface, a photocurrent will occur. These LEDs can be used to measure either vertical or horizontal oscillations.

The aim of using light-emitting diodes, in this type of experiments, is to measure the heave and pitch oscillations of the model. They were positioned on the deck of the model at station 8 1/2 and at the after perpendicular on the starboard side. These LED were mounted on a vertical slidy rod for ease of calibration of the selspot cameras. The longitudinal distance between the LEDs is the same distance between the selspot cameras and this is about 2.125 metres. This distance is important for pitch oscillations calculation. Hence using the recorded data from the selspot cameras during the experiments heave and pitch amplitudes are calculated using the following identities:

1) Heave:

$$z = \frac{S_B - S_s}{2} \tag{4.1}$$

2) Pitch:

$$\theta = \frac{s_B - s_s}{x} \qquad (4.2)$$

where:

s_B : bow vertical displacement
s_s : stern vertical displacement
x : distance between LEDs = 2.125 metres
z : heave response
θ : pitch response.

All relations for calibration of the selspot system with the LEDs are converted to linear motion responses.

4.4.3 Pressure Transducers, Location and Measurement

The pressure transducer used for this test is called Mediamate. This transducer is a bonded semiconductor strain gage pressure transducer which has been fully compensated and calibrated. The pressure port of the Mediamate is a brazed assembly of 302, 304, or 310 stainless steel, depending on the range. The range of this pressure transducer used for the slamming test is in the range of 0 to 15 (psi) pound per square inch.

The purpose of using this pressure transducer is to measure the impact pressure due to bottom slamming at a discrete location in the bottom of the model of the S175 container ship. The measurement of slamming impact pressure on the bottom of the model was taken at two positions in the bow region where frequent slamming phenomenon was expected to occur. According to Belik et al (1982) the maximum length of hull to leave the water during the course of the slam is 0.3L from the bow, and where L is the length between perpendiculars. For this reason, two pressure transducers were placed at station 8 and 8 1/2, or at distance of 0.2L and 0.15L from the forward perpendicular. Due to the dimensions of the pressure transducer as given in Fig. 4.4, the constraints on size of the model in the fore region, there was not enough space to insert another pressure transducer beyond station 8 1/2 towards the fore end.

Each pressure transducer was calibrated before the experiments. A hand gauge device, called the Hand Held Test Pump Superb Instrumentation, was used for calibration procedure. The pressure transducer was attached to the hand gauge, and the handle was operated until a required pressure was reached and the reading was recorded. This reading corresponds to a voltage which is keyed into the computer for calibration purposes. This operation was repeated for different readings until all the output voltages were linear and the calibration factor was determined.

4.4.4 Accelerometer

A gravity type accelerometer was used to measure the vertical bow acceleration at a position of 0.15 L from FP and this corresponds to station 8 1/2. The calibration of the accelerometer was carried out before it was mounted on the deck of the transverse beam of the model at station 8 1/2. The accelerometer was rotated 90 degrees and the position of the pen corresponding to 9.81 m/sec^2 was marked on the chart recorder.

4.5 DATA ACQUISITION AND TEST PROCEDURE

During acquisition of the test data a software package called LabView was run on Apple Macintosh IICi terminal and this was mounted on the mobile carriage. The electronic signals from the instrumentation were collected through an amplifier data collecting system (32 channel analogue to digital convertor) and then stored in a 40 MByte built in hard disc in the form of an ASCII code data file. Such Storage allows the data to be released to another computer network, such as VAX-3100 workstation computer system, for further test data analysis.

The data collected during each test has been automatically converted into the corresponding unit of any measured mode. This was made possible by inputting the calibration factors into the data acquisition software prior to the test. For further data analysis, the magnitude of any response can be read directly from the recorded measurements. Fig. 4.5 illustrates the electronic equipment on the mobile observation platform.

The experimental data are sampled at a rate of two thousand (2000) samples per second per channel. The length of each run was between 12 and 20 seconds depending on forward speed. As mentioned by Hamoudi et al (1993 b), the aim behind the choice of high number of samples is to pick up the transient impact loading during a slam, and as

this occurs in a very small interval of time (between 20 and 100 milliseconds) according to Gatzer et al (1992). The length of each run was taken as twelve seconds due to limitation in the capacity of the micro computer system. The comparison study of results between theory and experiments was carried out on Macintosh Plus micro computer.

The set up was for the ship moving in head sea condition, i.e when a train of regular waves are incident on her. The model of the container ship S175 was run for different forward speeds corresponding to Froude numbers namely 0.1, 0.15, 0.2, 0.278 and 0.3 respectively. Two draughts, ballast and loaded draught conditions were tested in order to notice the effect of draught on the occurrence of bottom slamming. The model was also tested for various frequencies and within the limit of those frequencies at which the tank wall interference are avoided as stated earlier. For the case of Fr=0.275, the runs were repeated three times for the same conditions, frequencies, wave heights and loaded draught, in order to investigate the occurrence of slamming and to evaluate the magnitude of the impact pressure.

A wave of particular height which depends on frequency and voltage was generated by the hydraulic type wave maker and its magnitude is measured by wave probes. This wave height was carefully selected by inputting various voltages for different frequencies in order to satisfy a rough weather for slamming occurrence and to avoid damage of the equipment which may be caused by large and severe pitching of the model and the set up of the equipment, specially when the model was restricted from other degrees of freedom. The range of frequencies chosen were between 0.5 Hz and 1.0 Hz, and the voltage that was input in order to generate the wave height was in the interval of 0.5 and 2.0 volts. Table 4.4 shows the range of wave amplitude, which can be generated in the towing tank, as function of the frequency volts. In the case of ballast draught the wave height was reduced in order to avoid any damage to the equipment due to severity of the motions on the light model.

4.6 DATA ANALYSIS, RESULTS AND DISCUSSION

The analysis of the results were performed in the frequency domain with the Fast Fourier Transform technique. As mentioned earlier, the data collected during the test is automatically converted into the corresponding unit.

4.6.1 Vertical Relative Motion

One of the conditions to satisfy the occurrence of slamming is bow emergence, i.e when the vertical relative motion exceeds the local draught. Wave probes were fixed to the model at station 8 1/2 port and starboard in order to measure the motion response (vertical relative motion) in relation to the elevation of the incident wave. During the analysis, the average of the two recorded values, namely relative motion on port and starboard, was taken after the standard deviation was calculated. Figs. 4.14 and 4.15 are a typical example of time history tracing the vertical relative motion, recorded during the experiment, port and starboard side respectively.

The magnitude of the vertical relative motion response is measured with respect to the amplitude of the incident wave.

4.6.1.1 Relative motion for Fr=0.1

Fig. 4.6 represents the nondimensional vertical relative motion v frequency history at station 8 1/2 for the loaded draught condition and for Fr=0.1 on the port and starboard side. The average of the two relative motions, port and starboard, is plotted. The relative motion on the port side is higher than the starboard side due to the set up of the model and also due to restriction from other degrees of freedom. The difference in the two recorded relative motions, on the port and starboard side becomes higher if the trend of the relative motion approaches the peak, and which is in the range of $2.75 \leq \omega\sqrt{\frac{L}{g}} \leq 3.25$. The difference in the peak is around 19%. The author also believes that the model was tending to roll (heel) slightly towards the port side, which may be due to the set up, as the values of the relative motion on the port side exceeds that of the starboard side. Another possible reason for this difference is believed to be due to the interaction between tank walls and model. This might, for example, be due to asymmetry in the wave maker motion, which has been noticed elsewhere, i.e. Fig. 4.91.

Fig. 4.7 represents the vertical relative motion for ballast draught. The variation in the peak value of the relative motion for the loaded and ballast draught conditions is of 57.4% as in Fig. 4.6 and 4.7. Also as in Fig. 4.7 the variation in the peak relative motion for the port and starboard side is 15.4%. The peak of the vertical relative motion takes place in the range of $2.25 \leq \omega\sqrt{\frac{L}{g}} \leq 2.5$.

4.6.1.2 Relative motion for Fr=0.15

Fig. 4.8 shows the trend of the vertical relative motion at station 8 1/2 for conditions of loaded draught and Fr=0.15. It is clear from this figure that the vertical relative motion increases with the forward speed.

The peak occurs in the range $2.75 \leq \omega\sqrt{\frac{L}{g}} \leq 3.25$ and with a difference of 22.3% higher on the port side than on the starboard side due to the asymmetric wave sent by the wavemaker.

Fig. 4.9 represents the vertical relative motion at station 8 1/2 for ballast draught. The relative motion in this case differs from the one in the loaded draught condition and with a difference of 52% higher in ballast draught. There is also a difference of 6.5% between the relative motion on the port and starboard side in the region of $2.25 \leq \omega\sqrt{\frac{L}{g}} \leq 2.55$ due to the asymmetric wave sent by the wavemaker.

4.6.1.3 Relative motion for Fr=0.2

Fig. 4.10 shows the vertical relative motion response at station 8 1/2 for loaded draught and Fr=0.2. The peak occurs in the range of $2.5 \leq \omega\sqrt{\frac{L}{g}} \leq 3.0$ and with a difference of 17.6% between the relative motion recorded on the port and starboard side due to the asymmetric wave sent by the wavemaker.

Fig. 4.11 represents the vertical relative motion at station 8 1/2 for ballast draught and Fr=0.2. For ballast draught condition, the relative motion becomes 42.9% higher than the loaded draught. The difference in the motion recorded on the port side is 7.1% higher than the starboard side and the peak range is in the region of $2.2 \leq \omega\sqrt{\frac{L}{g}} \leq 2.5$ due to the asymmetric wave sent by the wavemaker.

4.6.1.4 Relative motion for Fr=0.278

Fig. 4.12 represents the vertical relative motion at station 8 1/2 for loaded draught and Fr=0.278. Two peaks appear in this figure. The first peak with a vertical relative motion higher than 1.3 occurs in the region $2.0 \leq \omega\sqrt{\frac{L}{g}} \leq 2.25$ and corresponds to resonance of heave mode as given in Fig. 4.24, while the second peak of 1.9 occurs in the region $2.25 \leq \omega\sqrt{\frac{L}{g}} \leq 2.5$ and can be associated with pitch resonance. The relative motion recorded on the port side is 18.4% higher than the starboard side due to the asymmetric wave sent by the wavemaker.

Fig. 4.13 gives the vertical relative motion at station 8 1/2 for ballast draught and Fr=0.278. In this case the peak approaches the value of 4.3 for a nondimensional frequency of 2.02 and the difference between the relative motion recorded on port side is only 5% higher than that on the starboard side.

The variation of the peak value of the relative motion for loaded and ballast draughts are as in Fig. 4.12 and 4.13 is 56%.

4.6.1.5 Relative motion for Fr=0.3

Fig. 4.16 represents the vertical relative motion at station 8 1/2 for loaded draught and Fr=0.3. The peak value of the vertical relative motion is 1.72 and occurs in the range of $2.0 \leq \omega\sqrt{\frac{L}{g}} \leq 2.25$. There is also a difference of nearly 19% between the recorded relative motion on port and starboard side due to the asymmetric wave sent by the wavemaker.

Fig. 4.17 shows the vertical relative motion at station 8 1/2 for ballast draught and Fr=0.3. The difference between the relative motion on port and starboard side is around 25% and the peak occurs in the region of $2.0 \leq \omega\sqrt{\frac{L}{g}} \leq 2.25$.

The difference between the peak of the relative motion is 65% higher at ballast draught conditions.

The main reason for the differences between the port and starboard relative motion measurements is due to the asymmetric wave pattern sent by the wave maker. Fig. 4.91 shows the discrepancy of the wave height measured by the three wave probes which were distributed across the tank.

4.6.2 Heave and pitch Motion

Heave and pitch amplitude are calculated using equations (4.1) and (4.2) respectively. Figs. 4.68 and 4.69 give a typical response of the fore and the aft vertical relative motion, using the above equations. Heave amplitude was nondimensionalised by the magnitude of the wave amplitude generated in the towing tank and pitch amplitude was nondimensionalised by the product of wave amplitude and the wave number.

Fig. 4.18 represents nondimensional heave response for loaded draught and Fr=0.1. The response in frequency domain is uncertain, and this is probably due to low forward speed and restriction of the model from other degrees of motion.

The heave responses in ballast draught and Fr=0.1 are as in Fig. 4.19. The variation in heave responses are good with the exception of the nondimensional frequency $\omega\sqrt{\frac{L}{g}}$ =2.02, where the values should have been higher and this is probably due to restriction of the model motions and some errors in the testing process.

The heave responses in loaded and ballast draught for Fr=0.15 are as in Fig. 4.20 and 4.21. In both cases, i.e the loaded and ballast draught, the trend of the curve is consistent.

Fig. 4.22 and 4.23 represent the nondimensional heave amplitudes for Fr=0.2 at loaded and ballast draughts respectively. One can notice that the trend of both curves is consistent except for some odd points and which are due to errors resulting from experiments.

Fig. 4.24 gives a comparison of the nondimensional heave response between the present set of experiments for the loaded draught condition with those of ITTC'78 for Fr=0.278 and 0.275 respectively. The trend of the two curves is good and the difference can be attributed to two main factors, i.e the slight difference in the forward speed and

restriction of the model motions during experiments. Results represented by the International Towing Tank Conference (1978) were obtained from model tests carried out with free-running model, whereas for this investigation only heave and pitch were allowed, and the difference in the results between the present investigation and those of ITTC (1978) is due to in the different equipment and test procedures used in different carriages (i.e bow and/or stern restrain mechanism).

Fig. 4.25 shows nondimensional heave amplitude, for ballast draught and Fr=0.278. The heave response are higher for the lower range of frequencies and they gradually decrease as the nondimensional frequency values increases.

Figs. 4.26 and 4.27 give the nondimensional heave amplitude response for Fr=0.3 at loaded and ballast draughts respectively.

Figs. 4.28 and 4.29 show a scatter behaviour of nondimensional pitch amplitude in frequency domain for Fr=0.1 at loaded and ballast draught conditions respectively. The behaviour of the pitch amplitude at low frequencies is the same as in the heave mode. In ballast draught, the model pitches very heavily.

Figs. 4.30 and 4.31 represent nondimensional pitch amplitude for loaded and ballast draught respectively at Fr=0.15. Large pitch amplitude is noticeable for ballast draught.

The pitch responses at loaded and ballast draught and Fr=0.2 are as in Figs. 4.32 and 4.33. On comparison of the loaded draught condition with the ballast draught condition it is noticed that the pitch amplitude is greater in the case of ballast draught, and this which is due to lightness of the model in response to undulations of head waves.

Fig. 4.34 gives a comparison of the nondimensional pitch between the present set of experiment for loaded draught condition with those of ITTC'78 for Fr=0.278 and 0.275 respectively. There is good agreement for high frequency range, but for lower frequencies the discrepancy is large and this may be attributed to restriction of the model motions. Fig. 4.35 shows nondimensional pitch amplitude for ballast draught at Fr=0.278.

Figs. 4.36 and 4.37 illustrate nondimensional pitch amplitude in frequency domain for Fr=0.3 for loaded and ballast draughts respectively. Although the trend is the same in both cases, the response at ballast draught is much higher than the loaded draught condition.

4.6.3 Vertical acceleration

Lewison (1970) reported that the slamming event can be observed when the vertical acceleration is of the order of 8.8 m/sec^2, in the case of Cargo ships named 'Lukuga' and 'Jordaens' of length 136 m and 146.15 m respectively. If one may associate the same order of magnitude for the vertical acceleration 8.8 m/sec^2 to the present container ship S175, and using kinematic similarity, the vertical acceleration becomes 0.36g for a model scale of 1:70. This value may be called the threshold vertical acceleration. The above reasoning was used as a basis for placing an accelerometer on the deck, to measure vertical acceleration.

Fig. 4.38 represents the vertical acceleration for Fr=0.1 and for loaded draught condition. In this particular case no appreciable vertical acceleration was recorded. However, Fig. 4.39 gives the vertical acceleration for ballast draught and at the same Froude number. The vertical acceleration exceeding its threshold value lies in the range

$2.4 \leq \omega\sqrt{\frac{L}{g}} \leq 3.0$ and with a maximum value of 0.47g.

At Fr=0.15, the vertical acceleration is presented in Fig. 4.40 for the loaded draught condition . For this case also there is no appreciable vertical acceleration which may cause slam. Fig. 4.41 shows the vertical acceleration for Fr=0.15 and for ballast draught condition. In the range of frequency $2.75 \leq \omega\sqrt{\frac{L}{g}} \leq 3.0$ the vertical acceleration exceeds the threshold value and the peak value recorded during model tests is of the order of 0.43g.

As shown in Fig. 4.42 and 4.43, for Fr=0.2 the vertical acceleration for loaded and ballast draught conditions are 0.4g and 0.39g respectively.

Increasing the forward speed means an increase in the probability of slamming occurrence. Fig. 4.44 is a good example of an increase in the vertical acceleration, as a result of increasing forward speed. For loaded draught and for Fr=0.278 the maximum vertical acceleration recorded during model test is 0.53g. Furthermore, Fig. 4.45 shows the vertical acceleration for ballast draught at the same Froude number. As the curve fluctuates, it is not possible to make any conclusive statement.

Fig. 4.46 is another example of a case where the vertical acceleration exceeds the threshold value, for the case of loaded draught and for Fr=0.3. The peak value of the vertical acceleration in this case is 0.46g. As in Fig. 4.47 the peak value for the ballast draught is lower than the loaded draught condition.

From the above results, we may conclude that there were more cases when the vertical acceleration exceeded the threshold value, for the case of loaded draught condition, than that of the ballast draught condition.

4.6.4 Impact pressure due bottom slamming

4.6.4.1 Impact pressure magnitude and occurrence

Lewison (1970) reported that if a pressure on the bottom plating is of the order of 0.098 MN/m^2, as in the case of cargo ships 'Lukuga' and 'Jordaens' of length 136 m and 146.15 respectively, there is occurrence of slam. If one scales down this magnitude of pressure to model scale using the ratio of the present investigation, one can get 1.39 kN/m2, and this can be called threshold value for model test.

Figs. 4.48.a, b and c give a time variation of hydrodynamic pressure followed by an impact at station 8 1/2 for frequency 0.95 Hz and for Fr=0.275. The impact pressure recorded for this run, during model experiment, is of the order of 1.53 kN/m2 (0.221 psi) and beyond the threshold value which Lewison reported. Fig. 4.49.a, b and c represent another example of impact pressure recorded during experiments, and in this case the pressure is of the order of 6.73 kN/m2 (0.975 psi).

Equation (3.4) and (3.7) are used to obtain the pressure coefficient by three and two parameter conformal mapping technique. The impact pressure obtained by the theoretical process is compared with the measured experimental value. This pressure coefficient is employed in equation (3.3) to predict the impact pressure due to bottom

slamming. Fig. 4.50 represents the measured and calculated impact pressure by the two methods i.e two and three parameter at station 8 1/2 for loaded draught and for Fr=0.1. The calculated pressure in the above result is higher than the measured value. Also as the vertical velocity increases the calculated pressure increases. The two parameter prediction technique also predicts higher values than the measured pressure.

For Fr=0.2 and loaded draught condition, Fig. 4.51 gives the measured impact pressure and the calculated pressure at station 8 1/2, using the above method. For a higher vertical relative velocity, the impact pressure is overpredicted. The measured impact pressure is always lower than the calculated value, and this may be the cause of compressibility of water and air and cushioning effect of air which are ignored in the calculation. The maximum impact pressure calculated by three parameter is of the order of 5.4 kN/m2 and by two parameter it is of the order of 4.02 kN/m2, these pressures correspond to vertical relative velocity of the order of 0.84 m/sec. However, for the same conditions the maximum impact pressure measured at station 8 1/2 is about 0.57 kN/m2. This value is lower than the threshold magnitude assumed by Lewison, and corresponds to a vertical relative velocity of 0.78 m/sec which is higher than threshold value.

A comparison of measured and calculated pressure using two and three parameter conformal mapping technique is shown in Fig. 4.52 for loaded draught and for Fr=0.278 at station 8 1/2. The maximum pressure measured is 0.78 kN/m2 (lower than threshold magnitude given by Lewison). This corresponds to a maximum vertical acceleration of 0.53g (higher than the threshold value) and vertical relative velocity of 0.61 m/sec (higher than its threshold value). The maximum impact pressure calculated by three parameter is 7.42 kN/m2 and 5.53 kN/m2 by two parameter, both these pressures correspond to a vertical relative velocity of 0.98 m/sec.

A comparison of measured and calculated pressure using two and three parameter conformal mapping technique is also shown in Fig. 4.53 for loaded draught and Fr=0.3 at station 8 1/2. The maximum pressure measured is 0.59 kN/m2 (lower than threshold magnitude given by Lewison). This corresponds to a vertical acceleration of 0.41 m/sec2 (higher than its threshold value) and vertical relative velocity of 0.51 m/sec (higher than its threshold value). The maximum impact pressure calculated by three parameter is 6.24 kN/m2 and 4.65 kN/m2 by two parameter, both these pressures correspond to a vertical relative velocity of 0.9 m/sec.

For ballast draught the comparison has been made only between measured and calculated pressure by three parameter. For example, Fig. 4.54 represents measured and calculated impact pressure by three parameter method at station 8 1/2 for Fr=0.1 and ballast draught condition. It is noticed in the results that the calculated pressure is always higher than the measured pressure except in the case where the vertical relative velocity is lower than the threshold value. The maximum impact pressure measured, for these conditions, is 0.91 kN/m2 (less than its threshold magnitude) and this corresponds to a vertical acceleration of 0.39g and vertical relative velocity of 0.81 m/sec. The maximum impact pressure calculated by three parameter method is 4.98 kN/m2, and this corresponds to a vertical acceleration of 0.39g and vertical relative velocity of 0.8 m/sec. The measured pressure in this case is much lower than the calculated pressure by a ratio of more than 5. For the same conditions where Froude number is increased to 0.15 as shown in Fig. 4.55, the maximum impact measured at station 8 1/2 is about 0.69 kN/m2 (less than threshold magnitude) and corresponds to vertical acceleration of 0.39g (higher than threshold value) and vertical relative velocity of 0.78 m/sec (higher than threshold value). However, the maximum impact pressure calculated by three parameter is of the order of 6.3 kN/m2 and corresponds to vertical relative velocity of 0.91 m/sec and acceleration of 0.43g. This calculated pressure is about 9 times higher than the measured pressure.

Fig. 4.56 shows a comparison of calculated (using three parameter method) and measured impact pressure for ballast draught at station 8 1/2 and for Fr=0.2. In this case the maximum impact pressure measured is 1.27 kN/m2, corresponding to a vertical acceleration 0.33g and relative velocity of 0.6 m/sec. The maximum impact pressure calculated is 6.55 kN/m2 for a vertical acceleration of 0.25g (less than its threshold value) and vertical relative velocity of 0.92 m/sec. The maximum calculated pressure is 5 times higher than the maximum measured pressure. For Fr=0.278 as shown in Fig. 4.57, the maximum measured impact pressure is 0.9 kN/m2 and this corresponds to an acceleration of 0.34g and vertical velocity of 0.86 m/sec. The scatter in the data of calculated pressure is quite large, and the increase in pressure with respect to increase of vertical velocity is clear. For this case the maximum impact pressure calculated is 8.38 kN/m2 for a vertical velocity of 1.04 m/sec. The same explanation follows for the case of Fr=0.3 as shown in Fig. 4.58. The maximum pressure recorded from this test is about 1.07 kN/m2, for an acceleration of 0.33g and vertical velocity of 0.56 m/sec. The maximum calculated pressure is of the order of 8.73 kN/m2 for a vertical velocity of 1.07 m/sec.

On the basis of the above discussion, one may conclude that the measured pressure is always lower than the calculated one. The results do not correlate very well, except for few points in the lower range of the vertical relative velocity, and this is due to the non-linearities, layer of air underneath the bottom of the investigated body and also some errors, which will be detailed in later section, resulting from the calibration or guides which restrict motions other than heave and pitch. Though the wide use of the empirical prediction of the impact pressure, due to bottom slamming is made, this empirical prediction is expected to give an approximate results.

The other reason for the difference between the calculated and measured impact pressure, due to bottom slamming, is due to the interaction between wave and model particularly at high frequencies.

According to Radev (1990), slamming pressure increases towards the fore part. Figs. 4.59 to 4.67 show a comparison of impact pressure at station 8 1/2 and station 8 for loaded and ballast draught for Fr 0.1, 0.15, 0.2,0.278 and 0.3 respectively. The pressure recorded at station 8 1/2 is always higher than the one recorded at station 8, except for few minor points and which may due to some errors in measurements. From this we can conclude that the stations in the fore part are subjected to severe slamming phenomenon. The pressure recorded at ballast draughts is much higher, and sometimes twice that of the loaded draught cases.

For the case when Fr=0.275, and as mentioned earlier, the runs were repeated three times for the same conditions, for different frequencies, forward speed, wave heights, loaded draught and set up of the model. In this case the set up of the model was different than the first set of test and the model was free to surge. Fig. 4.70 represents nondimensional heave amplitude for loaded draught and for Fr=0.275. For high frequencies range, i.e $\omega\sqrt{\frac{L}{g}} > 2.5$, the amplitude is almost the same but for low frequencies range, i.e $\omega\sqrt{\frac{L}{g}} < 2.5$, there were some discrepancies although the testing

conditions were exactly the same. This can only be explained by two factors, i.e due to the error in calibration and also due to different wave heights generated by the wavemaker for the same frequency and voltage. Results are the same for pitch amplitude and are as shown in Fig. 4.72.

Fig. 4.71 shows comparison of the heave amplitude obtained from test results and of results from the International Towing Tank Conference (1978). Results agree very well at high frequencies, however there are significant discrepancies at the low frequency range, due to the set up of the model and the restriction of the motions. The model had a limited range of motion for heave and pitch motions in order to avoid the damage of the equipment when motions were large, whereas results represented by the International Towing Tank Conference (1978) were obtained from model tests carried out with free-running model. Error effects can be attributed to the instrumentation errors and the errors due to the procedure and experiment conditions. The same explanation can be given to the comparison of pitch amplitude as given in Fig. 4.73.

Fig. 4.74 illustrates nondimensional vertical relative motion amplitude, at station 8 1/2, for the three attempts performed during the experiments. The trend of the relative motion is the same for the three tests with some small variations in the amplitudes due to the asymmetric wave sent by the wavemaker. These variations are large when the amplitudes of the relative motion are high.

The relative velocity is obtained by differentiating the relative motion with respect to time. The amplitude of the vertical relative velocity is obtained by multiplying the measured amplitude of vertical relative motion with the frequency of encounter of the ship with the waves, and the results are as in Fig. 4.75. Also any error in the relative motion measurements will influence the relative velocity. It is clear in this figure that in the range of $\omega\sqrt{\frac{L}{g}} \geq 2.45$ the vertical relative velocity exceeds its threshold velocity (0.46 m/sec, model test) for slamming occurrence except for test 1 where the amplitude is around 0.45 m/sec (less than its threshold value).

The maximum vertical acceleration recorded during the three tests is around 0.89g as shown in Fig. 4.76. In this figure most of the accelerations, recorded during the

three tests, exceed the threshold value for slamming occurrence except for $\omega\sqrt{\frac{L}{g}} \geq 3.0$.

Fig. 4.77 to 4.79 show the dependence of the impact pressure on the vertical relative velocity at station 8 1/2 for loaded draught and for Fr=0.275. It is very interesting to observe the behaviour of slamming pressure as a function of the vertical relative velocity, derived from the corresponding relative motion elevation, of the test results. In some case though the velocity is lower than its threshold value (0.46 m/sec), the measured impact pressure exceeds its threshold magnitude (1.39 kN/m2). For example, in Fig. 4.77 (test 1) the vertical velocity recorded is about 0.112 m/sec and the pressure is of the order of 1.48 kN/m^2. For the same conditions, as in Fig. 4.78 (test 2), the vertical velocity is 0.14 m/sec and this corresponds to an impact pressure of 2.297 kN/m2. Furthermore, for test 3 presented in Fig. 4.79, the velocity and the pressure are recorded as 0.196 m/sec and 1.166 kN/m2 respectively, and are less than their threshold values. It is difficult to draw a final conclusion from model test as some of the conclusions may eliminate some prediction methods.

It is also very interesting to observe the occurrence of some discrepancies in the occurrence of slamming, even when the conditions are the same. Fig. 4.80 shows the impact pressure for three repeated tests at station 8 1/2. As mentioned earlier, the conditions of wave frequency, loaded draught, forward speed, wave height and the same set-up technique for the model are the same. Although the tests were repeated three times, the occurrences of slamming were different, as also the magnitude of the slamming pressure. In certain cases the variation in the magnitude of the slamming pressure was as high as twice.

Fig. 4.81 to 4.83 give a comparison of the measured and calculated impact pressure for loaded draught at station 8 1/2 and for Fr=0.275. One can notice that for the low range of vertical relative velocity the measured pressure is higher than the calculated one, but for the high vertical relative velocity range the calculated pressure is higher than the recorded pressure. Although there are discrepancies in the comparison, the magnitude of the measured and calculated are reasonable.

The nondimensional pressure coefficient at station 8 1/2 calculated by the three parameter and two parameter methods are of the order of 15.10 and 11.5 respectively. This nondimensional coefficient is calculated by dividing the measured impact pressure by

the vertical relative velocity derived from the vertical relative motion and the results are as in Fig. 4.84. This coefficient for station 8 1/2 should be constant for the frequencies, as it is not frequency or speed dependant, and it is a function of the bottom shape of the section under consideration.

4.6.4.2 Distribution of impact pressure

Equation (3.32) gives the distribution of the slamming pressure over the girth of the section at one tenth of the design draught. This pressure is zero at one tenth of the design draught and is a maximum at the keel. Figs. 4.85 to 4.90 give the pressure distribution over the girth of the section at 8 and 8 1/2 and at one tenth of the design draught, for different frequencies and for Fr=0.275. The magnitude of the pressures given in these figures are obtained from test results during the experimental investigation and represent the maximum pressure at the keel. For example, Fig. 4.85 represents the impact pressure of the order of 0.478 psi at the keel and equation (3.32) can be used to calculate the pressure at any point over the girth and the pressure at one tenth of the design draught is zero.

4.6.4.3 Time interval of an impact pressure

From Ochi's (1973) investigation, it was found that the gifle, which is the transient response due to bottom slamming, of an impact pressure is of triangular shape, and the time duration of pressure at any location is 0.1 seconds (100 milliseconds) as an average for 520 ft vessel. Using Froude scaling law, the duration time at any point for a ship of length L (in feet) may be given by:

$$t = 0.1\sqrt{\frac{L}{520}} \tag{4.3}$$

According to this assumption, the duration time for the S175 container ship (full scale) is approximately 105 milliseconds, and the model is about 12.5 milliseconds.

From the present investigation, the expression which assumes the duration time of an impact, is not valid and the interval time of an impact is found by Hamoudi (1993 a) and (1993 b) to lie between 1 and 10 milliseconds. Hence, the average time can be assumed as 5.5 milliseconds for the model of S175 container ship of 2.5 metres length. These results confirm that more research needs to be done in this field.

4.6.5 Relative Motion and Swell-Up

The swell-up is in fact the effect of water being pushed around the bow higher than can be accounted for by considering heave, pitch and wave fluctuations alone. Swell-up is an important parameter on shipping of water. Lloyd (1989) mentioned that as the hull dips into the water the increasing submerged volume causes a local swell-up of the water surface and as the hull rises this effect disappears. Block et al (1983) mentioned in their investigation that the swell-up coefficient is usually of the order of 1.1 to 1.5 and if one supposes there is no occurrence of swell-up this factor reduces to unity.

Swell-up coefficient is defined by Lloyd (1989) as follows:

$$C_s = \frac{\text{actual relative motion amplitude}}{\text{notional relative motion amplitude}} \tag{4.4}$$

Swell-up is a function of the relative motion, ship speed and hull shape. Blok et al (1983) found that swell-up coefficients show very little frequency dependency and is still the subject of research.

For the present investigation comparison is made for the vertical relative motion predicted by the NSM program and results obtained from measurements of the three repeated tests as shown in Fig. 4.92. The calculated vertical relative motion is higher than the measured one in the frequency range of $\omega\sqrt{\frac{L}{g}} < 2.5$, this may due to the shift in the heave response, as given in Fig. 2.42 in chapter 2, caused by the end effect, and also some experimental errors, however in the range of the frequency where $\omega\sqrt{\frac{L}{g}} > 2.5$ the measured vertical relative motion is higher than the calculated one which is due to the exclusion of the swell-up effect. There are also other factors such as the asymmetric wave heights sent by the wave maker, restriction of the model from other degrees of freedom and also some errors in the measurements. These factors have some influence on the swell-up coefficient as given in Fig. 4.93.

4.7. ERROR EFFECT

The effect of errors is an important factor to be looked at in all fields of theoretical or experimental investigations. The magnitude of errors differs depending upon the source, therefore it is important to determine the magnitude as well as the source of the error in order to introduce a correction factor.

The performance committee of the 15th International Towing Tank Conference (1978) has attempted to determine precisely the magnitude of the different sources of errors. It was found that the sources of errors can be classified as model test errors (these errors result from instrumentation errors and procedure and experiment conditions errors), prediction method errors (these errors result from approximate assumptions) and sea trial error (including instrumentation errors and other errors such as influence of sea water, temperature propeller cavitation etc..).

In the present investigation, it is possible to perform some error investigation for the three repeated tests. To start with, the main experimental error, which should be taken into account in every step of this investigation, is due to the asymmetric wave sent by the wavemaker, the set up of the model and also the restriction of the model from other degrees of freedom.

The error, for heave, pitch, vertical relative motion and measured impact pressure, is calculated as follows:

$$\text{Mean} = \frac{\sum_{i=1}^{n} \text{Test}_i}{n} \tag{4.5}$$

i=1, 2 and 3 (1 for test 1, 2 for test 2 and 3 for test 3)

n : number of tests

Mean : average of n values

$$\text{Error}_i = \frac{\text{Mean} - \text{Test}_i}{\text{Mean}} \tag{4.6}$$

$Error_i$: error for test i

$$\text{Mean error} = \frac{\sum_{i=1}^{n} Error_i}{n} \tag{4.7}$$

Mean error is the mean value of the errors obtained from the n tests.

For example, Table 4.5 represents the error for heave amplitude where the maximum is about 22.5% and the minimum is 0.7%, for pitch amplitude the error is represented in Table 4.6 and one can notice that the maximum error is 19.5% and the minimum is 0.3%. Furthermore, the error for vertical relative motion is also represented in Table 4.7 with a maximum of 20.5% and a minimum of 0.2%. The impact pressure measurements are also affected by the error effect as given in Table 4.8, the maximum error calculated from the three repeated tests is nearly 40% and the minimum error is 1.4. One can notice that the maximum error in the measured impact pressure is the highest one more than the one obtained from heave amplitude, pitch amplitude and vertical relative motion; this is due to the nonlinearities in the vicinity of the pressure transducers measuring the impact pressure.

4.8 CONCLUSIONS

Experimental investigation to predict the occurrence of slamming and its pressure magnitude has been reported in order to study this phenomenon on a high speed vehicle type.

A model of the S175 container ship was used in the present study. Characteristics associated with slamming phenomenon were also investigated by taking their measurements from model tests for different conditions, such as draught, forward speed and wave frequency.

Vertical relative motion was measured and its differentiation with respect to time was taken, in order to obtain vertical relative velocity. Using this vertical relative velocity, calculation of the impact pressure was performed. The measurement of impact pressure was first made by using pressure transducers located at station 8 and 8 1/2 on the

bottom of the model. These measurements were repeated three times in order to gather a big population of scatter.

The pressures recorded at ballast draught are much higher, and sometimes twice that of the loaded draught cases.

Though the vertical relative velocity and vertical acceleration are lower than predicted threshold values but slamming occurs. The magnitude of the slamming pressure and its occurrence was different for the three tests. This difference is believed to be due to some nonlinearities which were ignored during the investigation, such as compressibility of water and air and the cushioning effect of air (air boundary layer, depression of the water surface just before impact), due to the limitations of the degrees of freedom and also due to the error resulting from experiments. The other reason for this difference is the interaction between the wave and model which may cause the pressure transducer to measure only a partial impact pressure and one has to bear in mind that the empirical prediction of the impact pressure due to bottom slamming is only an approximate method and not a universal established method. The maximum measured magnitude of impact pressure due to bottom slamming is found to be 3.476 kN/m2 for the S175 container ship model, this corresponds to a vertical relative velocity of 0.724 m/sec and a vertical acceleration of 0.63g for loaded draught and for Fr=0.275. The maximum impact pressure calculated by three parameter is 7.42 kN/m2 and by two parameter it is 5.53 kN/m2, these pressures correspond to vertical relative velocity of 0.84 m/sec for loaded draught.

As the measured impact values are lower than the calculated values, three repetitive tests were conducted for the same set of conditions. However when the calculated pressures were compared with the measured pressures for the three test cases, it is noticed there was not much consistency, but results were believable. From this one can conclude that it is more appropriate to use the theoretical three parameter prediction method, due to consistency of the results.

Heave and pitch motions results agree very well for high frequencies, however there are discrepancies at the low frequency range, due to the set up of the model. The model had a limited range of motion for heave and pitch motions in order to avoid the damage of the equipment when motions were large, whereas results represented by the International Towing Tank Conference (1978) were obtained from model tests carried out

with free-running model.

The calculated pressure coefficient for station 81/2 is 15.1 by using conformal mapping (three parameter), but some measured values, for the same relative velocity at the instant of impact, are approximately 4 times higher than the calculated values and this is attributed to the errors obtained from the experimental measurements.

The average time interval of an impact is found to be 5.5 milliseconds for the 2.5 metre length model of the S175 container ship. The impact time interval is compared with the experimental measurements of Verhagen (1967) and is in a good agreement.

The vertical relative motion, by which the vertical relative velocity is calculated to predict the impact pressure due to bottom slamming, is affected by the so-called swell-up coefficient, therefore for a well designed experiment this coefficient can be determined and incorporated in the prediction of the vertical relative motion.

One has to take into account the error effects resulted from the present investigation particularly for the measurement of the impact pressure due to bottom slamming where the maximum error is approaching 40% which is significant.

Results of the present investigation will be useful for development of further study on ship slamming for high speed marine vehicles. Setting up a data bank, of the measured results will be useful in the near future for enhancement of the present method.

It must also be noted that in towing tanks, the conditions of rough weather cannot be satisfied because of the following reasons:

- motions are limited by the set up of the equipments (guides),
- avoid damage of the equipment,
- slam may not occur during very limited time of the run length, which is 12 seconds on an average.

Table 4.1 Principle particulars of S175 ship

Ship S175	
Lpp (m)	175.000
B (m)	25.400
D (m)	15.400
T (m)	9.500
Displacement (t)	24742.000
L/B	6.890
B/T	2.670
LCB (%Lpp)	1.417
CB	0.572
$C_{\text{棱}}$	0.970
KM (m)	10.520
GM (m)	1.000
Kyy/Lpp	0.240
Kxx/B	0.328

Stations	x/l	$B/B_{\varnothing}$	$T/T_{\varnothing}$	$S/S_{\varnothing}$	B/2T	S/BT	Weight
F.P.	1.0	0.000	0.985	0.050	0.000		0.119
9.5	0.9	0.123	1.000	0.117	0.164	0.923	0.260
9.0	0.8	0.248	1.000	0.192	0.331	0.751	0.402
8.5	0.7	0.395	1.000	0.293	0.527	0.720	0.502
8.0	0.6	0.553	1.000	0.419	0.738	0.735	0.601
7.5	0.5	0.702	1.000	0.559	0.837	0.772	0.701
7.0	0.4	0.828	1.000	0.698	1.105	0.818	0.802
6.5	0.3	0.920	1.000	0.823	1.228	0.868	0.900
6.0	0.2	0.978	1.000	0.922	1.306	0.914	1.000
5.5	0.1	0.999	1.000	0.980	1.334	0.952	1.000
5.0	0.0	1.000	1.000	1.000	1.335	0.970	1.000
4.5	0.1	1.000	1.000	0.996	1.336	0.966	1.000
4.0	0.2	1.000	1.000	0.969	1.335	0.940	1.000
3.5	0.3	0.995	1.000	0.913	1.328	0.890	0.920
3.0	0.4	0.970	1.000	0.825	1.295	0.825	0.840
2.5	0.5	0.921	1.000	0.708	1.230	0.746	0.759
2.0	0.6	0.839	1.000	0.569	1.120	0.658	0.679
1.5	0.7	0.716	1.000	0.417	0.956	0.565	0.599
1.0	0.8	0.555	1.000	0.263	0.741	0.460	0.519
0.5	0.9	0.354	1.000	0.101	0.473	0.277	0.352
A.P.	1.0	0.122	0.074	0.005	0.163		0.185

x/l : distance from the midship

$B/B_{\varnothing}$: ratio of breadth to the midship breadth

$T/T_{\varnothing}$: ratio of draught to the midship draught

$S/S_{\varnothing}$: ratio of sectional areas

Water line	Station 0	Station 0.25	Station 0.5	Station 0.75	Station 1	Station 1.5	Station 2	Station 2.5
0.0	0.000	0.000	0.200	0.240	0.300	0.530	1.025	1.910
0.5	0.000	0.000	0.320	0.625	0.970	1.770	2.790	4.190
1.0	0.000	0.000	0.400	0.865	1.355	2.425	3.725	5.300
2.0	0.000	0.000	0.550	1.180	1.845	3.265	4.910	6.750
3.0	0.000	0.000	0.645	1.400	2.180	3.880	5.800	7.790
4.0	0.000	0.000	0.730	1.600	2.495	4.445	6.565	8.640
5.0	0.000	0.000	0.845	1.940	2.880	5.080	7.370	9.400
6.0	0.000	0.000	1.040	2.210	3.455	5.860	8.170	10.060
7.0	0.000	0.000	1.410	2.890	4.300	6.785	8.940	10.615
8.0	0.000	0.000	2.200	3.920	5.380	7.750	9.670	11.090
9.0	0.650	2.190	3.770	5.210	6.500	8.670	10.340	11.510
9.5	1.550	3.070	4.500	5.850	7.050	9.090	10.650	11.690
10.0	2.280	3.800	5.180	6.450	7.600	9.520	10.940	11.860
11.0	3.430	4.950	6.270	7.480	8.560	10.270	11.450	12.150
12.0	4.340	5.060	7.180	8.360	9.380	10.940	11.890	12.390
13.0	5.140	6.630	7.950	9.100	10.070	11.500	12.240	12.550

Water line	Station 3	Station 3.5	Station 4	Station 4.5	Station 5	Station 5.5	Station 6	Station 6.5
0.0	3.330	5.245	7.495	9.430	9.905	8.950	7.320	5.580
0.5	5.930	7.885	9.605	10.760	10.960	10.160	8.800	7.100
1.0	7.150	9.065	10.660	11.620	11.740	11.040	9.660	8.020
2.0	8.640	10.340	11.375	12.350	12.440	11.860	10.680	9.150
3.0	9.640	11.105	12.090	12.610	12.680	12.280	11.310	9.880
4.0	10.380	11.630	12.355	12.680	12.700	12.500	11.710	10.380
5.0	10.955	11.980	12.510	12.700	12.700	12.600	11.980	10.730
6.0	11.415	12.240	12.600	12.700	12.700	12.630	12.140	11.010
7.0	11.750	12.400	12.660	12.700	12.700	12.650	12.600	11.240
8.0	12.030	12.520	12.690	12.700	12.700	12.660	12.350	11.440
9.0	12.240	12.600	12.700	12.700	12.700	12.670	12.400	11.600
9.5	12.320	12.640	12.700	12.700	12.700	12.685	12.420	11.680
10.0	12.400	12.650	12.700	12.700	12.700	12.695	12.450	11.760
11.0	12.520	12.680	12.700	12.700	12.700	12.700	12.490	11.910
12.0	12.610	12.700	12.700	12.700	12.700	12.700	12.530	12.060
13.0	12.670	12.700	12.700	12.700	12.700	12.700	12.570	12.200

Water line	Station 7	Station 7.5	Station 8	Station 8.5	Station 9	Station 9.25	Station 9.5	Station 9.75	Station 10
0.0	3.940	2.480	1.330	0.590	0.250	0.190	0.150	0.150	0.000
0.5	5.520	4.000	2.780	1.920	1.420	1.200	1.100	1.000	0.660
1.0	6.340	4.750	3.400	2.480	1.880	1.670	1.490	1.320	1.050
2.0	7.420	5.700	4.180	3.010	2.280	2.000	1.770	1.570	1.340
3.0	8.140	6.330	4.700	3.340	2.390	2.020	1.750	1.520	1.320
4.0	8.670	6.860	5.110	3.580	2.400	1.950	1.600	1.360	1.100
5.0	9.100	7.280	5.450	3.780	2.390	1.860	1.450	1.160	0.820
6.0	9.460	7.660	5.790	3.990	2.420	1.800	1.320	0.950	0.560
7.0	9.800	8.040	6.100	4.210	2.520	1.830	1.270	0.800	0.350
8.0	10.100	8.380	6.450	4.480	2.700	1.950	1.300	0.740	0.200
9.0	10.380	8.760	6.810	4.820	2.970	2.160	1.400	0.800	0.100
9.5	10.510	8.920	7.020	5.200	3.150	2.310	1.560	0.870	0.000
10.0	10.660	9.110	7.240	5.240	3.360	2.490	1.700	0.960	0.110
11.0	10.930	9.500	7.710	5.770	3.870	2.440	2.070	1.230	0.280
12.0	11.210	9.900	8.250	6.400	4.480	3.510	2.550	1.610	0.540
13.0	11.480	10.340	8.830	7.100	5.200	4.200	3.160	2.120	0.890

Table 4.3 (cont'd)

Water line	Station 0	Station 0.25	Station 0.5	Station 0.75	Station 1	Station 1.5	Station 2	Station 2.5
14.0	5.830	7.310	8.620	9.740	10.650	11.920	12.500	12.660
15.0	6.440	7.930	9.220	10.280	11.150	12.240	12.650	12.700
Upper Deck S.L.	6.800	8.250	9.500	10.540	11.350	12.340	12.580	12.700
Bulwark Top	7.350	8.830	10.050	11.030	11.750	12.540	12.700	12.700
17.0								
18.0								
19.0								
F'CLE DK S.L.								
Shell Top S.K.L.								
Bowchock Top								
WL								

Table 4.3 (cont'd)

Water line	Station 3	Station 3.5	Station 4	Station 4.5	Station 5	Station 5.5	Station 6	Station 6.5
14.0	12.700	12.700	12.700	12.700	12.700	12.700	12.610	12.360
15.0	12.700	12.700	12.700	12.700	12.700	12.700	12.650	12.510
Upper Deck S.L.	12.700	12.700	12.700	12.700	12.700	12.700	12.670	12.570
Bulwark Top	12.700	12.700	12.700	12.700	12.700	12.700	12.700	12.700
17.0								
18.0								
19.0								
F'CLE DK S.L.								
Shell Top S.K.L.								
Bowchock Top								
WL								

Table 4.3 (cont'd)

Water line	Station 7	Station 7.5	Station 8	Station 8.5	Station 9	Station 9.25	Station 9.5	Station 9.75	Station 10
14.0	11.760	10.780	9.470	7.870	6.000	4.970	3.890	2.760	1.350
15.0	12.050	11.260	10.150	8.700	6.880	5.830	4.700	3.500	1.920
Upper Deck S.L.	12.170	11.480	10.500	9.170	7.460	6.440	5.330	4.140	2.490
Bulwark Top	12.470	12.010	11.300						
17.0				10.490	8.820	7.750	6.580	5.260	3.400
18.0				11.440	9.870	8.850	7.630	6.270	4.290
19.0							8.750	7.350	5.280
F'CLE DK S.L.				11.850	10.660	9.820	8.810	7.600	5.700
Shell Top S.K.L.				1.196	1.074	0.990	0.890	0.770	5.800
Bowchock Top								0.789	6.170
WL									

Table 4.3 (cont'd)

Water line	Station 0	Station 0.25	Station 0.5	Station 0.75	Station 1	Station 1.5	Station 2	Station 2.5
E	8.800	8.170	0.000					
0.5 BL	8.980	8.270	0.000					
1 BL	9.170	8.460	5.830	1.370	0.530	0.130	0.000	
2 BL	9.800	8.900	7.820	5.500	2.420	0.650	0.220	0.300
3 BL	10.600	9.460	8.550	7.130	5.250	1.620	0.600	0.160
Upper DK C.L.	15.900	15.900	15.900	15.900	15.900	15.900	15.900	15.900
Upper DK S.L.	15.650	15.590	15.560	15.490	15.450	15.410	15.400	15.400
Bolwarf Top	16.750	16.690	16.660	16.590	16.550	16.410	16.500	16.500
F'CLE DK C.C.								
F'CLE DK S.L.								
Shell Top F.L.								
BowChock Top								

Table 4.3 (cont'd)

Water line	Station 3	Station 3.5	Station 4	Station 4.5	Station 5	Station 5.5	Station 6	Station 6.5
E								
0.5 BL								
1 BL								
2 BL								
3 BL	0.600							
Upper DK C.L.	15.900	15.900	15.900	15.900	15.900	15.900	15.900	15.900
Upper DK S.L.	15.400	15.400	15.400	15.400	15.400	15.400	15.405	15.410
Bolwarf Top	16.500	16.500	16.500	16.500	16.500	16.500	16.505	16.510
F'CLE DK C.C.								
F'CLE DK S.L.								
Shell Top F.L.								
BowChock Top								

Table 4.3 (cont'd)

Water line	Station 7	Station 7.5	Station 8	Station 8.5	Station 9	Station 9.25	Station 9.5	Station 9.75	Station 10
E									9.500
0.5 BL				0.000	0.500	0.700	0.100	0.130	6.220
1 BL			0.000	0.600	0.220	0.300	0.380		13.230
2 BL		0.300	0.130	0.570	1.220		10.830	12.780	15.120
3 BL	0.600	0.120	0.660	1.960	9.050	11.100	12.730	14.330	16.320
Upper DK C.L.	15.900	15.900	15.900	15.900	15.900	15.900	15.900	15.900	15.900
Upper DK S.L.	15.420	15.460	15.500	15.560	15.620	15.670	15.710	15.760	0.830
Bolwarf Top	16.520	16.560	16.600	16.660	16.720	16.770	16.810	16.860	1.930
F'CLE DK C.C.				18.900	16.499	16.499	16.499	16.499	19.500
F'CLE DK S.L.				18.450	18.730	18.890			19.440
Shell Top F.L.				18.550	18.830	18.990			19.540
BowChock Top				19.550	19.830	19.990			20.540

	0.4 Hz	0.6 Hz	0.8 Hz	1.0 Hz	1.2Hz	1.4 Hz
0.4 volts	0.7587 cm	1.1300 cm	1.1812 cm	1.2257 cm	1.1664 cm	1.0125 cm
0.8 volts	1.3156 cm	2.2336 cm	2.4447 cm	2.7666 cm	2.4470 cm	2.1018 cm
1.0 volts	1.5683 cm	2.6953 cm	2.8734 cm	3.2154 cm	3.0361 cm	2.6772 cm
1.2 volts	1.9672 cm	3.3574 cm	3.6105 cm	4.0004 cm	3.5978 cm	3.1628 cm
1.6 volts	2.6375 cm	4.5545 cm	4.8695 cm	5.1897 cm	4.5914 cm	4.1183 cm
1.8 volts	3.2590 cm	4.9060 cm	5.3345 cm	5.3731 cm	4.9945 cm	4.3200 cm
2.0 volts	3.3638 cm	5.2792 cm	6.6355 cm	5.7882 cm	5.5491 cm	4.4072 cm
3.0 volts	4.8416 cm	8.5293 cm	8.6531 cm			
4.0 volts	5.7286 cm	9.5754 cm	10.9065 cm			

Table 4.5 Error measurement for heave amplitude

Test 1	Test 2	Test 3	n	Mean	Error 1	Error 2	Error 3	Mean error	Error in %
0.446	0.669	0.537	3	0.551	0.190	0.215	0.025	0.143	14.3
0.593	0.470	0.563	3	0.542	0.094	0.133	0.039	0.089	8.9
0.632	0.508	0.594	3	0.578	0.093	0.121	0.028	0.081	8.1
0.611	0.666	0.609	3	0.629	0.028	0.059	0.031	0.040	4.0
0.411	0.641	0.658	3	0.570	0.279	0.125	0.154	0.186	18.6
0.588	0.653	0.612	3	0.618	0.048	0.057	0.009	0.038	3.8
0.563	0.614	0.589	3	0.589	0.044	0.043	0.001	0.029	2.9
0.583	0.596	0.578	3	0.586	0.005	0.018	0.013	0.012	1.2
0.604	0.556	0.537	3	0.566	0.068	0.017	0.051	0.045	4.5
0.465	0.514	0.514	3	0.498	0.066	0.033	0.033	0.044	4.4
0.232	0.410	0.409	3	0.350	0.338	0.170	0.167	0.225	22.5
0.480	0.355	0.401	3	0.412	0.165	0.138	0.027	0.110	11.0
0.390	0.335	0.350	3	0.358	0.088	0.065	0.023	0.059	5.9
0.252	0.255	0.257	3	0.255	0.010	0.001	0.009	0.007	0.7
0.179	0.195	0.182	3	0.185	0.034	0.052	0.018	0.035	3.5
0.157	0.132	0.117	3	0.135	0.160	0.025	0.135	0.107	10.7
0.083	0.084	0.089	3	0.085	0.027	0.016	0.043	0.029	2.9
0.045	0.045	0.050	3	0.047	0.036	0.036	0.071	0.048	4.8
0.031	0.028	0.026	3	0.028	0.094	0.012	0.082	0.063	6.3
0.031	0.031	0.023	3	0.028	0.094	0.094	0.188	0.125	12.5
0.041	0.033	0.037	3	0.037	0.108	0.108	0.000	0.072	7.2

n is the number of measured heave amplitude
Error 1 is the error obtained from test 1
Error 2 is the error obtained from test 2
Error 3 is the error obtained from test 3

Table 4.6 Error measurement for pitch amplitude

Test 1	Test 2	Test 3	n	Mean	Error 1	Error 2	Error 3	Mean error	Error in %
0.418	0.670	0.468	3	0.519	0.194	0.292	0.098	0.195	19.5
0.583	0.400	0.544	3	0.509	0.145	0.214	0.069	0.143	14.3
0.599	0.390	0.567	3	0.519	0.155	0.248	0.093	0.165	16.5
0.572	0.610	0.564	3	0.582	0.017	0.048	0.031	0.032	3.2
0.419	0.510	0.572	3	0.500	0.163	0.019	0.143	0.108	10.8
0.587	0.600	0.567	3	0.585	0.004	0.026	0.030	0.020	2.0
0.551	0.540	0.527	3	0.539	0.022	0.001	0.023	0.015	1.5
0.585	0.520	0.495	3	0.533	0.097	0.025	0.072	0.065	6.5
0.544	0.480	0.462	3	0.495	0.098	0.031	0.067	0.066	6.6
0.447	0.450	0.450	3	0.449	0.004	0.002	0.002	0.003	0.3
0.300	0.350	0.384	3	0.345	0.130	0.015	0.114	0.086	8.6
0.404	0.370	0.399	3	0.391	0.033	0.054	0.020	0.036	3.6
0.416	0.360	0.376	3	0.384	0.083	0.063	0.021	0.056	5.6
0.291	0.300	0.287	3	0.293	0.006	0.025	0.019	0.017	1.7
0.225	0.240	0.232	3	0.232	0.032	0.033	0.001	0.022	2.2
0.208	0.180	0.167	3	0.185	0.124	0.027	0.097	0.083	8.3
0.126	0.130	0.134	3	0.130	0.031	0.000	0.031	0.021	2.1
0.086	0.090	0.097	3	0.091	0.055	0.011	0.066	0.044	4.4
0.059	0.060	0.062	3	0.060	0.022	0.006	0.028	0.018	1.8
0.032	0.030	0.036	3	0.033	0.020	0.082	0.102	0.068	6.8
0.022	0.020	0.017	3	0.020	0.119	0.017	0.136	0.090	9.0

n is the number of measured pitch amplitude
Error 1 is the error obtained from test 1
Error 2 is the error obtained from test 2
Error 3 is the error obtained from test 3

Table 4.7 Error measurement for vertical relative motion amplitude

Test 1	Test 2	Test 3	n	Mean	Error 1	Error 2	Error 3	Mean error	Error in %
0.278	0.350	0.485	3	0.371	0.251	0.057	0.307	0.205	20.5
0.321	0.370	0.348	3	0.346	0.073	0.068	0.005	0.049	4.9
0.534	0.490	0.539	3	0.521	0.025	0.060	0.035	0.040	4.0
0.554	0.550	0.625	3	0.576	0.039	0.046	0.084	0.056	5.6
0.595	0.590	0.757	3	0.647	0.081	0.089	0.169	0.113	11.3
0.790	0.820	0.864	3	0.825	0.042	0.006	0.048	0.032	3.2
0.875	0.910	0.917	3	0.901	0.028	0.010	0.018	0.019	1.9
0.984	0.890	0.968	3	0.947	0.039	0.061	0.022	0.040	4.0
1.132	0.960	1.009	3	1.034	0.095	0.071	0.024	0.063	6.3
0.810	0.940	0.912	3	0.887	0.087	0.059	0.028	0.058	5.8
0.820	0.870	0.907	3	0.866	0.053	0.005	0.048	0.035	3.5
0.857	1.230	1.375	3	1.154	0.257	0.066	0.192	0.172	17.2
1.743	1.550	1.885	3	1.726	0.010	0.102	0.092	0.068	6.8
1.361	1.360	1.547	3	1.423	0.043	0.044	0.087	0.058	5.8
1.322	1.320	1.602	3	1.415	0.066	0.067	0.132	0.088	8.8
1.467	1.260	1.490	3	1.406	0.044	0.104	0.060	0.069	6.9
1.106	1.150	1.362	3	1.206	0.083	0.046	0.129	0.086	8.6
1.029	1.080	1.301	3	1.137	0.095	0.050	0.145	0.096	9.6
1.019	0.950	1.138	3	1.036	0.016	0.083	0.099	0.066	6.6
0.896	0.900	0.901	3	0.899	0.003	0.001	0.002	0.002	0.2
0.938	0.760	0.840	3	0.846	0.109	0.102	0.007	0.072	7.2

n is the number of measured vertical relative motion
Error 1 is the error obtained from test 1
Error 2 is the error obtained from test 2
Error 3 is the error obtained from test 3

Table 4.8 Error measurement for impact pressure (psi)

Pressure from test 1	Pressure from test 2	Pressure from test 3	n	Mean	Error 1	Error 2	Error 3	Mean error	Error in %
0.214	0.330	0.170	3	0.238	0.101	0.387	0.286	0.258	25.8
0.495	0.300	0.340	3	0.378	0.308	0.207	0.101	0.206	20.6
0.214	0.220	*	2	0.217	0.014	0.014	*	0.014	1.4
0.252	0.270	0.360	3	0.294	0.143	0.082	0.224	0.150	15.0
0.146	0.340	*	2	0.243	0.399	0.399	*	0.399	39.9
0.224	0.280	*	2	0.252	0.111	0.111	*	0.111	11.1
*	0.280	0.360	2	0.320	*	0.125	0.125	0.125	12.5
0.347	0.330	*	2	0.338	0.027	0.024	*	0.025	2.5
0.203	*	0.280	2	0.242	0.161	*	0.157	0.159	15.9
*	0.250	0.370	2	0.310	*	0.194	0.194	0.194	19.4
0.409	0.220	*	2	0.315	0.298	0.302	*	0.300	30.0
*	0.270	0.250	2	0.260	*	0.038	0.038	0.038	3.8

n is the number of measured pressures
Error 1 is the error obtained from test 1
Error 2 is the error obtained from test 2
Error 3 is the error obtained from test 3

Fig. 4.1 Body plan for the S175 container ship

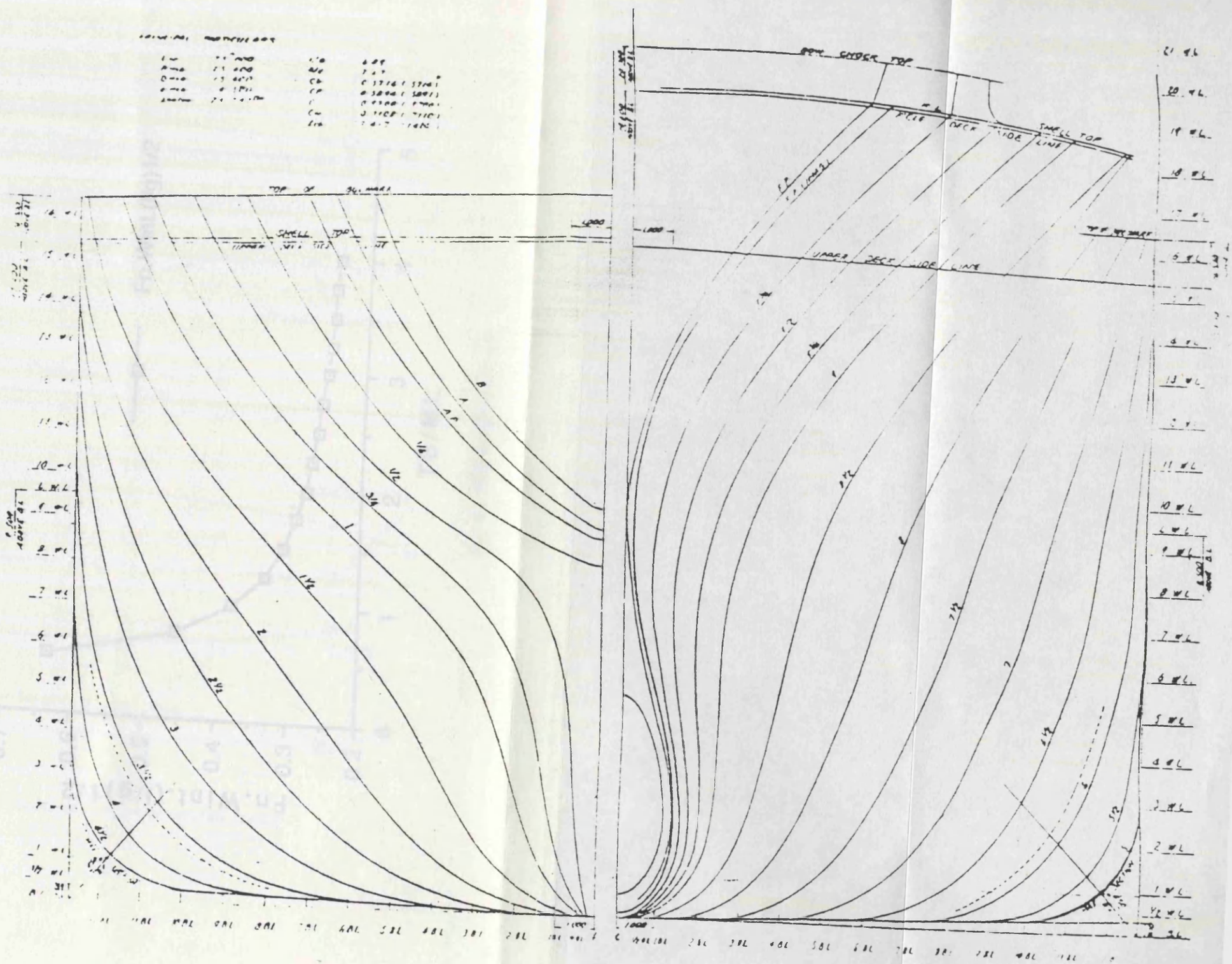

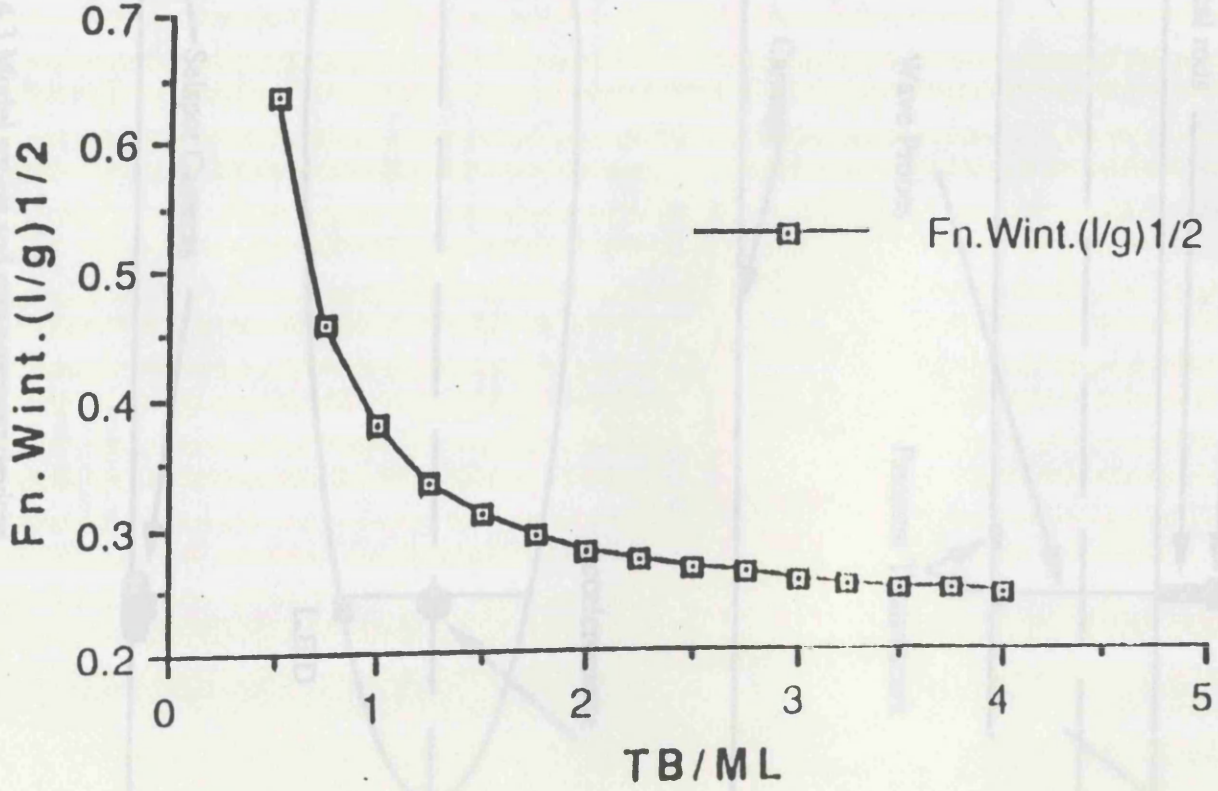

Fig. 4.2 Blockage phenomenon

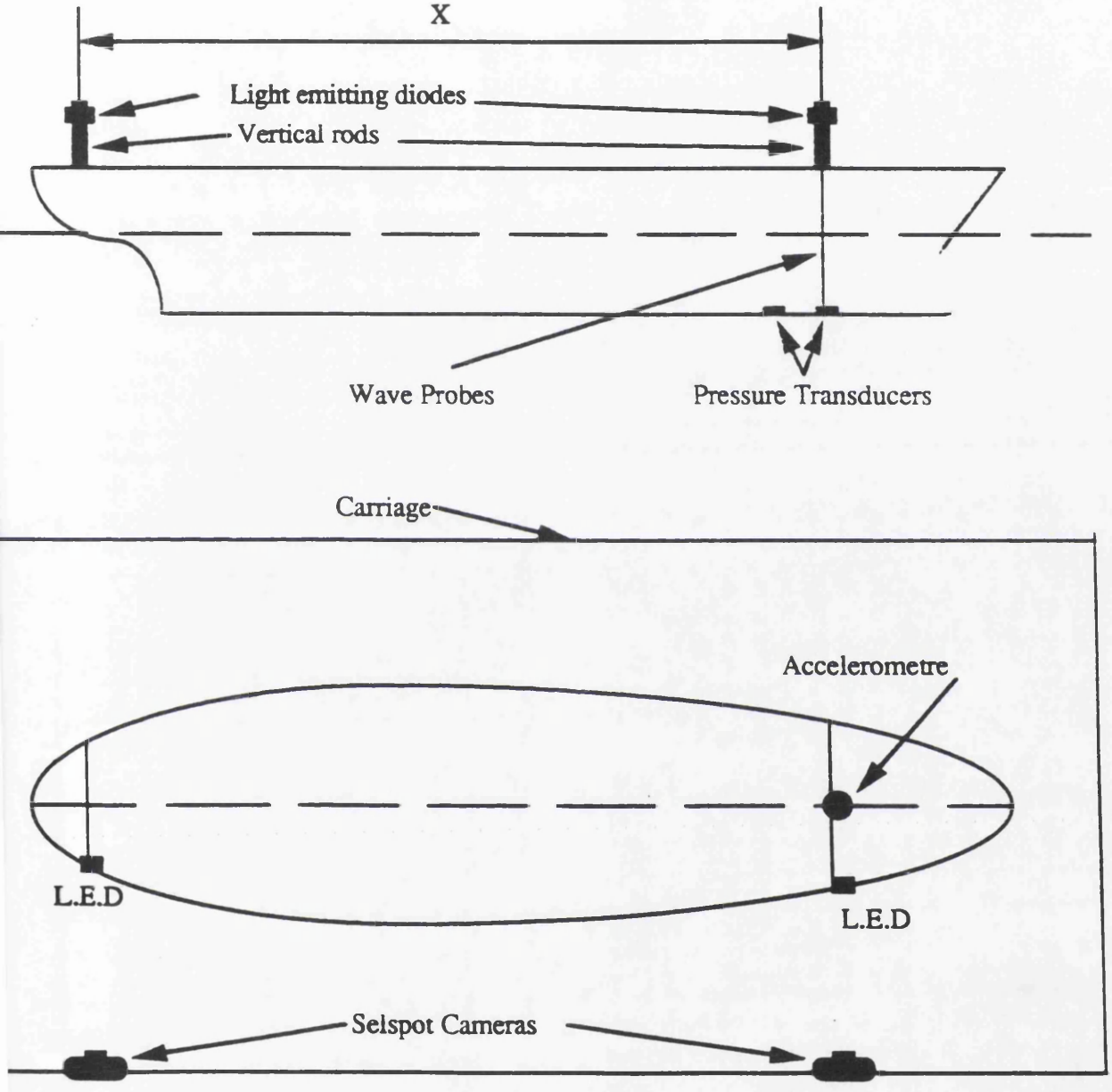

Fig. 4.3 Model set-up and measurement devices

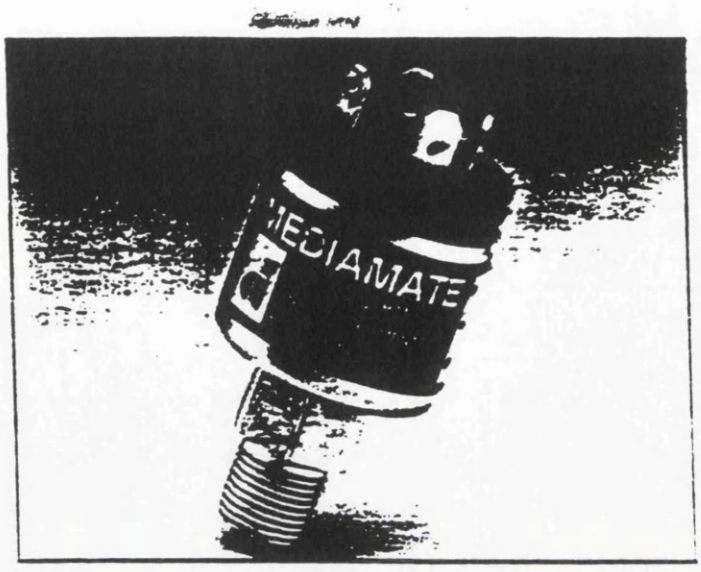

DIMENSIONS

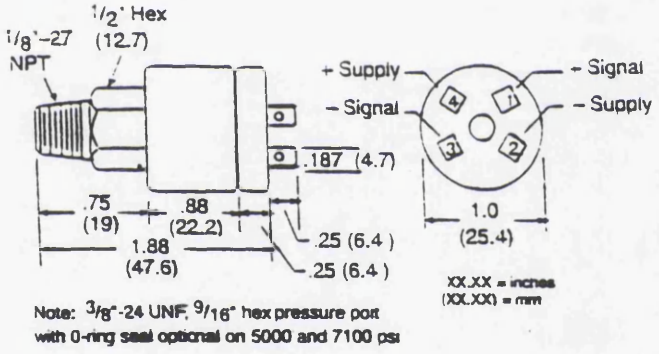

Mediamate

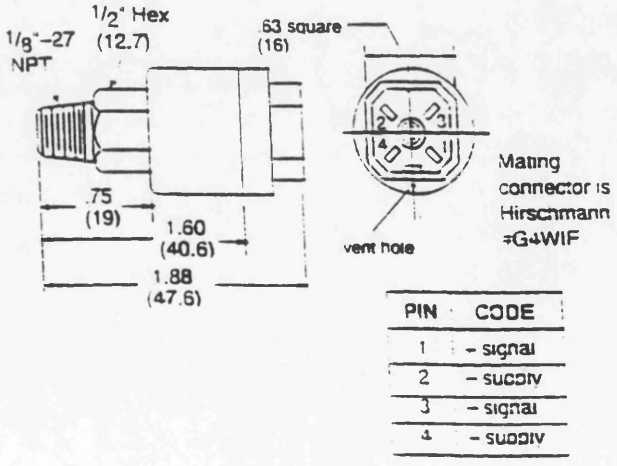

PIN	CODE
1	– signal
2	– supply
3	– signal
4	– supply

Fig. 4.4 Mediamate pressure transducer

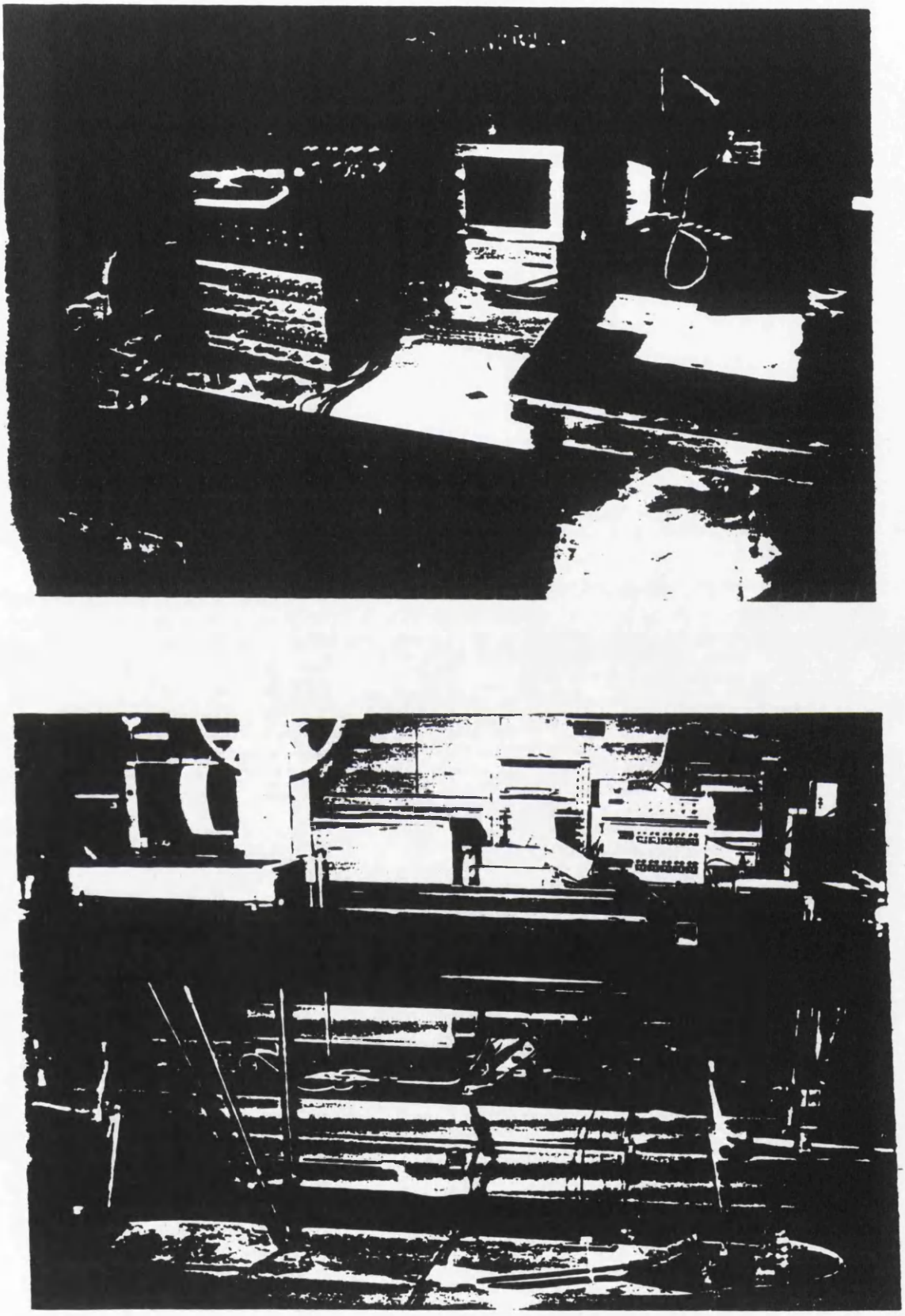

Fig. 4.5 Electronic equipment on the carriage

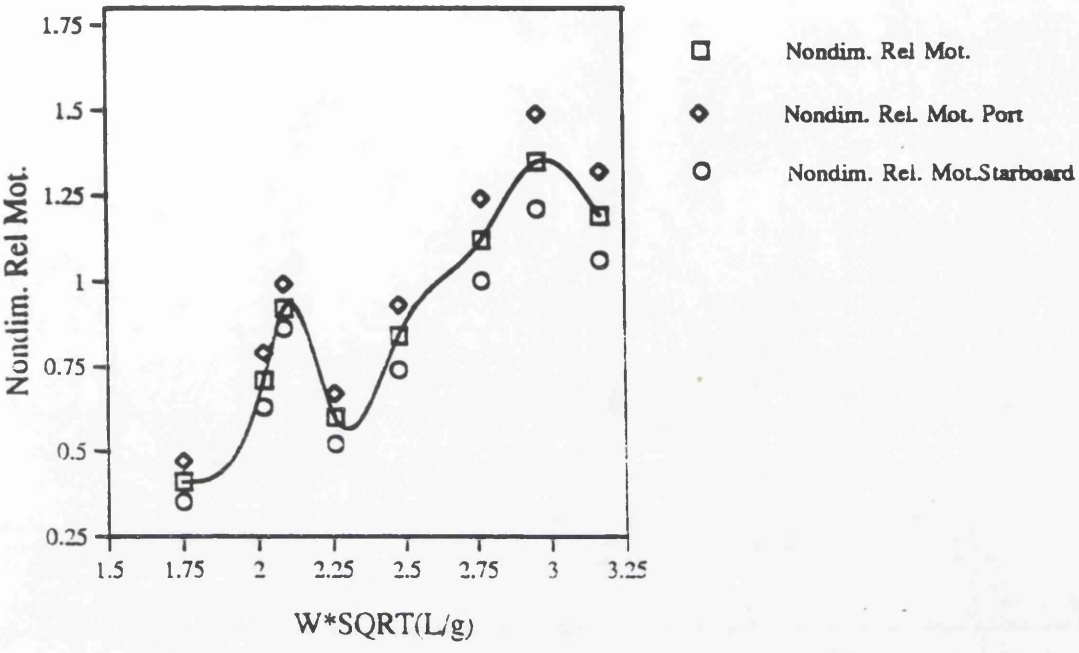

Fig. 4.6 Nondimensional relative motion at station 8 1/2 for loaded draught, Fr=0.1

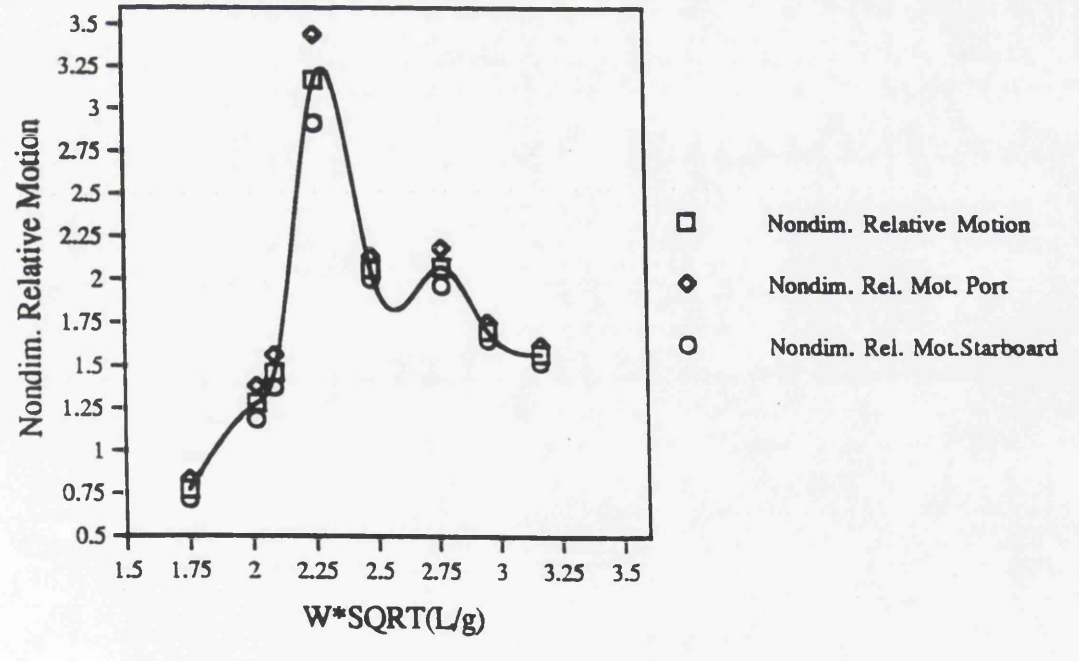

Fig. 4.7 Nondimensional relative motion at station 8 1/2 for ballast draught, Fr=0.1

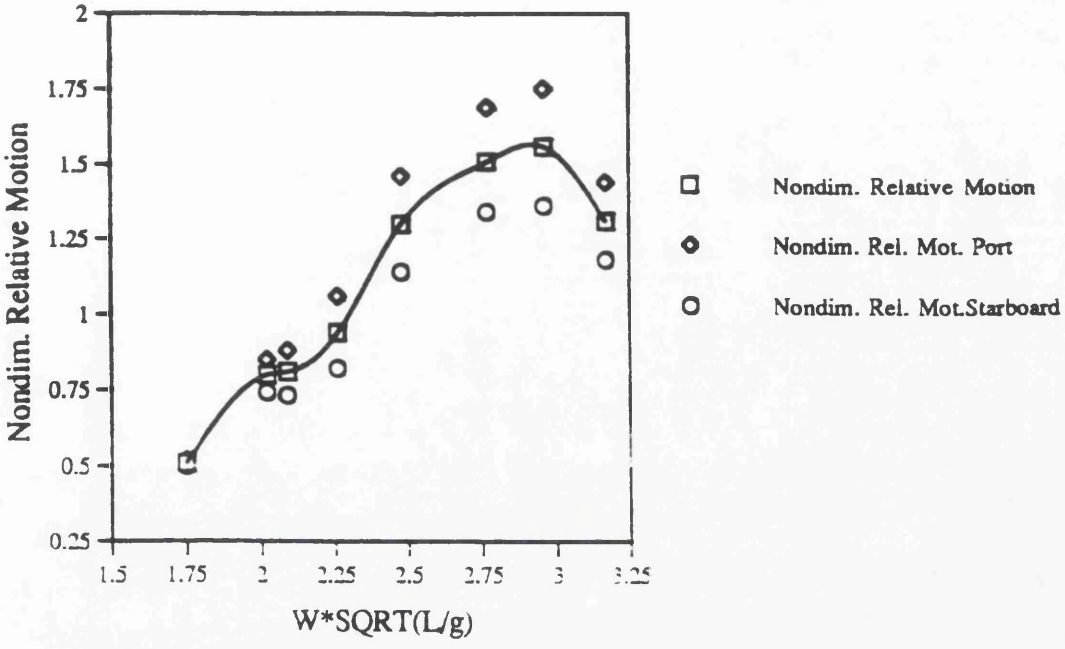

Fig. 4.8 Nondimensional relative motion at station 8 1/2 for loaded draught, Fr=0.15

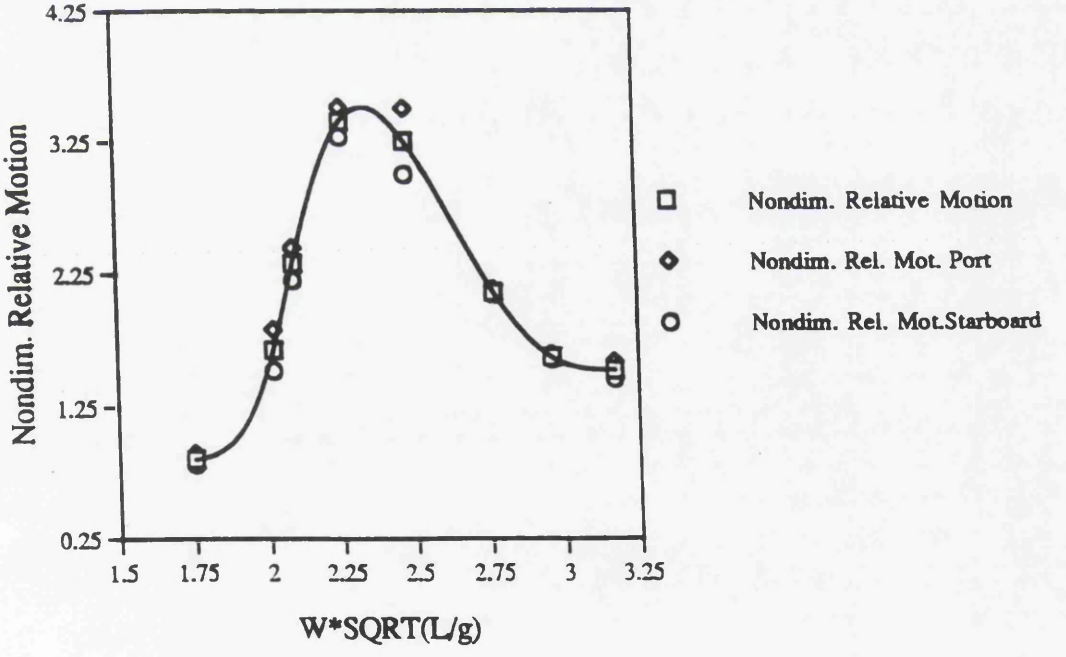

Fig. 4.9 Nondimensional relative motion at station 8 1/2 for ballast draught, Fr=0.15

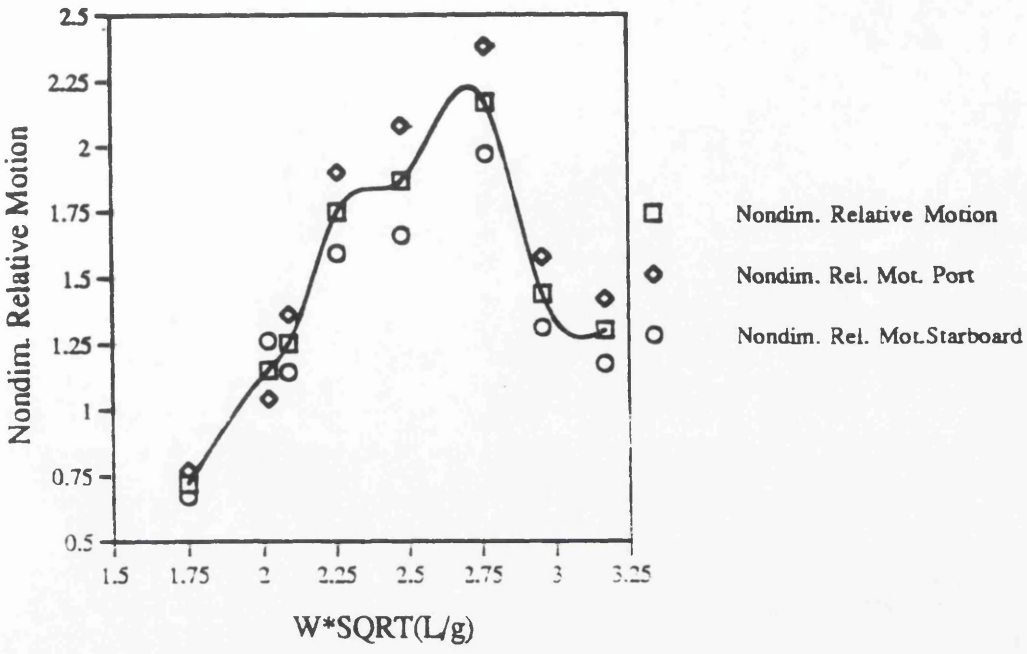

Fig. 4.10 Nondimensional relative motion at station 8 1/2 for loaded draught, Fr=0.2

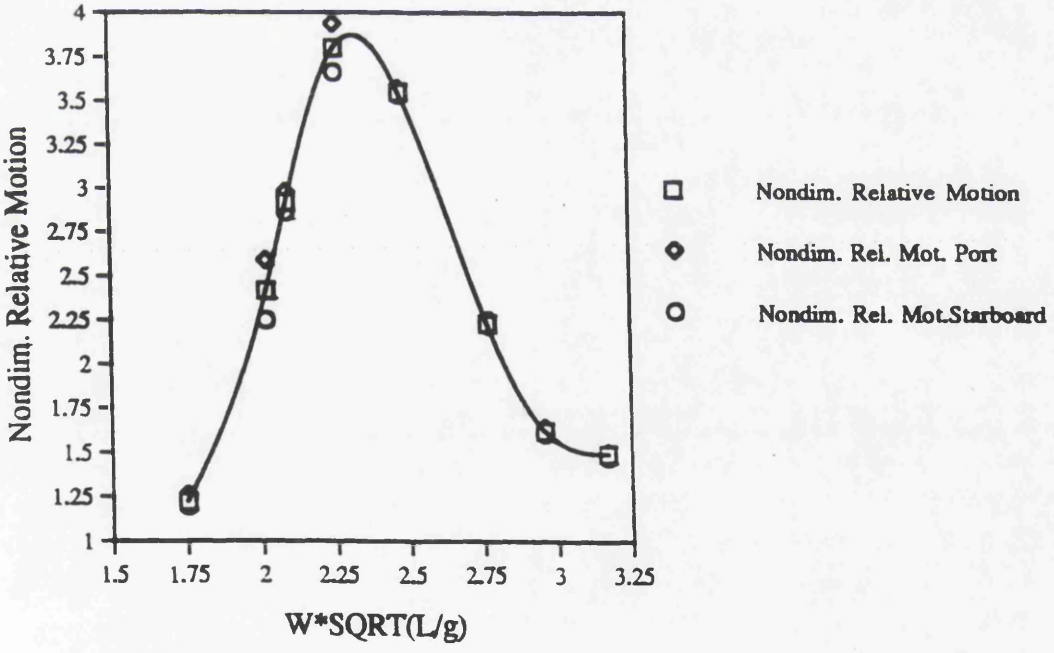

Fig. 4.11 Nondimensional relative motion at station 8 1/2 for ballast draught, Fr=0.2

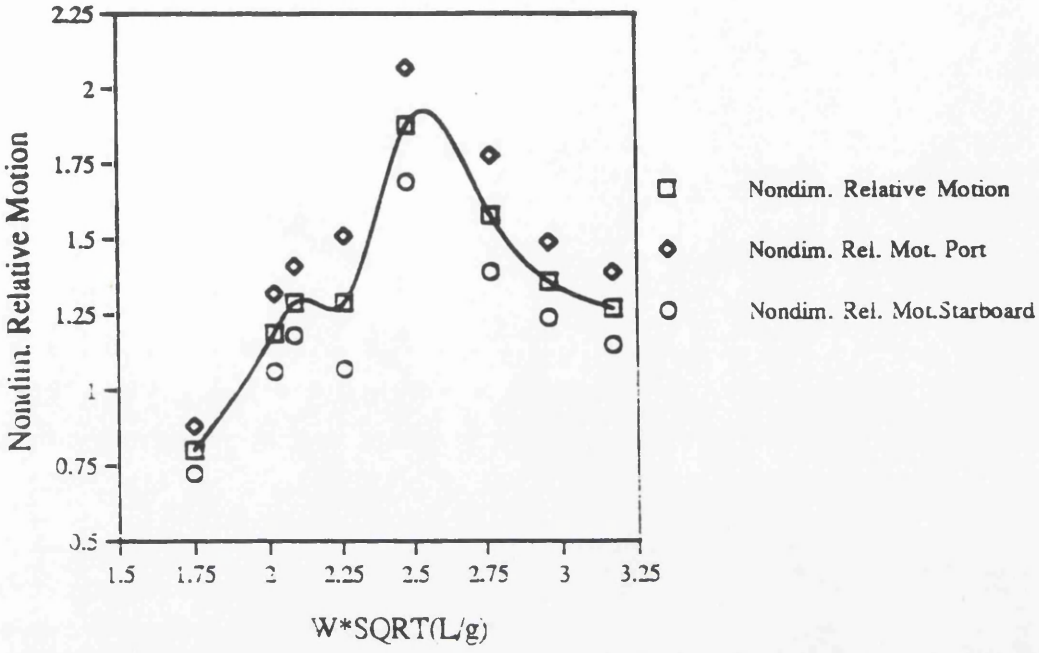

Fig. 4.12 Nondimensional relative motion at station 8 1/2 for loaded draught, Fr=0.278

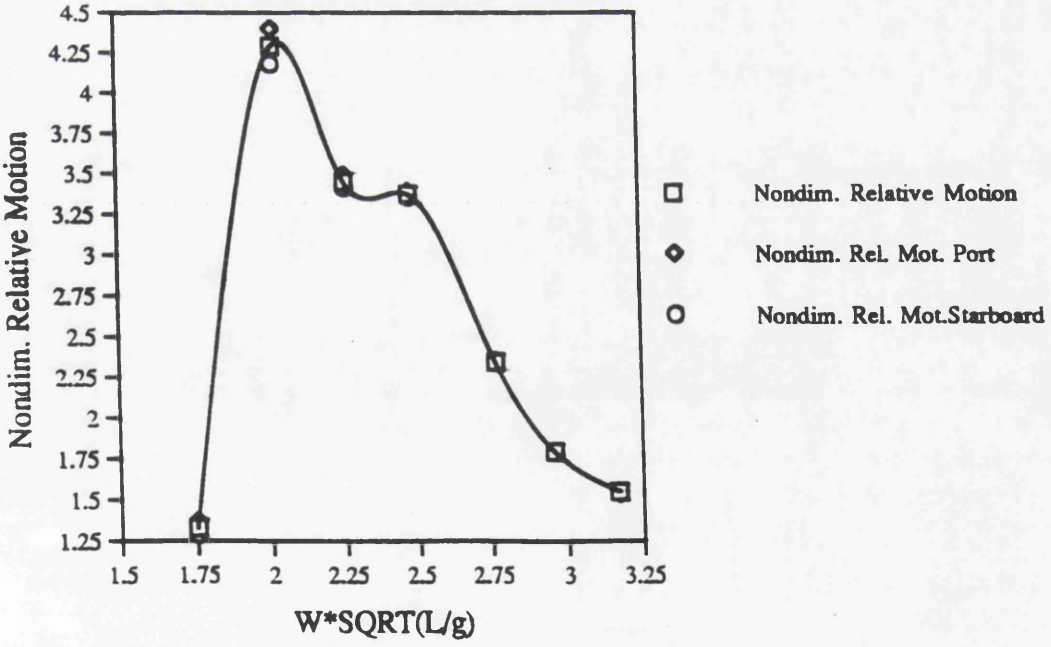

Fig. 4.13 Nondimensional relative motion at station 8 1/2 for ballast draught, Fr=0.278

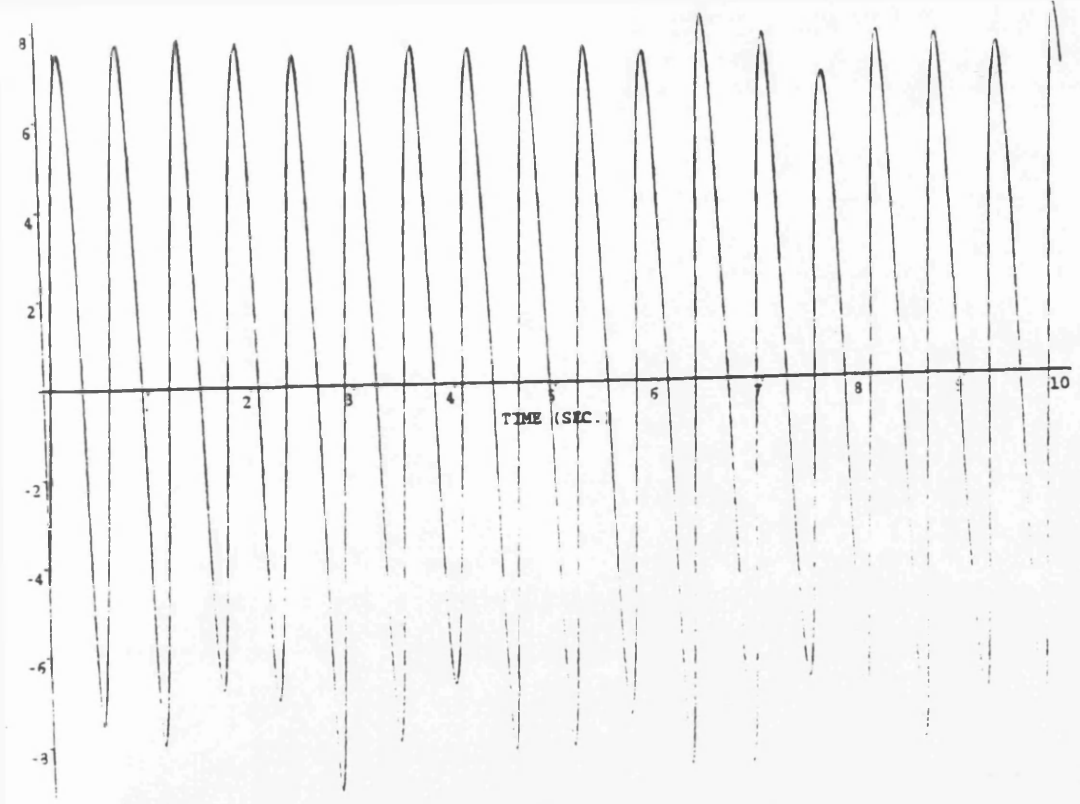

Fig. 4.14 Time history of vertical relative motion at starboard side at station 8 1/2 for f=0.95 Hz and Fr=0.275

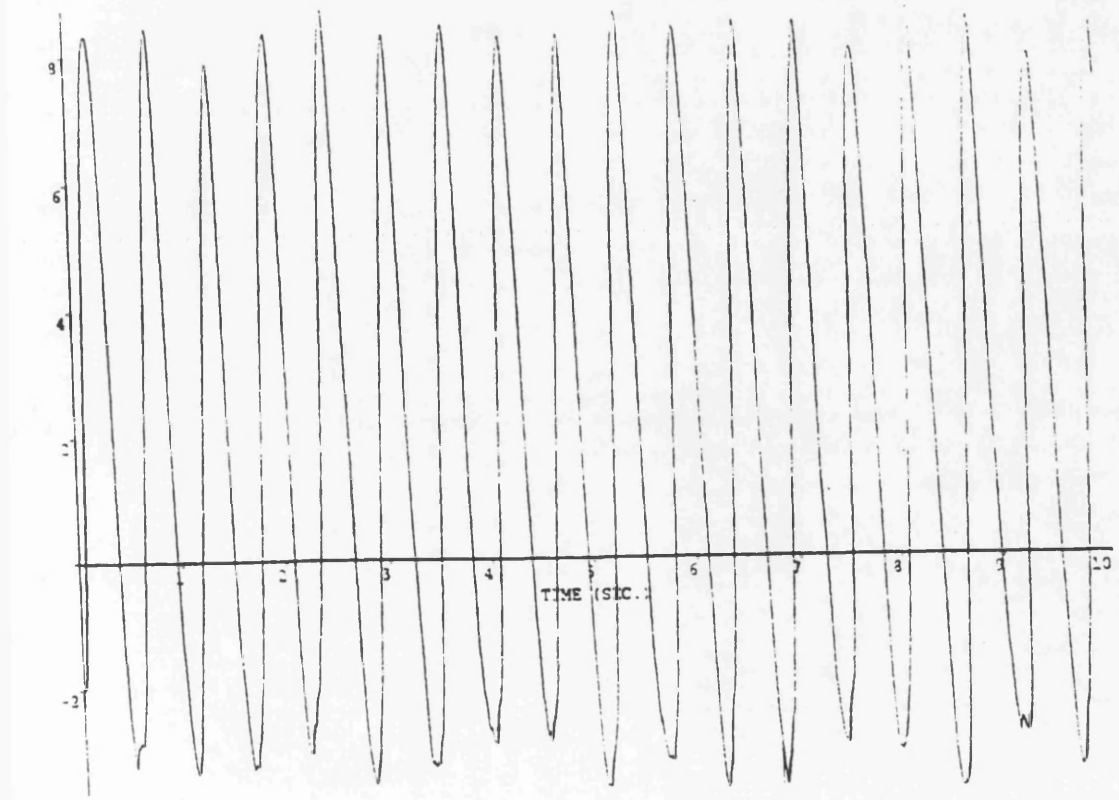

Fig. 4.15 Time history of vertical relative motion at port side at station 8 1/2 for f=0.95 Hz and Fr=0.275

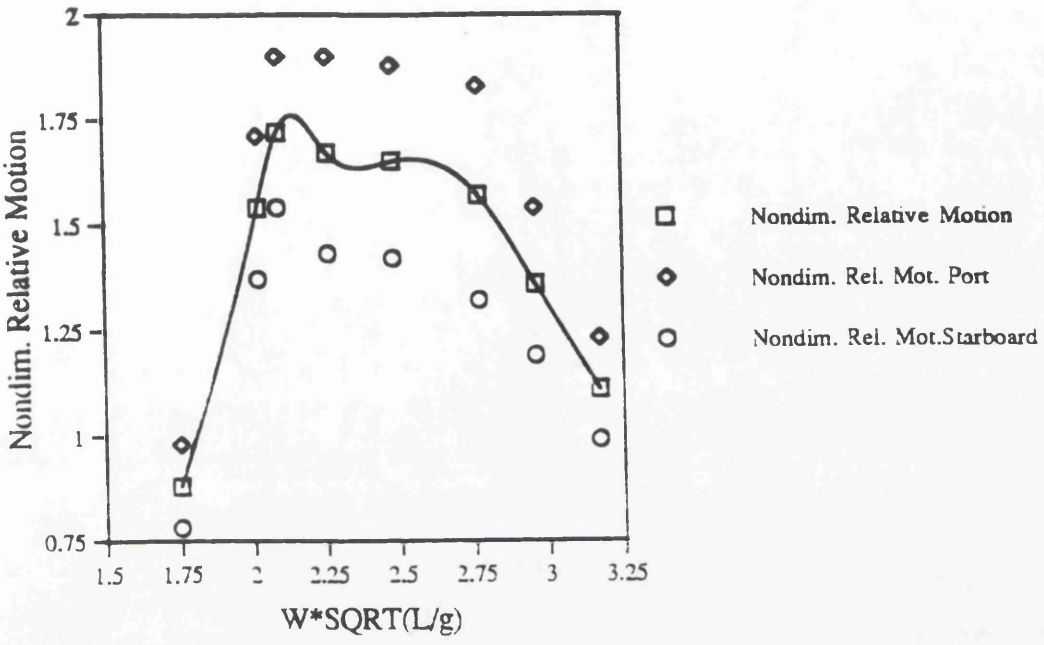

Fig. 4.16 Nondimensional relative motion at station 8 1/2
for loaded draught, Fr=0.3

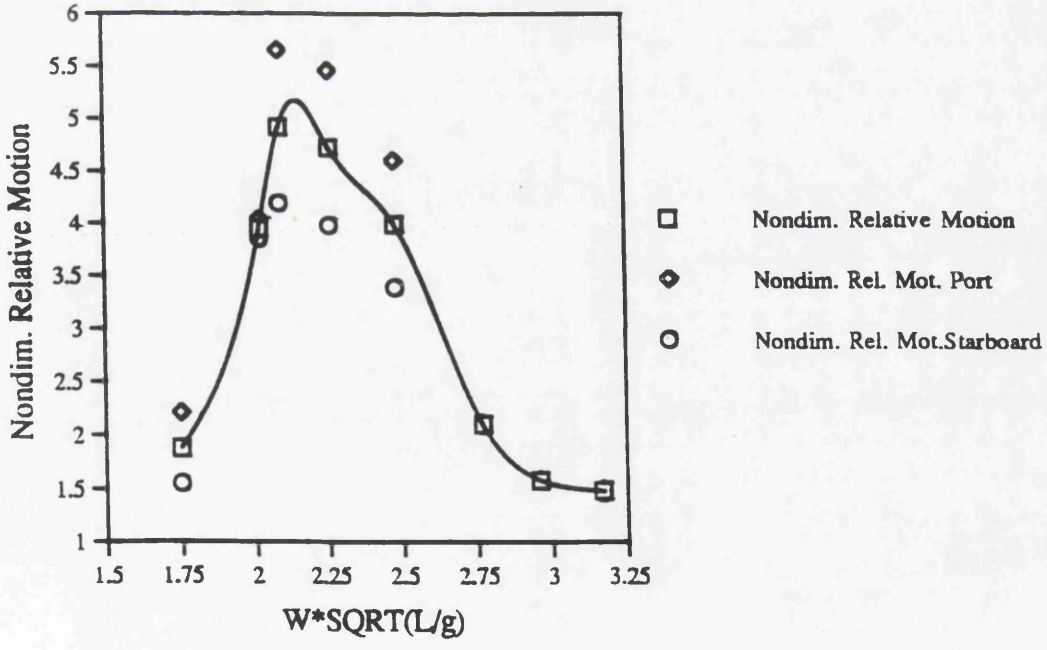

Fig. 4.17 Nondimensional relative motion at station 8 1/2
for ballast draught, Fr=0.3

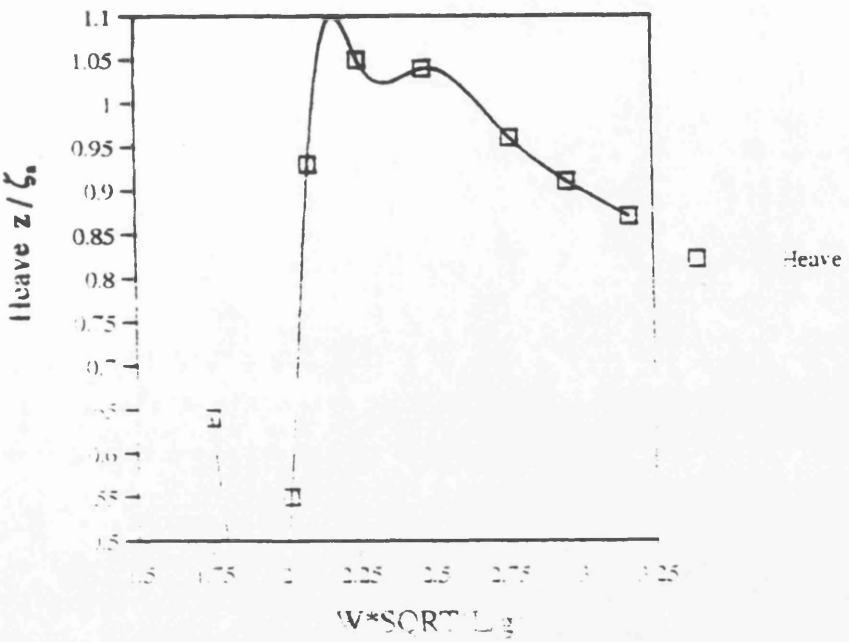

Fig. 4.18 Nondimensional heave amplitude for loaded draught at Fr=0.1

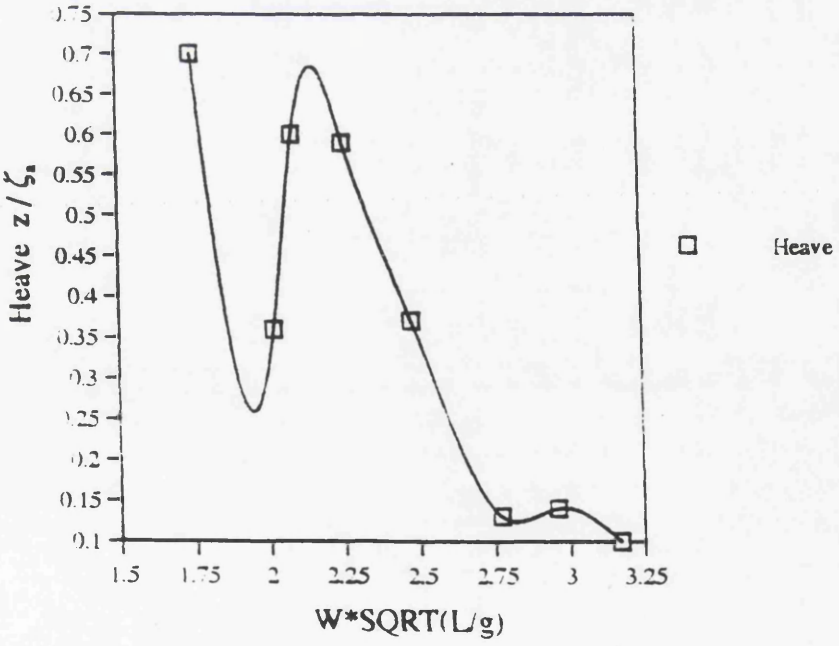

Fig. 4.19 Nondimensional heave amplitude for ballast draught at Fr=0.1

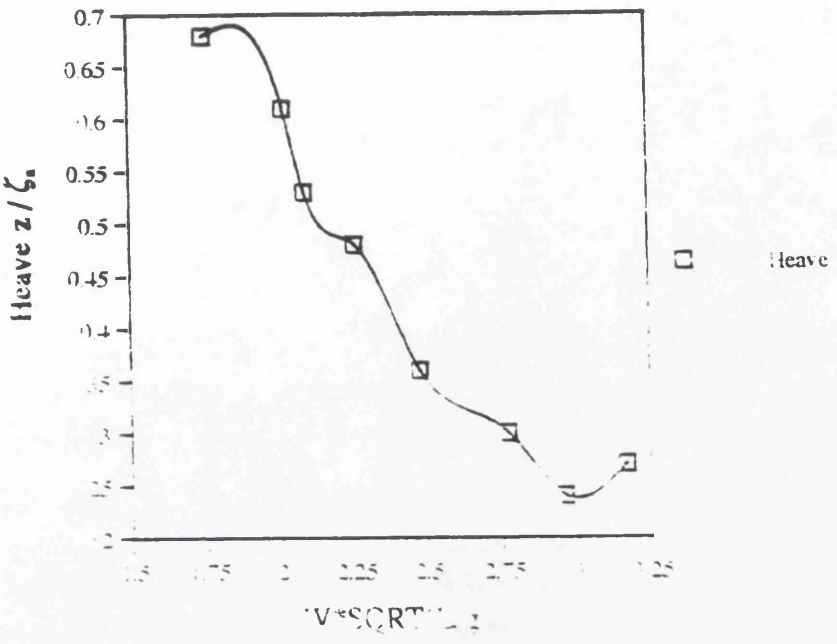

Fig. 4.20 Nondimensional heave amplitude for loaded draught at Fr=0.15

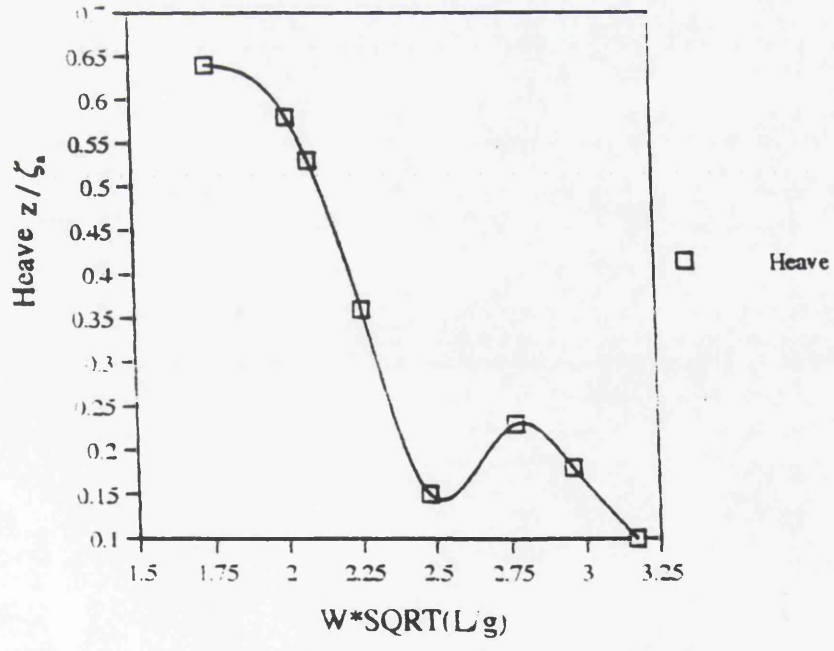

Fig. 4.21 Nondimensional heave amplitude for ballast draught at Fr=0.15

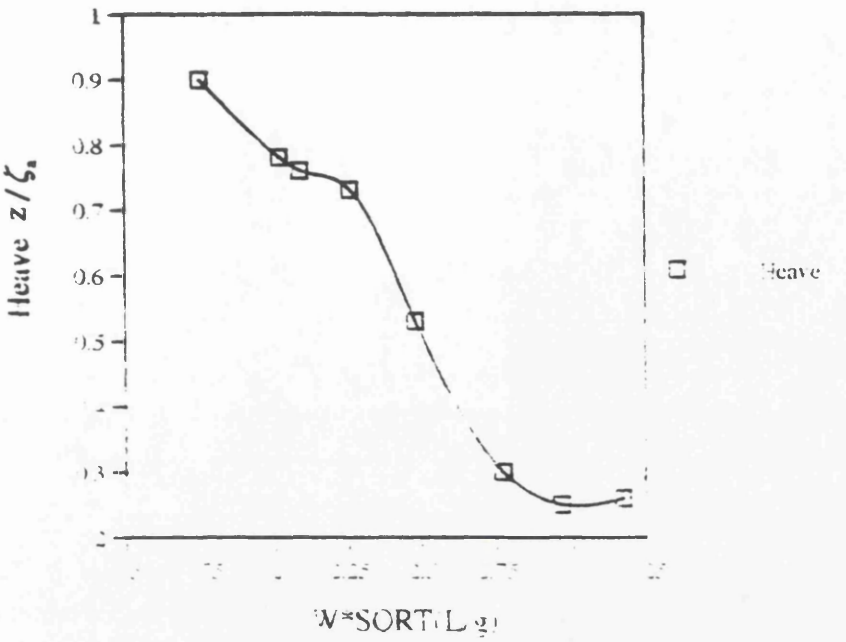

Fig. 4.22 Nondimensional heave amplitude for loaded draught at Fr=0.2

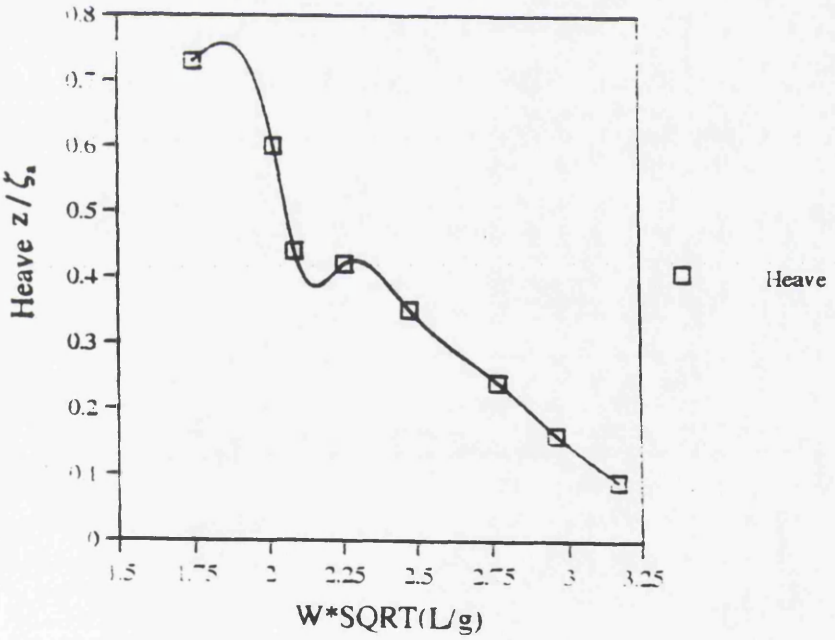

Fig. 4.23 Nondimensional heave amplitude for ballast draught at Fr=0.2

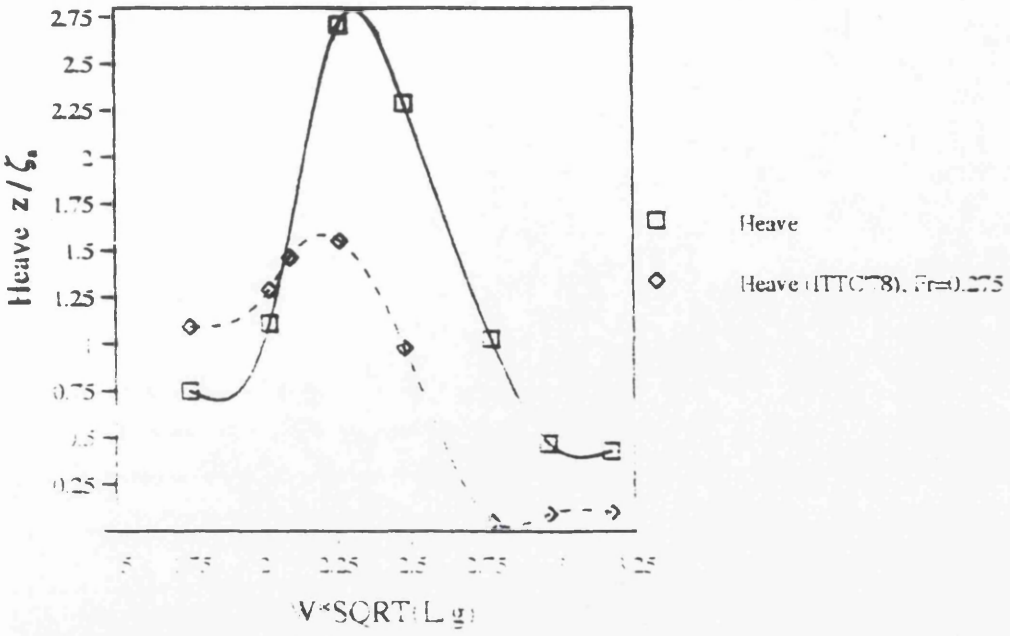

Fig. 4.24 Comparison of nondimensional heave amplitude obtained from experiment for loaded draught at Fr=0.278 and results given in ITTC'78 for Fr=0.275

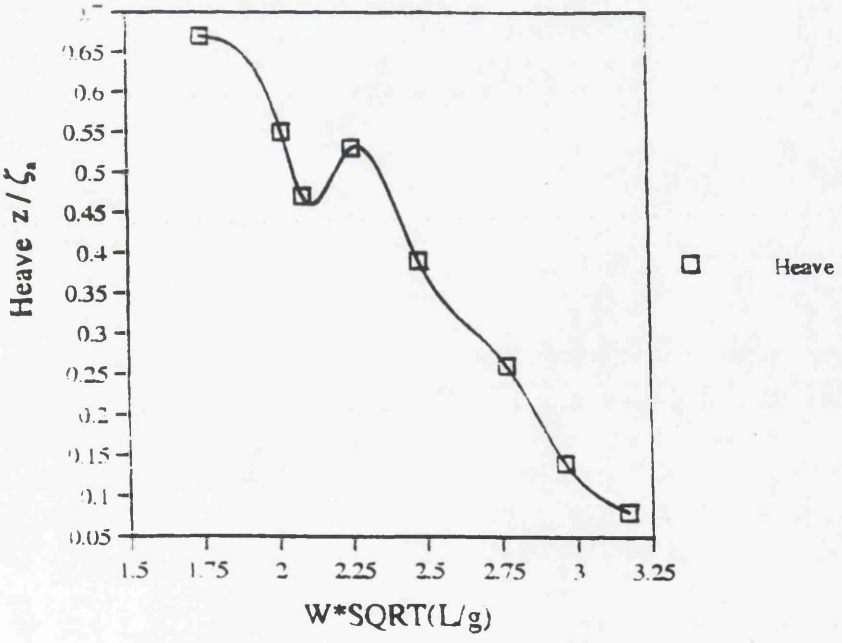

Fig. 4.25 Nondimensional heave amplitude for ballast draught at Fr=0.278

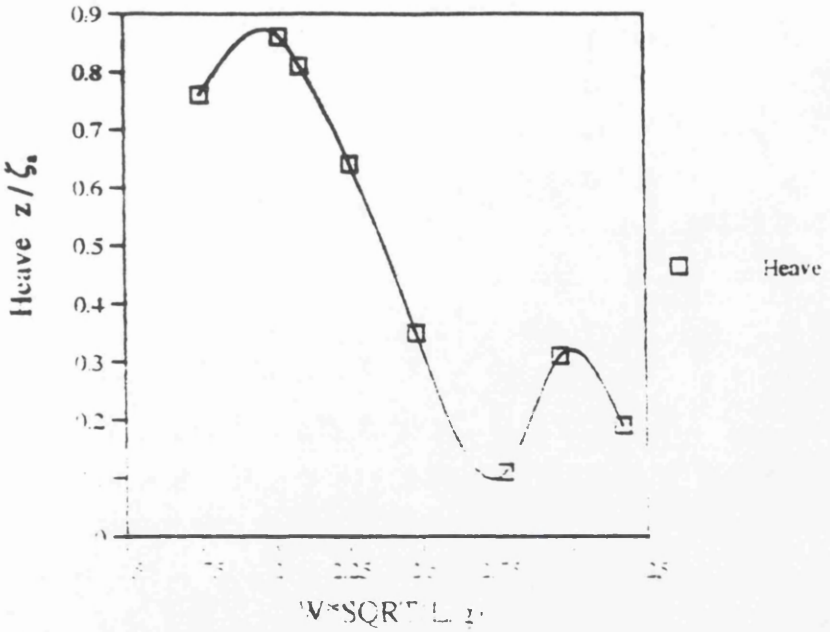

Fig. 4.26 Nondimensional heave amplitude for loaded draught at Fr=0.3

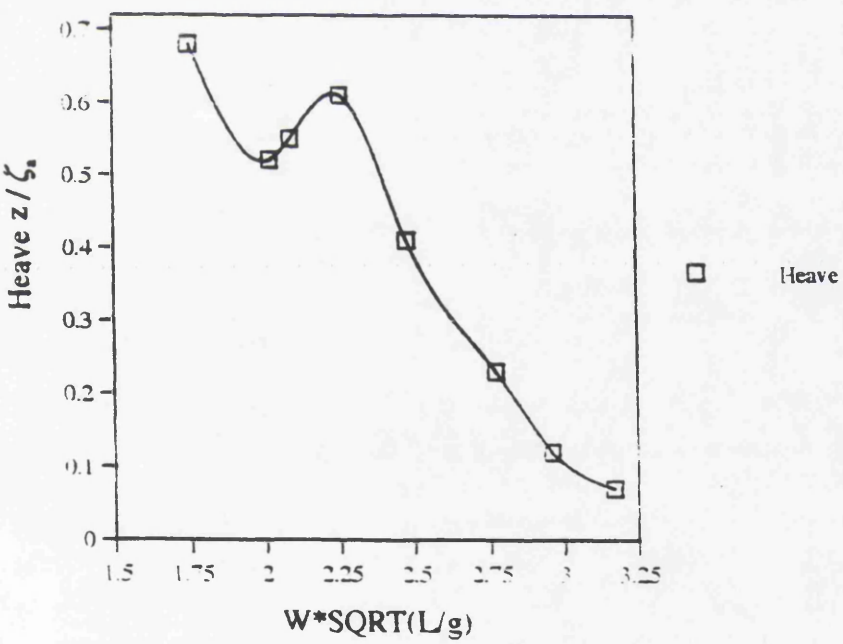

Fig. 4.27 Nondimensional heave amplitude for ballast draught at Fr=0.3

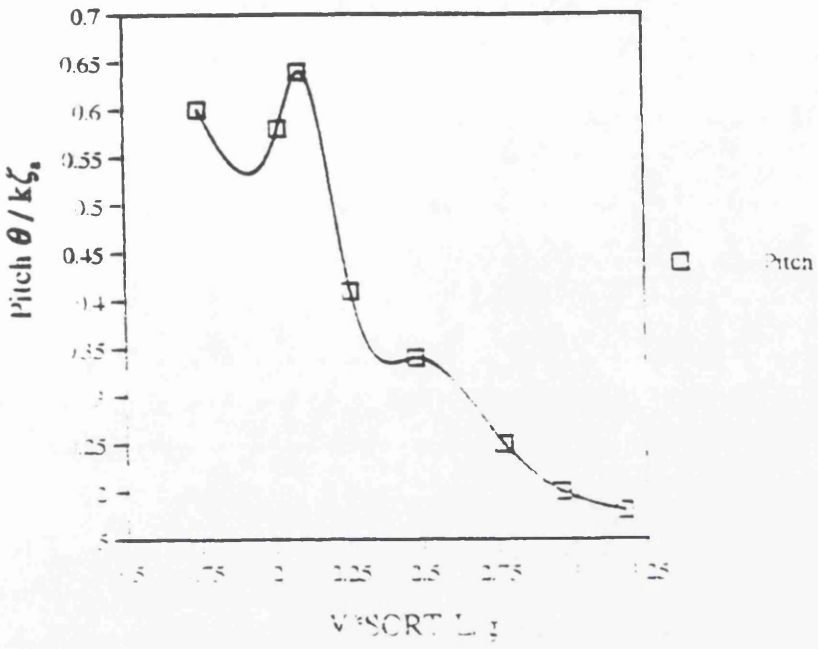

Fig. 4.28 Nondimensional pitch amplitude for loaded draught at Fr=0.1

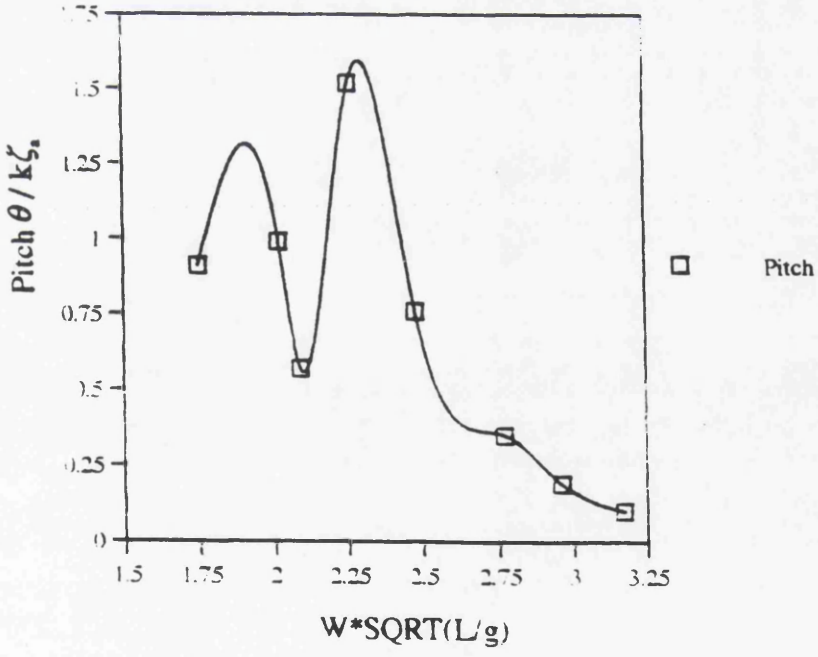

Fig. 4.29 Nondimensional pitch amplitude for ballast draught at Fr=0.1

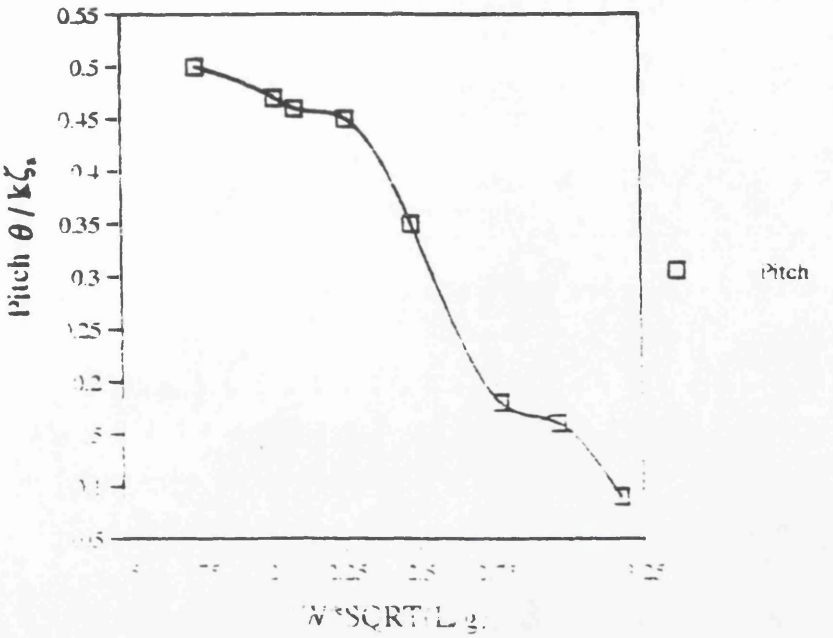

Fig. 4.30 Nondimensional pitch amplitude for loaded draught at Fr=0.15

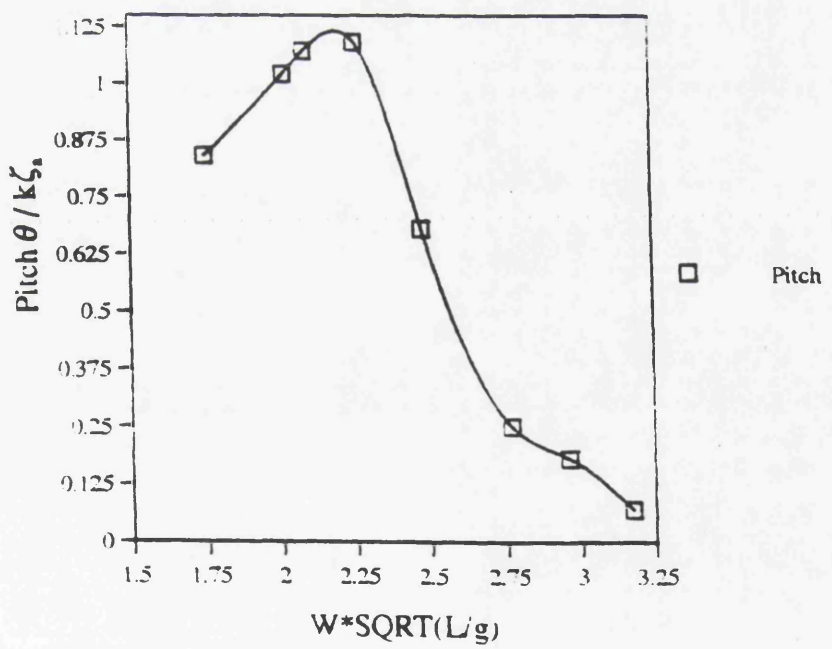

Fig. 4.31 Nondimensional pitch amplitude for ballast draught at Fr=0.15

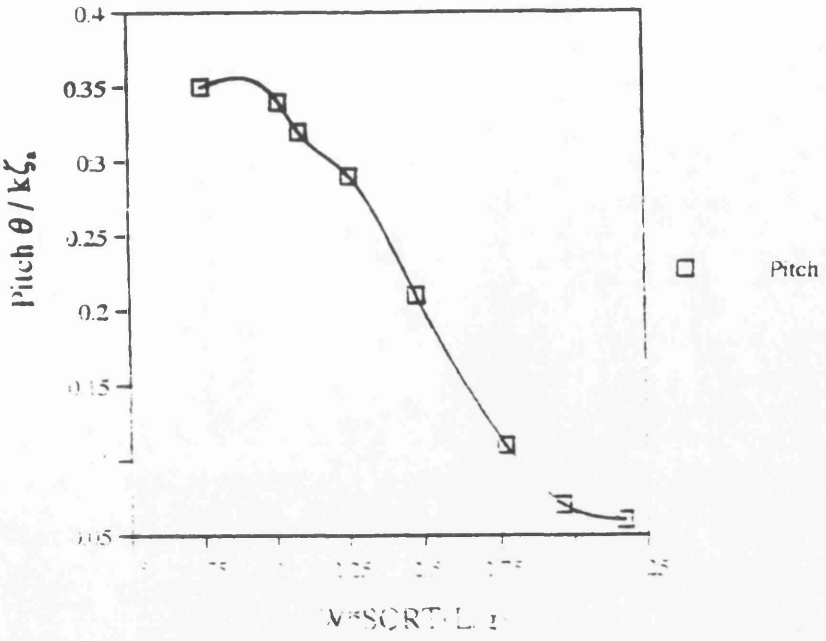

Fig. 4.32 Nondimensional pitch amplitude for loaded draught at Fr=0.2

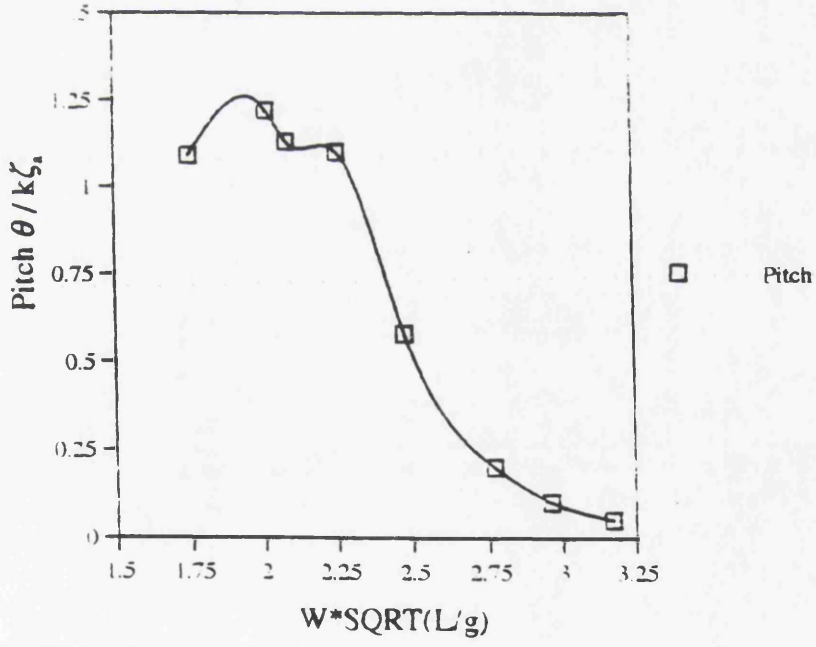

Fig. 4.33 Nondimensional pitch amplitude for ballast draught at Fr=0.2

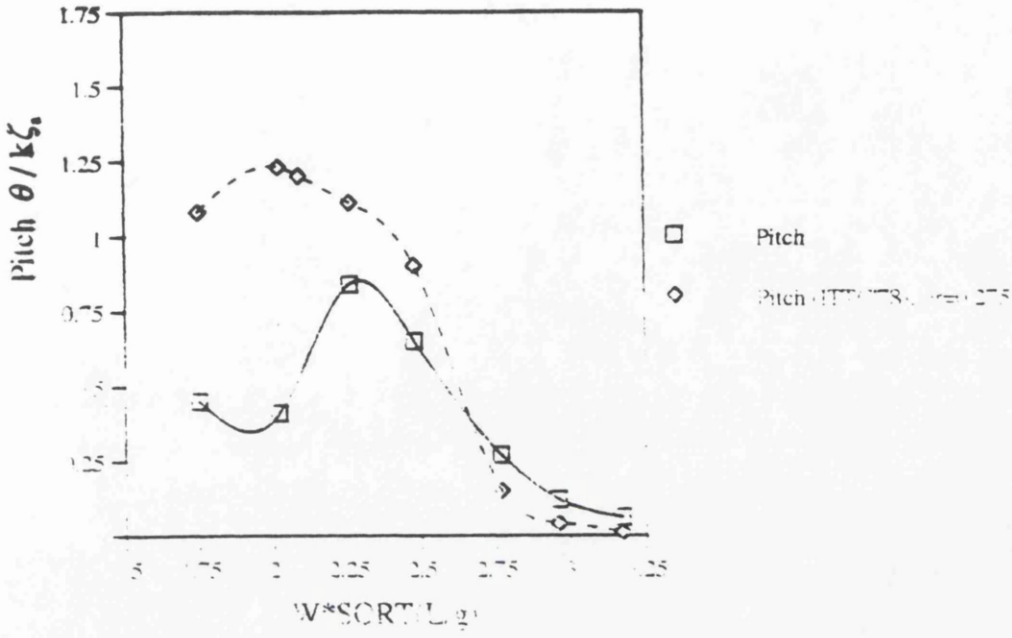

Fig. 4.34 Comparison of nondimensional pitch amplitude obtained from experiment for loaded draught at Fr=0.278 and results given in ITTC'78 for Fr=0.275

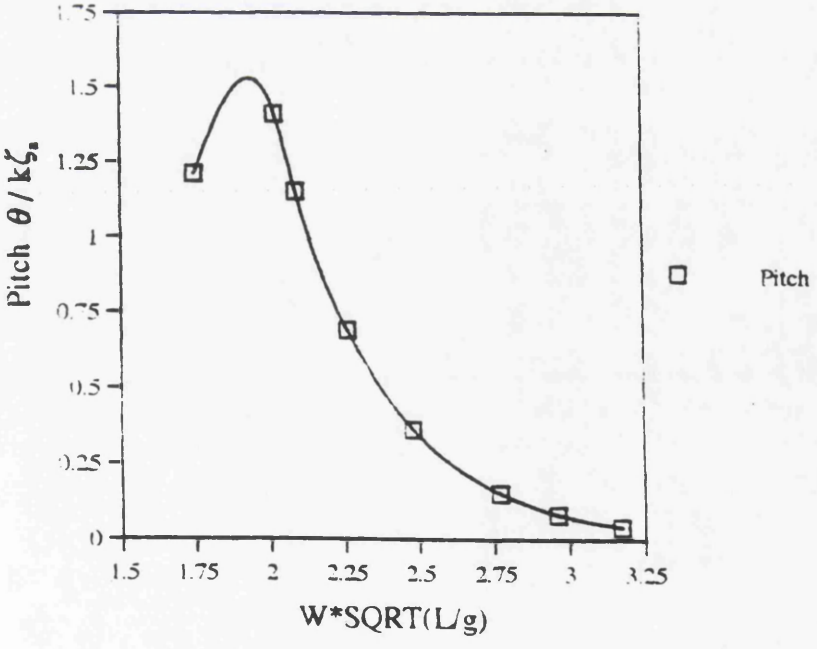

Fig. 4.35 Nondimensional pitch amplitude for ballast draught at Fr=0.278

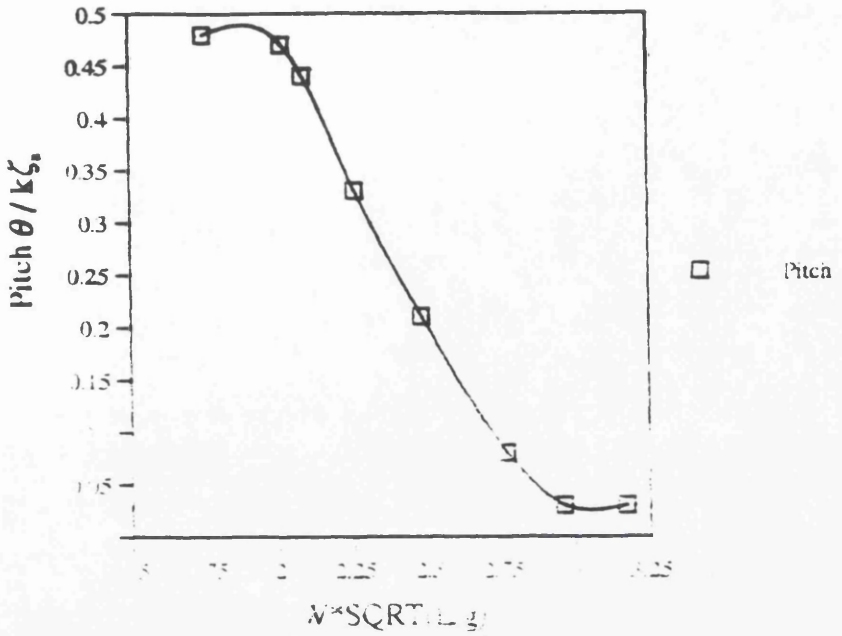

Fig. 4.36 Nondimensional pitch amplitude for loaded draught at Fr=0.3

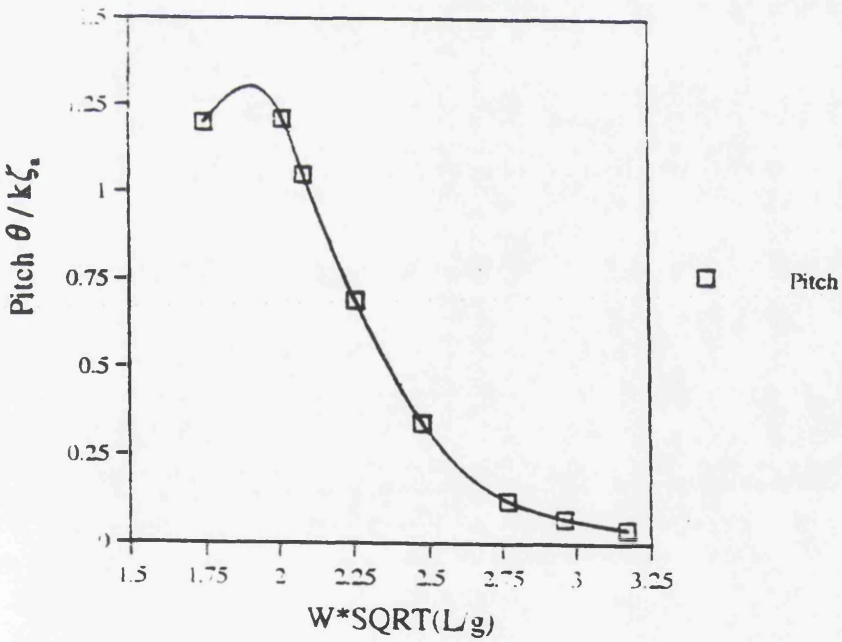

Fig. 4.37 Nondimensional pitch amplitude for ballast draught at Fr=0.3

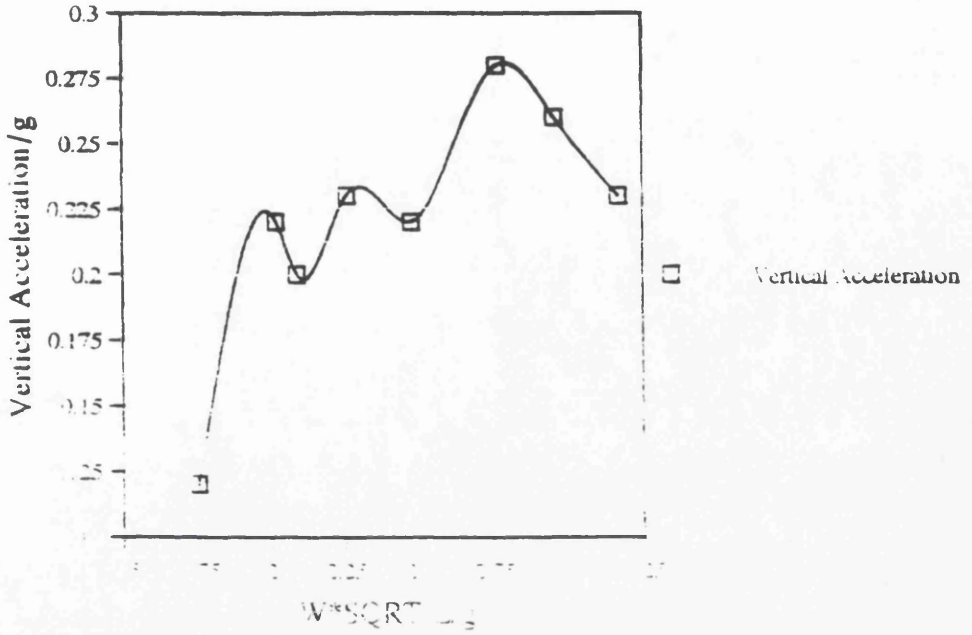

Fig. 4.38 Nondimensional vertical acceleration for loaded draught at Fr=0.1

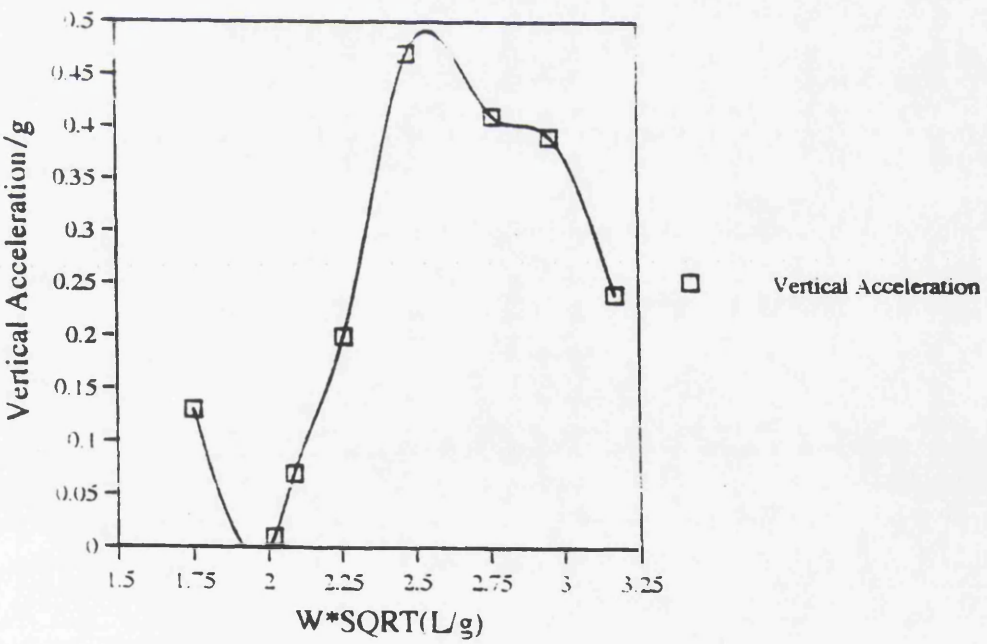

Fig. 4.39 Nondimensional vertical acceleration for ballast draught at Fr=0.1

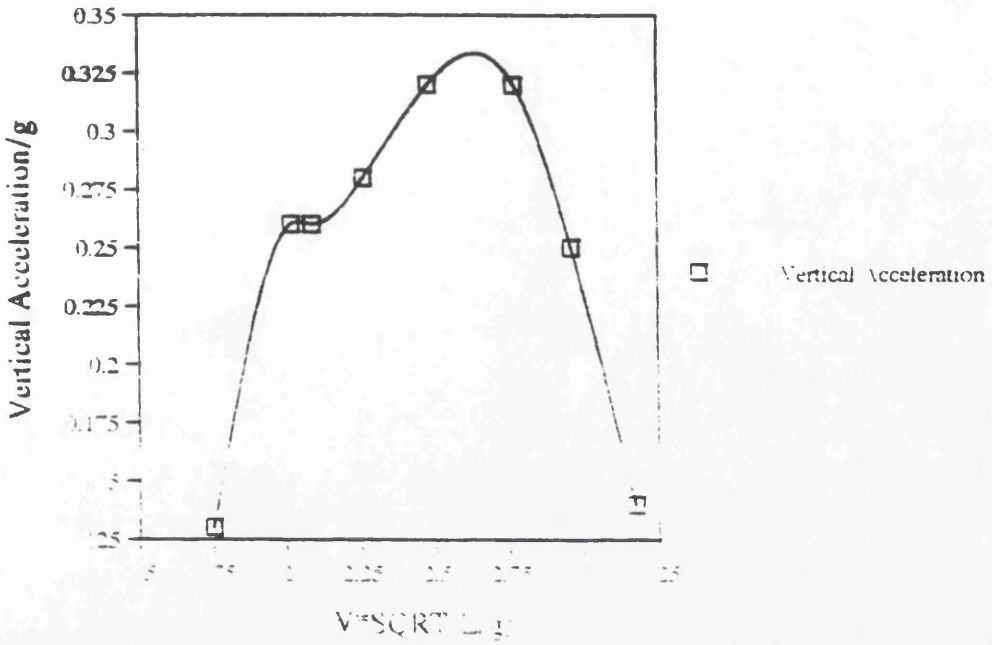

Fig. 4.40 Nondimensional vertical acceleration for loaded draught at Fr=0.15

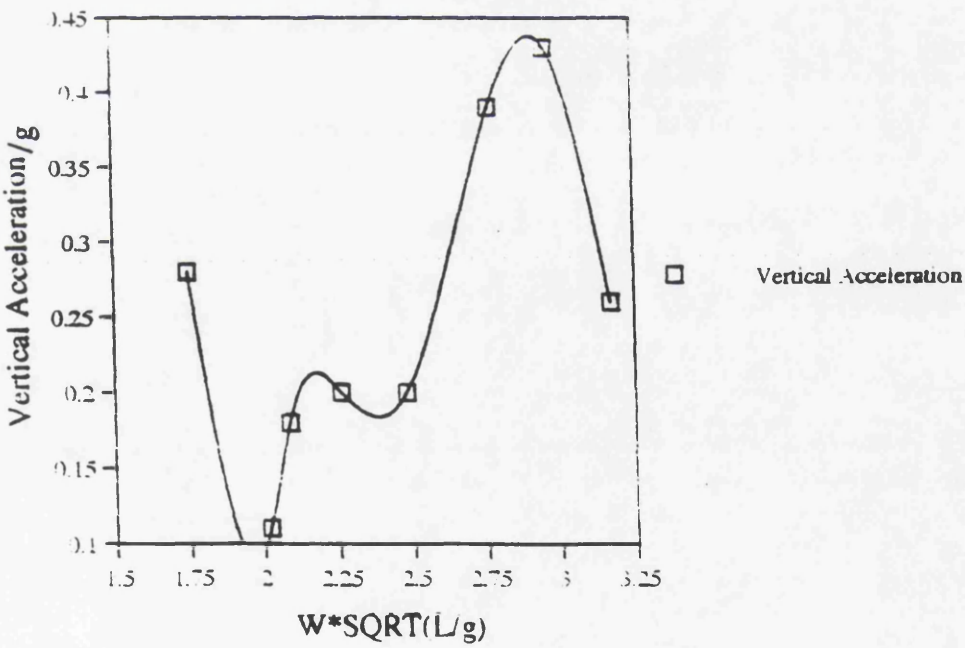

Fig. 4.41 Nondimensional vertical acceleration for ballast draught at Fr=0.15

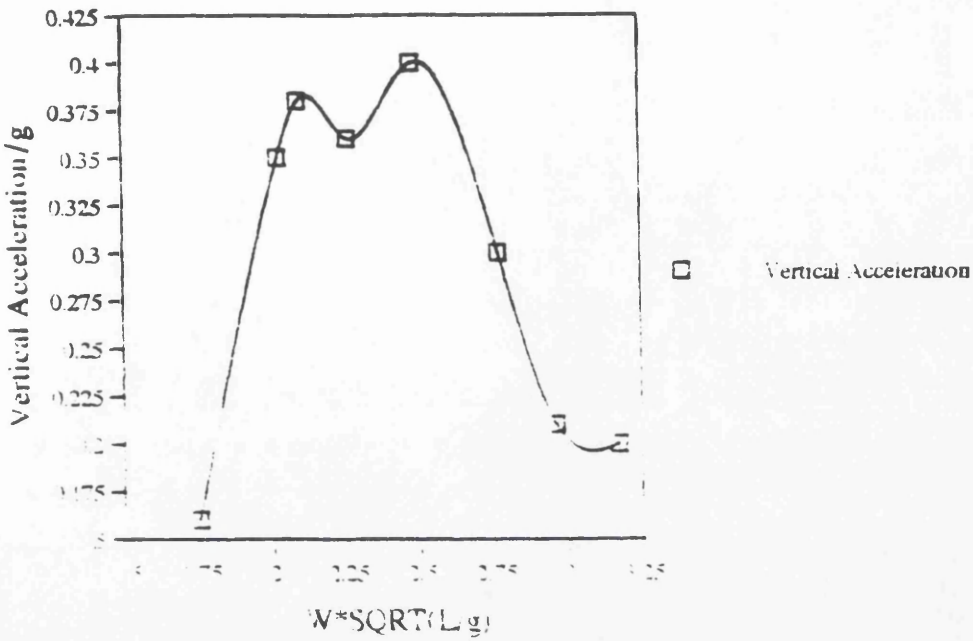

Fig. 4.42 Nondimensional vertical acceleration for loaded draught at Fr=0.2

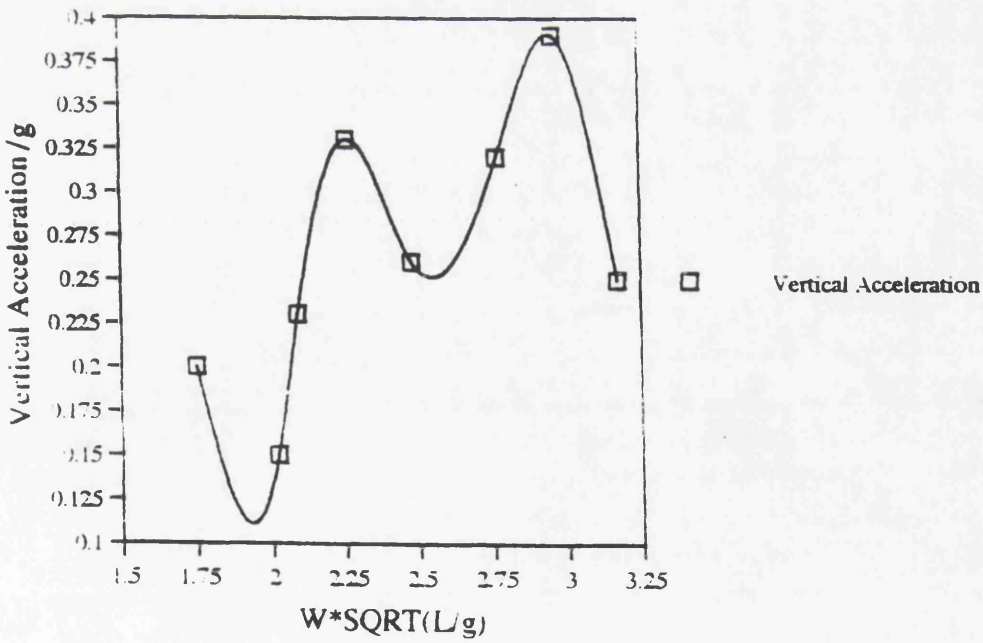

Fig. 4.43 Nondimensional vertical acceleration for ballast draught at Fr=0.2

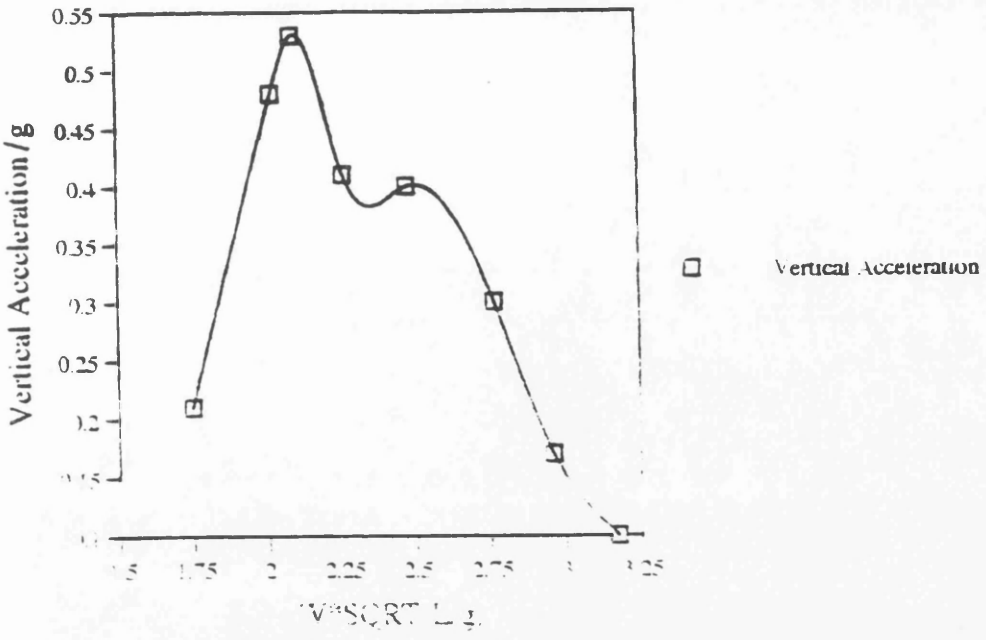

Fig. 4.44 Nondimensional vertical acceleration for loaded draught at Fr=0.278

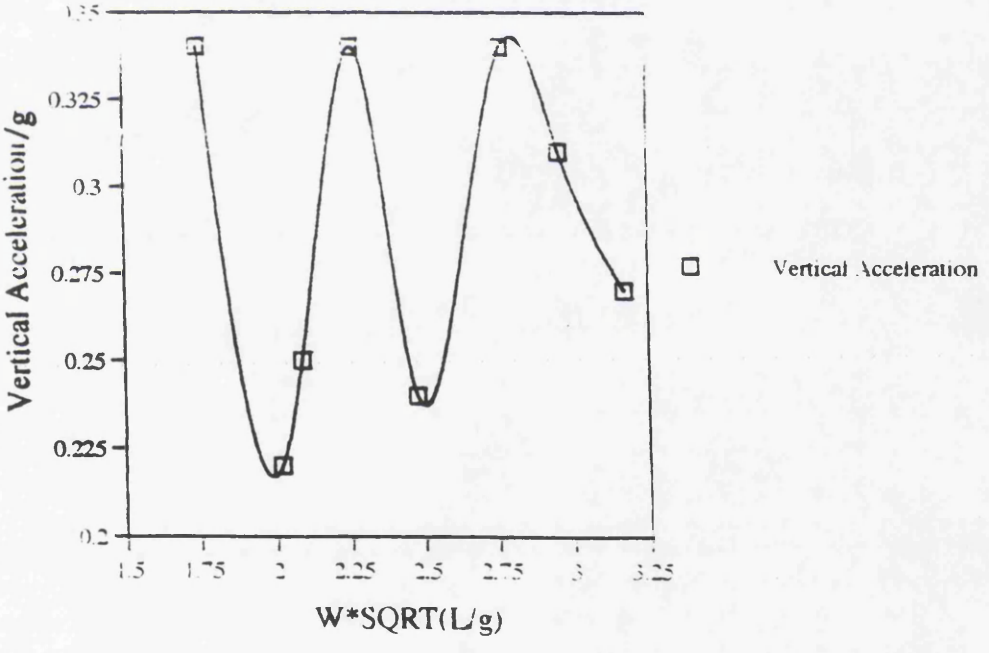

Fig. 4.45 Nondimensional vertical acceleration for ballast draught at Fr=0.278

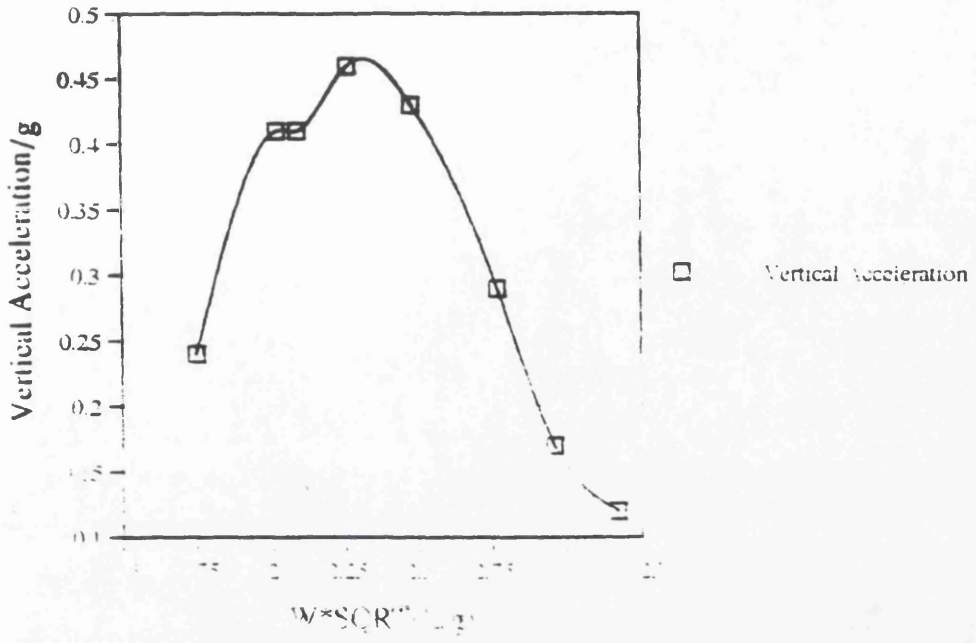

Fig. 4.46 Nondimensional vertical acceleration for loaded draught at Fr=0.3

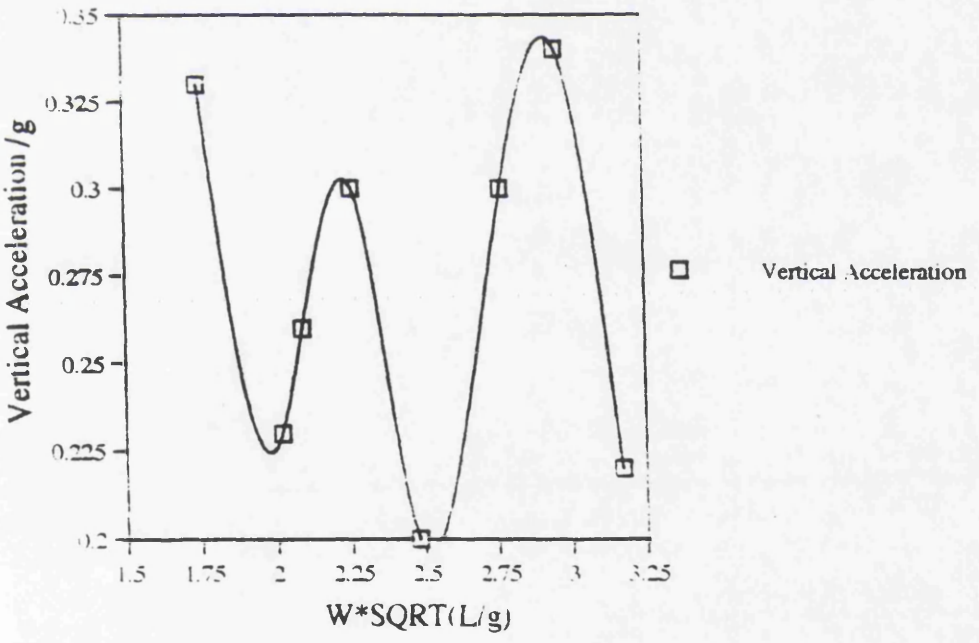

Fig. 4.47 Nondimensional vertical acceleration for ballast draught at Fr=0.3

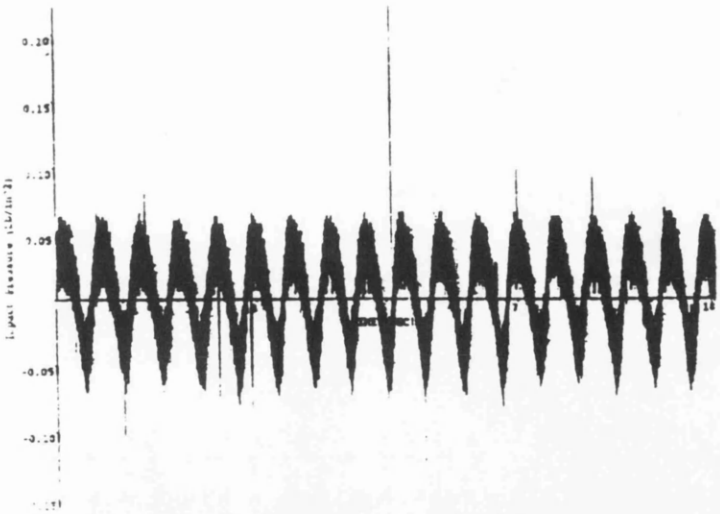

Fig. 4.48.a 10 second time trace of an impact pressure due to bottom slamming at 8 1/2 station for f=0.95 Hz and Fr=0.275

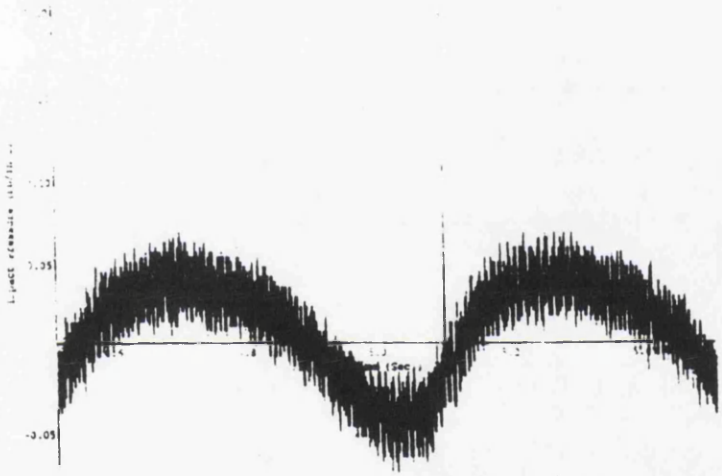

Fig. 4.48.b 1 second time trace of an impact pressure due to bottom slamming at 8 1/2 station for f=0.95 Hz and Fr=0.275

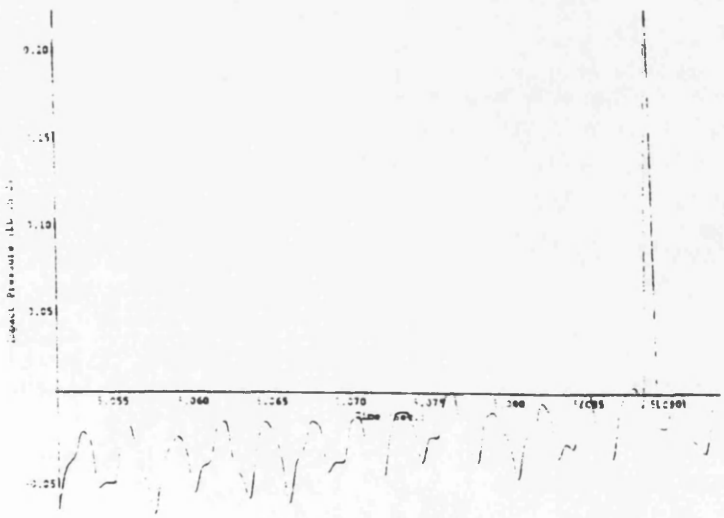

Fig. 4.48.c Typical impact peak due to bottom slamming at station 8 1/2 for f=0.95 Hz and Fr=0.275

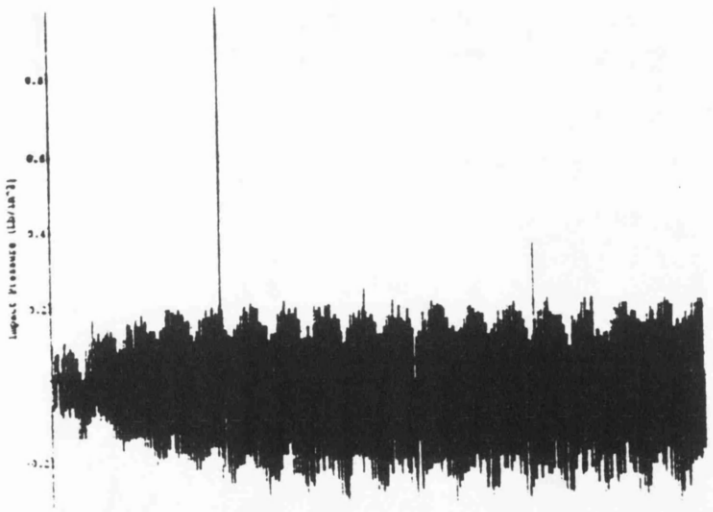

Fig. 4.49.a 10 second time trace of an impact pressure due to bottom slamming at 8 station for f=0.95 Hz and Fr=0.275

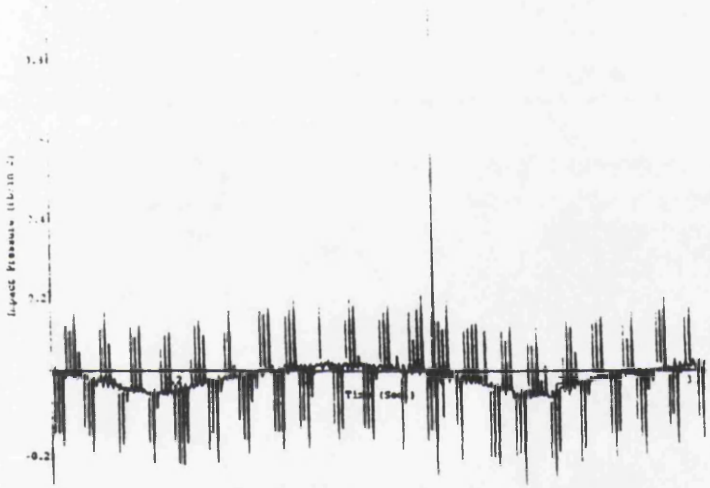

Fig. 4.49.b 1 second time trace of an impact pressure due to bottom slamming at 8 station for f=0.95 Hz and Fr=0.275

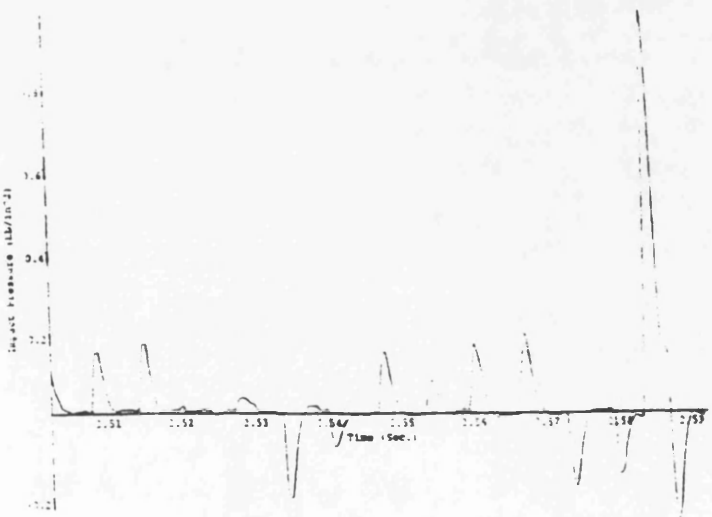

Fig. 4.49.c Typical impact peak due to bottom slamming at station 8 for f=0.95 Hz and Fr=0.275

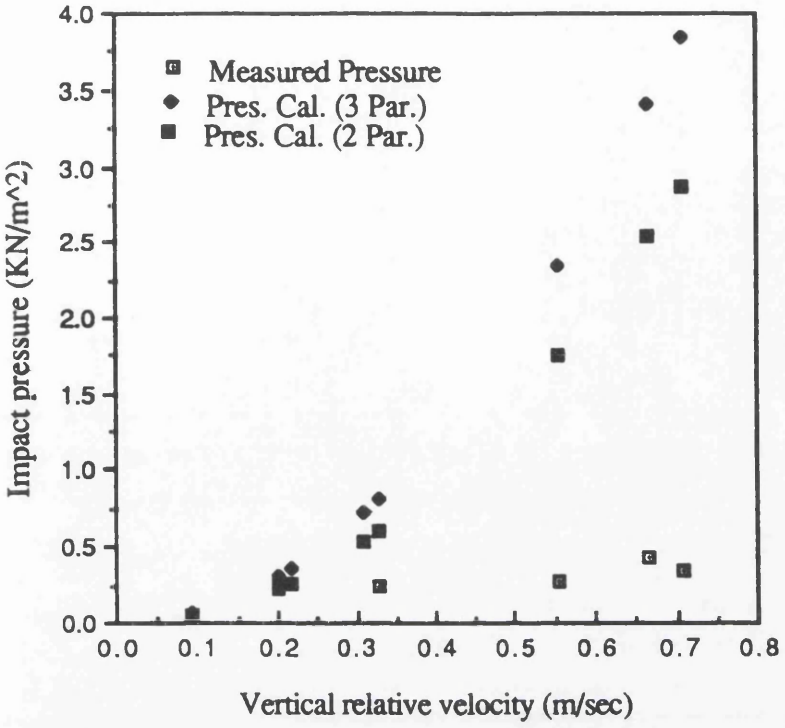

Fig. 4.50 Comparison of measured pressure and calculated pressure with 2 and 3 parameter for loaded draught at station 8 1/2, Fr=0.1

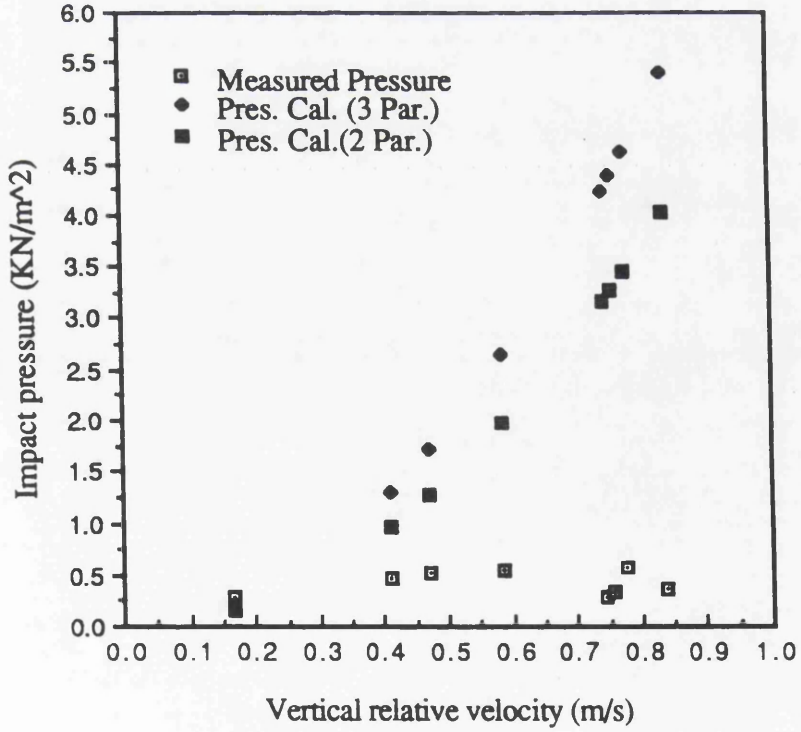

Fig. 4.51 Comparison of measured pressure and calculated pressure with 2 and 3 parameter for loaded draught at station 8 1/2, Fr=0.2

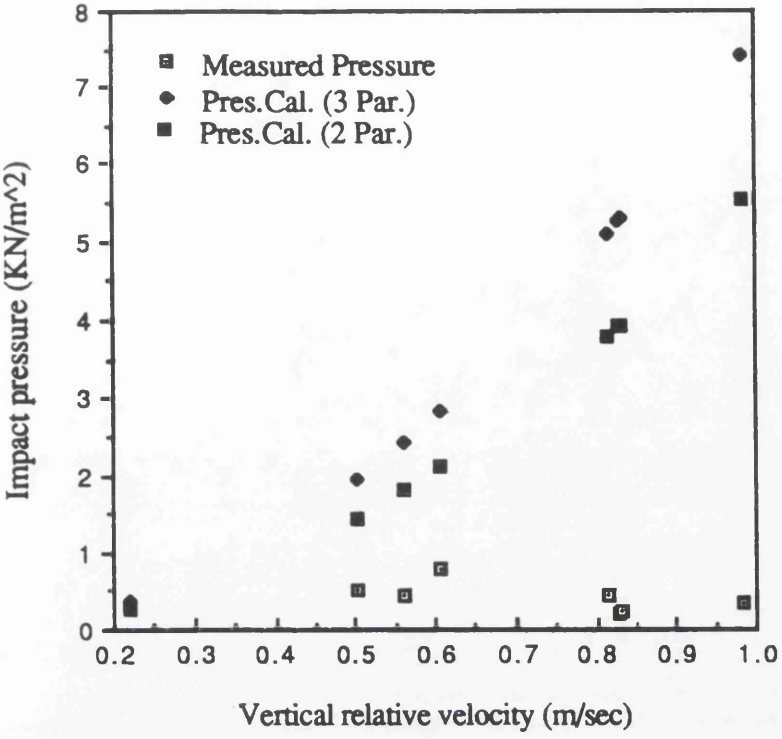

Fig. 4.52 Comparison of measured pressure and calculated pressure with 2 and 3 parameter for loaded draught at station 8 1/2, Fr=0.278

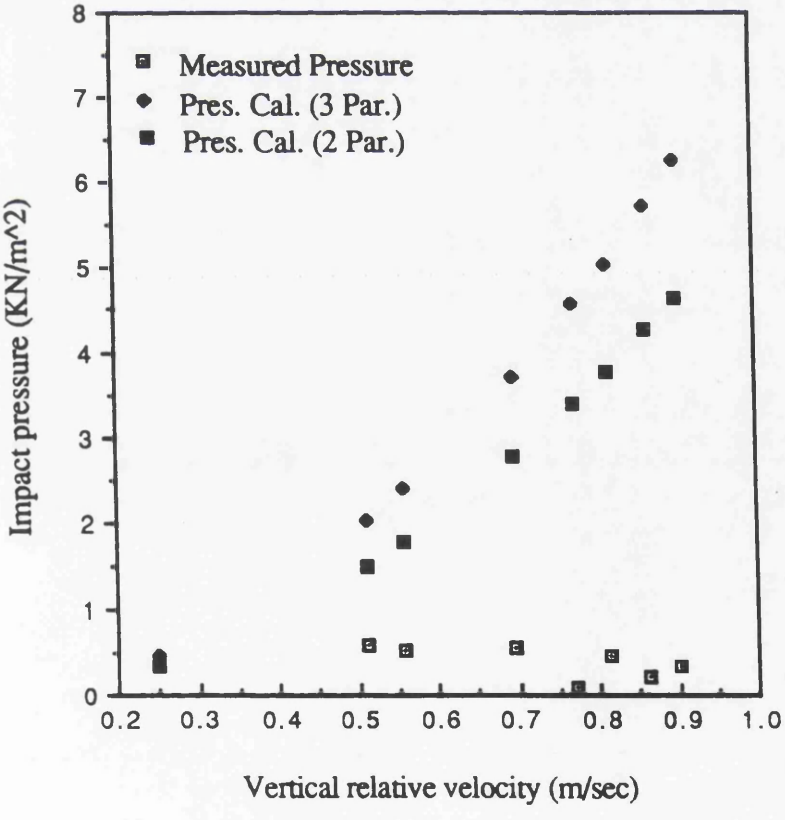

Fig. 4.53 Comparison of measured pressure and calculated pressure with 2 and 3 parameter for loaded draught at station 8 1/2, Fr=0.3

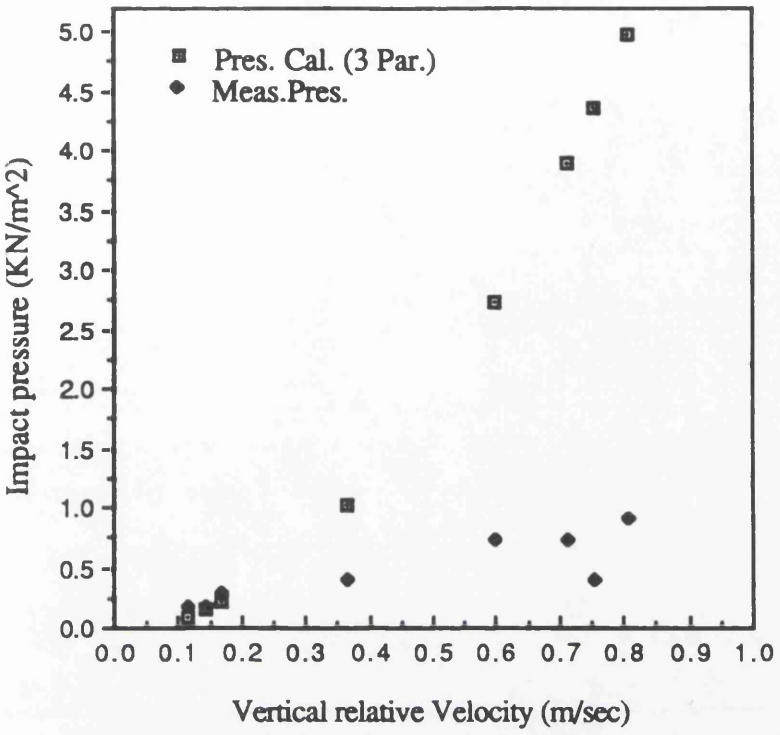

Fig. 4.54 Comparison of calculated and measured impact pressure for ballast draught at station 8 1/2, Fr=0.1

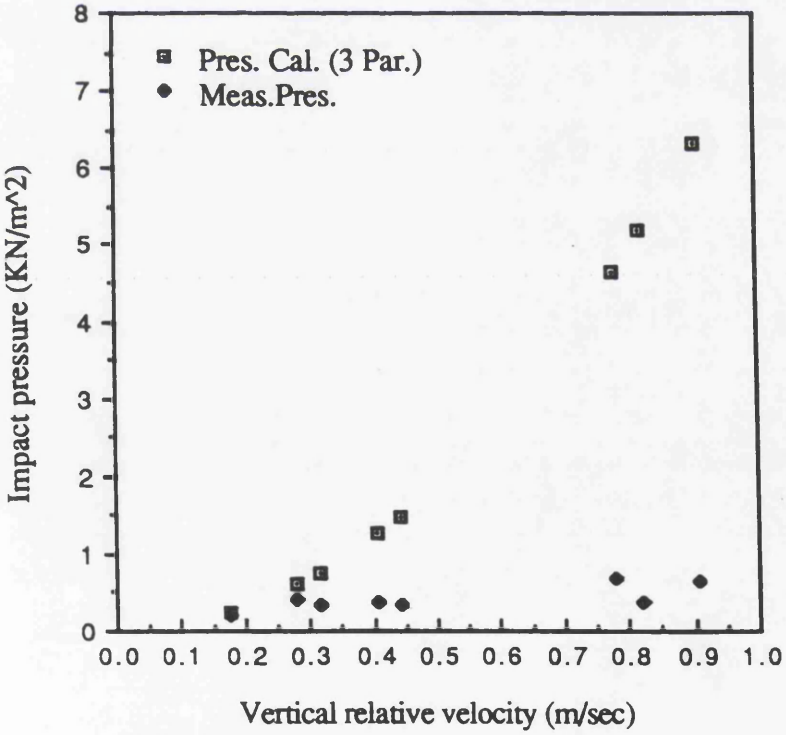

Fig. 4.55 Comparison of calculated and measured impact pressure for ballast draught at station 8 1/2, Fr=0.15

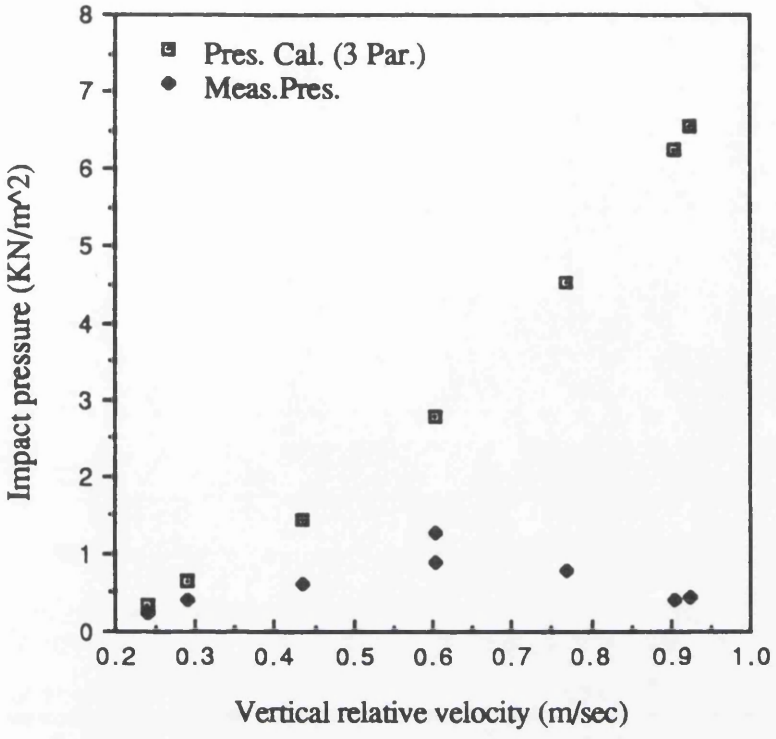

Fig. 4.56 Comparison of calculated and measured impact pressure for ballast draught at station 8 1/2, Fr=0.2

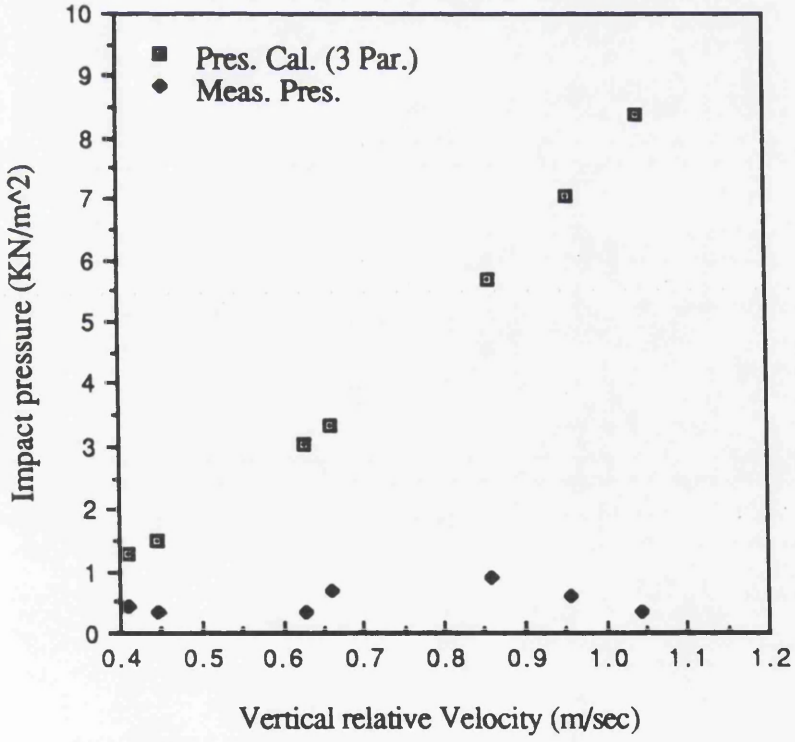

Fig. 4.57 Comparison of calculated and measured impact pressure for ballast draught at station 8 1/2, Fr=0.278

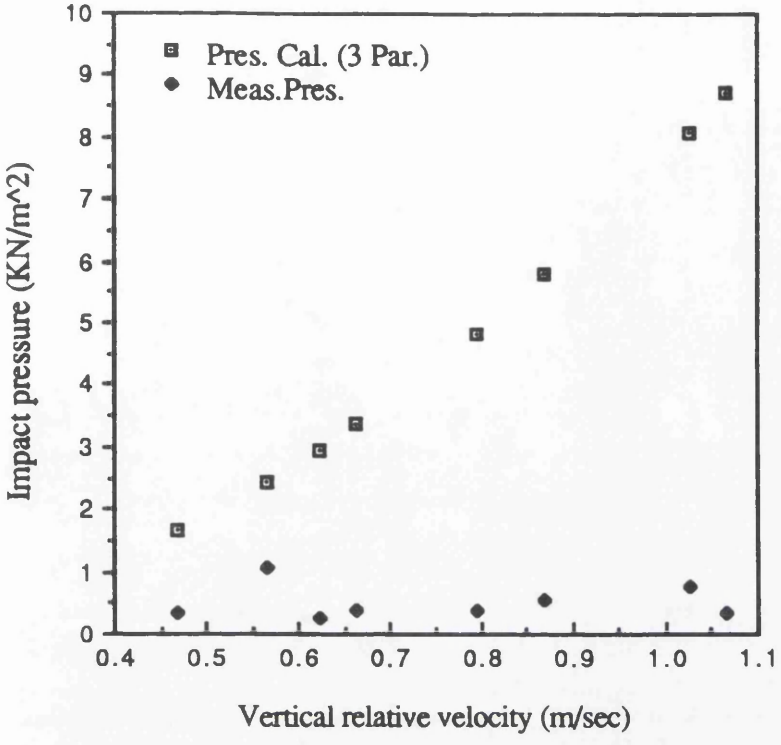

Fig. 4.58 Comparison of calculated and measured impact pressure for ballast draught at station 8 1/2, Fr=0.3

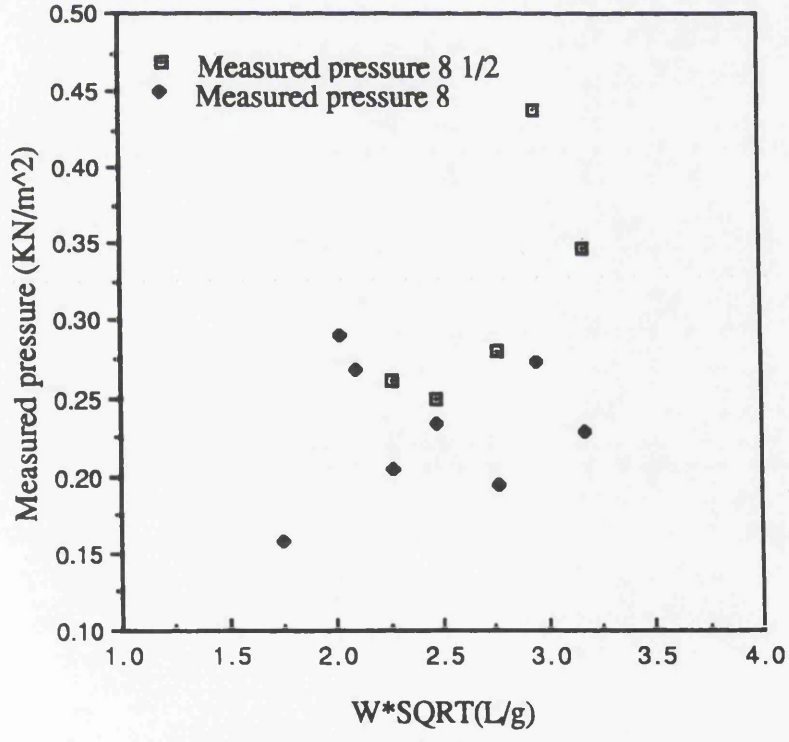

Fig. 4.59 Comparison of impact pressure at station 8 1/2 and station 8 for loaded draught, Fr=0.1

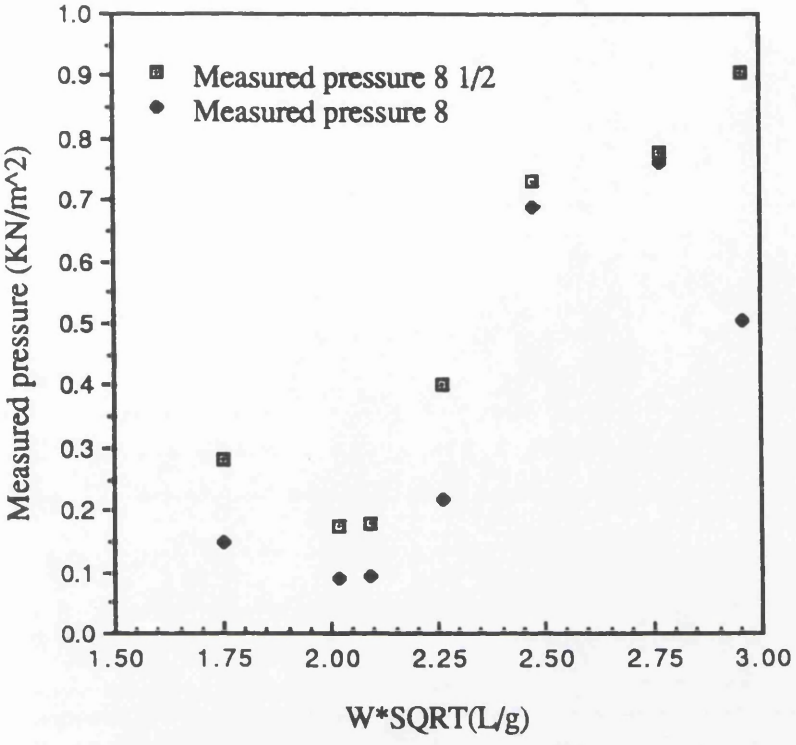

Fig. 4.60 Comparison of impact pressure at station 8 1/2 and station 8 for ballast draught, Fr=0.1

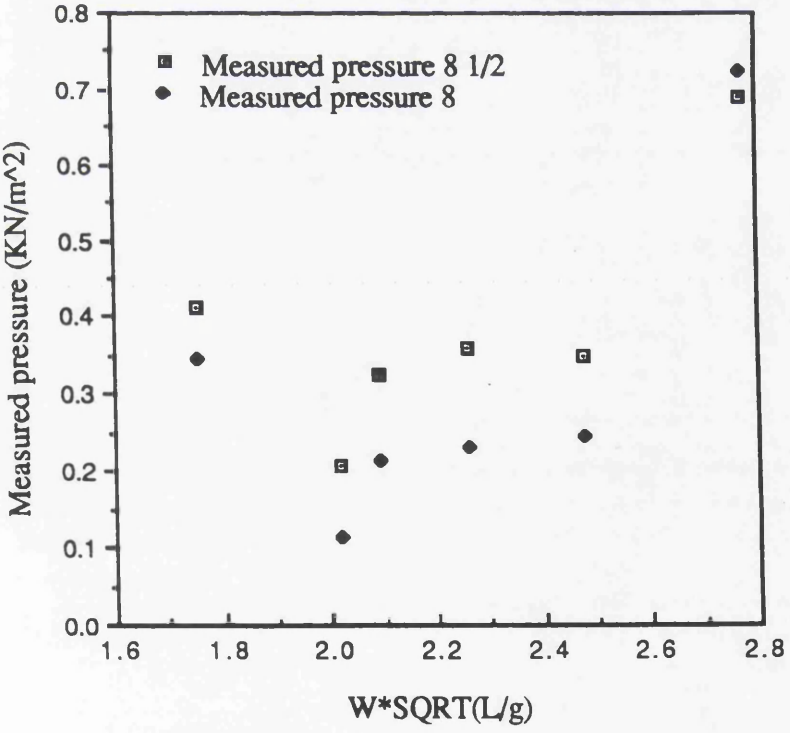

Fig. 4.61 Comparison of impact pressure at station 8 1/2 and station 8 for ballast draught, Fr=0.15

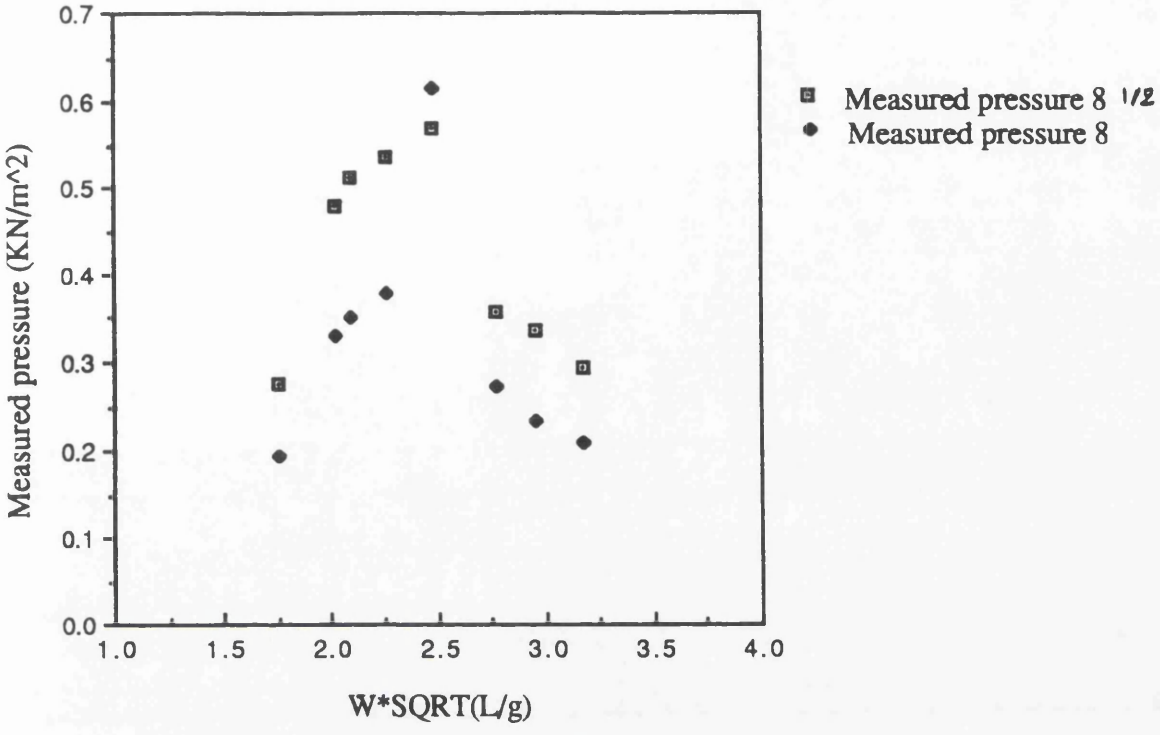

Fig. 4.62 Comparison of impact pressure at station 8 1/2 and station 8 for loaded draught, Fr=0.2

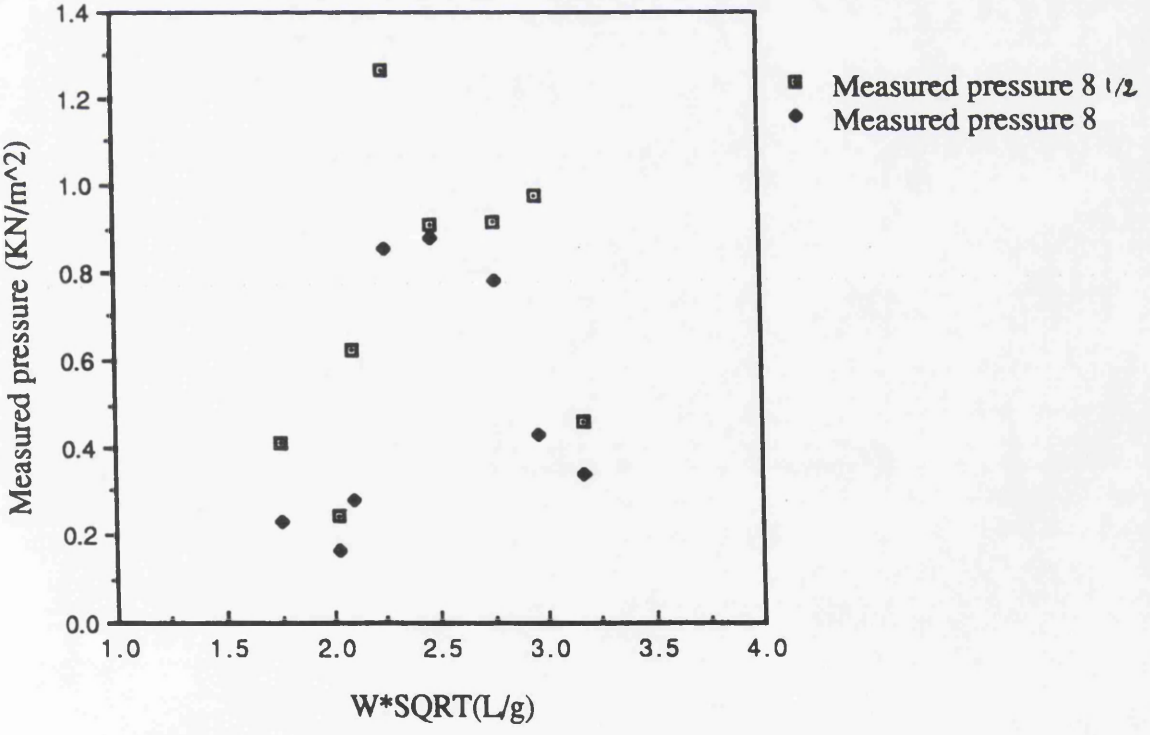

Fig. 4.63 Comparison of impact pressure at station 8 1/2 and station 8 for ballast draught, Fr=0.2

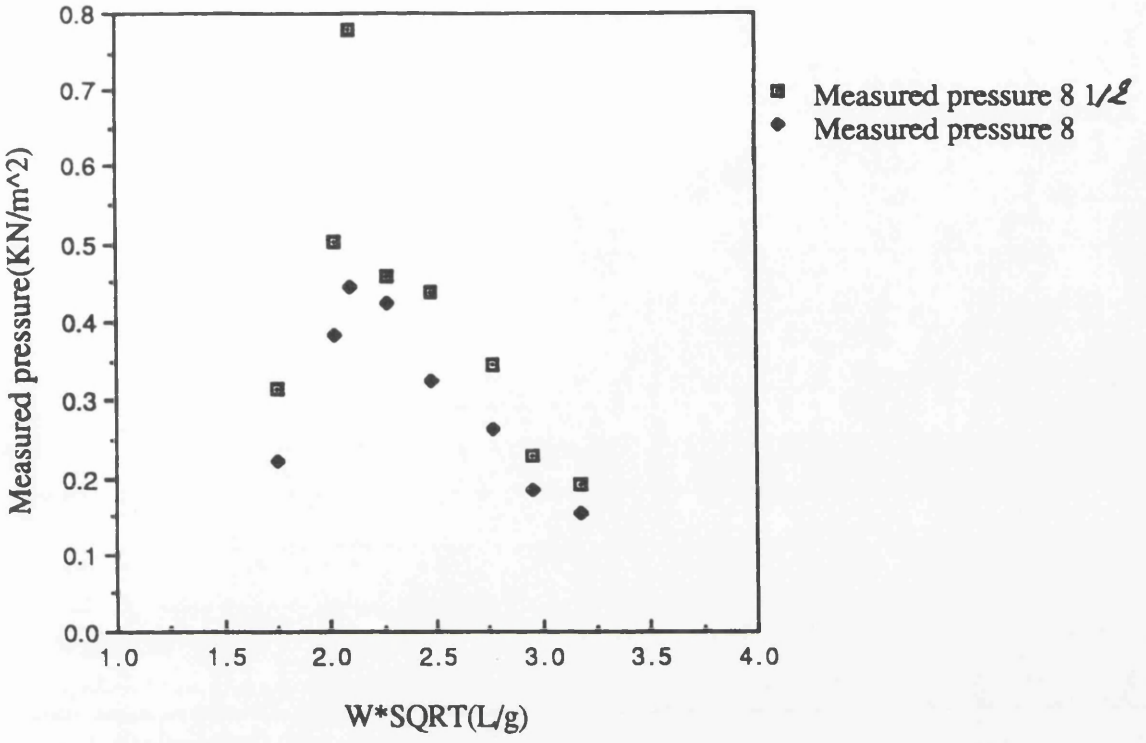

Fig. 4.64 Comparison of impact pressure at staion 8 1/2 and station 8 for loaded draught, Fr=0.278

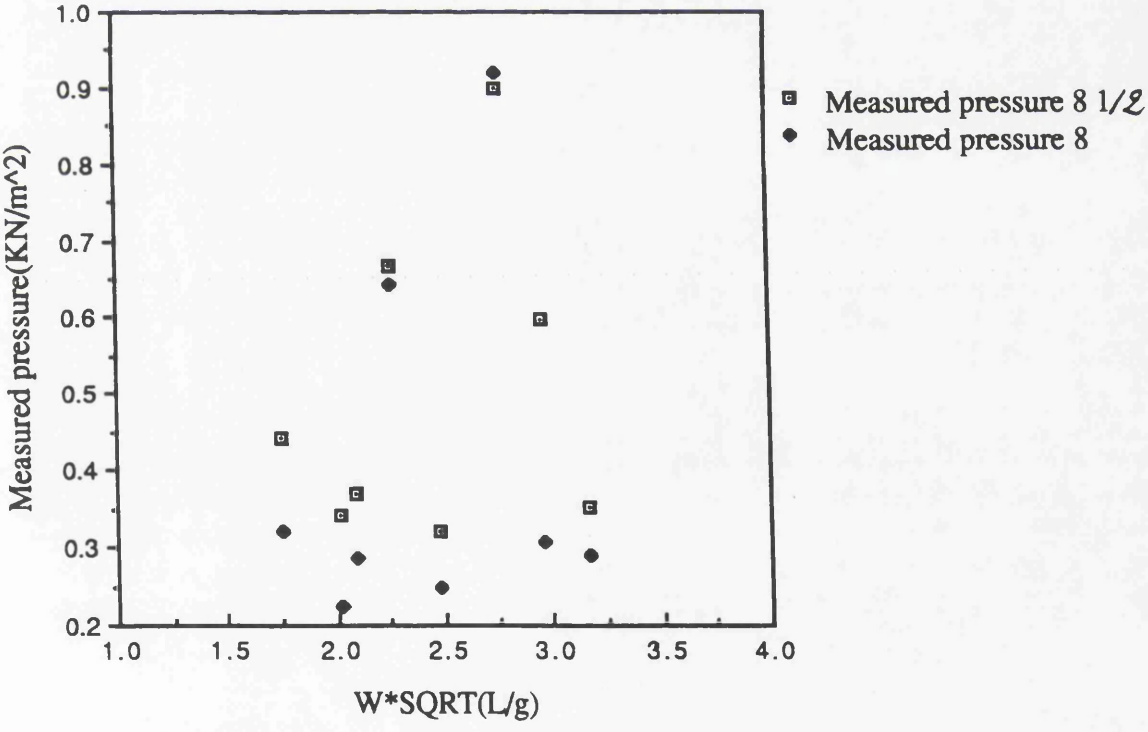

Fig. 4.65 Comparison of impact pressure at station 8 1/2 and station 8 for ballast draught, Fr=0.278

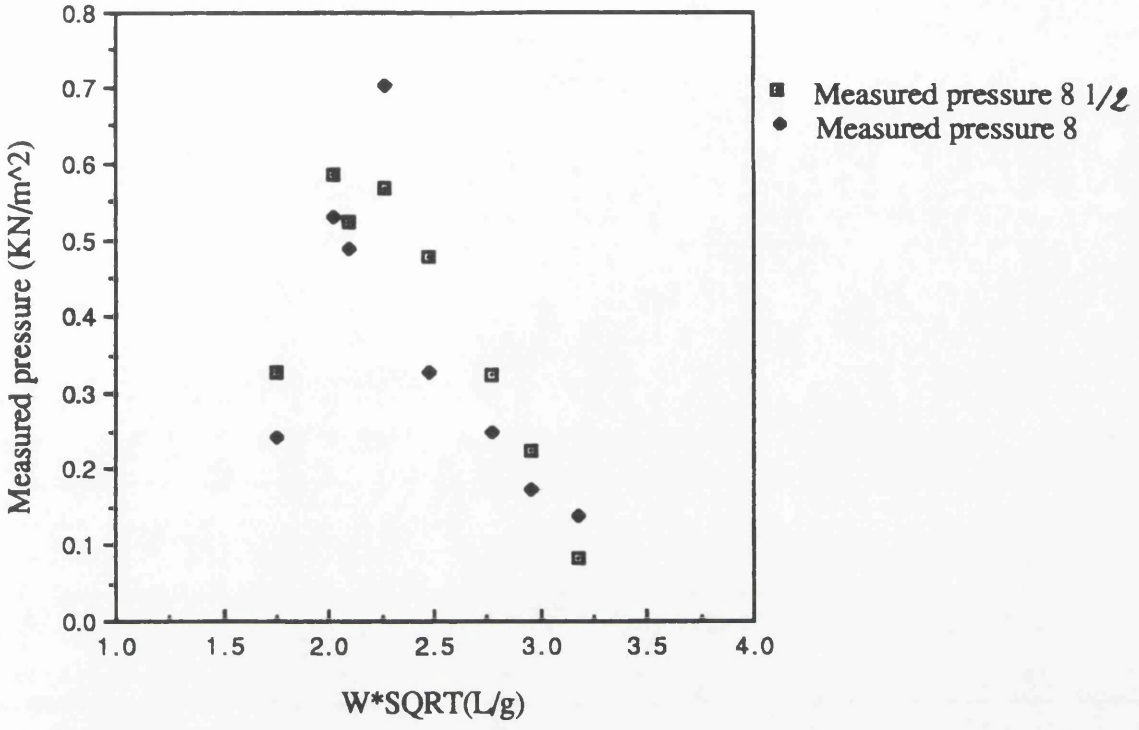

Fig. 4.66 Comparison of impact pressure at station 8 1/2 and station 8 for loaded draught, Fr=0.3

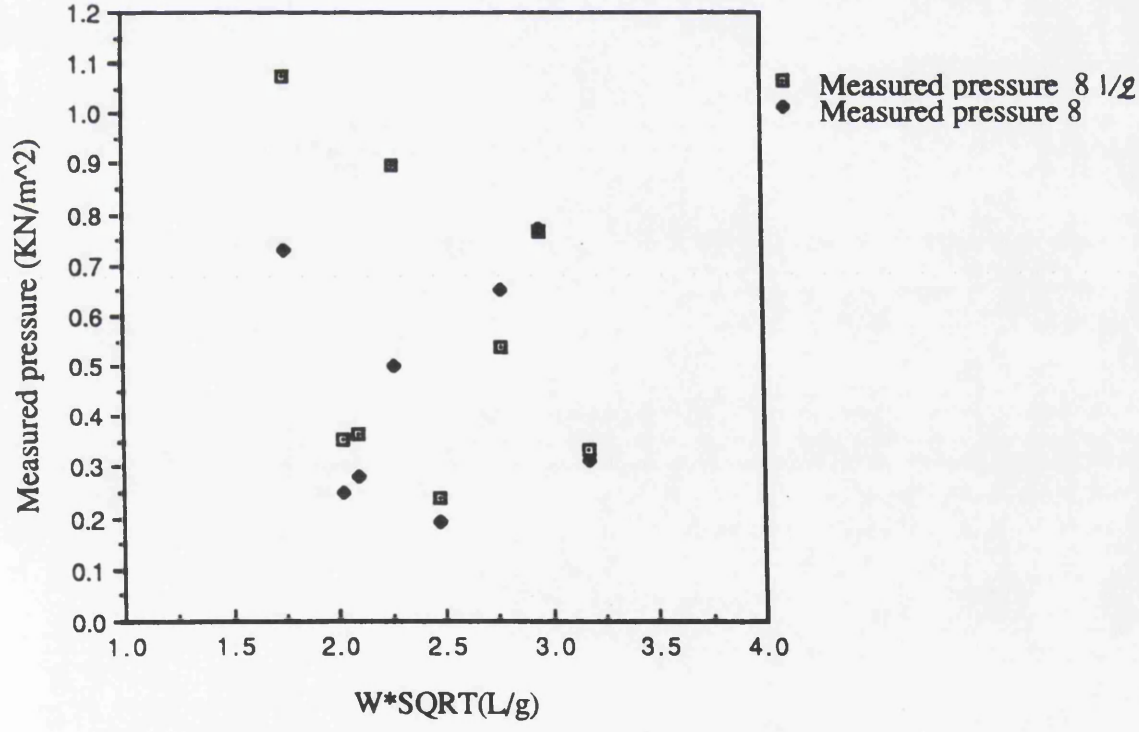

Fig. 4.67 Comparison of impact pressure at station 8 1/2 and station 8 for ballast draught, Fr=0.3

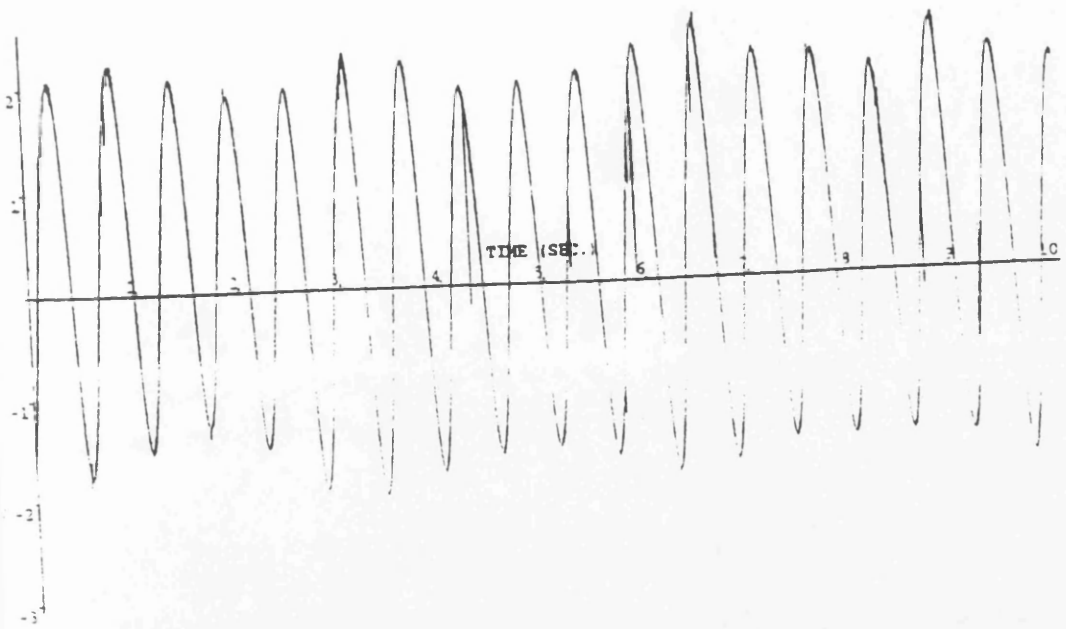

Fig. 4.68 Time history of the forward vetical motion for f=0.95 Hz and Fr=0.275

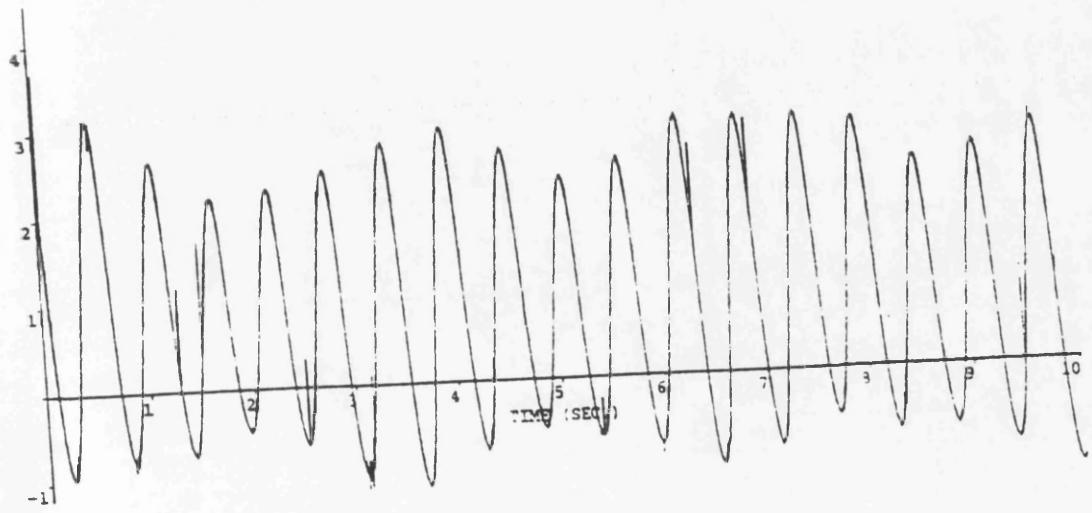

Fig. 4.69 Time history of the aftward vetical motion for f=0.95 Hz and Fr=0.275

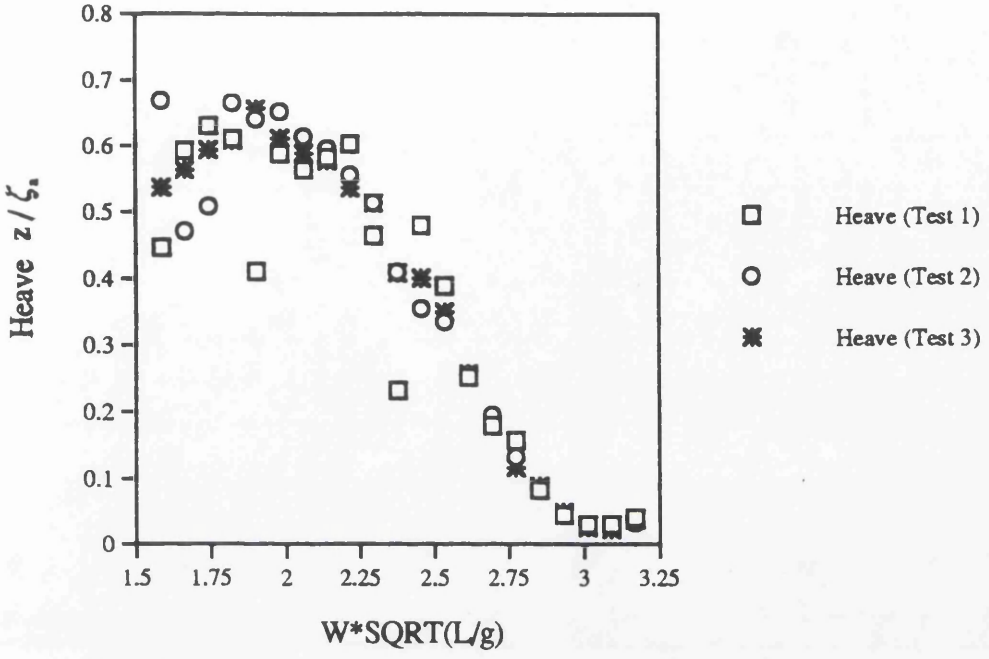

Fig. 4.70 Nondimensional heave amplitude for loaded draught at Fr=0.275

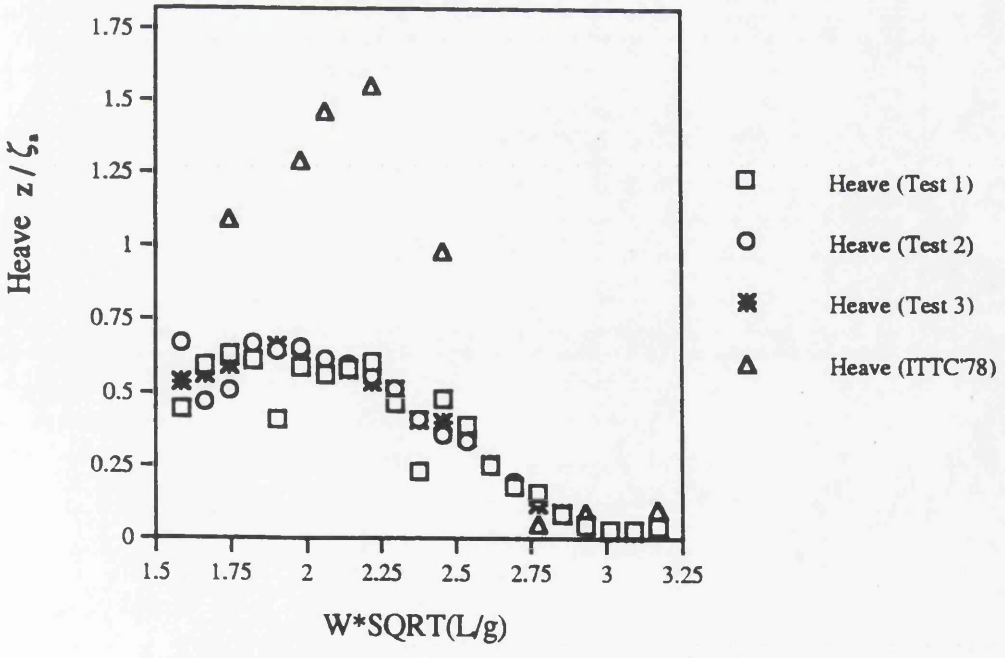

Fig. 4.71 Comparison of heave amplitude for loaded draught at Fr=0.275

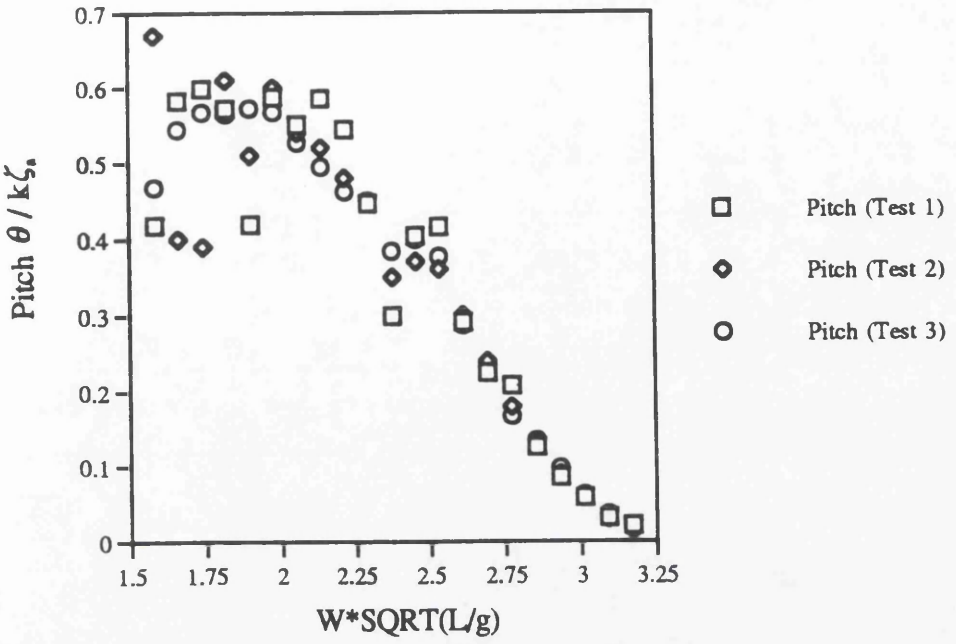

Fig. 4.72 Nondimensional pitch amplitude for loaded draught at Fr=0.275

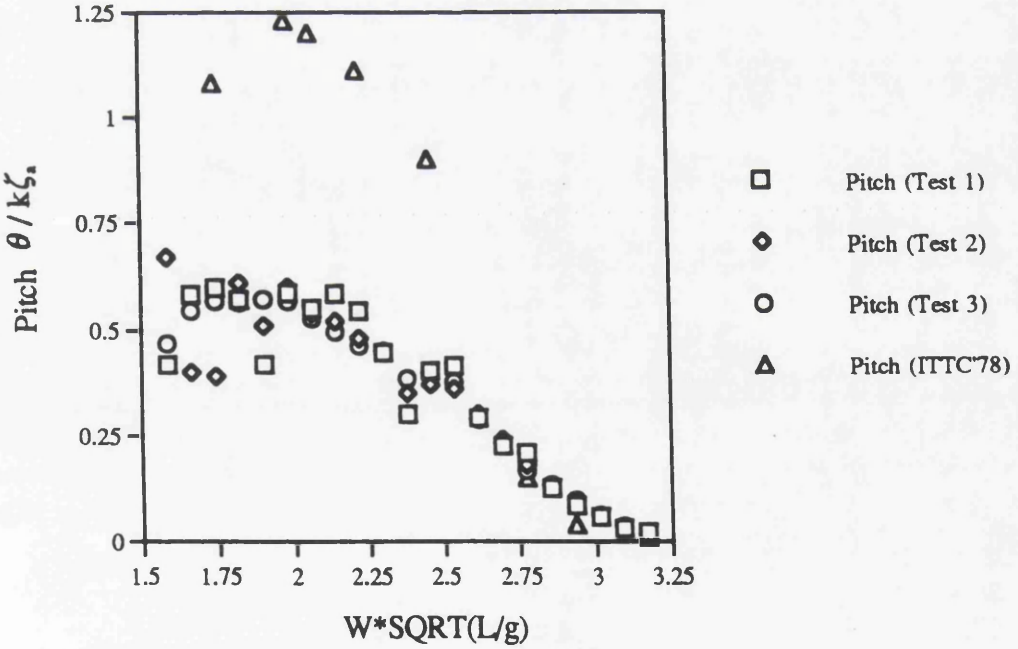

Fig. 4.73 Comparison of nondimensional pitch amplitude for loaded draught at Fr=0.275

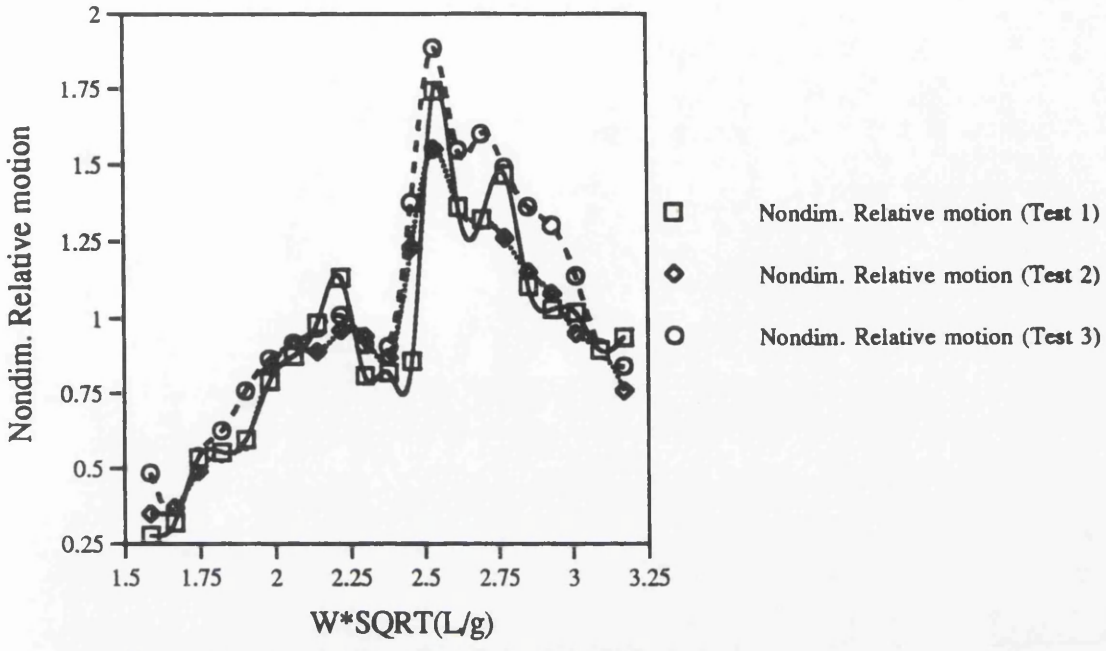

Fig. 4.74 Nondimensional vertical relative motion amplitude at Fr=0.275

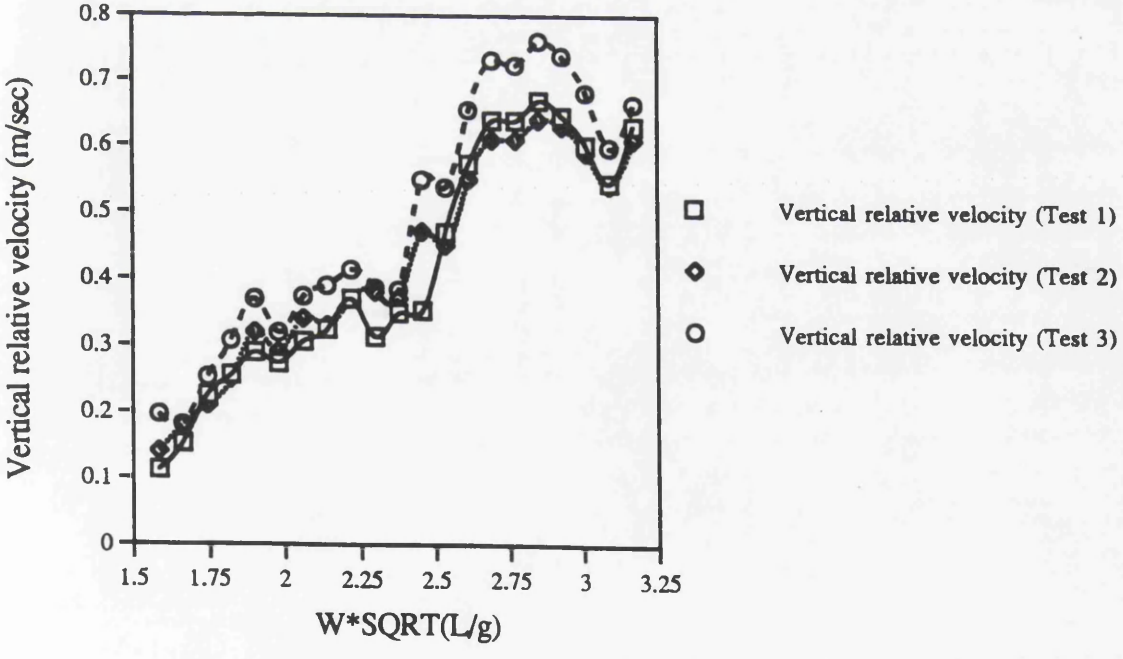

Fig. 4.75 Vertical relative velocity at Fr=0.275

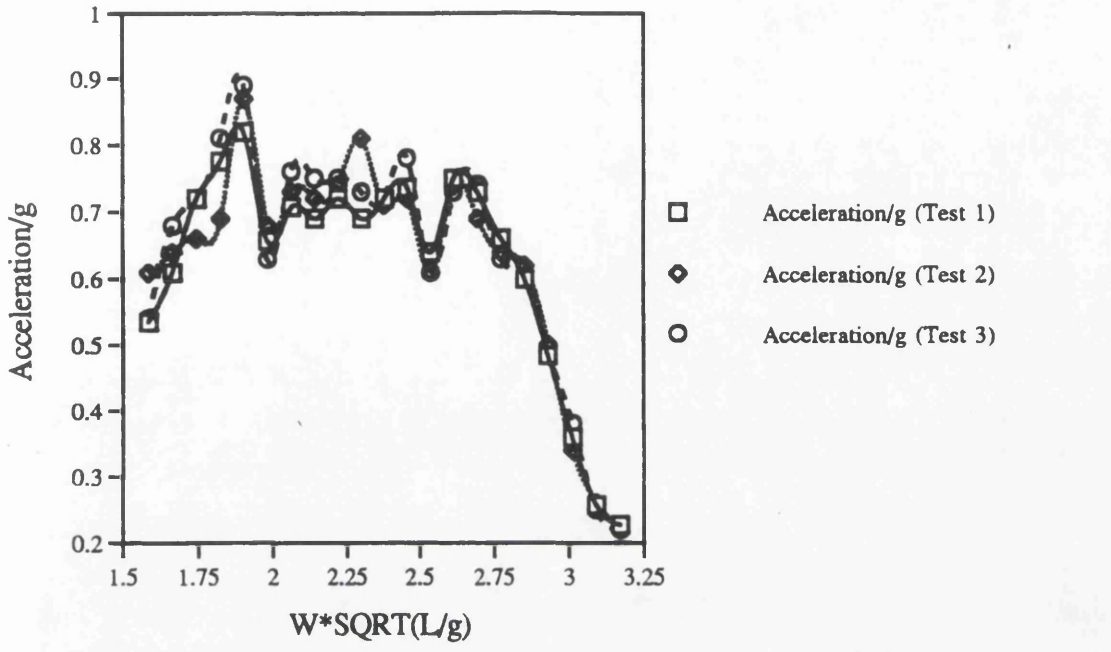

Fig. 4.76 Nondimesional vertical acceleration at Fr=0.275

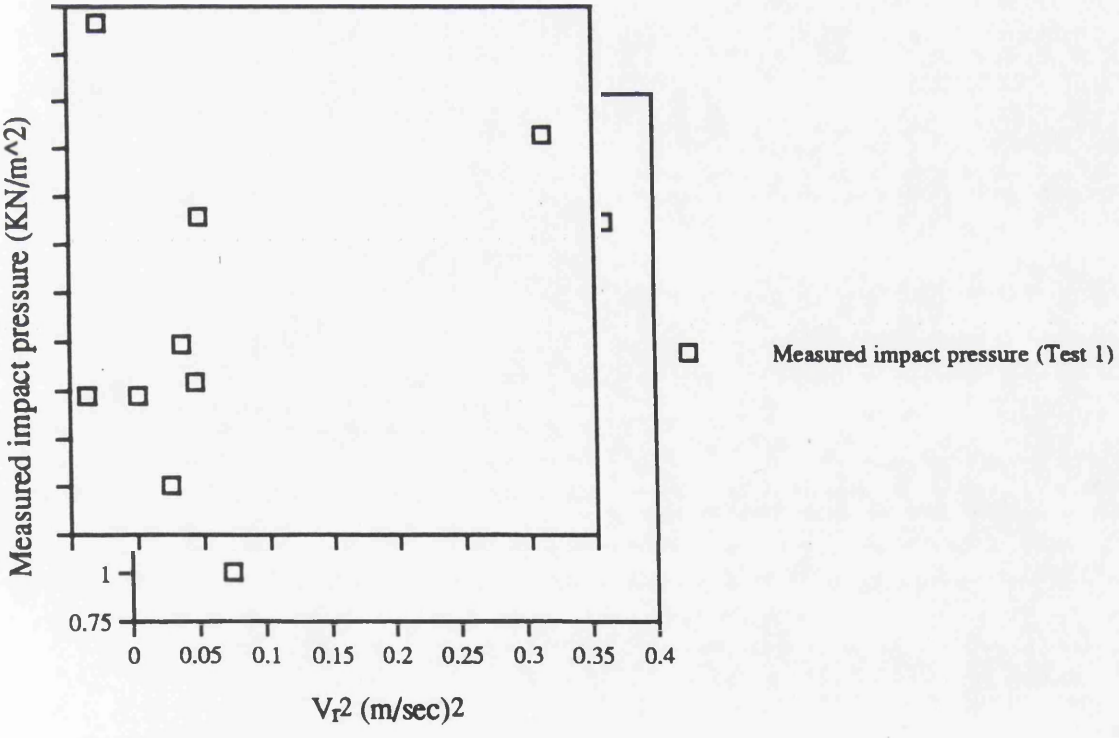

Fig. 4.77 Dependence of the impact pressure on the vertical relative velocity at station 8 1/2 for Fr=0.275

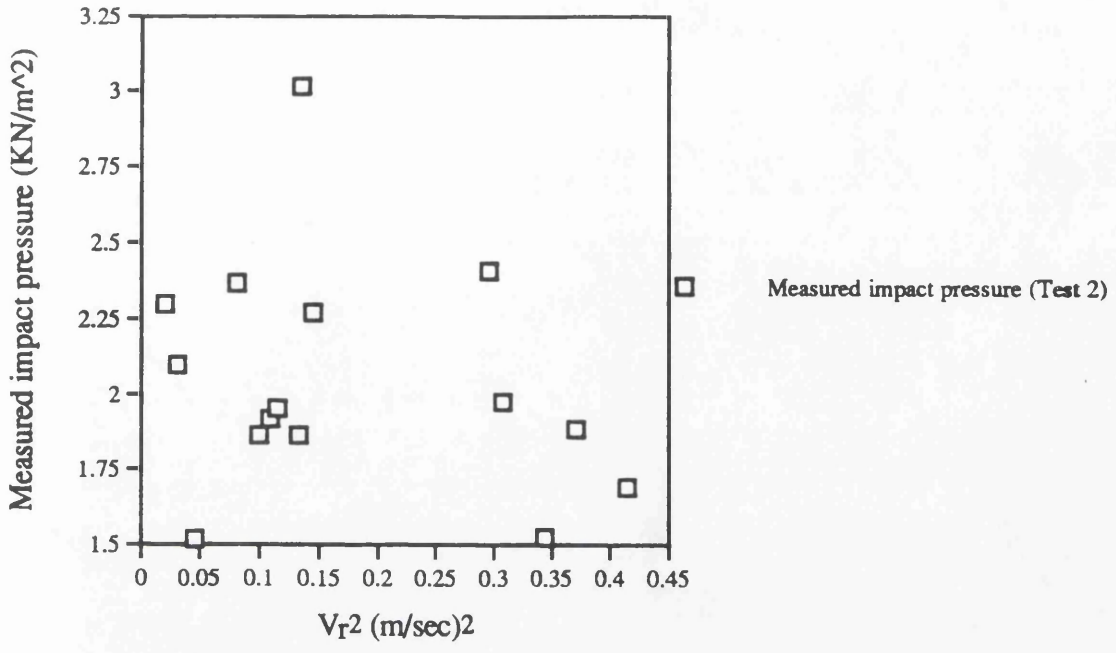

Fig. 4.78 Dependence of the impact pressure on the vertical relative velocity at station 8 1/2 for Fr=0.275

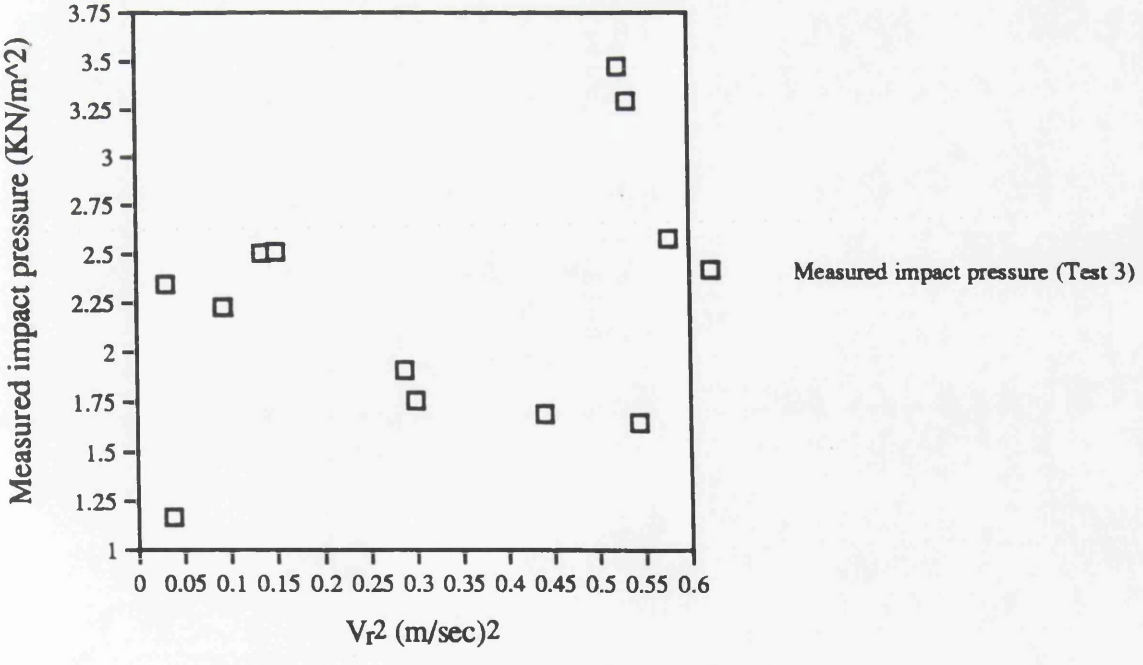

Fig. 4.79 Dependence of the impact pressure on the vertical relative velocity at station 8 1/2 for Fr=0.275

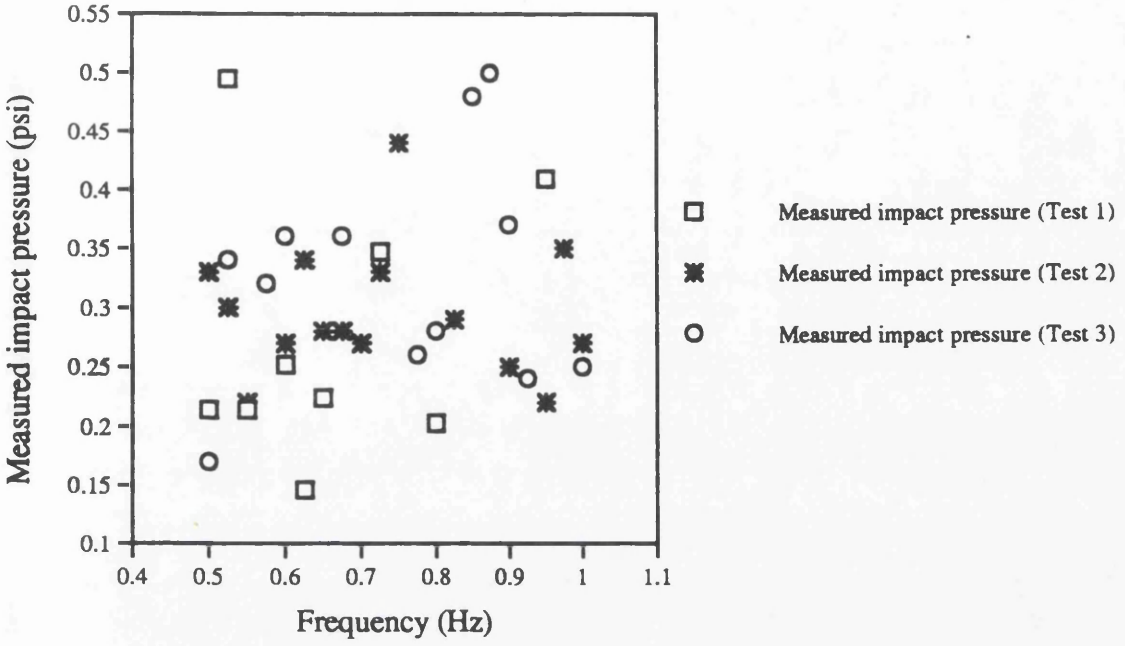

Fig. 4.80 Discrepancy in slamming pressure magnitude at station 8 1/2 for Fr=0.275

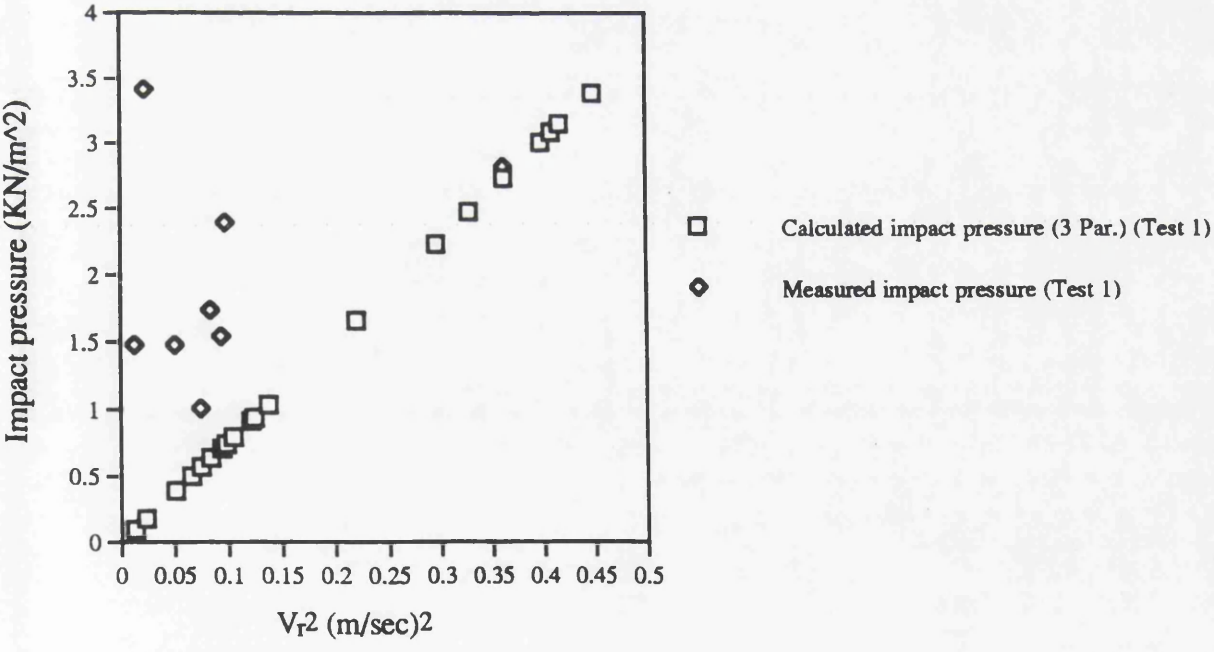

Fig. 4.81 Comparison of measured and calculated impact pressure for loaded draught at station 8 1/2, Fr=0.275

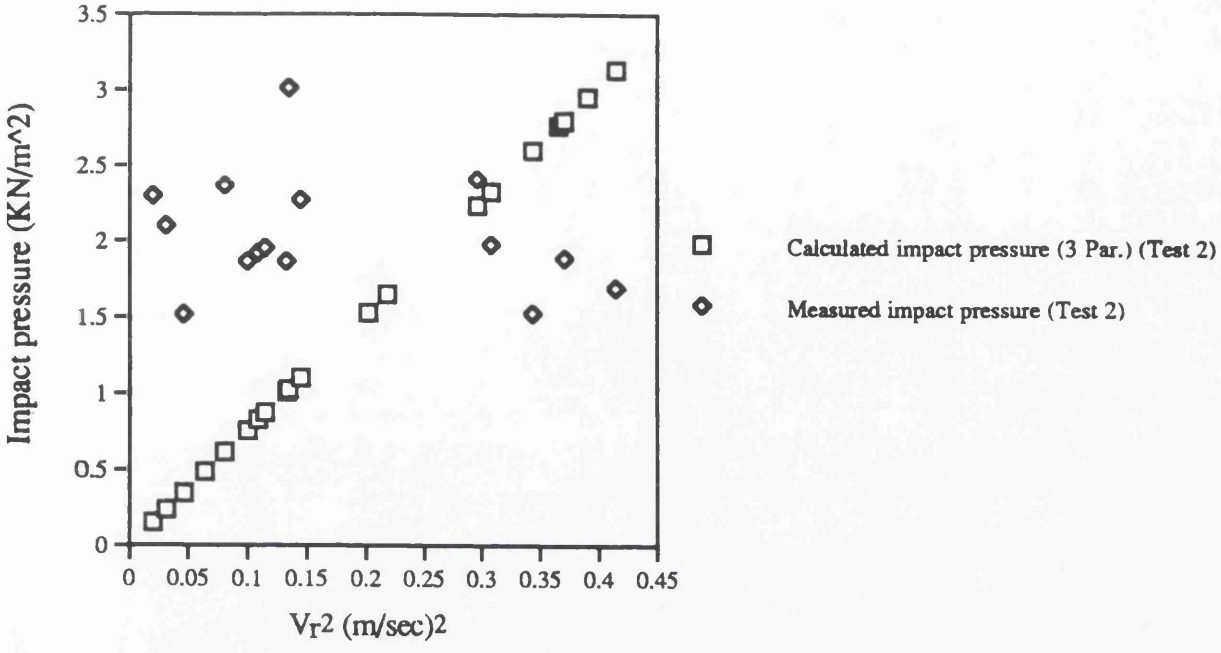

Fig. 4.82 Comparison of measured and calculated impact pressure for laded draught at station 8 1/2, Fr=0.275

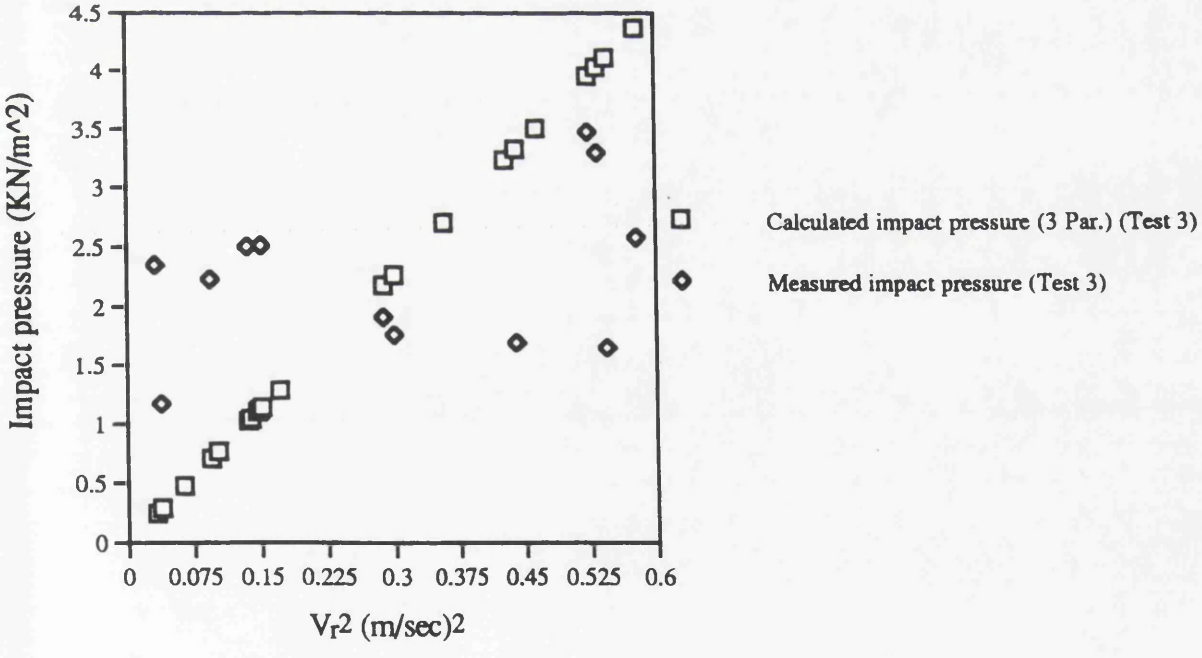

Fig. 4.83 Comparison of measured and calculated impact pressure for loaded draught at station 8 1/2, Fr=0.275

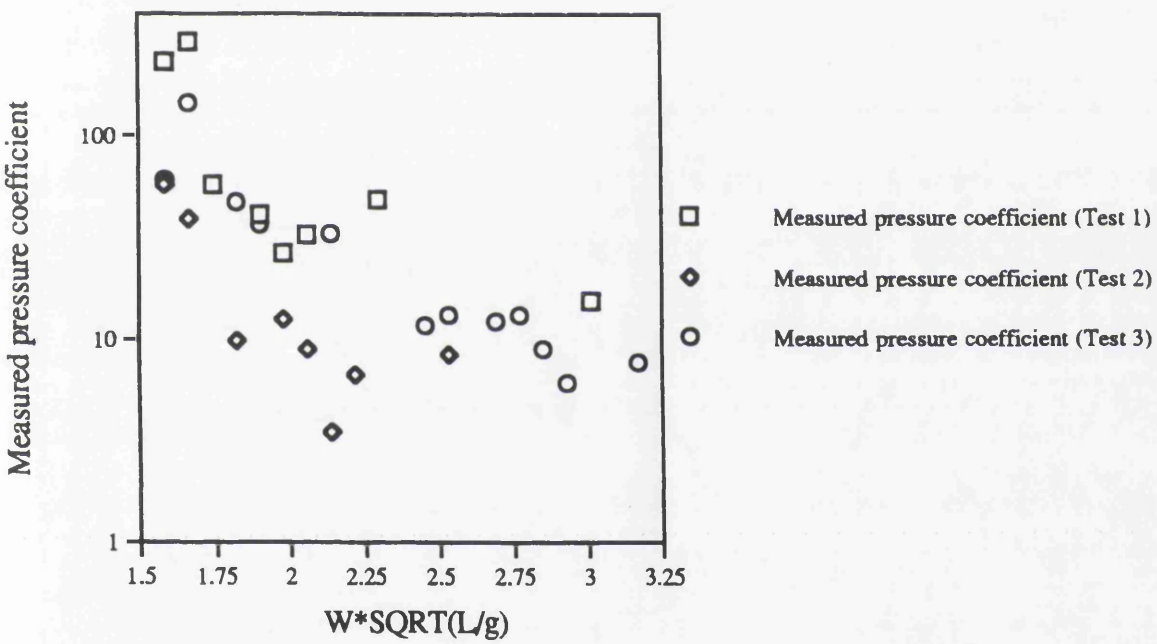

Fig. 4.84 Measured pressure coefficient for station 8 1/2

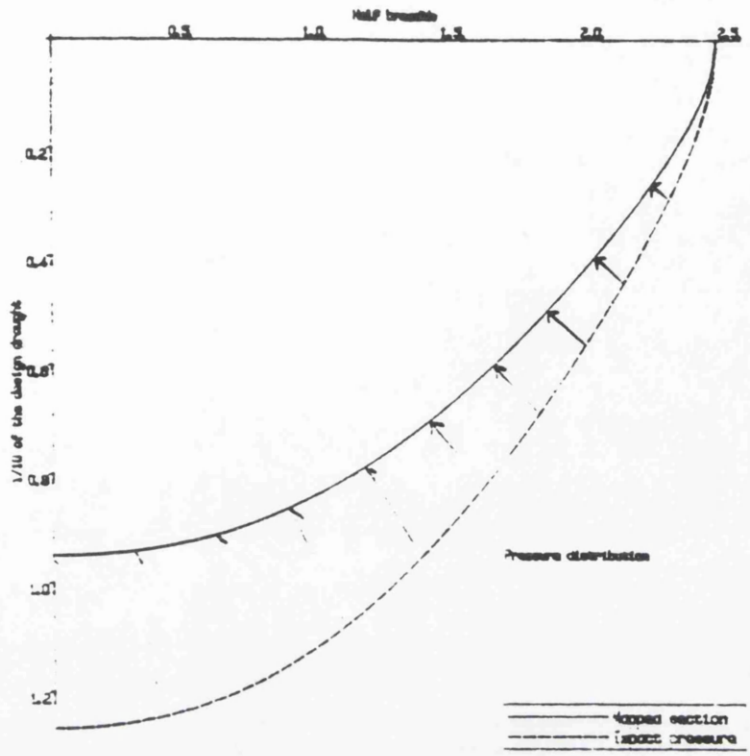

Fig. 4.85 Distribution of slamming pressure over the bottom on one tenth of the design draught, pressure=0.478 psi at the centre of station 8 1/2 for Fr=0.275 and f=0.85 Hz

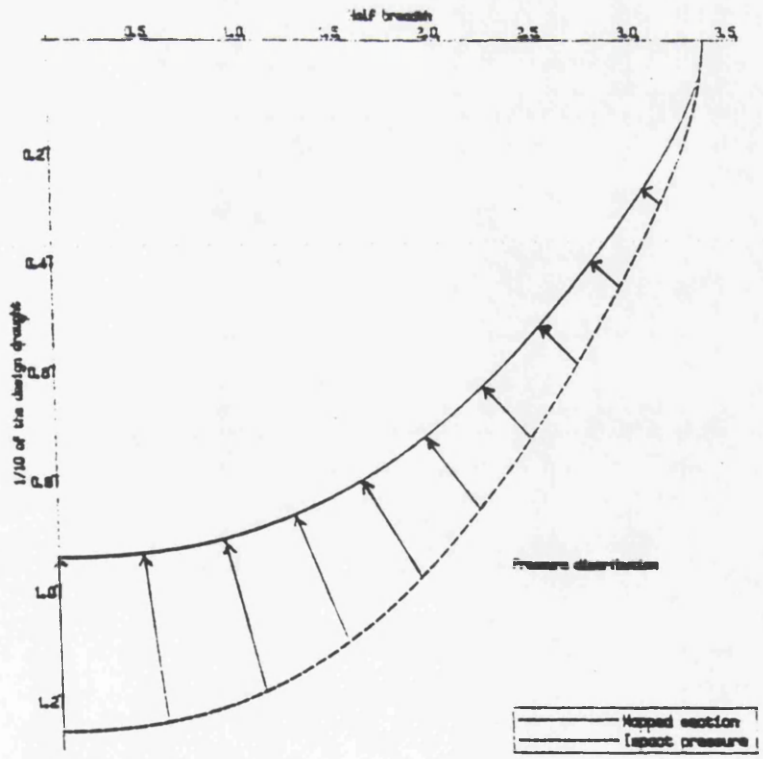

Fig. 4.86 Distribution of slamming pressure over the bottom on one tenth of the design draught, pressure=0.438 psi at the centre of station 8 for Fr=0.275 and f=0.85 Hz

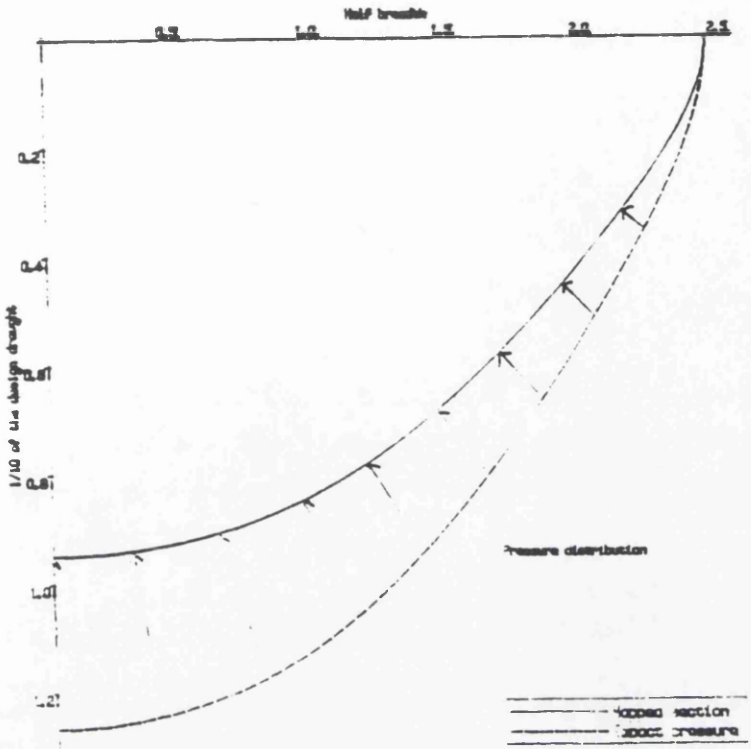

Fig. 4.87 Distribution of slamming pressure over the bottom on one tenth of the design draught, pressure=0.504 psi at the centre of station 8 1/2 for Fr=0.275 and f=0.875 Hz

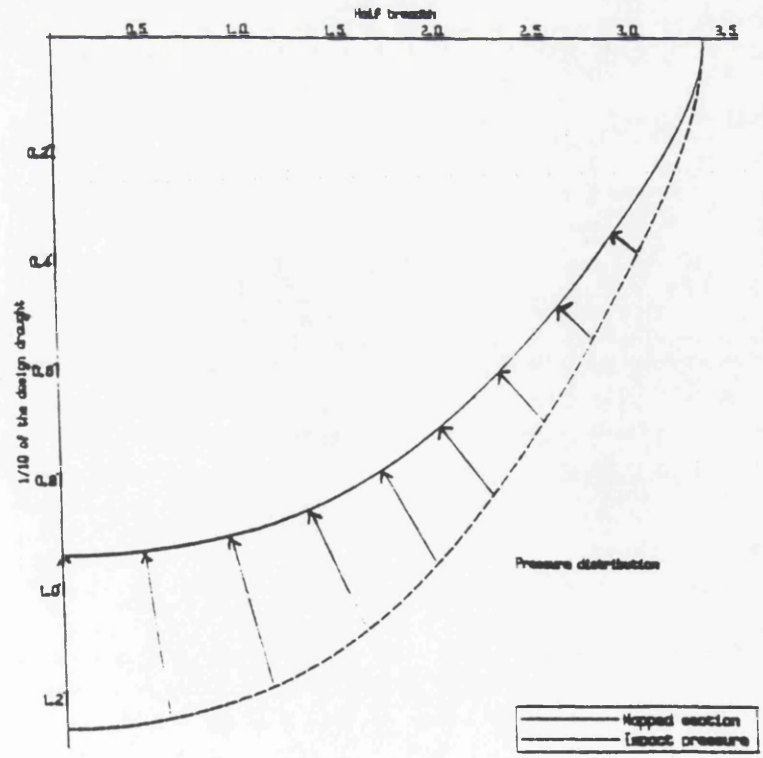

Fig. 4.88 Distribution of slamming pressure over the bottom on one tenth of the design draught, pressure=0.417 psi at the centre of station 8 for Fr=0.275 and f=0.875 Hz

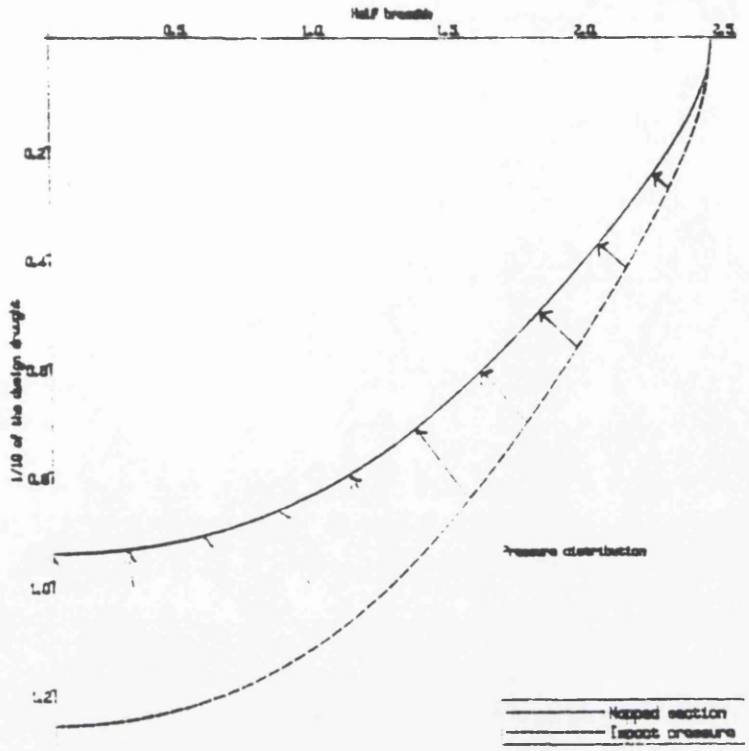

Fig. 4.89 Distribution of slamming pressure over the bottom on one tenth of the design draught, pressure=0.214 psi at the centre of station 8 1/2 for Fr=0.275 and f=0.55 Hz

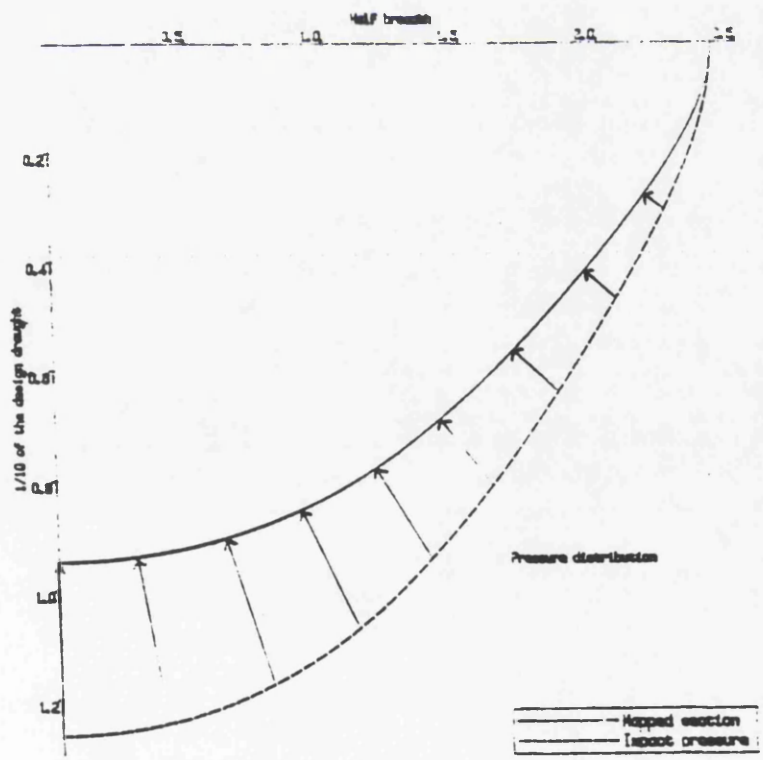

Fig. 4.90 Distribution of slamming pressure over the bottom on one tenth of the design draught, pressure=0.333 psi at the centre of station 8 1/2 for Fr=0.275 and f=0.5 Hz

Fig. 4.91 Discrepancy in the wave height sent by the wavemaker
(Run Nr. 25812, f=0.933 Hz, V=1.5 Volts)

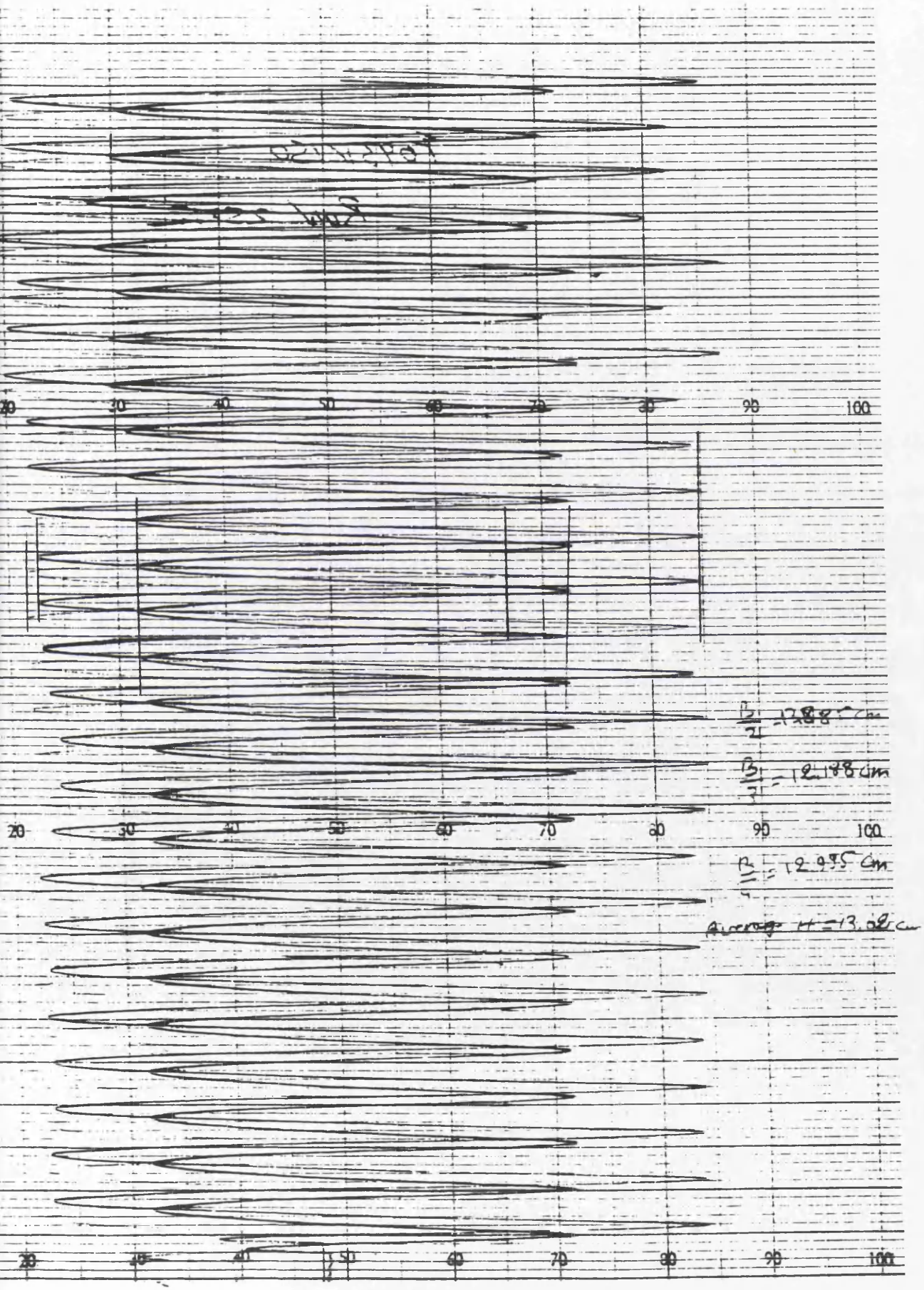

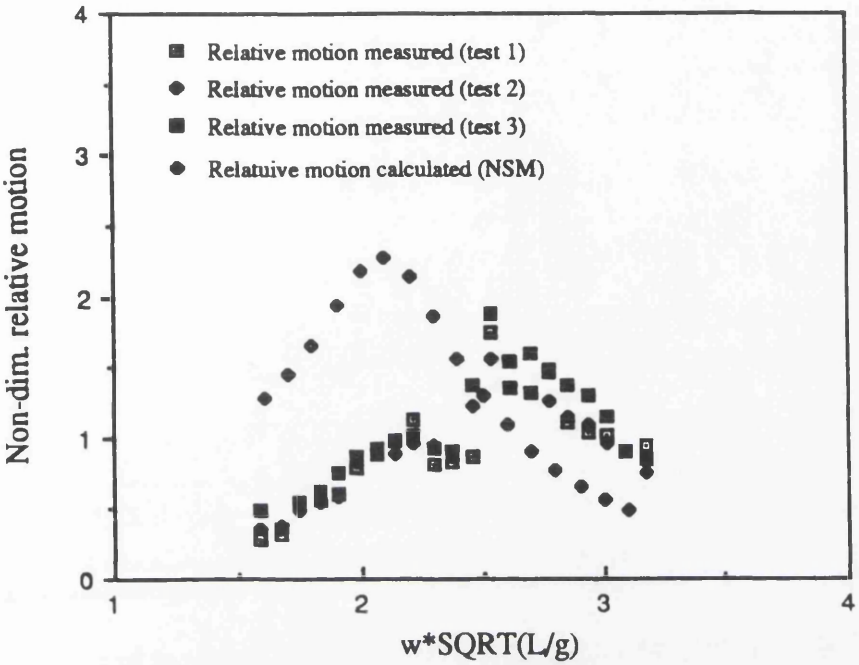

Fig. 4.92 Comparison between calculated and measured vertical relative motion for Fr=0.275

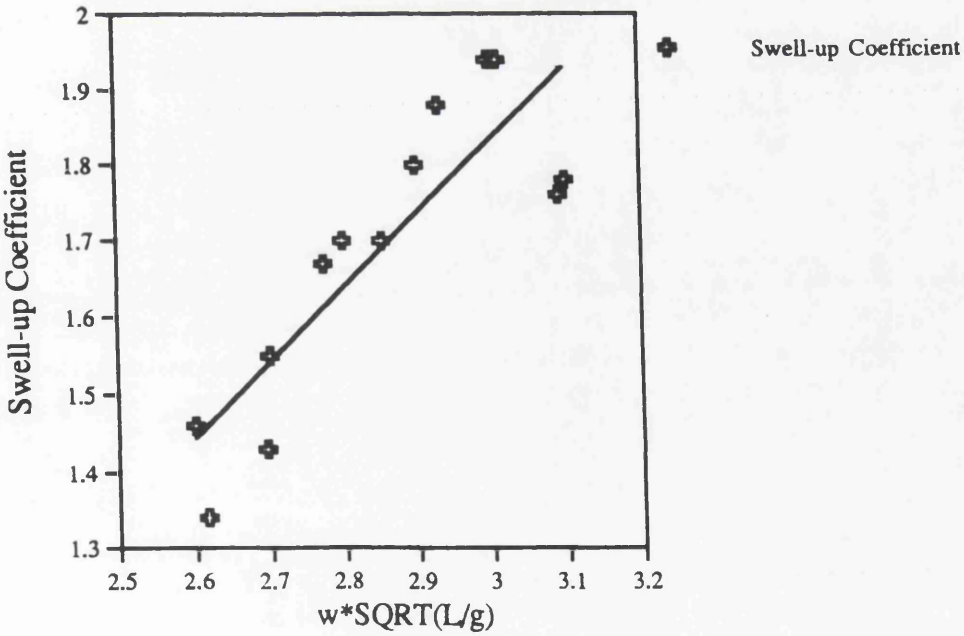

Fig. 4.93 Swell-up coefficient for the S175 container ship at Fr=0.275

CHAPTER 5

PROBABILITY APPROACH AND DESIGN SLAMMING PRESSURE

CHAPTER 5

PROBABILITY APPROACH AND DESIGN SLAMMING PRESSURE

5.1 PROBABILITY APPROACH

It is meaningful to consider the probability approach as a useful tool for predicting ship behaviour due to bottom slamming phenomenon. This chapter explains the probability approach for the occurrence of bottom slamming event.

The two parameter spectrum recommended by the 12th I.T.T.C. is given and is used as a tool to predict the variance of the vertical relative motion and velocity which are derived from heave, pitch and wave elevation for the S175 container ship using the developed computer program on the basis of the New Strip Method (NSM) given in chapter 2. These two variances are used for the prediction of probability of occurrence of slamming event. Furthermore, the number of slamming impacts are calculated as a function of ship operation time.

The ship designer is interested in the extreme pressure which may cause significant damage to the bottom of the structure of the hull. This extreme pressure is calculated for a given probability of occurrence, number of impacts and ship navigation time.

Slamming is a phenomenon associated with extreme motions of a vessel due to large amplitude of an incident waves. The moving vessel experiences an impact due to slamming when the forefoot hits the water surface during a severe pitching motion. As mentioned earlier, this impact is due to bottom slamming and it occurs if the vertical relative velocity between ship and sea surface for the station under consideration is greater than a critical velocity called the threshold velocity.

This phenomenon can be investigated by experiment and theory. Both methods can be used in probabilistic and statistical analysis in order to predict the occurrence of the event.

Fig. 5.1 represents the Response Amplitude Operator (RAO) for the relative motion which is calculated by superposition of heave, pitch and wave elevations for a given ship speed, wave amplitude and wave direction.

Fig. 5.2 represents Response Amplitude Operator for the relative vertical velocity which is the first derivative of the vertical relative motion with respect to time.

It is of great interest to know the occurrence of an event, such as a motion exceeding a certain critical level. The above motions are calculated in the frequency domain, as mentioned earlier, and can be easily used in probabilistic approach for predicting the slamming behaviour (probability of occurrence, number of impact per unit time and extreme magnitude of the pressure).

The spectrum (Bretschneider spectrum) in the two parameter form, with significant wave height and characteristic period, is recommended by the 12th I.T.T.C..

This spectrum is presented in Fig. 5.3 and it is given by the following expression as:

$$S(\omega) = \frac{A}{\omega^5} e^{-\frac{B}{\omega^4}} \tag{5.1}$$

with

$$A = 173 \frac{\zeta_{1/3}^2}{T_1^4} \tag{5.2}$$

$$B = \frac{691}{T_1^4} \tag{5.3}$$

where:

$\zeta_{1/3}$: significant wave height,
T_1 : characteristic wave period and
ω : wave frequency.

It is necessary to transform the wave spectrum in terms of frequencies of encounter instead of frequencies of the waves. As plotted in Fig. 5.4, the wave spectrum as encountered by the ship is obtained as:

$$S(\omega_e) = S(\omega)\frac{1}{[1-(\frac{4\omega_e U}{g})\cos\chi]^{1/2}} \tag{5.4}$$

where the frequency of encounter is given in term of the frequency of the wave:

$$\omega_e = \omega - \frac{\omega^2 U}{g}\cos\chi \tag{5.5}$$

where:

U	:	forward speed of the ship
χ	:	angle of the incident wave
g	:	acceleration of gravity.

Fig. 5.5 and 5.6 represent the response spectrum for the vertical relative motion and velocity respectively.

5.2 PROBABILITY OF SLAMMING OCCURRENCE

The occurrence of an impact, i.e Fig. 5.7, at a given location is a function of vertical relative motion and velocity relative to wave elevations. The probability of slamming impact can be evaluated by applying the following formula given by Ochi et al (1973) as:

$$\Pr\{\text{slam impact}\} = e^{-(\frac{H^2}{R_r}+\frac{V_{cr}^2}{R_{\dot{r}}})} \tag{5.6}$$

where:

H	:	ship draught at station where the slamming may occur
V_{cr}	:	threshold velocity
R_r	:	twice variance of relative motion
$R_{\dot{r}}$	:	twice variance of relative velocity.

The variance of the relative motion and vertical velocity as referred by Djatmiko (1992) is:

$$R_r = 2\int_0^\infty (r/\zeta_a)^2 S(\omega_e)d\omega_e \tag{5.7}$$

$$R_{\dot{r}} = 2\int_0^\infty (\omega_e r/\zeta_a)^2 S(\omega_e)d\omega_e \tag{5.8}$$

r : relative motion amplitude
ζ_a : wave amplitude
$S(\omega_e)$: spectrum given in equation (5.4).

Table 5.1 lists the probability of impact occurrence as a function of characteristic wave period and significant wave height for two draught conditions.

5.3 NUMBER OF IMPACTS

Marine vehicles are experiencing a number of slam impacts during their operation time. The number of these impacts per unit time is as shown in Fig. 5.8 and can be expressed by the following expression:

$$N_s = \frac{1}{2\pi}\sqrt{\frac{R_{\dot{r}}}{R_r}}\, e^{-\left(\frac{H^2}{R_r}+\frac{V_{cr}^2}{R_{\dot{r}}}\right)} \tag{5.9}$$

Furthermore the number of impacts (in hours) can be evaluated if the operation time of ship is given, i.e:

$$N = 3600TN_s \tag{5.10}$$

where:

T : ship operation time (hours).

Table 5.1 presents the probability of occurrence for different characteristic wave periods and for a different significant wave heights. On the basis of probabilistic results,

it can be concluded that the high number of occurrence depends on high probability and vice versa. For a characteristic wave period of 10 seconds and significant wave height of 10 m the probability of occurrence is 0.005 for loaded draught and 0.213 for ballast draught conditions. This is also true in the real state.

If the ship maintains the same speed and the same environment the number of impacts increase with ship operation time and the probability of occurrence is presented in Table 5.2 and 5.3 .

5.4 EXTREME IMPACT PRESSURE

The extreme impact pressure is also of importance to the designer as it may induce significant damage to the bottom structure of the ship, i.e Fig. 5.9. This extreme pressure depends on the probability of exceedance and can be evaluated as:

$$\hat{p}_s(\alpha) = p_* - \frac{1}{2}\rho k_1 R_r \ln\{1-(1-\alpha)^{\frac{1}{N}}\} \tag{5.11}$$

the threshold slamming pressure given as:

$$p_* = \frac{1}{2}\rho k_1 V_{cr}^2 \tag{5.12}$$

where:

ρ : density of water

k_1 : slamming pressure coefficient, depends on the shape of the section.

In order to use the above formula to predict the extreme pressure, the designer has to specify the probability of exceedance α. The ship is more safe from experiencing an extreme pressure if the value of the probability of exceedance α is smaller. Also the extreme pressure depends on the number of slamming impacts which in turn is a function of the operation time, and it increases with an increase in time of navigation for the same environment.

Table 5.2 and 5.3 also presents the influence of the number of impacts per hour on the extreme pressure. One of the conclusions that can be drawn from these results and

also from Hamoudi (1994), is that the extreme pressure increases with increase in the number of impact. Using Bretschneider spectrum the extreme pressure (with probability of occurrence 0.025) exceeds 1540 kPa. This extreme pressure is predicted when the significant wave height of 12.0 metres and the characteristic period of 10.0 seconds are imposed. It can also be concluded that the extreme slamming pressure depends on the environmental condition.

5.5 OTHER EMPIRICAL FORMULA FOR SLAMMING PRESSURE PREDICTION

Various model tests and investigations in the same field led to different approaches and empirical formulae to be used in the design and to predict the slamming pressure. This prediction is important in order to implement the strength requirement for the forward structure of the vessel. Some rules are generally revised annually and the designer is advised to consult the latest version of these rules.

These predictions are listed in Djatmiko's work (1992) and also in PANEL HS-2 (Impact Loading and Response) (1993) and are given as follows:

5.5.1 Sellars Method:

The pressure main equation is given bellow as:

$$p_2 = \frac{p_1}{2}\left[\left(1 + C\frac{V_0}{V_1} - \frac{C}{\delta_v}\right) + \sqrt{\left(1 + C\frac{V_0}{V_1} - \frac{C}{\delta_v}\right)^2 + 4\frac{C}{\delta_v}}\right] \quad \text{(psi)} \qquad (5.13)$$

where:

p_2 : absolute impact pressure

p_1 : absolute ambient pressure

C : structure impedance ratio, given in Djatmiko's work (1992)

V_0 : relative velocity at impact

$V_1 = \frac{p_1}{\rho_0 C_0}$

C_0 : speed of sound for pure liquid

ρ_0 : mass density for pure liquid

δ_v : liquid-air mixture volumetric impedance ratio (=0.0236).

5.5.2 Allen and Jones Method:

This method is based on theoretical and experimental data. The design limit pressure is given, as the average pressure over the impact reference area, by the following equation:

$$\bar{p} = \frac{N_z \Delta (2240)}{A_R} \quad \text{(psi)} \tag{5.14}$$

N_z : impact load factor or maximum amplitude vertical acceleration
Δ : full load displacement in long tons
A_R : impact reference area (in^2).

the impact reference area can be determined as:

$$A_R = \frac{25\Delta}{d}(144) \tag{5.15}$$

where d is the full load static draught in feet.

The maximum pressure (p_m) over the reference area can be calculated from the following equations:

$$p_m = \frac{\bar{p}}{0.14} \quad \text{(psi)} \tag{5.16}$$

The structural design pressure (p_D) is then determined by the following equation:

$$p_D = p_m F K_D \quad \text{(psi)} \tag{5.17}$$

where:

F : longitudinal pressure distribution factor
K_D : pressure reduction coefficient

5.5.3 Det norske Veritas (DnV):

This method estimates the design slamming pressure on flat cross structure as the greater of the following:

$$p_s = 2.6 k_t (\frac{\Delta}{A})^{0.3} a_{cg} (1 - \frac{H_c}{0.07L}) \quad \text{(kPa)} \tag{5.18}$$

and

$$p_s = 125 + \frac{L}{2.6} \quad \text{(kPa)} \tag{5.19}$$

where:

k_t : longitudinal pressure distribution factor

Δ : fully loaded displacement (tonnes)

$A = 2.5s^2$, design load area and not to be taken less than $0.002\Delta / T$

s : load factor

T : service draught

a_{cg} : design vertical acceleration

H_c : vertical distance from waterline to load point (m)

L : ship length.

According to DnV Classification and Registry of Shipping [(1978), the magnitude of impact pressure and the duration time depends on several factors, and which are cited as follows:

- Liquid density
- Relative velocity between panel and the liquid surface
- Angle between the panel and the liquid surface
- The panel flexibility.

The impact pressure due to slamming is taken by DnV is not as the peak pressure but the impact tail pressure (the following portion of the pressure and as is shown in Fig. 5.7). This decision has been taken on basis of the very short duration of the peak.

Under-estimating the peak pressure and taking the tail pressure only is a very serious matter. Perhaps the decision taken by DnV, is valid for a certain type of structure, and construction. Hence this may not be valid for other structures which differ in the type of construction. Furthermore, the magnitude of slamming pressure is proportional to the amplitude of the vertical relative velocity at the instant of impact (at the time of the peak) and not at the time which follows the impact (tail portion of the pressure).

5.5.4 American Bureau of Shipping (ABS):

The american bureau of shipping adopts the same formulation used by Allen and Jones, and this formulation is given as follows:

$$p_{max} = \frac{2240 N_z \Delta}{0.09 A_R} \quad \text{(psi)} \tag{5.20}$$

where:

N_z : impact load factor (or acceleration due to impact)
Δ : limiting displacement for strength (long tons)
$A_R = 0.06 L_{cr} B$, reference area (in^2)
L_{cr} : length of cross structure (in)
B : total ship breadth (in).

5.5.5 Lloyd's Register of Shipping

The equivalent slamming pressure is expressed as a head of water and calculated from the following expressions:

1) $65 < L \leq 169$ m:

$$h_{max} = 10\sqrt{L}F \quad \text{m} \tag{5.21}$$

2) $169 < L \leq 180$ m:

$$h_{max} = 130F \quad \text{m} \tag{5.22}$$

3) $L \geq 180$ m:

$$h_{max} = 130Fe^{-0.0125(L-180)^{0.705}} \quad m \tag{5.23}$$

where:

$$F = 5.95 - 10.5(\frac{T_{FB}}{L})^{0.2} \tag{5.24}$$

e : base of natural logarithm

L : distance from the forward side of the stem to the after side of rudder post

T_{FB} : minimum draught forward between 0.01L and 0.045L.

Besides these there are other empirical formulae used for the prediction of impact pressure due to slamming for design purposes. These formulae vary with variation of the type of the vessel.

5.6 DESIGN SLAMMING PRESSURE

As the pressure due to bottom slamming may damage the structure subjected to the transient impact, it is important to determine this slamming load which is referred to as design slamming pressure.

In open literature, the information on impact pressure due to bottom slamming is limited due to lack of measurement of full scale. The only information available is described as below.

Lewison (1970) reported in his paper that Aertssen attempted to measure the highest impact pressure due to slamming of the Jordaens ship which is 146.15 metres. This pressure was in the order of 175 kPa (25.4 psi).

Bledsoe et al (1960) reported from their seakeeping trials, conducted under the joint sponsorship of the Royal Netherlands and the United States Navies, that the maximum impact pressure recorded was of the order of 48 psi (331.2 kPa) for a Destroyer ship of 2988 tons and length 112 metres at speed of 25 knots. These impact pressures were measured using pressure gauge (Dynisco gauge with capacity of 500 psi). In other words, the recorded pressures were measured on the reference area of the

pressure gauge.

It is good practice to apply some of the empirical formulae given by different classification rules in order to compare the data obtained from the application of these rules, the measured data taken from the open literature and the present investigation.

Using Allen and Jones method the design pressure calculated for a flat panel size of an area of 30x100 in^2 (0.76x2.54 m^2), located at the bottom of the S175 container ship (24742 tons) is found to be 30.35 psi (209.4 kPa). The design pressure is calculated for the same panel using Det norske Veritas and found to be of the order of 27.87 psi (192 kPa). Moreover if one applies Lloyd's Register of Shipping method, the maximum pressure will be of the order of 16 psi (110.4 kPa).

As given in Table 4.4 the methods by Allen and Jones and Det norske Veritas correlate well and the difference is only 8% higher in Allen and Jones prediction. However the Lloyd's Register of Shipping prediction method gives a design pressure of 16 psi (110.4 kPa), this pressure is 47% lower than Allen and Jones prediction method and 43% lower than Det norske Veritas prediction method.

As there is no restriction given by Allen and Jones method for the determination of the design pressure, one may apply it to model scale for the S175 container ship. The design pressure for the model of the S175, for the same reference area scaled down to model scale, is found to be 1.285 psi (8.865 kPa). This pressure magnitude is not far from the measured pressures if the reference area is not taken into account. For example, the maximum pressure measured, on an area of the pressure transducer with the dimensions given in Fig. 4.4, for the S175 container ship model is found to be 0.503 psi (3.476 kPa) for loaded draught condition and Fr=0.275 when the model was underway in a head sea condition and the maximum impact pressure calculated by three and two parameter conformal mapping technique are 1.075 psi (7.42 kPa) and 0.801 psi (5.53 kPa) respectively, for loaded draught condition and Fr=0.278. According to Ohkusu and Hamoudi (1993) that the pressure transducer picks the average pressure applied on all over the area of the device. One may conclude that the design pressures calculated by Allen and Jones method for model scale which is 1.285 psi (8.865 kPa) and the maximum impact pressure calculated by three parameter which is 1.075 psi (7.42 kPa), for loaded draught condition and Fr=0.278, are in good agreement.

One may also determine the scale factor for the pressure between model scale and full scale for the S175 container ship by applying Allen and Jones method for both ship and model. By using this method the pressure scale factor can be obtained and is found to be 23.62 approximately. Further, all the measured data, from model test, of the impact pressure may be scaled up to ship scale.

5.7 CONCLUSIONS

This investigation can be used for better assessment of the performance of ship in a given seaway. The investigation has been focused on the probabilistic approach of slamming and design pressure. The main points of interest and which may be required by ship designer during the design stage are:

The probability of occurrence of slamming event depends mainly on motion response of the ship and the sea environment. The highest probability of occurrence of slamming for Fr=0.275 and a significant wave height of 4 m and characteristic wave period of 10 seconds is 0.188. For a characteristic wave period of 10 seconds and significant wave height of 10 m the probability of occurrence is 0.005 for loaded draught and 0.213 for ballast draught conditions.

The number of slamming impacts depend on the probability of occurrence and ship operation time. The highest value for the probability of occurrence occurs in the longest navigation time and results in a large number of impacts.

The extreme pressure depends mainly on the probability of occurrence, the number of impact and the ship operation time. The extreme pressure (with probability of occurrence 0.025) exceeds 1540 kPa. This extreme pressure is predicted when the significant wave height of 12.0 metres and the characteristic period of 10.0 seconds are imposed.

The design pressure by the Allen and Jones method for the model of the S175 container ship is found to be 1.285 psi (8.865 kN/m^2). This pressure magnitude is not far from the measured pressures given in chapter 4, if the reference area is not taken into account. The maximum pressure measured for the S175 container ship model is 0.503 psi (3.476 kN/m^2) for loaded draught condition and Fr=0.275 when the model was underway in a head sea condition and the corresponding maximum impact pressure

calculated by the three and two parameter conformal mapping technique are 1.075 psi (7.42 kN/m^2) and 0.801 psi (5.53 kN/m^2) respectively. One may conclude that the design pressures calculated by the Allen and Jones method for model and the maximum impact pressure calculated by three parameter for loaded draught condition and Fr=0.278, are in a good agreement.

The equivalent full scale pressures would be 23.62 times as great. This scaling factor is determined by applying Allen and Jones method for the ship and model.

Table 5.1 Probability of occurrence for different significant wave heights and characteristic wave periods at loaded and ballast draughts

		Pr.=Probability of occurrence	
H1/3 (m)	T (sec.)	H1=9.5 m	H2 =3.15m
4	6	*	*
	8	*	*
	10	*	*
	12	*	0.0001
6	6	*	*
	8	*	0.0009
	10	*	0.014
	12	*	0.012
8	6	*	*
	8	*	0.019
	10	0.0003	0.09
	12	0.0004	0.082
10	6	*	*
	8	0.0001	0.08
	10	0.005	0.213
	12	0.0065	0.202
12	6	*	*
	8	0.001	0.172
	10	0.025	0.342
	12	0.03	0.33

H1/3 : Significant wave height

T : Characteristic wave period

H1 : loaded draught

H2 : ballast draught

* : no slamming occurrence

Table 5.2 Extreme pressure as function of number of impacts and ship operation time for different significant wave heights and periods

T(sec.)	Probability	Operation time (Hour)	Nr. impacts	Extreme pressure (KN/m^2)
6.0	*	1.0	*	-
		5.0	*	-
		10.0	*	-
		15.0	*	-
		20.0	*	-
		24.0	*	-
8.0	*	1.0	0	397.37
		5.0	0.001	469.99
		10.0	0.001	501.27
		15.0	0.002	519.57
		20.0	0.002	532.56
		24.0	0.002	540.79
10.0	0.0003	1.0	0.114	532.67
		5.0	0.571	642.28
		10.0	1.143	689.51
		15.0	1.714	717.14
		20.0	2.285	736.74
		24.0	2.742	749.16
12.0	0.0004	1.0	0.16	494.02
		5.0	0.801	594.92
		10.0	1.603	638.4
		15.0	2.404	663.83
		20.0	3.205	681.87
		24.0	3.846	693.31

Conditions: H1/3=8.0 m, Fr=0.275, loaded draught

Table 5.3 Extreme pressure as function of number of impacts and ship operation time for different significant wave heights and periods

T(sec.)	Probability	Operation time (Hour)	Nr. impacts	Extreme pressure (KN/m^2)
		1.0	*	-
		5.0	*	-
6.0	*	10.0	*	-
		15.0	*	-
		20.0	*	-
		24.0	*	-
		1.0	0.546	750.64
		5.0	2.73	914.03
8.0	0.001	10.0	5.46	984.42
		15.0	8.19	1025.6
		20.0	10.92	1054.8
		24.0	13.105	1073.3
		1.0	11.505	1053.2
		5.0	57.524	1299.8
10.0	0.025	10.0	115.05	1406.1
		15.0	172.57	1468.3
		20.0	230.1	1512.36
		24.0	276.12	1540.3
		1.0	12.75	966
		5.0	63.72	1193.1
12.0	0.03	10.0	127.45	1290.88
		15.0	191.17	1348.1
		20.0	254.9	1388.7
		24.0	3.587	1414.4

Conditions: H1/3=12.0 m, Fr=0.275, loaded draught

Table 5.4 Comparison of design slamming pressure (kPa) calculated by various method for the S175 container ship

Allen & Jones Eq. (5.17)	DnV Eq. (5.19)	LR Eq. (5.22)
209.4	192	110.4

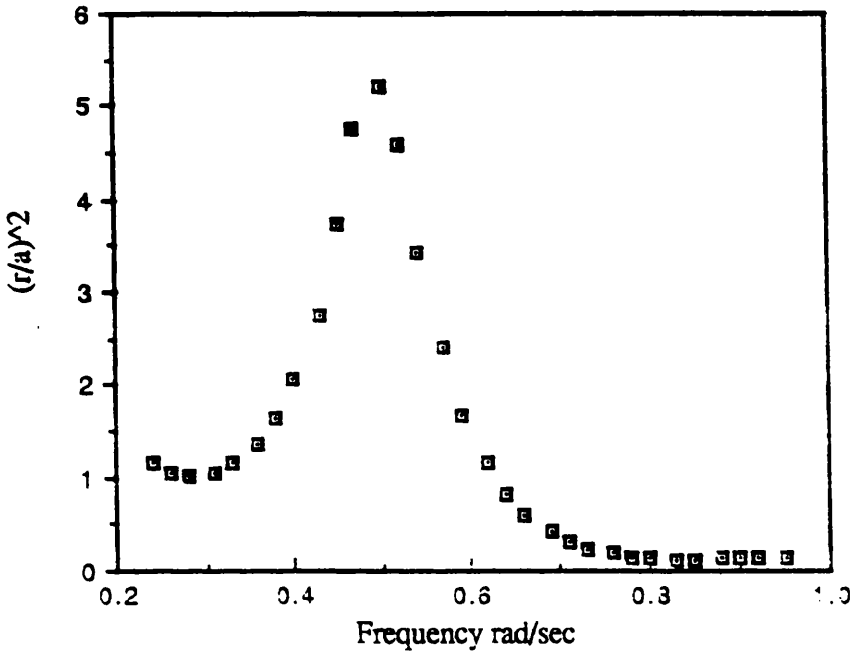

Fig. 5.1 Response amplitude operator
of relative motion (Fr=0.275)

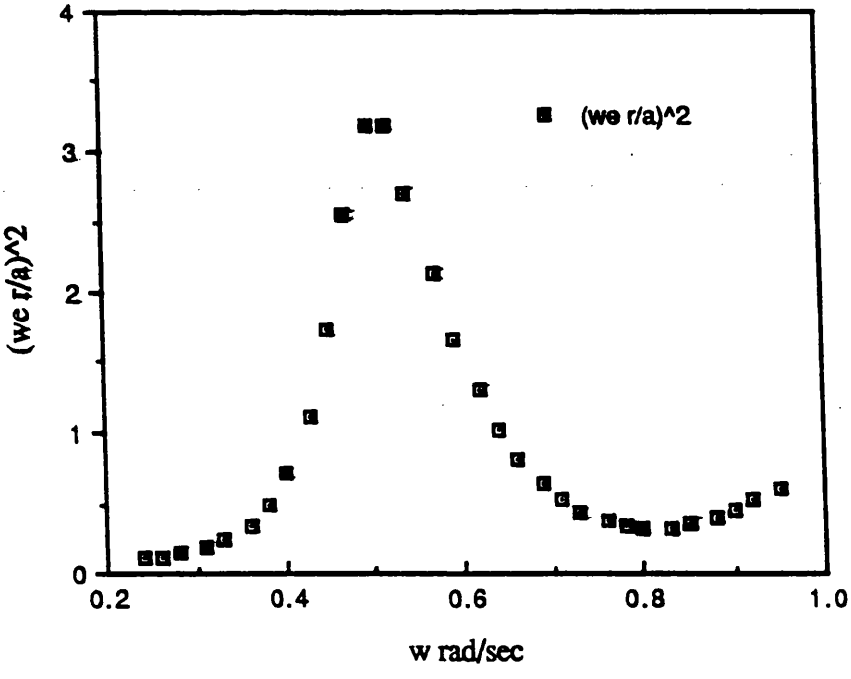

Fig. 5.2 Response amplitude operator
of vertical relative velocity (Fr=0.275)

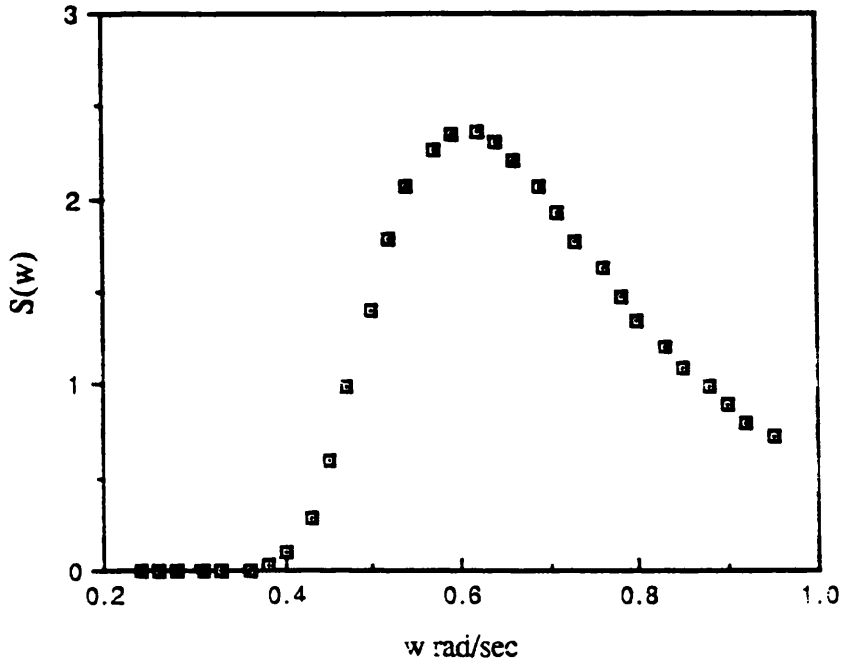

Fig. 5.3 Bretschneider spectrum with significant wave height 4m and wave characteristic period 8 seconds

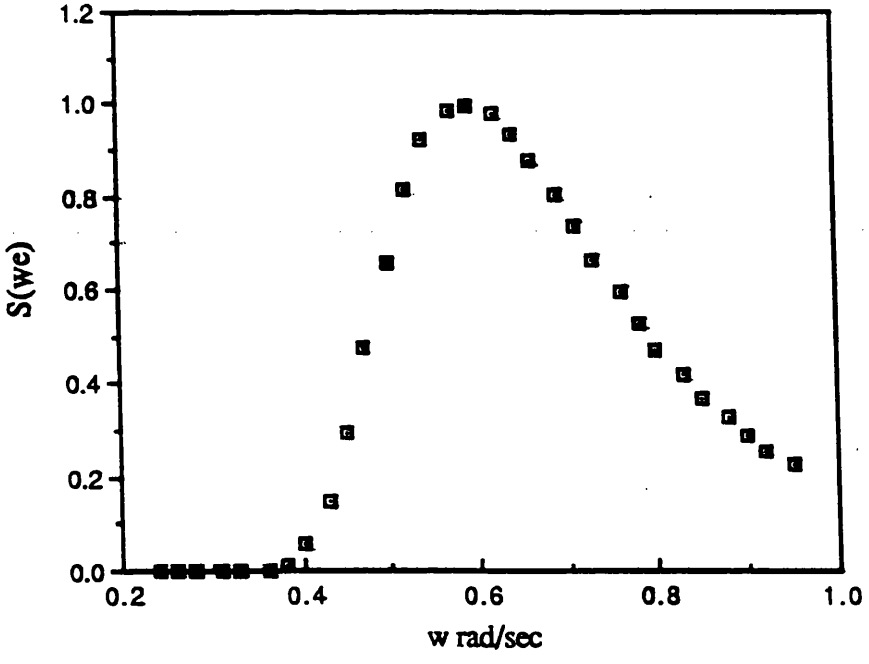

Fig. 5.4 Encountering wave spectrum for Fr=0.275

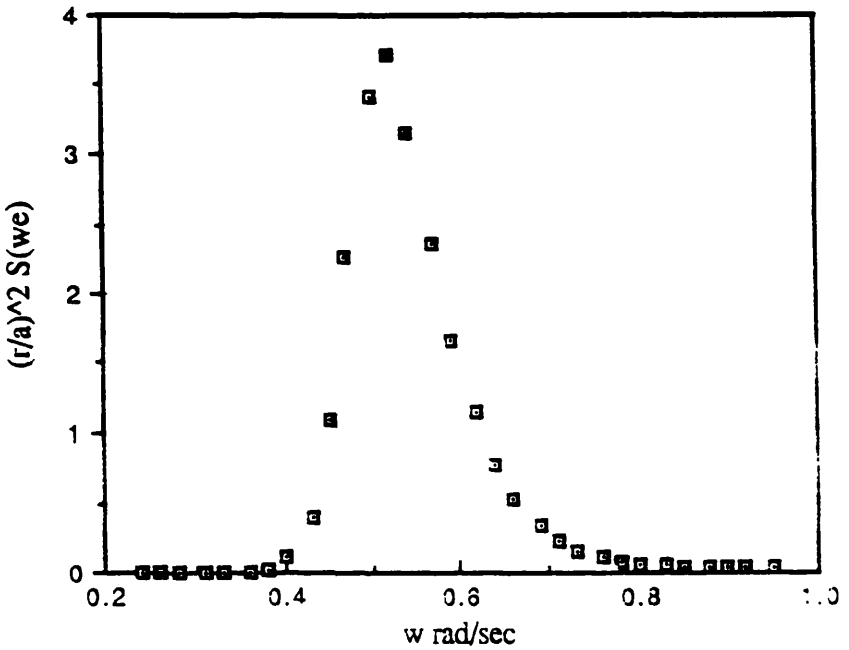

Fig. 5.5 Response spectrum for vertical relative motion for Fr=0.275

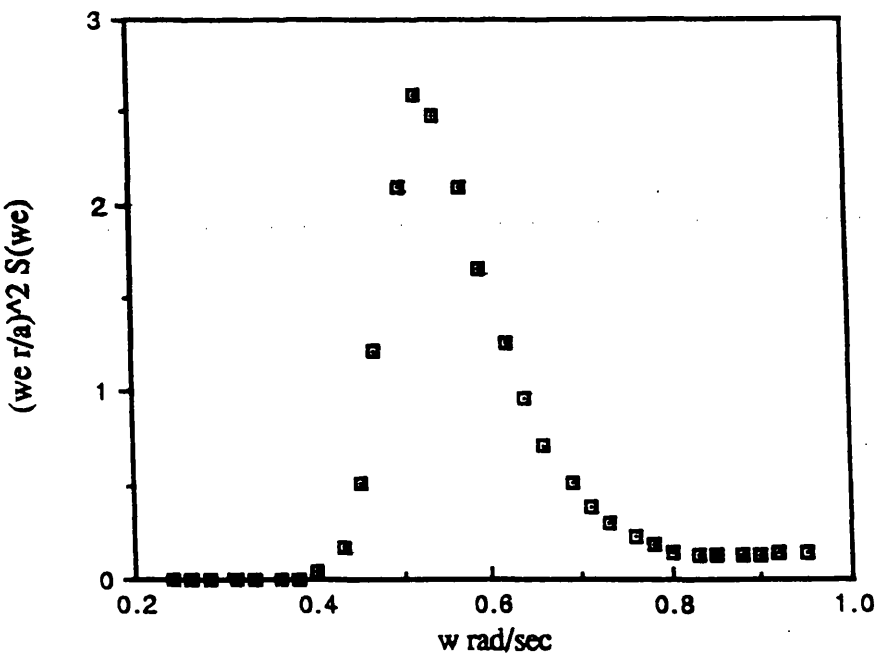

Fig. 5.6 Response spectrum for vertical relative velocity for Fr=0.275

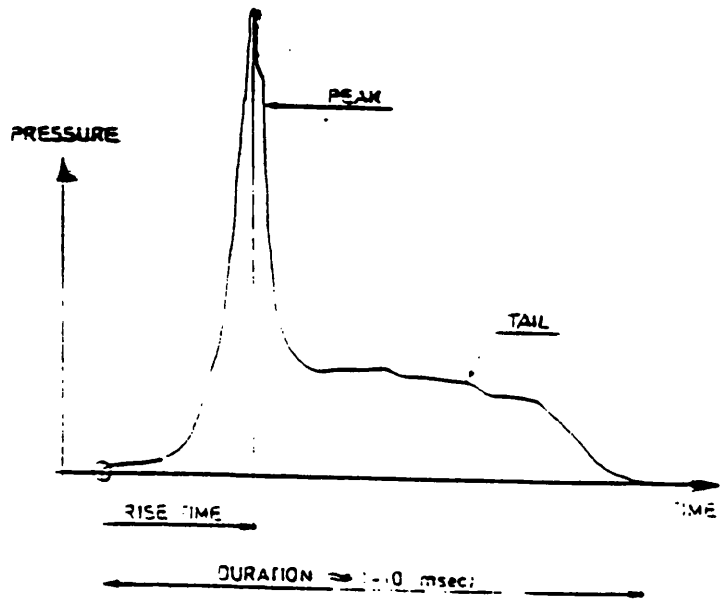

Fig. 5.7 Typical impact peak and tail pressure

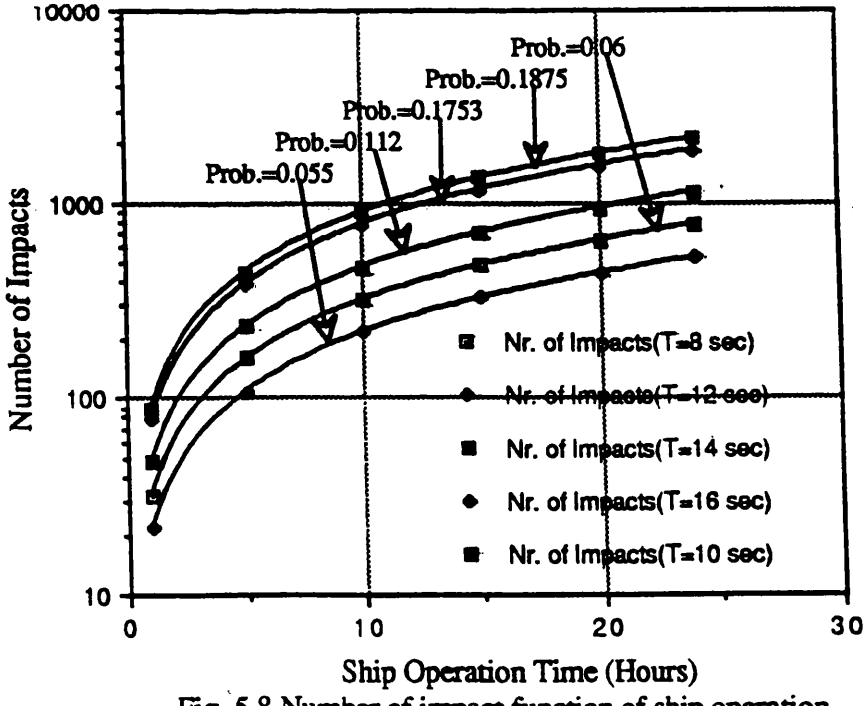

Fig. 5.8 Number of impact function of ship operation time for significant wave height H=4m, Fn=0.275.

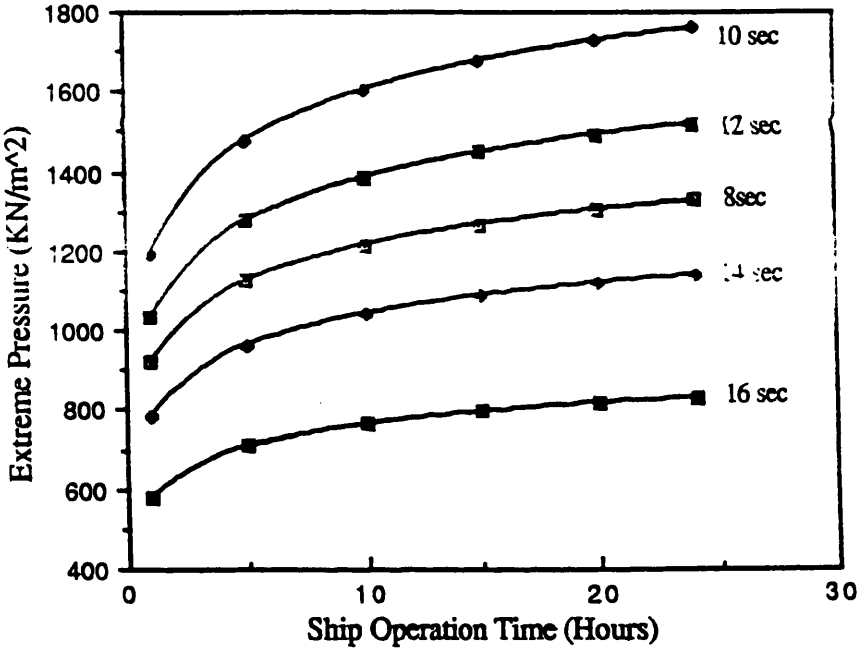

Fig. 5.9 Extreme pressure as function of ship operation time for significant wave height H=4m, Fn=0.275

CHAPTER 6

DECK WETNESS PHENOMENON

The qualitative and quantitative data collected by Lloyd are very useful for the given ship (the narrow beam LEANDER), but deck wetness is a common event for other ships and in particular for high speed vessels. Besides these other conditions for ship navigation also need to be taken into account.

In order to investigate the complex phenomenon of shipping water on deck Mizoguchi (1988) measured the impact pressure acting on water breaker and carried out numerical simulation on a model of S-175 container ship in regular head waves. In this investigation the impact pressure acting on water breaker is predicted using the empirical equation for impact pressure due to water jet. The conclusions from the measured wave height contours indicate that at the beginning of shipping of water, the flow is similar to a dam break water. For the case when the wave height is high the water is concentrated in the forepart of the fore castle deck and it crashes against the aft water breaker. For the lower wave height case, the water is concentrated in the forepart of the fore castle deck and it spreads in all directions. It was also found that the wave height and the deck area are the most important parameters related to shipping water on deck.

In the above numerical simulation, ship motions were not taken into consideration. However in reality ship motions play a vital role in predicting the deck wetness phenomenon and it is also known that the deck wetness phenomenon occurs when the relative motion exceeds the freeboard of the vessel.

A technique to evaluate the duration of threshold crossing of a random process was applied for the first time to shipping of green water by Oliver (1981). This technique predicts the probability of occurrence of deck wetness event. Unlike Mizoguchi, Oliver has taken into account the relative motion of the vessel with respect to the sea surface. The amplitude of threshold crossing was evaluated by Rayleigh distribution. Furthermore, the volume of shipping water on deck and the total pressure on the deck was also calculated.

Edward and Todd (1938-39) reported that deck wetness is one of the factors which determine seakindliness or seaworthiness. Three models were tested with forward freeboards of 11.75 ft, 8.5 ft and 11.75 ft respectively. The tests in regular waves showed the importance of sufficient forward freeboard. The second model sank, whilst the first and the third remained nearly dry. However, these conclusions are not significant, as they did not mention the speed at which the models were run.

The present chapter investigates a set of experiments in regular waves with the S175 container ship model for different forward speeds. Deck wetness was quantified by measuring the forces in the longitudinal direction and by collecting the mass of water shipped on deck.

6.2 EXPERIMENTAL INVESTIGATION ON DECK WETNESS

6.2.1 Model

The event of deck wetness occurs mostly with high speed vessels. For this reason the chosen model is S175 high speed container ship and is made of glass reinforced plastic (GRP) to a ratio of 1/70. This is also the same model used for slamming tests. The ratio between freeboard and ship length for stations FP, 9 1/2 and 9 are given in Table 6.1. Main dimensions and offset table for the container ship S175 are given in detail in Tables 4.1 and 4.2 of chapter 4.

6.2.2 Instrumentation Setup and Calibration

While carrying out slamming tests, investigation on deck wetness was also carried out. As both of these phenomena occur in the fore region of the vessel under consideration, most of the measurement apparatus was concentrated in this region of the model.

6.2.2.1 Wave Probes

As stated for slamming test, the undisturbed wave heights were measured with three resistance type wave probes fixed to a bridge across the tank width at distance of about 5 metres in front of the wave-maker. The calibration process is the same as in the case of slamming tests. The average of these wave heights was taken for analysis.

Another resistance wave probe of the same type was fixed at the bow in order to measure the relative bow motion. This wave probe was inclined by an angle of more than 50 degrees in order to take the same shape of the bow, therefore any measurement from the wave probe must be multiplied by a correction factor which is the cosine of this angle to give the vertical relative motion. The calibration process of the wave probe in the fore region of the ship was the same as that of the wave probe at station 8 1/2, used for

slamming tests.

6.2.2.2 Load cells

The wetness impact forces (longitudinal forces or impact pressures) were measured using nine square plates mounted in a array over the deck at station 9 1/2 and is as in Fig. 6.1. Each plate is mounted on a load cell (Sensotec 'D' series, range 0.5 lbs). As three load cells failed before the set of experiments commenced, the runs were conducted with the remaining six load cells only. Fig. 6.2 represents load measurement device (load cells) located at station 9 1/2 on the deck of container ship model S175.

The nine load cells were individually calibrated before assembly by applying different weights from 100 grams to 1000 grams, with an incremental step of 100 grams. Six of the nine load cells behaved similarly while three failed. Fig. 6.3 shows the response of the load cells which is linear and within the range of calibration. Once the load cells were calibrated, they were built into plates mounted in an array and positioned in the desired orientation on the deck to receive (measure) the longitudinal force due to the incoming water on deck.

Lloyd et al (1985) mentioned in their paper that an impact due to wetness is accepted as true wetting if:

- it was recorded on at least two pressure transducers
- it exceeded a threshold pressure (10 kN/m^2 full scale)
- it occurred at least 4 seconds (full scale) after the previous impact.

It was also recommended by Lloyd et al (1985) that the most frequent freeboard exceedance occurs between the forward perpendicular and station 9 if the ship is divided into 10 stations, and for this reason the plates were mounted at station 9 1/2.

6.2.2.3 Accelerometer

As shown in Fig. 6.1 this device was installed on the deck to measure the deck acceleration. This device is a gravity type accelerometer. The calibration procedure is given in section 4.4.4 of chapter 4.

6.2.2.4 Selspot System and Light-Emitting Diodes

Selspot system and light-emitting diodes were used to measure heave and pitch oscillations of the model using equation (4.1) and (4.2).

6.2.2.5 Water Container

As water was expected to be shipped on deck, a water container was placed inside the model (at the centre of gravity) and linked to the forecastle deck side line by tube. A pump was used to pump the water out from the container to avoid any effect on the motions and the quantity of water was weighed after each test.

6.2.3 Test Procedure and Data Acquisition system

A set of experiments were carried out in the Hydrodynamics Laboratory of Naval Architecture and Ocean Engineering, University of Glasgow. The model of the container ship was run in ballast and loaded draught conditions in regular head waves and at zero trim. All the running conditions are similar to the bottom slamming tests. Heave and pitch are the only degrees of freedom allowed during the test.

As mentioned earlier, the model was run for different Froude number, namely 0.1, 0.15, 0.2, 0.278 and 0.3 and for different wave frequencies. The range of these frequencies are calculated using Hamoudi's (1992 a) computer program developed to determine the frequencies at which the tank wall interferences (blockage phenomenon) are avoided, and also in accordance to the 15th ITTC recommendations (Seakeeping Committee) (1978).

The runs were recorded by a Panasonic MC20 VHS type video camera. All the signals are collected by the Data Collecting System (32 channel analogue to digital converter) and recorded into Macintosh-2CLA micro computer system. The experimental data are sampled at the rate of two thousands (2000) samples per second per channel and for 20 seconds. For higher speeds the running time was 12 seconds because of the length of the tank. Fig. 4.5 illustrates the electronic equipment on the moving platform.

All relations of calibration data converted from induced voltage to actual responses or loads are linear. All experimental data acquired by Macintosh-2CLA

computer are analysed in frequency domain, using the Fast Fourier Transform technique on the VAX-3100 workstation computer system and also in time domain on the VAX/VMS computer system.

The data collected during the test are automatically converted into the corresponding unit of magnitude recorded by using the calibration factor determined from the calibration process.

6.3 ANALYSIS TECHNIQUE FOR DECK WETNESS

The analysis was done in the frequency domain and no deck wetness was encountered for ballast draught condition (high freeboard). The vertical relative motions, vertical deck acceleration and the impact pressure (impact force in the longitudinal direction on the area of the plate) recorded during the experiments are plotted against nondimensionalised frequency.

6.3.1 Threshold Vertical Relative Motion

In the case of green seas, threshold vertical relative motion is the limit of the relative motion at which deck wetness phenomenon may occur. This relative motion is compared with the freeboard value to determine the occurrence of deck wetness. Freeboard value for the S175 container ship model is 9.975 cm at the forward perpendicular station (FP).

Fig. 6.5 represents the nondimensional vertical relative motion with respect to wave amplitude (6 cm in amplitude) at the bow for Fr=0.1. For this case the recorded vertical motion exceeds the freeboard value except for $\omega\sqrt{\frac{L}{g}} < 2.0$. In this region the relative motion measured is far less than the value of the freeboard but for $\omega\sqrt{\frac{L}{g}} > 2.0$ the relative motion is higher than the value of the freeboard. The highest relative motion recorded for Fr=0.1 is recorded for nondimensional frequency of $\omega\sqrt{\frac{L}{g}} = 2.02$.

Fig. 6.6 illustrates the bow vertical relative motion for Fr=0.15. In this case the relative motion exceeds the freeboard at FP and shipping of water on deck takes place in

the frequency range $2.0 < \omega\sqrt{\frac{L}{g}} < 2.8$. The highest vertical relative motion at the bow for this case is recorded for $\omega\sqrt{\frac{L}{g}} = 2.5$.

Fig. 6.7 shows the recorded vertical relative motion at the bow for Fr=0.2, where the highest value is recorded for $\omega\sqrt{\frac{L}{g}} = 2.5$ and this relative motion exceeds the freeboard in the nondimensional frequency range $2.0 < \omega\sqrt{\frac{L}{g}} \leq 2.5$.

Fig. 6.8 represents the bow vertical relative motion recorded for Fr=0.278. The freeboard exceedance occurs when the relative motion exceeds its threshold value at the bow in the nondimensional frequency range $2.0 < \omega\sqrt{\frac{L}{g}} \leq 2.5$ and the highest value occurred at $\omega\sqrt{\frac{L}{g}} = 2.1$.

Fig. 6.9 illustrates the relative motion for Fr=0.3. The freeboard exceedance occurs also in the nondimensional frequency range $2.0 < \omega\sqrt{\frac{L}{g}} \leq 2.5$ and the highest relative motion occurred at $\omega\sqrt{\frac{L}{g}} = 2.26$.

The effect of forward speed on freeboard exceedance is consistent, as explained in the above figures of bow vertical relative motion, this effect is consistent except for some vagaries resulting from the setup of the model or the calibration of the instrumentations used during the experimental investigations. For example at Fr=0.2 and nondimensional frequency $\omega\sqrt{\frac{L}{g}} = 2.26$ the nondimensional relative motion recorded is more than 1.5 and for the same frequency and Fr=0.278 the relative motion recorded is less than 1.5. However for Fr=0.3 the relative motion is more than 1.5.

6.3.2 Heave and Pitch Motion

Heave was obtained by using equation (4.1). Figs. 4.34, 4.36, 4.38, 4.40 and 4.42 represent the nondimensional heave amplitude response for Fr=0.1, 0.15, 0.2,

0.278 and 0.3 respectively and for loaded draught at which the deck wetness phenomenon is more likely to occur.

Pitch was obtained by using equation (4.2). Figs. 4.44, 4.46, 4.48, 4.50 and 4.52 represent the nondimensional heave amplitude response for Fr=0.1, 0.15, 0.2, 0.278 and 0.3 respectively and for loaded draught at which the deck wetness phenomenon is more likely to occur.

The bow vertical relative motion of the model is affected by heave and pitch motions. As the model was restricted from other motion, the recorded relative motion values may have been affected slightly.

6.3.3 Measured Force in the Longitudinal Direction

For most of the runs in the loaded draught conditions, water was shipped on deck and was impinging the load cells.

All the loads recorded during deck wetness tests are presented in figures, including the loads which did not exceed the pressure (10 kN/m^2 full scale) reported by Lloyd (1982). Figs. 6.10 to 6.19 represent the measured impact forces (impact pressure) on top and bottom row of plates for different Froude number, i.e Fr=0.1, 0.15, 0.2, 0.278 and 0.3 respectively. Also Table 6.2 represents the impact pressures scaled to full scale values by using linear dynamical similarities. These impact pressures follow the same trend as the bow vertical relative motion except for some points which are believed to be vagaries of the experiments.

In most of the cases the magnitude of the impact pressures recorded on the bottom row of plates are higher than the one recorded on the top row of plates. Among the bottom plates the middle load cell recorded the highest impact as shown in the Fig. 6.10 to 6.19. For Fr=0.2 plate 5 in the centre of the bottom row recorded more than 1.945 kN/m^2 model scale (i.e more than 136 kN/m^2 full scale) and plate 2 which is in the centre of the upper row recorded 0.418 kN/m^2 (29.4 kN/m^2 full scale), this load is not far the design load given by Lloyd's Register of Shipping (1982). On comparison of the results between the top and bottom row of plates, one can say that there is a good agreement between the present set of experimental results and those by Lloyd (1982).

Increasing the forward speed also makes remarkable changes in the magnitude of the pressures recorded on the plates, particularly the load cell which is in the centre of the bottom row.

The impact pressures recorded on the top row of plates were in most cases lower, but were not far to be unbelievable from those recorded on the bottom row of plates. Also for certain Froude number plate 1 on the starboard side of the top row recorded a higher pressure than plate 3 on the port side. As concluded by Hamoudi (1993 a), heave and pitch were the only two degrees of freedom allowed during experiments and to a certain extent experimental results show that the recorded results of these plates are symmetrical in regular waves, except for some odd points which are believed to be caused by restriction of the model from other degrees of freedom.

6.3.4 Shipping of Water on Deck

As mentioned earlier, a pump was used to pump the incoming water out from the model. Fig. 6.20 represents the weighed mass of water shipped on deck for different speeds (Froude number) and various frequencies. The total mass shipped on deck depends mainly on forward speed of the model and the relative motion exceeding the freeboard. In the case of high speeds, deck wetness occurred more frequently and violently as more water was shipped on deck. The water was not only coming from the fore part of the vessel but also from the sides.

For Fr=0.3 and frequency 4.48 rad/sec, the mass of water collected is more than 42 kg, in this case the nondimensional relative motion recorded exceeded the value of 1.5 and the model nearly sank.

6.3.5 Vertical Acceleration

Vertical deck acceleration increases by increasing forward speed, as in Figs. 4.54, 4.56, 4.48, 4.60 and 4.62 respectively. For example, the peak acceleration recorded during the set of experiments, for Froude number 0.278, is 5.189 m/sec^2 (0.53 g). This is more than half the acceleration of gravity, and as a result of this, the nondimensional relative motion exceeding the freeboard recorded is more than 1.5, and a huge mass of water (12.4 kg) was shipped on deck.

6.4 PREDICTION OF THE IMPACT FORCE (PRESSURE) IN THE LONGITUDINAL DIRECTION

Deck wetness phenomenon can be very severe and may cause serious damage on the deck level. This makes the crew's task on the wet deck difficult and may be impossible to handle. The performance and effectiveness of the vehicle will be degraded as result of this event and her mission will not be completed in good condition.

The severity of deck wetness event can be decreased by slowing down the speed of the marine vehicle if moving or changing the heading angle until the storm is over. This decision affects the operational effectiveness.

Conclusions given by Lloyd (1983, 1985) and Bales (1979) state that the main parameters which influence this event is the freeboard (the above water-line structure) and to a certain extent the forward speed Fukuda (1983).

6.4.1 Definition

The impact force in the longitudinal direction is the force due to the mass of water hitting the vertically positioned equipment. The mass of water is randomly distributed in space after the occurrence of deck wetness.

6.4.2 Formulation of the Impact Force

As in Fig. 6.21, the relative vertical motion exceeds the freeboard, and as a result of which deck wetness occurs and an undefined mass of water, in its quantity, which has high velocity, comes on deck and impacts the superstructure or any equipment mounted on deck such as gun ... etc.. This force is a variable, and it is a function of the velocity of the undefined mass of water, the forward speed of the marine vehicle and the level of the relative vertical motion exceeding the freeboard.

It is a very complex task to predict the volume of mass shipped on deck, but some assumptions have to be made in order to linearise the complexity of the problem.

Because the vessel is navigating in head seas with a certain forward speed if any, the mass of the water is moving in the opposite direction with a certain velocity and

which is the wave velocity plus the forward speed of the vehicle.

The mass of the water is estimated from the water shipped on deck and it can be calculated from the volume of water as follows:

$$m = \rho \nabla \tag{6.1}$$

where:

ρ : water density and

∇ : volume of water.

The volume of water as given by Oliver (1981) is the summation of parallel sectional elements as follows:

$$\nabla = \int_0^L A(x)dx \tag{6.2}$$

where:

$$A(x) = B(x)Z(x) \tag{6.3}$$

B(x) : deck beam at x

Z(x) : longitudinal wave shape function.

The phenomenon is very complex and highly disturbed and for this reason the volume calculated in equation (6.2) consists of a mixture of water and air. A dispersion factor is incorporated in the above equation, and the volume of water can be rewritten as follows:

$$\nabla = \int_0^L kA(x)dx \tag{6.4}$$

where:

$$0 < k \leq 1.0$$

The dispersion coefficient k depends on how homogenous the mass is, which is a mixture of water and air. It can be chosen by intuition and/or can be calculated from experiments as is the case in this investigation. Moreover, this coefficient can be predicted approximately by comparing the calculated and the measured forces.

If the water is crossing a certain distance called the wetted length 'L', this length can be easily identified by specifying at which station the impact force is going to be exerted, and from each reference point in the fore end, from where the water is coming. It is assumed by Hamoudi et al (1994) that the crossing time can be approximated by dividing the crossed length by the velocity of the mass of the water. The approximate expression for the impact force in the longitudinal direction is then written as follows:

$$F = m\frac{(U+C)^2}{L} \tag{6.5}$$

The force in the longitudinal direction can then be rewritten as follows:

$$F = \rho\nabla\frac{(U+C)^2}{L} \tag{6.6}$$

The calculated force in the longitudinal direction in equation (6.6) is predicted under some strongly idealistic assumptions and which are cited as follows:

- mass of water does not vary along the crossed length
- mass collected in the catch tank did hit the vertical wall without any water coming from other directions
- mass of water has got a constant energy till it hits the obstacle
- crossed length reference starts from the very end of the overhang
- mass of water moves in the longitudinal direction only.

Equation (6.6) can be interpreted as the force exerted in the longitudinal direction to be inversely proportional to the crossed length of the mass of water under consideration. In other words, if the vertical wall (superstructure, appendages, deck mounted equipment, guns...etc.) is at a larger distance from where the water is getting shipped, the impact force applied decreases. These conclusions also agree with the results presented by Oliver (1981). Fig. 6.22 presents the impact force per unit mass as

a function of the crossed length, and it increases for decreased crossed length.

The mass of water, while moving, is varying in its quantity and shape before hitting the vertical wall. This mass of water, which will be shipped on deck, after hitting the wall, depends on the shape of the forebody of different type of ships (freeboard, flare angle...etc). Furthermore, the knowledge of quantifying the mass of water is still at its formative stage. For example, Mizoguchi (1988) found that the water heights on the triangular deck form with narrower deck area, are higher than that of the semi-circle deck form with wider deck area. And the speed of the water particle of the triangle deck form are faster than that of the semi-circle deck form. Also Lloyd et al (1982) found from his experimental investigation that the effect of deck shapes, bluntness or sharpness, are less conclusive. He also noticed that for a speed of 17.5 knots of the narrow beam LEANDER frigate both blunt and sharp stems appear beneficial but sharpness has much less effect at 20 knots.

6.4.3 Calculation of the Impact Force from the Experimental Data

Because of difficulties in the analytical approach of deck wetness, predictions of wetness is often made directly by testing a model in regular or irregular waves, and observing the phenomenon of shipping of water. A video tape records and catch tank technique are often used to clarify the event.

In order to quantify theoretically the wetness impact force in the longitudinal direction acting on a vertical wall, a catch tank technique was placed inside (at the centre of gravity) of the model of S175 container ship, to collect the incoming water on deck. The mass of water collected by the catch tank technique mentioned above was used as an input data into equation (6.6) to predict the force in the longitudinal direction acting on a vertical wall due to impingement of water. Table 6.2 presents the magnitude of the impact force acting on vertical wall in the longitudinal direction converted to impact pressure (impact load/plate area).

6.4.4 Dispersion Factor

The dispersion factor proposed by Oliver (1981) is calculated by dividing the impact pressure obtained from experiment with the calculated pressure from equation (6.6) and is as in Table 6.3. This dispersion factor lies between 0 and 1.0. It equals 0 when there is no force applied on the vertical wall, but is always lower than 1.0 due to

non-homogeneousity of the mass of water. The dispersion factor can be calculated by the following equation:

$$k = \frac{\text{Measured Load}}{\text{Calculated Load}} \tag{6.7}$$

The dispersion factor presented in Table 6.3 may not be accurate at this stage, due to the assumptions given above. However, it can be used as a first approximation of design. For example the minimum value of the dispersion factor calculated in the present research is 0.012 and the maximum value is around 0.94. The reason for large variation in certain cases of the measured and calculated load can be attributed to the fact that water was slipping from the sides, and top of the plates. The mass of water which is a good indicator in these calculations is represented in histogram format as in Fig. 6.20.

6.5 PROBABILITY APPROACH FOR DECK WETNESS

The probability of deck wetness occurrence depends mainly on relative motion exceeding the freeboard. Furthermore, the occurrence of deck wetness depends on other parameters, such as environmental conditions and to certain extent forward speed of the marine vehicle.

6.5.1 Probability and Number of Deck Wetness Occurrence

Deck wetness can be predicted by using probability tool. The probability of occurrence of the deck wetness process by Price et al (1974) is:

$$\Pr\{\text{wetness occurrence}\} = e^{-\frac{f^2}{R_r}} \tag{6.8}$$

where:

f : freeboard
R_r : twice variance of the bow relative motion.

The variance of the bow vertical relative motion is calculated from equation (5.7) using the spectrum given in equation (5.4).

Bretschneider spectrum in the two parameter form, with significant wave height and characteristic wave period, is used for the investigation of deck wetness.

The number of deck wetness per hour can be calculated from the following expression given by Price et al (1974):

$$N_w = \frac{3600}{2\pi}\sqrt{\frac{R_{\dot{r}}}{R_r}}e^{-\frac{F^2}{R_r}} \qquad (6.9)$$

where:

$R_{\dot{r}}$: twice variance of the bow relative velocity calculated from equation (5.8).

The measured bow vertical relative motion was used in order to determine the probability of occurrence and number of wetness per hour. Fig. 6.23 to 6.82 represent the probability of occurrence and number of impact per hour. These data were calculated for different significant wave heights (represented as H in the figures) varying from 4 metres to 14 metres and for characteristic wave periods varying from 4 seconds to 14 seconds in intervals of 2 seconds (as recommended in the 12th ITTC (1969)).

From the result obtained, it appears that the highest probability of deck wetness occurrence is 0.582 and the number of wetness is 228 per hour (model scale), i.e in the region of F/L=0.053 (F is the freeboard and L is the length). These data were calculated for significant wave height of 14 m, wave period 10 seconds and Fr=0.1. The probability of deck wetness occurrence increases by increasing the significant wave height. Increasing the characteristic wave period does not lead to an increase in the probability of occurrence nor does it lead to an increase in the number of deck wetness occurrence.

For a significant wave height of 6 m the highest probability of occurrence is 0.053 and the number of wetness is 20 wetting per hour. These results are for wave period of 10 seconds, ratio of freeboard to length of 0.053 and for Fr=0.1. At the forward perpendicular where F/L=0.057, the probability of occurrence is 0.034 and the number of wetting is 13 per hour. The difference in the results is due to the differences in the freeboard.

Table 6.4 represents a comparison of wetting per hour from the present investigation along with other results obtained from Lloyd et al (1982). The number of wetting obtained by Lloyd is higher than the present result and this due to different models used and also different forward speed. However, the results obtained here are more or less consistent and one can notice the effect of freeboard, as the number of wetting per hour decreases by increasing the freeboard level.

6.5.2 Significant Load

The impact force (pressure) in the longitudinal direction impacting the plates is not a Gaussian process and is not linear with regular waves. An assumption has to be made to calculate the significant load using spectrum analysis. This assumption is a linearisation between the energy of the waves and the impact force in the longitudinal direction resulting from exceedance of a certain level of motion (relative motion exceeding the freeboard).

From equation (6.6) the force "F" is proportional to the square of the wave velocity. The second order force can then be written as:

$$m_0 = \iint (\frac{F}{\zeta^2})^2 S^2(\omega_e) d\omega_e d\omega_e \qquad (6.10)$$

where:

F : : force in the longitudinal direction
$S(\omega_e)$: spectrum given in equation (5.4)
ω_e : frequency of encounter
ζ : wave amplitude

If the variance of the force is calculated by using the data obtained from the set of experiments, then the significant load can then be obtained as:

$$F_{\frac{1}{3}} = 2.0\sqrt{m_0} \qquad (6.11)$$

$F_{\frac{1}{3}}$: significant force (load).

Table 6.5, 6.6 and 6.7 illustrate a comparison of significant load with Lloyd's (1982) results for significant wave height of 6 metres and characteristic wave period of 11 seconds at the bottom row of plates (i.e plate 4, 5 and 6). The results are not far from each other but there is some difference and which may be due to the different conditions satisfied during the test.

6.6 CONCLUSIONS

This chapter has described model experiments to investigate the deck wetness event. A set of experiments were carried out in ballast and loaded draught conditions in regular waves. A model of S175 container ship was equipped with plates mounted on load cells in order to quantify the impact pressure due to the force in the longitudinal direction. The conclusions from this investigation are as follows:

Deck wetness occurs when the relative motions exceeds the freeboard. There is no occurrence of deck wetness at the ballast draught condition except for some sprays, but for the loaded draught condition the phenomenon was very violent. Hence this event depends mainly on the freeboard.

The forward speed of the vessel plays an important role. At high speed (for example Fr=0.3) deck wetness event becomes more violent. The force in the longitudinal direction (impact pressures) follows the same trend as the vertical relative motions. The impact pressures due to the impact forces recorded are larger at high speeds (Fr=0.278 and 0.3).

The impact pressures on the bottom row of plates are higher than the top row of plates. For example, at Fr=0.2 and for the frequency $\omega\sqrt{\frac{L}{g}}=2.5$, plate 5 in the middle of the bottom row recorded 1.945 kN/m^2 (corresponding 136 kN/m^2 for full scale) and plate 2 in the middle of the upper row recorded 0.418 kN/m^2 (29.4 kN/m^2 for full scale), this load can be compared with that of the design load which 24.6 kN/m^2 (full scale) given by Lloyd's Register of Shipping (1982).

The mass of water shipped on deck mainly depends on the forward speed of the vessel the relative motion exceeding the freeboard. For example, at Fr=0.3 the highest mass of water is more than 40 kg. The trend of the curve of mass of water collected is

the same as the relative motion curve.

An approximate method, to predict load in the longitudinal direction on a vertical superstructure or deck mounted equipment due to green water shipped on the deck of floating bodies (ship, platforms) with /or without forward speed.

The force per unit mass in the longitudinal direction presented has only been recently formulated and it is inversely proportional to the distance at which the vertical wall is positioned from where the water is shipped.

The measured load is always lower than the calculated load, and that is why the dispersion factor always lies in the range of 0.0 and 1.0. This is also clear from the fact that not all the mass of water collected, did hit the load cells wall, for example at Fr=0.3 the collected mass of water is more than 40 kg. In other words, a certain quantity of water comes from other directions, such as the sides and from above the wall. The histogram of the mass of water shipped on the deck of the container ship model, serves as a good design data for the dispersion factor. The minimum value of the dispersion factor calculated in the present research is 0.13 and the maximum value is around 0.94.

The probability of deck wetness occurrence and number of wetting depends mainly on the freeboard parameter. There are also other parameter such forward speed, significant wave height and characteristic wave period. The number of wettings resulting from this investigation differs from that of Lloyd et al (1982). The maximum number of wettings obtained from the present investigation, for the ratio of freeboard to ship length of 0.05, Fr=0.1, significant wave height of 6 m and characteristic wave period of 11 seconds, is about 15 wetting per hour.

The results of significant loads compared with those of Lloyd et al (1982) are not far from each other but there is some difference and this may be due to the different conditions satisfied during the test.

The difference in the result obtained in the present research and that of Lloyd et al (1982) investigation can be explained by one statement, i.e results of one type of ship are not applicable to another type of ship. In other words a data bank should be prepared for different high speed vessels, so that future researchers can make use of these data for investigating loads on deck mounted equipment.

Table 6.1 Ratio between freeboard and ship length
for station FP. 9 1/2 and 9

Station	F/L
FP	0.057
9 1/2	0.055
9	0.053

F: Freeboard
L: Ship Length

Overhang/Length	Sharpness (deg.)	Flare Angle (deg.)	Rake Angle (deg.)
0.024	86.000	35.000	84.000

Table 6.2 Impact pressure (KN/m^2) measured from experiment

Fr	Plate 1	Plate 2	Plate 3	Plate 4	Plate 5	Plate 6
	0.422	0.563	0.493	0.422	0.563	1.056
	0.563	0.704	0.634	0.634	0.985	0.845
0.100	1.197	1.478	1.126	0.985	1.197	0.985
	1.689	1.126	1.408	0.915	1.549	1.197
	1.549	1.126	1.478	1.337	1.337	2.041
	3.871	4.646	5.350	6.194	8.658	5.702
	0.845	0.845	0.774	1.830	2.745	1.830
	3.590	4.223	5.561	0.563	6.969	6.335
	0.493	0.704	10.699	0.422	0.634	0.985
	0.845	32.591	21.610	1.267	2.112	2.604
	1.056	1.337	14.078	2.745	3.942	2.604
0.150	1.337	35.617	0.985	4.012	6.546	4.223
	3.520	3.801	2.534	7.039	10.347	6.265
	1.478	2.112	2.041	1.971	2.534	2.112
	0.634	0.634	0.634	0.563	0.704	0.493
	0.563	0.493	0.493	0.352	0.563	0.352
	0.634	0.563	0.634	0.563	8.095	0.915
	1.619	8.517	1.689	9.784	43.079	7.602
	1.408	13.093	1.337	14.148	7.391	12.600
0.200	3.027	20.202	3.168	19.287	18.442	19.005
	6.405	29.423	6.546	26.044	136.909	26.889
	0.845	0.845	0.845	0.704	0.563	0.774
	0.563	0.634	11.966	0.422	0.634	0.845
	1.267	2.886	12.318	1.197	0.985	1.901
	1.197	2.112	1.549	1.619	46.176	2.041
	3.308	22.173	3.449	57.790	16.894	20.624
	5.420	29.916	5.420	22.595	20.343	26.889
0.278	25.833	46.880	48.921	37.096	56.805	42.164
	2.745	17.809	2.886	16.964	10.629	16.471
	1.760	0.634	1.197	0.915	36.110	1.197
	0.563	0.563	0.563	0.493	0.493	0.915
	1.478	1.056	1.337	1.478	1.971	1.337
	1.830	2.323	2.041	2.182	34.139	2.182
	9.784	32.098	9.432	25.763	10.981	28.719
	12.881	30.831	9.995	26.044	11.262	28.367
0.300	24.214	44.627	24.988	35.758	81.723	40.263
	6.194	17.809	6.405	15.838	96.294	17.668
	1.056	1.126	1.126	0.774	0.774	0.704
	0.493	0.634	0.704	0.422	5.279	0.563
	0.845	0.704	0.845	0.493	0.704	0.493

Table 6.3 Calculation of the dispersion factor k (load in KN/m^2)

Fr	w (rad/sec)	Calculated Load	Measured Load	Dispersion factor k
	3.467	-	0.050	-
	4.000	1.274	0.062	0.049
	4.145	1.395	0.099	0.071
0.100	4.478	4.645	0.112	0.024
	4.905	4.522	0.126	0.028
	5.482	11.976	0.489	0.041
	5.859	3.215	0.126	0.039
	6.280	1.661	0.387	0.233
	3.467	-	0.198	-
	4.000	1.761	0.867	0.492
	4.145	5.299	0.366	0.069
0.150	4.478	8.549	0.749	0.088
	4.905	9.293	0.476	0.051
	5.482	8.311	0.174	0.021
	5.859	-	0.052	-
	6.280	-	0.040	-
	3.467	-	0.162	-
	4.000	48.044	1.027	0.021
	4.145	51.113	0.710	0.014
0.200	4.478	43.138	1.181	0.027
	4.905	100.416	3.299	0.033
	5.482	0.121	0.065	0.536
	5.859	-	0.214	-
	6.280	4.333	0.292	0.067
	3.467	0.829	0.777	0.938
	4.000	61.415	1.765	0.029
	4.145	90.431	1.571	0.017
0.278	4.478	278.210	3.661	0.013
	4.905	54.605	0.959	0.018
	5.482	4.148	0.594	0.143
	5.859	-	0.051	-
	6.280	0.156	0.123	0.786
	3.467	5.455	0.635	0.116
	4.000	118.870	1.659	0.014
	4.145	102.528	1.696	0.017
0.300	4.478	299.698	3.574	0.012
	4.905	50.913	2.276	0.045
	5.482	-	0.079	-
	5.859	0.633	0.115	0.182
	6.280	0.195	0.058	0.298

Table 6.4 Comparison of number of wetting per hour with other work for significant wave height 6 m and characteristic wave period 11 seconds.

		F/L= 0.05		F/L= 0.053		F/L= 0.055		F/L= 0.057		F/L= 0.06		F/L= 0.07	
		Wetting/ Hour		Wetting/ Hour		Wetting/ Hour		Wetting/ Hour		Wetting/ Hour		Wetting/ Hour	
Fr	Source	Present Experiment S175	Lloyd's Experiment NBL	Present Experiment S175	Lloyd's Experiment NBL	Present Experiment S175	Lloyd's Experiment NBL	Present Experiment S175	Lloyd's Experiment NBL	Present Experiment S175	Lloyd's Experiment NBL	Present Experiment S175	Lloyd's Experiment NBL
0.1	S175	15	*	16	*	12	*	10	*	10	*	11	*
0.15	S175	9	*	10	*	7	*	6	*	6	*	7	*
0.2	S175	8	*	9	*	7	*	5	*	5	*	6	*
0.275	NBL	*	146	*	125	*	112	*	104	*	87	*	32
0.278	S175	4	*	4	*	3	*	2	*	11	*	13	*
0.3	S175	10	*	11	*	8	*	6	*	6	*	7	*
0.314	NBL	*	244	*	165	*	147	*	125	*	102	*	46
0.392	NBL	*	340	*	204	*	183	*	163	*	142	*	62

*: not investigated
S175: Container Ship S175
NBL: Narrow Beam LEANDER
: Interpolated

Table 6.5 Comparison of significant load with other work for significant wave height 6 m and characteristic wave period 11 seconds. Load in (KN/m^2). (Plate 4)

		F/L= 0.05		F/L= 0.053		F/L= 0.055		F/L= 0.057		F/L= 0.06		F/L= 0.07	
		Sig. Load Plate 4		Sig. Load Plate 4		Sig. Load Plate 4		Sig. Load Plate 4		Sig. Load Plate 4		Sig. Load Plate 4	
Fr	Source	Present Experimen S175	Lloyd's Experimen NBL	Present Experimen S175	Lloyd's Experimen NBL	Present Experimen S175	Lloyd's Experimen NBL	Present Experimen S175	Lloyd's Experimen NBL	Present Experimen S175	Lloyd's Experimen NBL	Present Experimen S175	Lloyd's Experiment NBL
0.1	S175	*	*	*	*	*	*	20.554	*	*	*	*	*
0.15	S175	*	*	*	*	*	*	14.078	*	*	*	*	*
0.2	S175	*	*	*	*	*	*	20.413	*	*	*	*	*
0.275	NBL	*	27.5	*	26	*	24	*	23	*	17.5	*	12.5
0.278	S175	*	*	*	*	*	*	10.84	*	*	*	*	*
0.3	S175	*	*	*	*	*	*	8.658	*	*	*	*	*
0.314	NBL	*	37.5	*	75	*	75	*	39	*	37.5	*	27.5
0.392	NBL	*	102.5	*	80	*	66	*	52.5	*	42.5	*	26.25

*: not investigated
S175: Container Ship S175
NBL: Narrow Beam LEANDER
: Interpolated

Table 6.6 Comparison of significant load with other work for significant wave height 6 m and characteristic wave period 11 seconds. Load in (KN/m^2). (Plate 5)

		F/L= 0.05		F/L= 0.053		F/L= 0.055		F/L= 0.057		F/L= 0.06		F/L= 0.07	
		Sig. Load Plate 5		Sig. Load Plate 5		Sig. Load Plate 5		Sig. Load Plate 5		Sig. Load Plate 5		Sig. Load Plate 5	
Fr	Source	Present Experimen S175	Lloyd's Experimen NBL	Present Experimen S175	Lloyd's Experimen NBL	Present Experimen S175	Lloyd's Experimen NBL	Present Experimen S175	Lloyd's Experimen NBL	Present Experimen S175	Lloyd's Experimen NBL	Present Experimen S175	Lloyd's Experiment NBL
0.1	S175	*	*	*	*	*	*	9.221	*	*	*	*	*
0.15	S175	*	*	*	*	*	*	21.61	*	*	*	*	*
0.2	S175	*	*	*	*	*	*	19.005	*	*	*	*	*
0.275	NBL	*	60	*	52.5	*	50	*	45	*	41.25	*	21.25
0.278	S175	*	*	*	*	*	*	11.122	*	*	*	*	*
0.3	S175	*	*	*	*	*	*	17.316	*	*	*	*	*
0.314	NBL	*	67.5	*	57	*	86	*	91	*	98.75	*	25.5
0.392	NBL	*	125	*	99	*	83	*	56	*	55	*	26.25

*: not investigated
S175: Container Ship S175
NBL: Narrow Beam LEANDER
: Interpolated

Table 6.7 Comparison of significant load with other work for significant wave height 6 m and characteristic wave period 11 seconds. Load in (KN/m^2). (Plate 6)

		F/L= 0.05		F/L= 0.053		F/L= 0.055		F/L= 0.057		F/L= 0.06		F/L= 0.07	
		Sig. Load Plate 6		Sig. Load Plate 6		Sig. Load Plate 6		Sig. Load Plate 6		Sig. Load Plate 6		Sig. Load Plate 6	
Fr	Source	Present Experimen S175	Lloyd's Experimen NBL	Present Experimen S175	Lloyd's Experimen NBL	Present Experimen S175	Lloyd's Experimen NBL	Present Experimen S175	Lloyd's Experimen NBL	Present Experimen S175	Lloyd's Experimen NBL	Present Experimen S175	Lloyd's Experiment NBL
0.1	S175	*	*	*	*	*	*	21.539	*	*	*	*	*
0.15	S175	*	*	*	*	*	*	14.43	*	*	*	*	*
0.2	S175	*	*	*	*	*	*	19.85	*	*	*	*	*
0.275	NBL	*	27.5	*	26	*	24	*	23	*	17.5	*	12.5
0.278	S175	*	*	*	*	*	*	8.165	*	*	*	*	*
0.3	S175	*	*	*	*	*	*	9.643	*	*	*	*	*
0.314	NBL	*	37.5	*	75	*	75	*	39	*	37.5	*	27.5
0.392	NBL	*	102.5	*	80	*	66	*	52.5	*	42.5	*	26.25

*: not investigated
S175: Container Ship S175
NBL: Narrow Beam LEANDER
: Interpolated

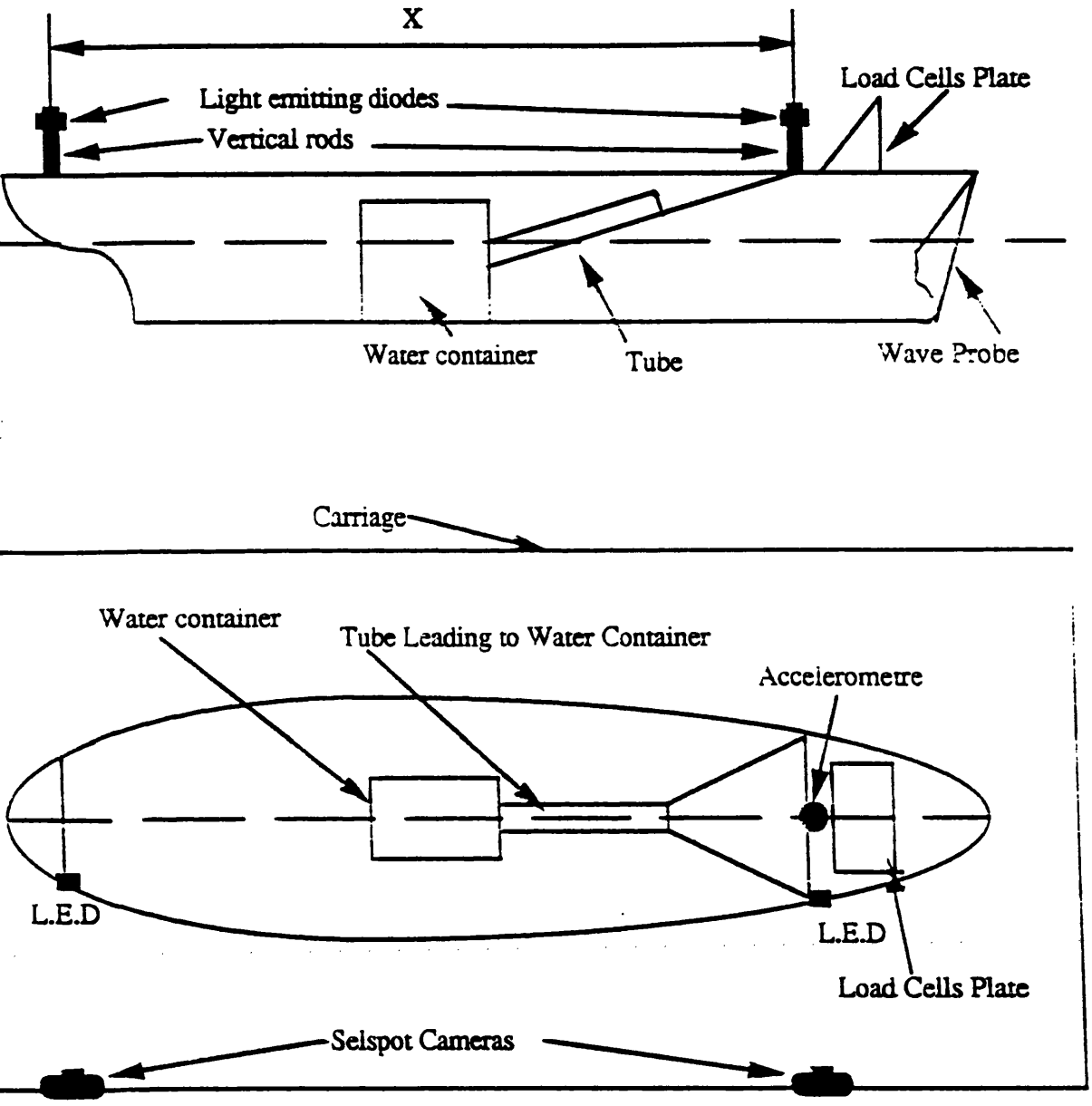

Fig. 6.1 Instrumentation set up

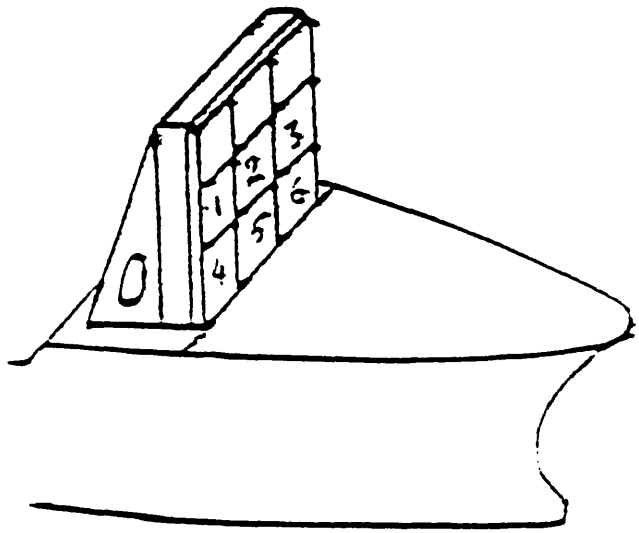

Fig. 6.2 Load measurement device mounted on the deck at station 9 1/2

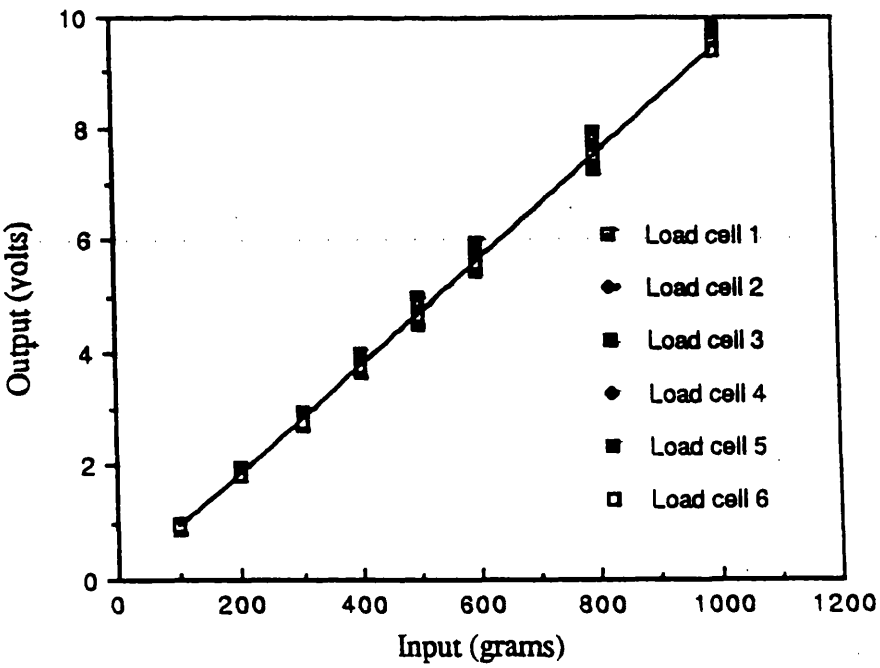

Fig. 6.3 Linear response of the calibration of load cells

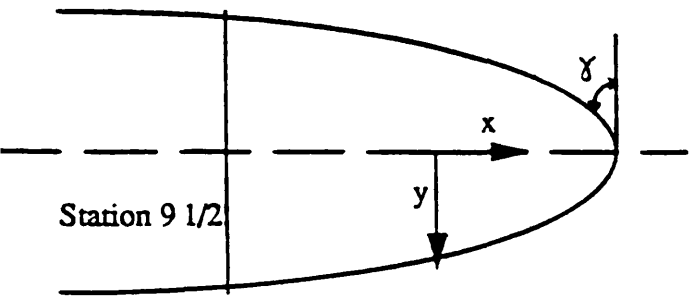

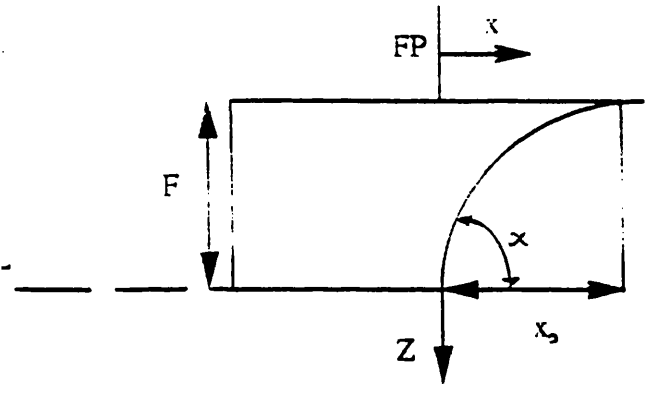

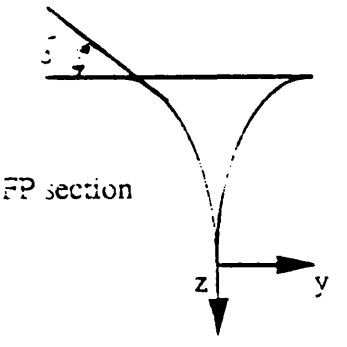

F : Freeboard

x_o : Overhang

γ : Sharpness

δ : Flare angle

α : Rake angle

Fig. 6.4 Notation

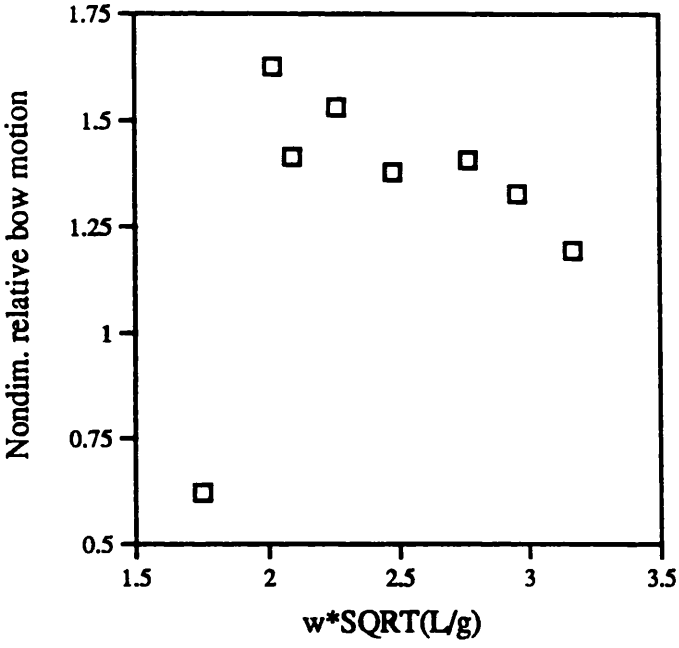

Fig. 6.5 Relative bow motion for Fr=0.1

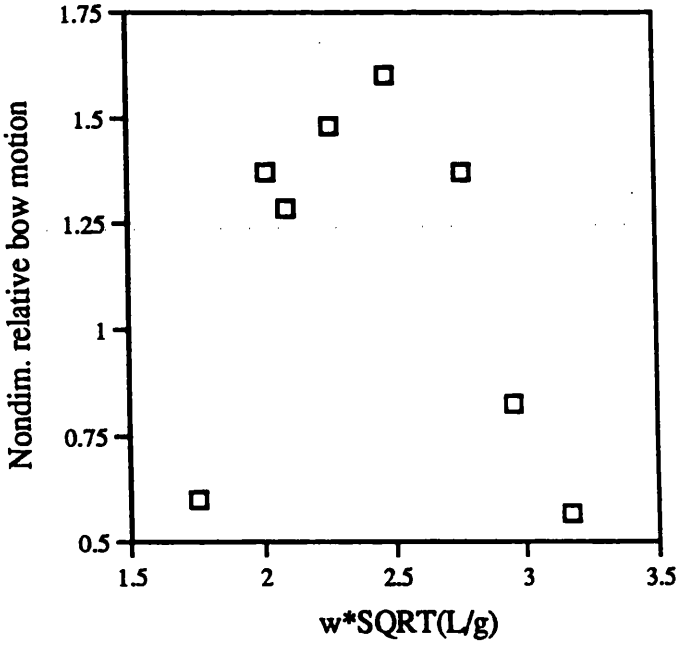

Fig. 6.6 Relative bow motion for fr=0.15

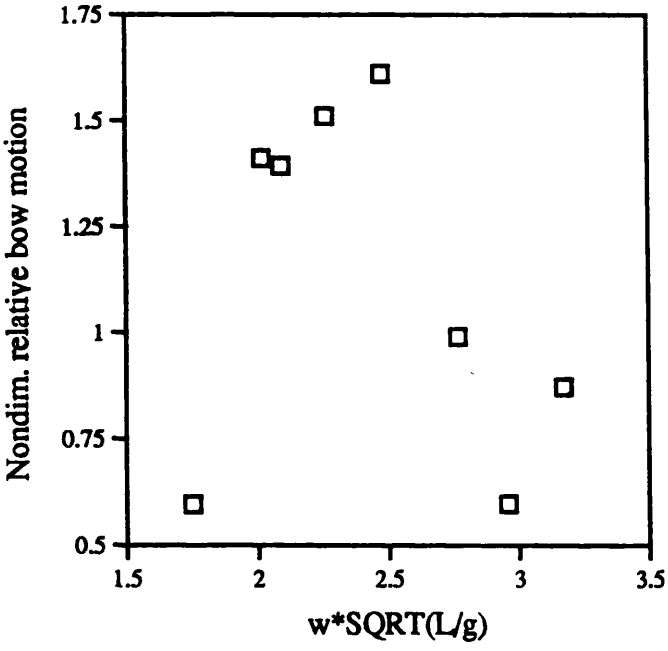

Fig. 6.7 Relative bow motion for Fr=0.2

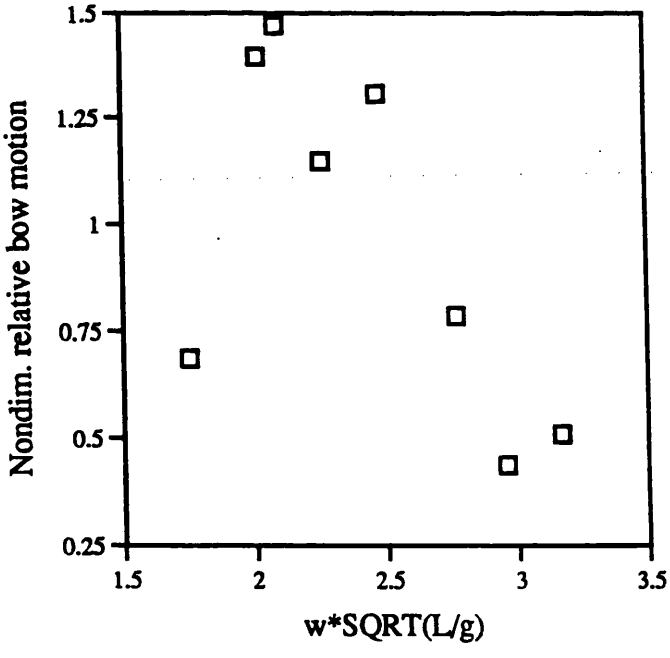

Fig. 6.8 Relative bow motion for Fr=0.278

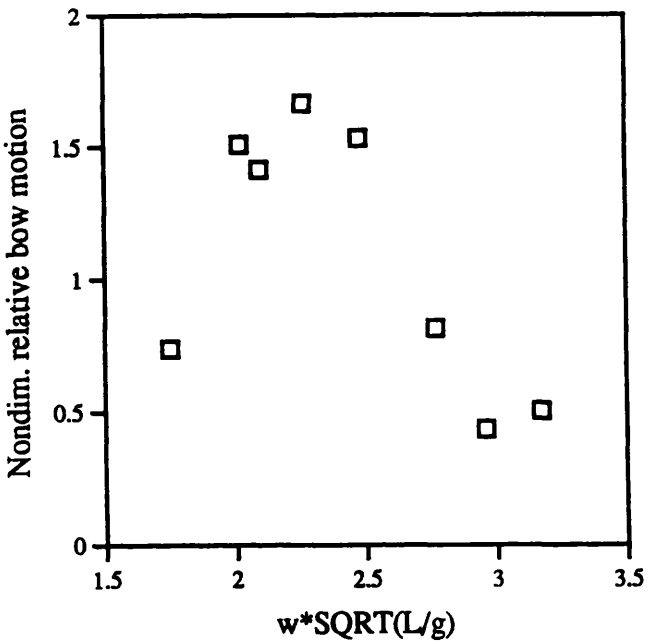

Fig. 6.9 Relative bow motion for Fr=0.3

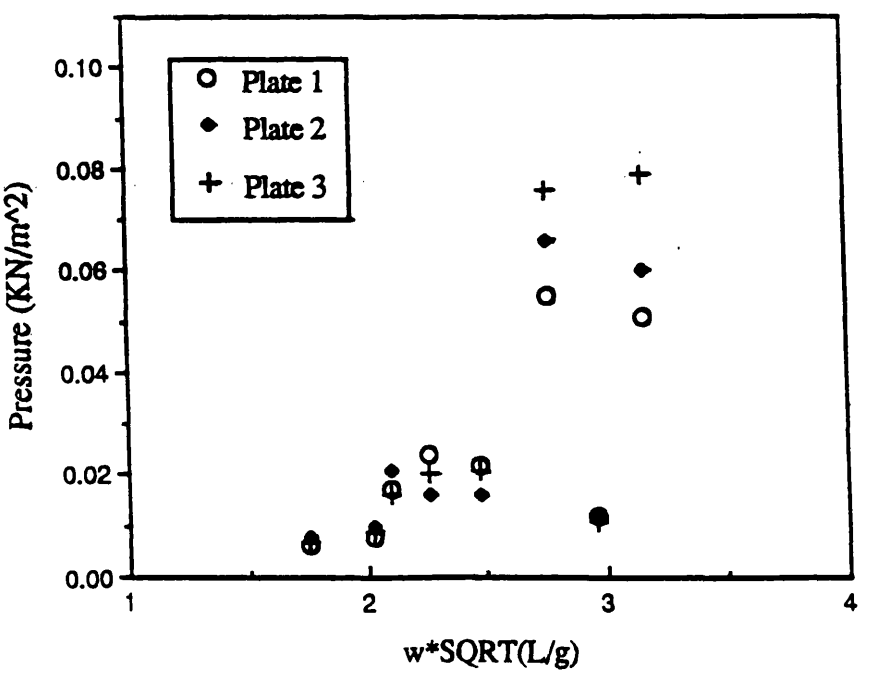

Fig. 6.10 Impact pressure on the top plates for Fr=0.1

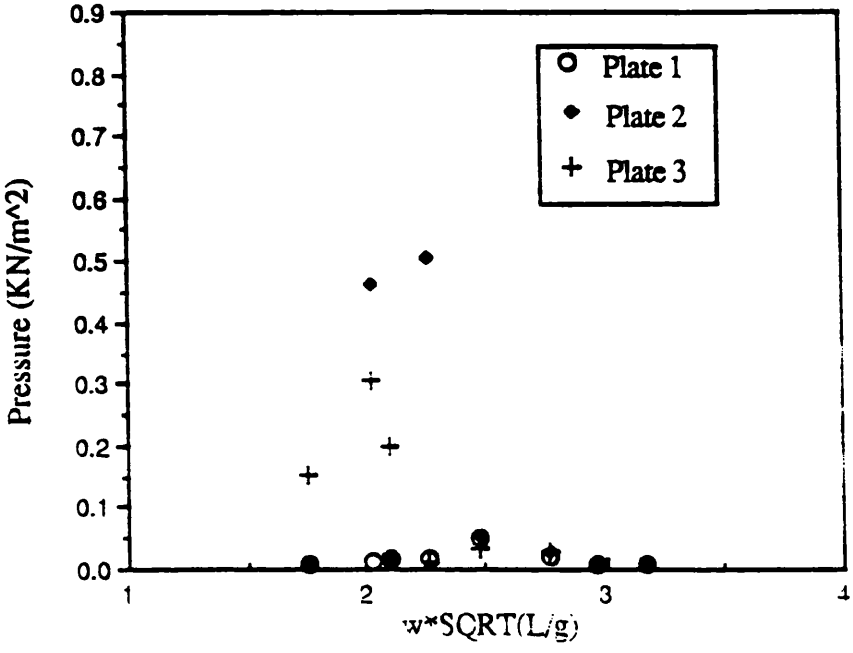

Fig. 6.11 Impact pressure on the top plates for Fr=0.15

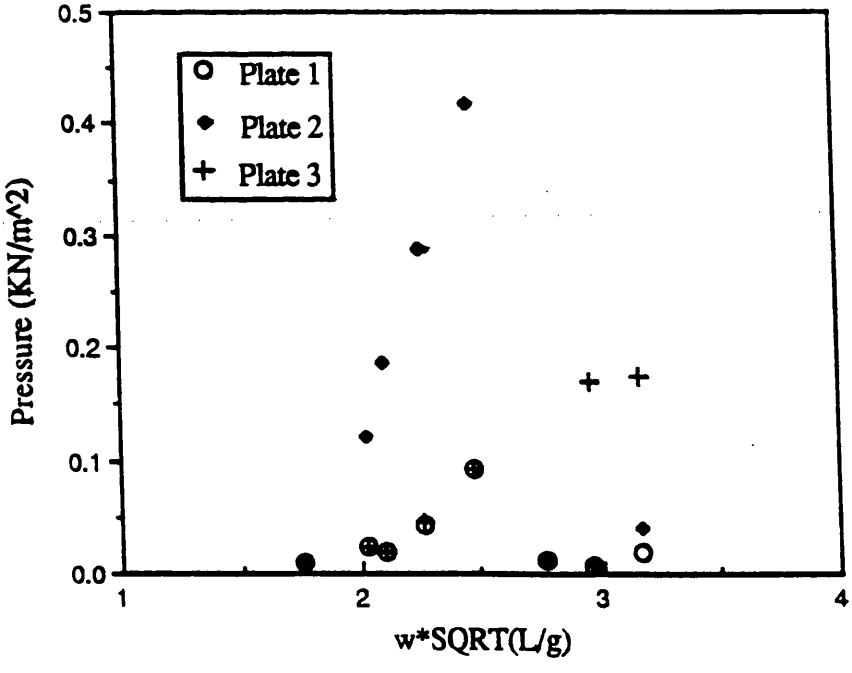

Fig. 6.12 Impact pressure on the top plates for Fr=0.2

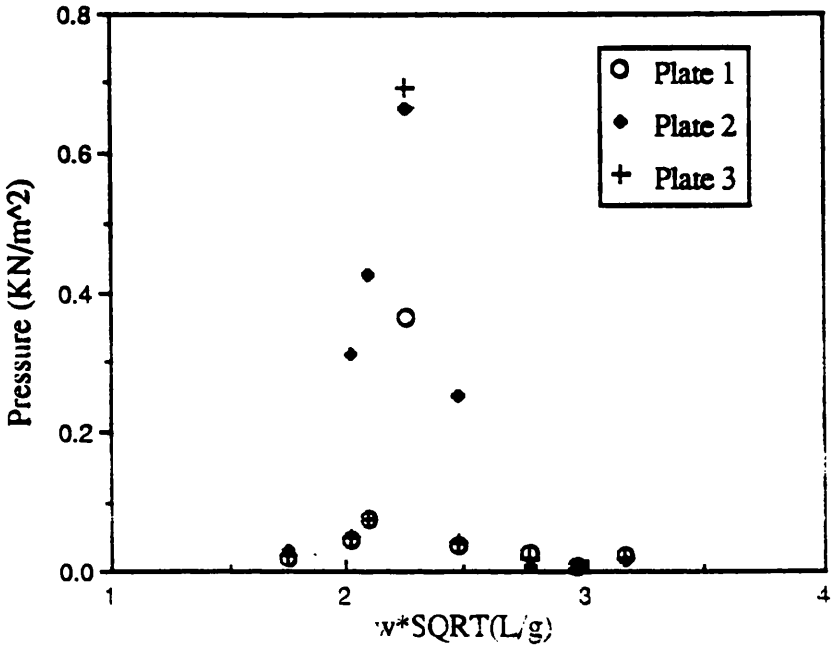

Fig. 6.13 Impact pressure on the top plates for Fr=0.278

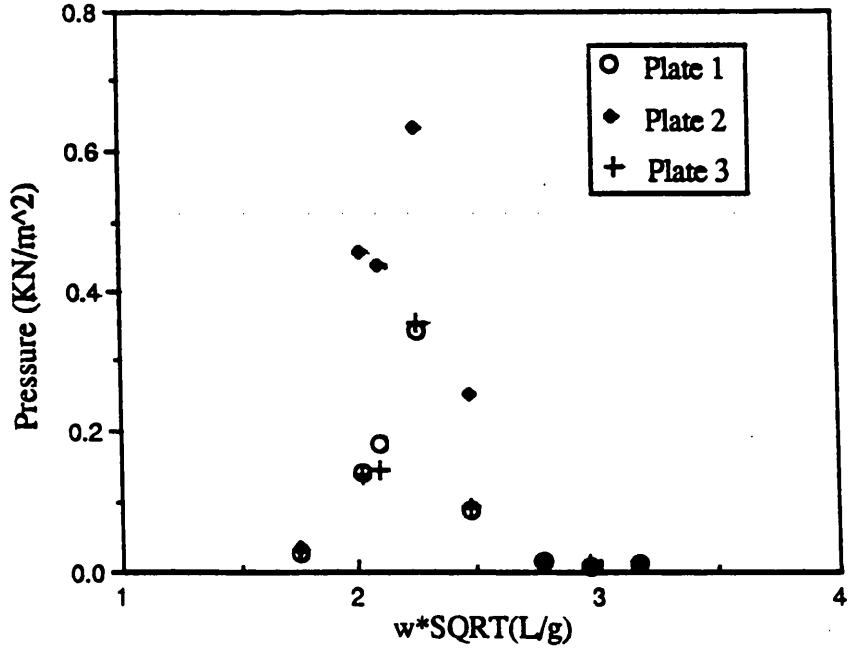

Fig. 6.14 Impact pressure on the top plates for Fr= 0.3

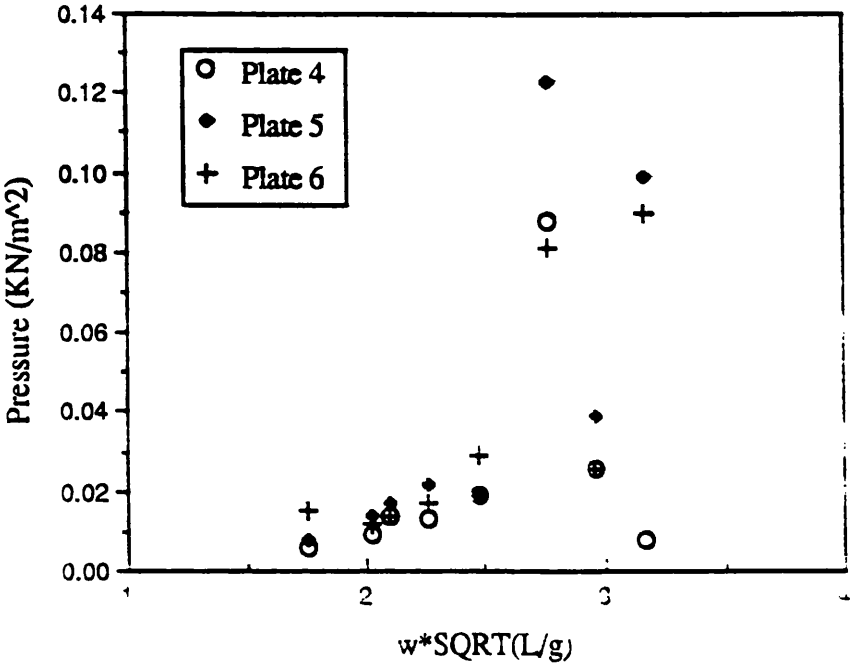

Fig. 6.15 Impact pressure on the bottom plates for Fr=0.1

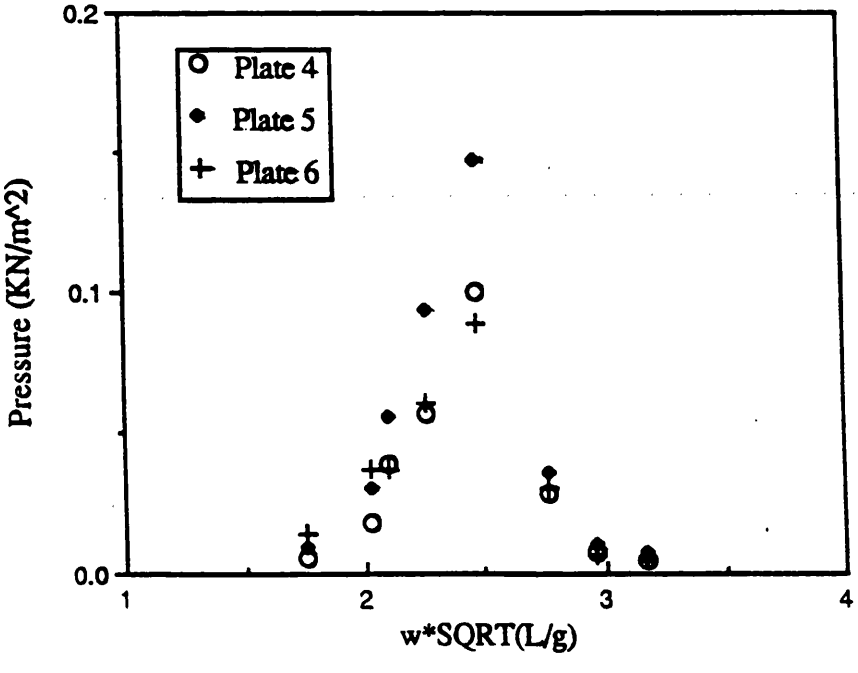

Fig. 6.16 Impact pressure on the bottom plates for Fr=0.15

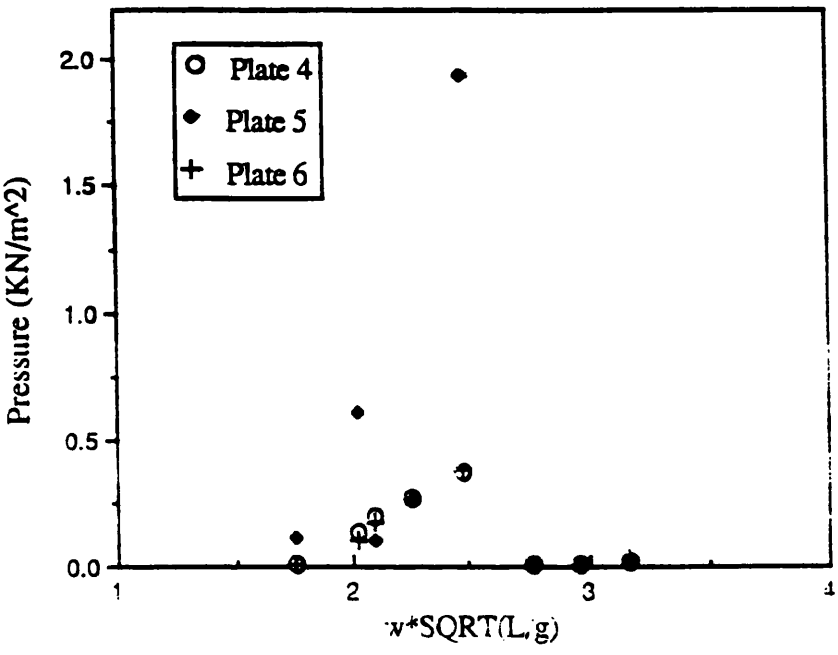

Fig. 6.17 Impact pressure on the bottom plates for Fr=0.2

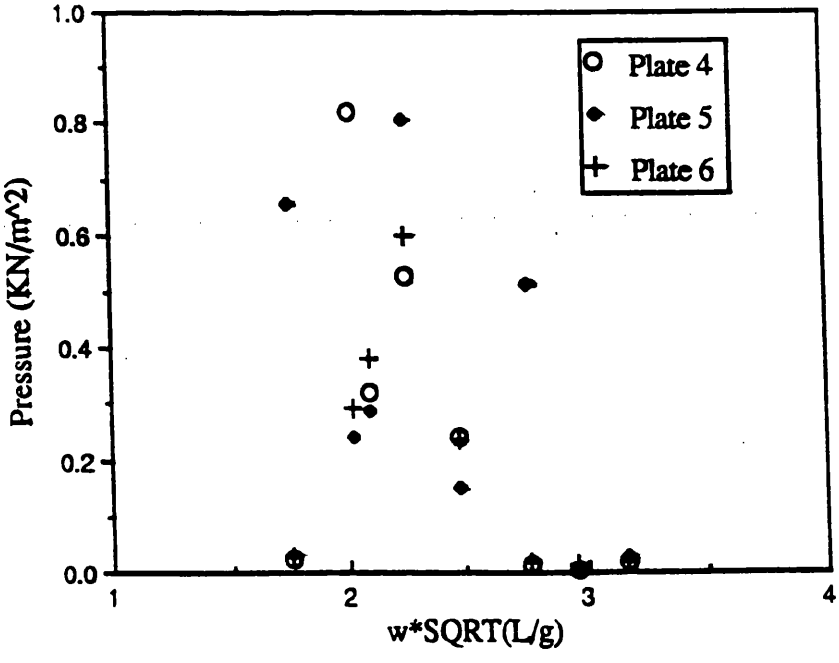

Fig. 6.18 Impact pressure on the bottom plates for Fr=0.278

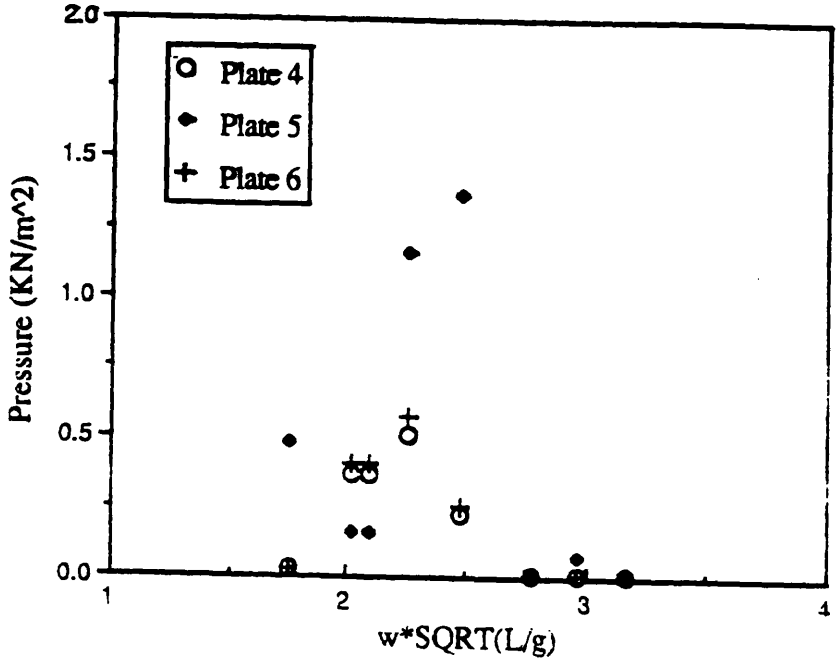

Fig. 6.19 Impact pressure on the bottom plates for Fr=0.3

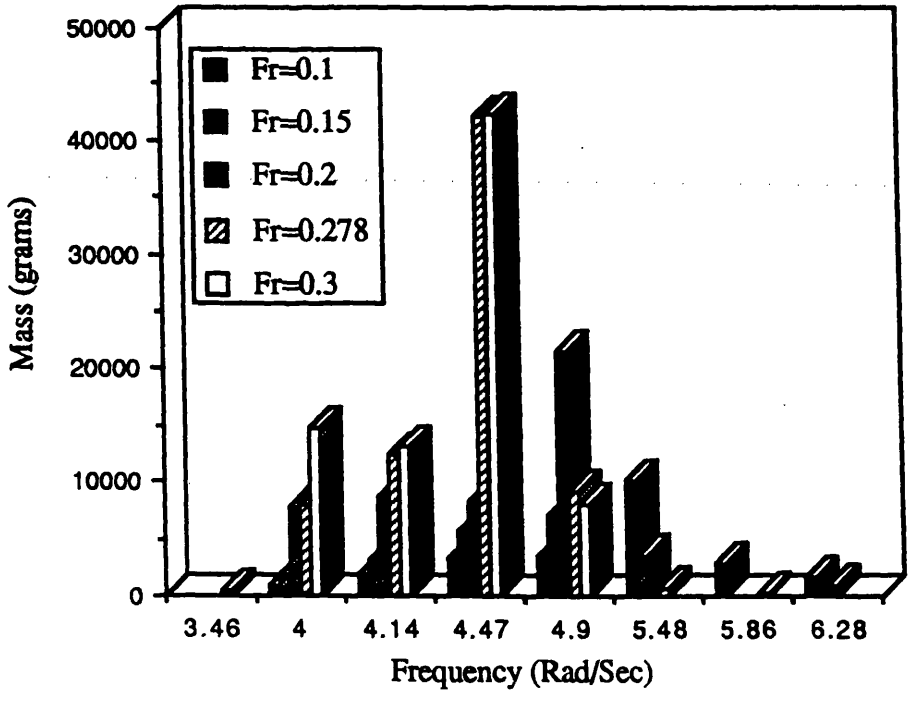

Fig. 6.20 Mass of water shipped on deck for different speeds and for loaded draught

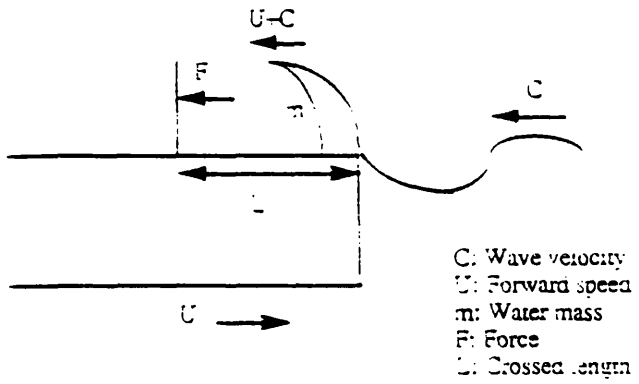

Fig. 6.21 Example of vertical relative motion excedding the freeboard

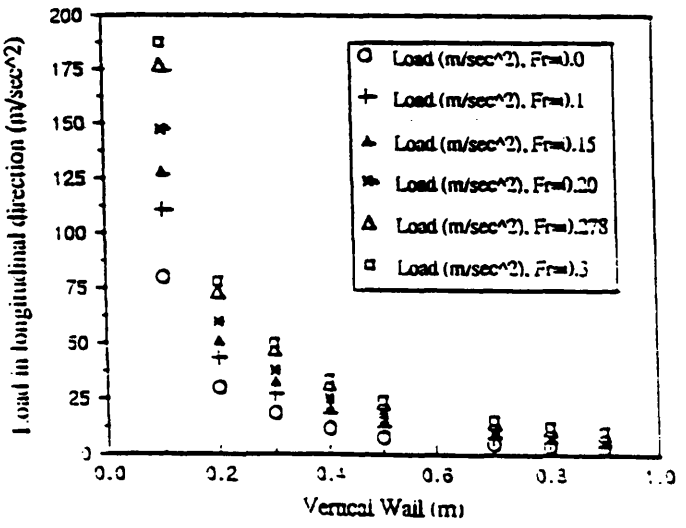

Fig. 6.22 Impact force per unit mass as function of crossed length

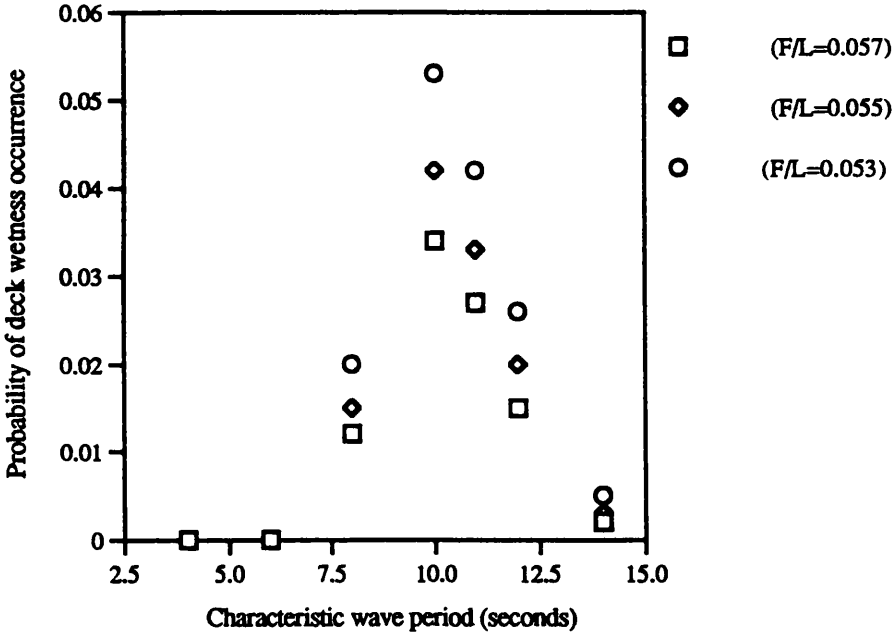

Fig. 6.23 Probability of deck wetness occurrence for Fr=0.1 and H=6 metres

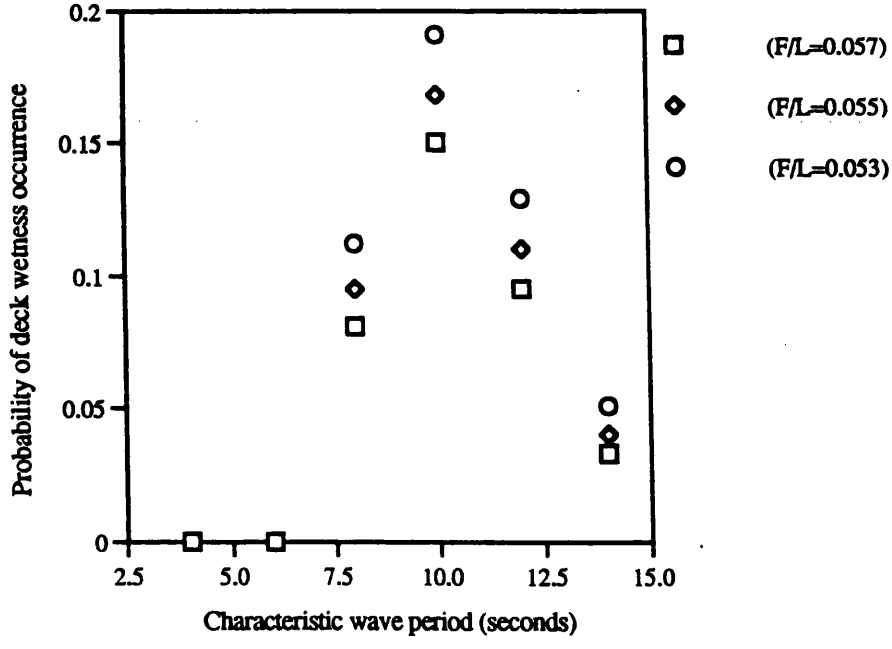

Fig. 6.24 Probability of deck wetness occurrence for Fr=0.1 and H=8 metres

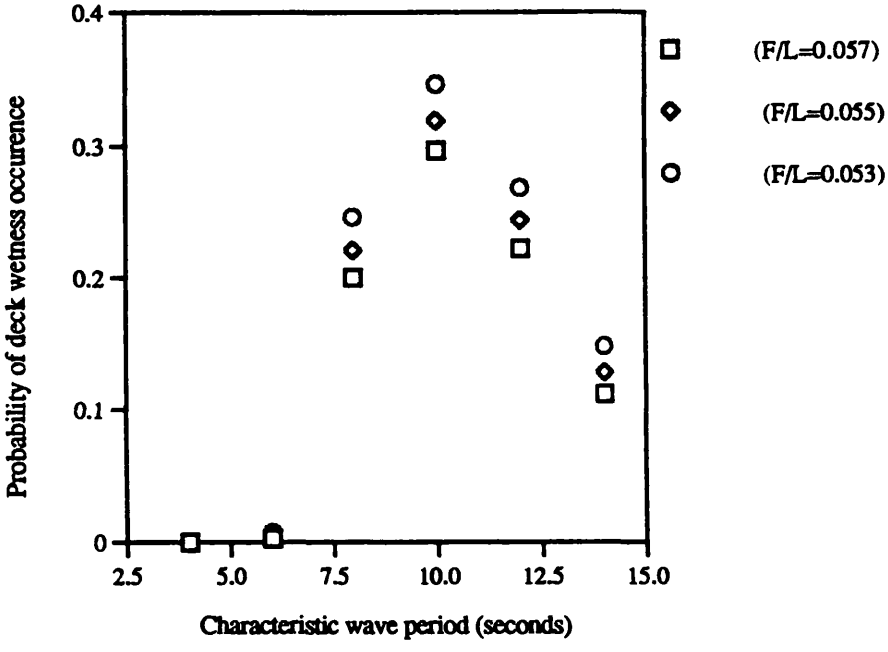

Fig. 6.25 Probability of deck wetness occurrence for Fr=0.1 and H=10 metres

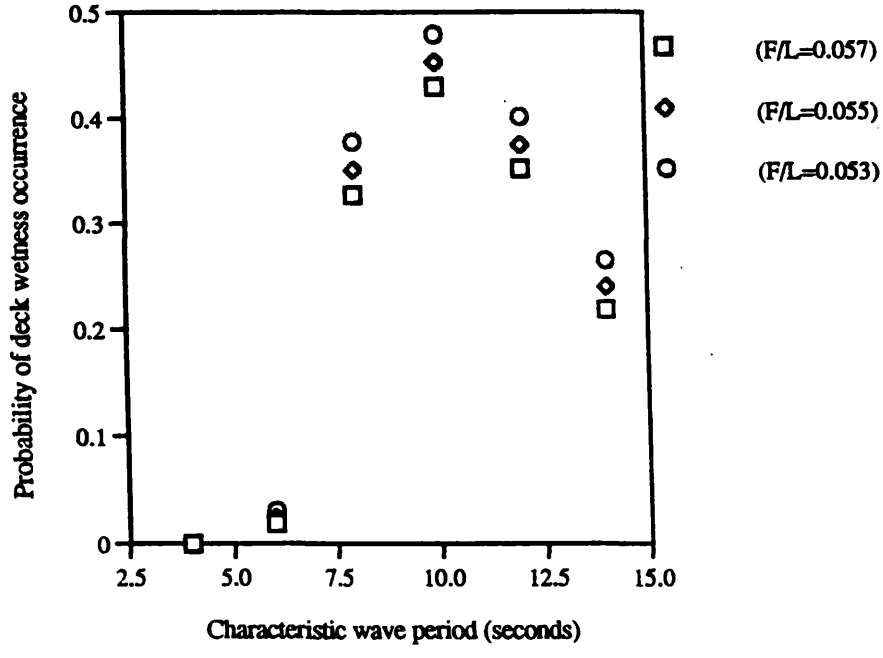

Fig. 6.26 Probability of deck wetness occurrence for Fr=0.1 and H=12 metres

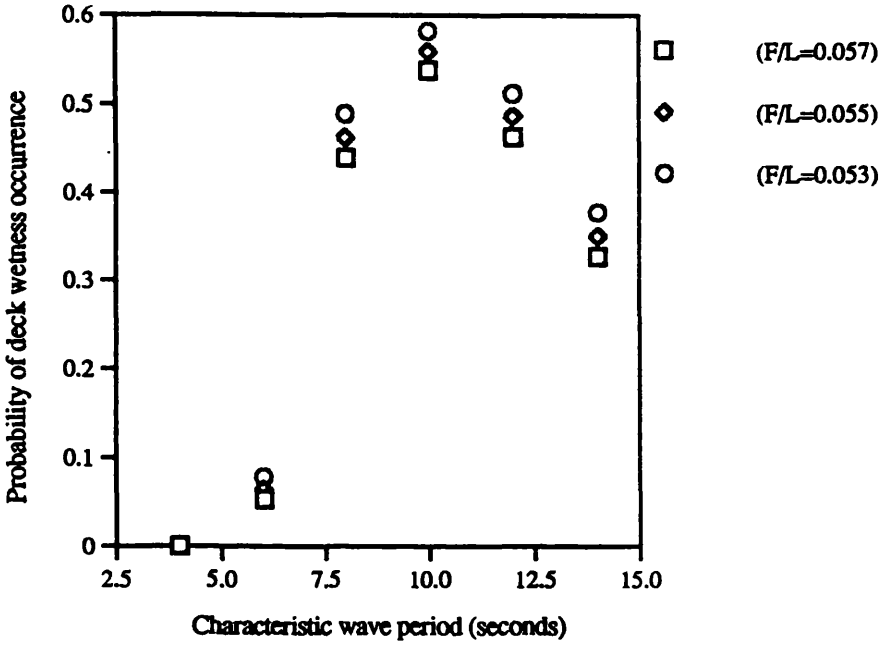

Fig. 6.27 Probability of deck wetness occurrence for Fr=0.1 and H=14 metres

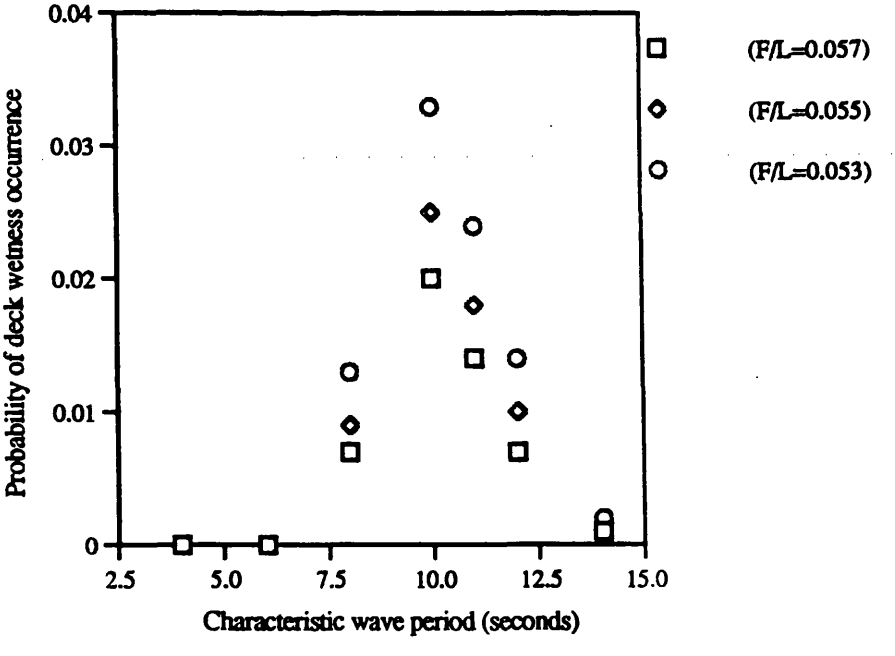

Fig. 6.28 Probability of deck wetness occurrence for Fr=0.15 and H=6 metres

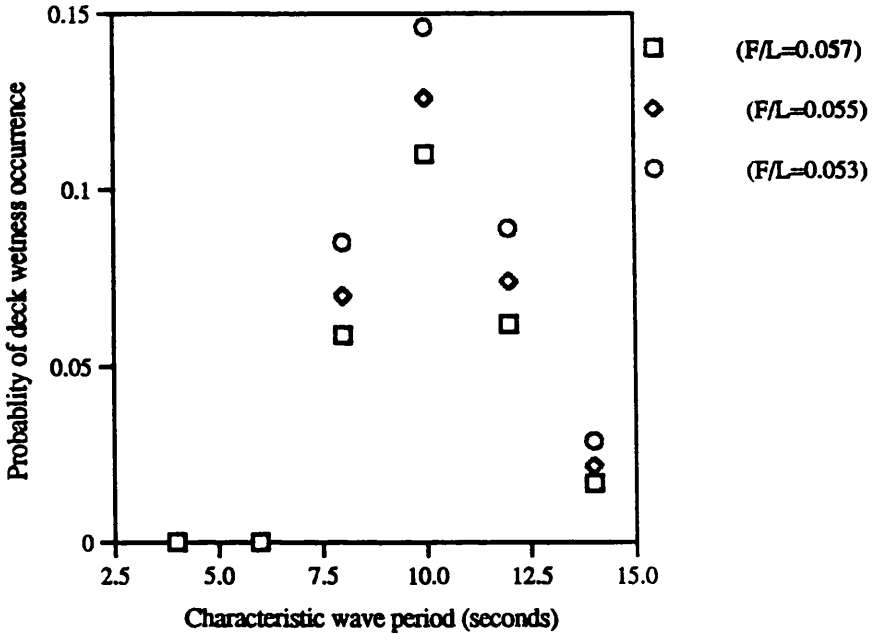

Fig. 6.29 Probability of deck wetness occurrence for Fr=0.15 and H=8 metres

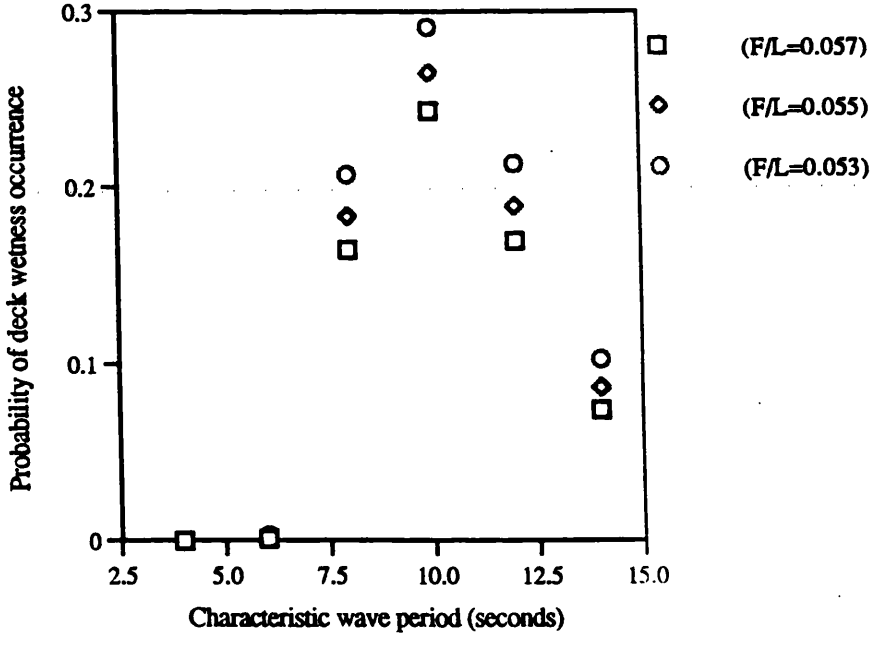

Fig. 6.30 Probability of deck wetness occurrence for Fr=0.15 and H=10 metres

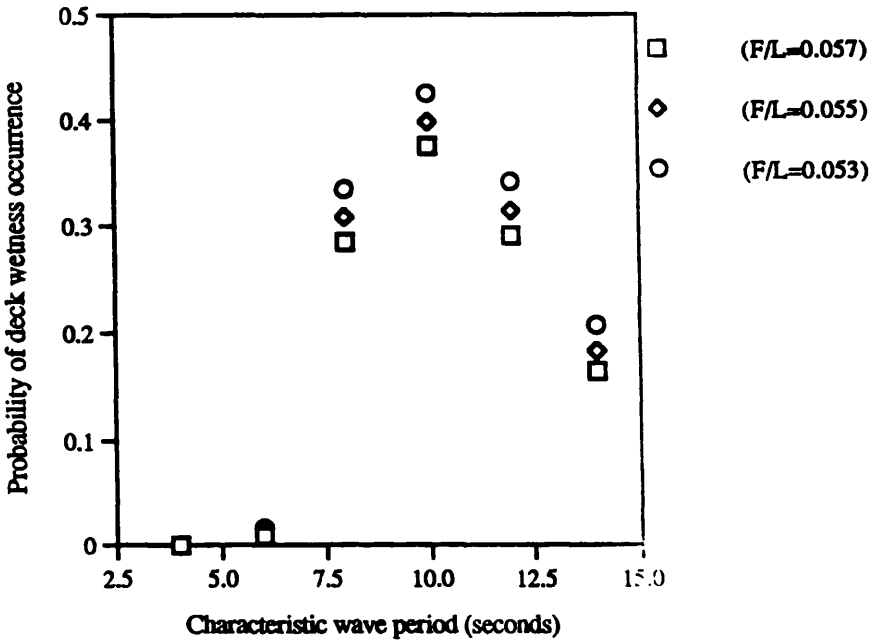

Fig. 6.31 Probability of deck wetness occurrence for Fr=0.15 and H=12 metres

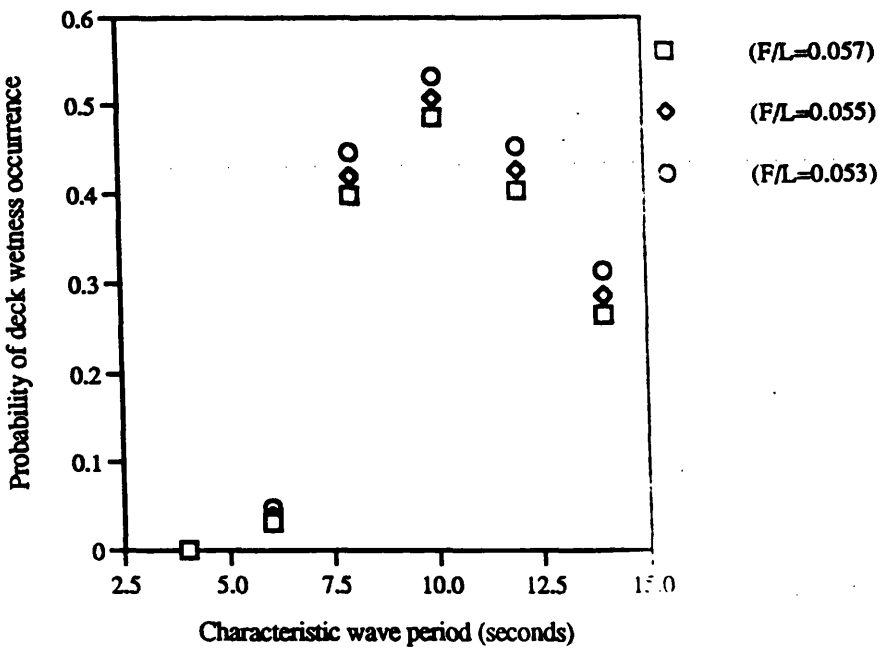

Fig. 6.32 Probability of deck wetness occurrence for Fr=0.15 and H=14 metres

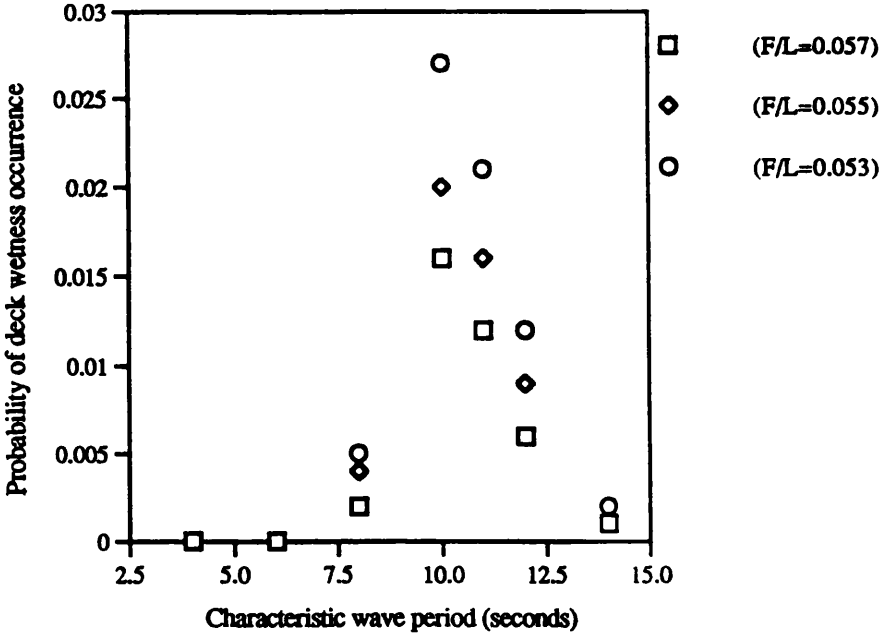

Fig. 6.33 Probability of deck wetness occurrence for Fr=0.2 and H=6 metres

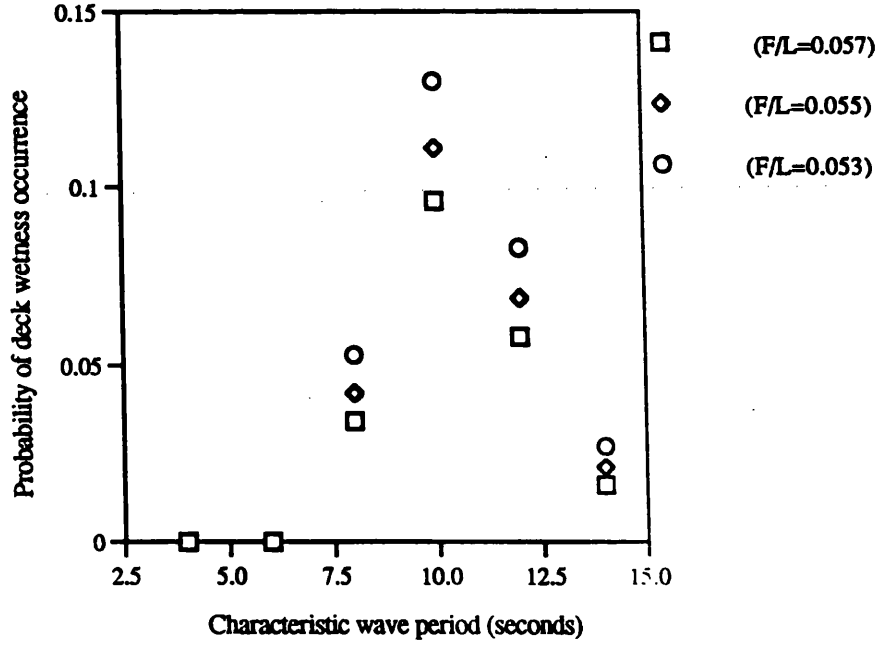

Fig. 6.34 Probability of deck wetness occurrence for Fr=0.2 and H=8 metres

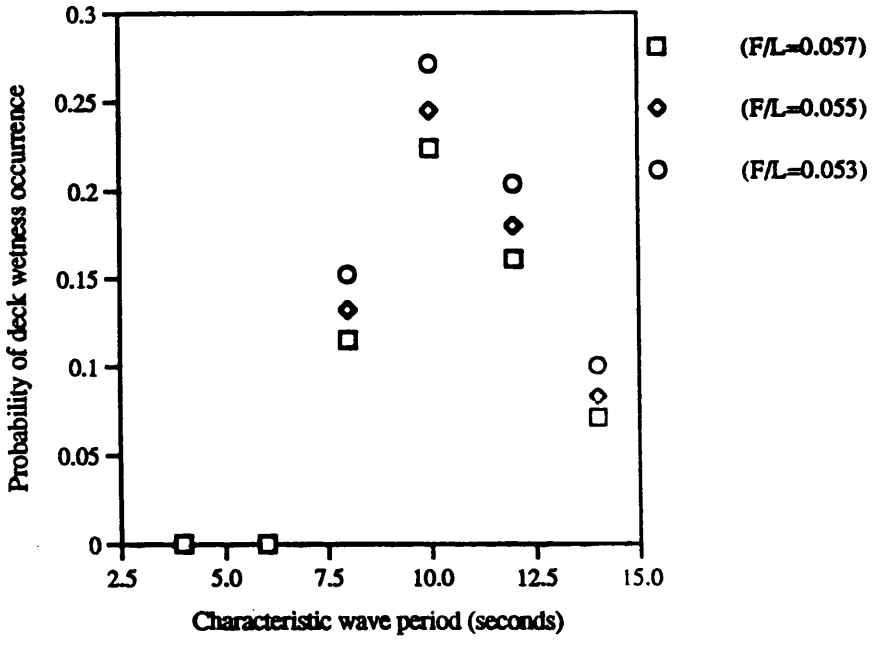

Fig. 6.35 Probability of deck wetness occurrence for Fr=0.2 and H=10 metres

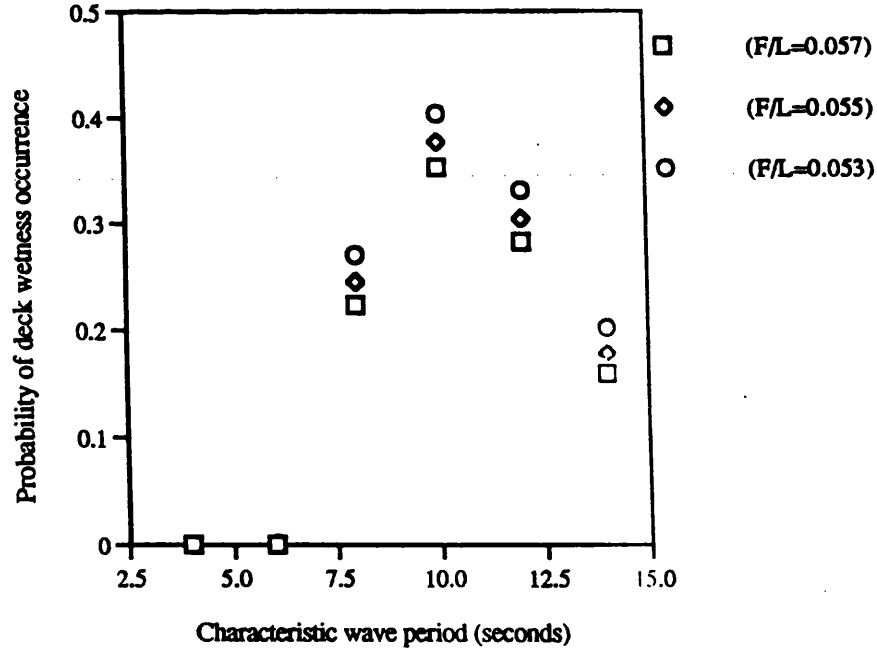

Fig. 6.36 Probability of deck wetness occurrence for Fr=0.2 and H=12 metres

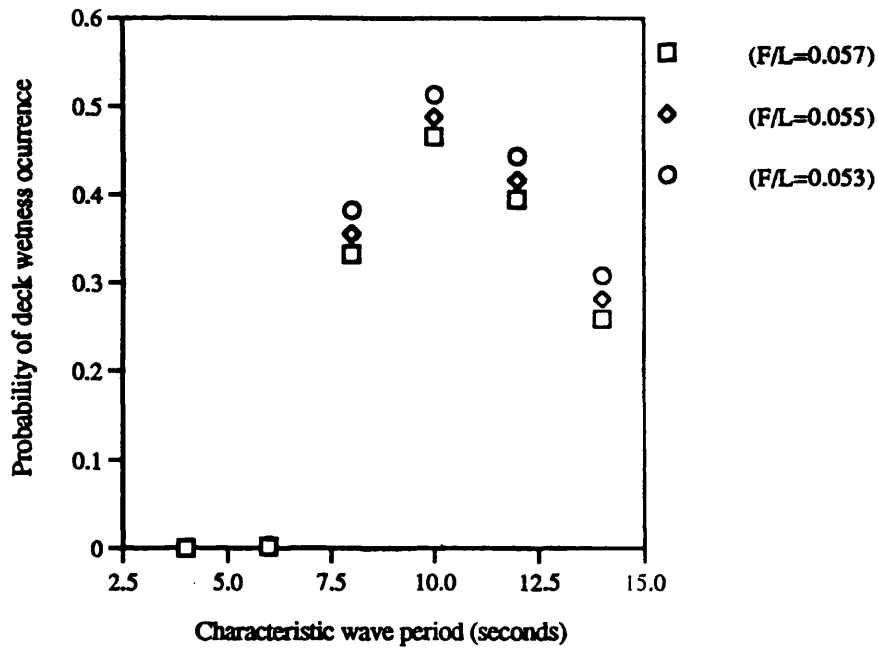

Fig. 6.37 Probability of deck wetness occurrence for Fr=0.2 and H=14 metres

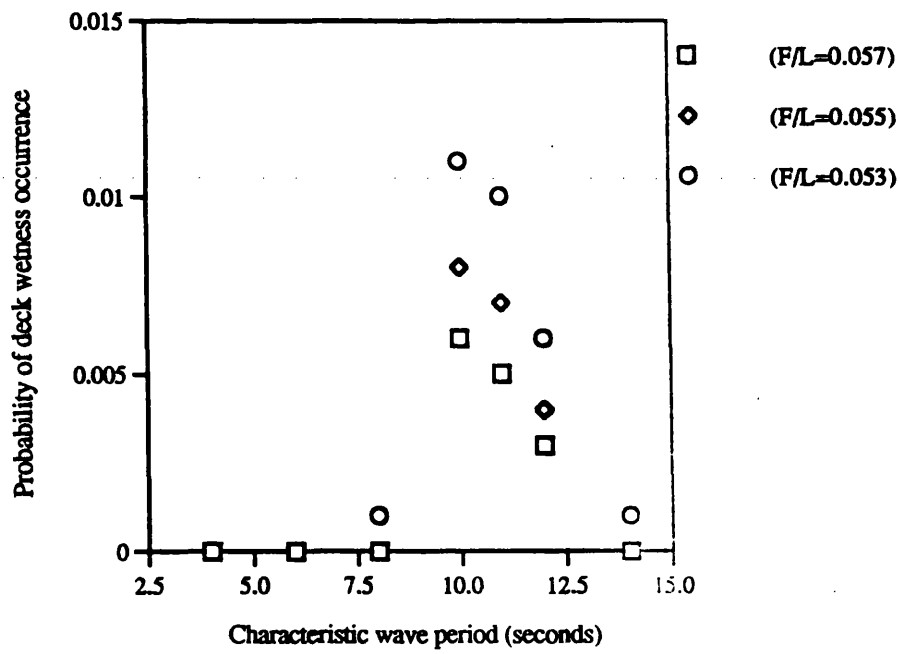

Fig. 6.38 Probability of deck wetness occurrence for Fr=0.278 and H=6 metres

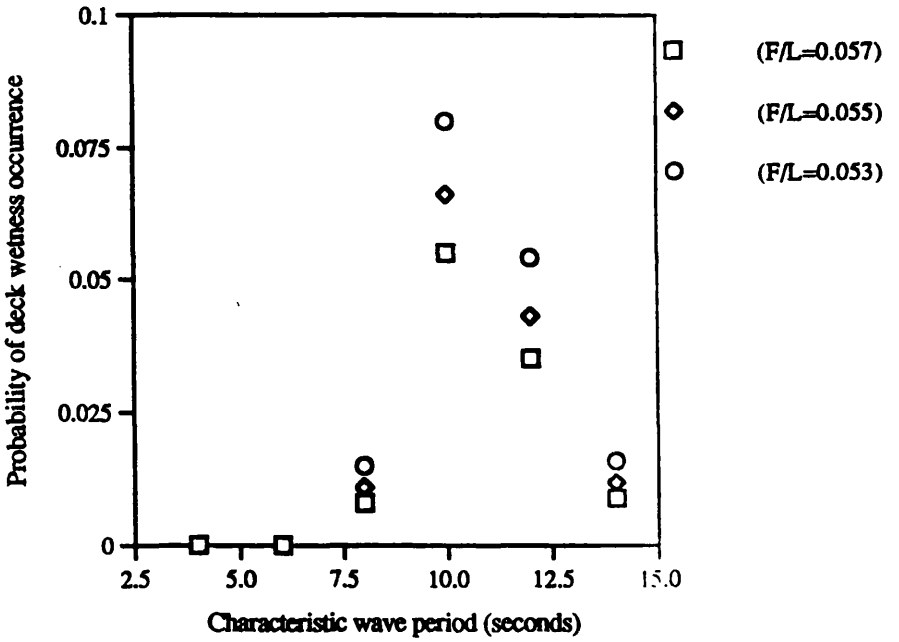

Fig. 6.39 Probability of deck wetness occurrence for Fr=0.278 and H=8 metres

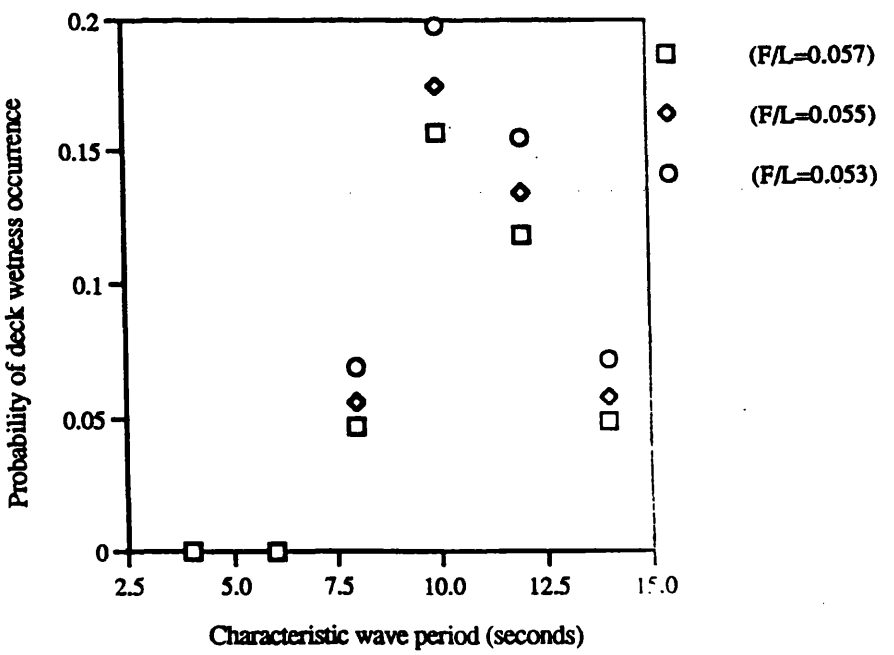

Fig. 6.40 Probability of deck wetness occurrence for Fr=0.278 and H=10 metres

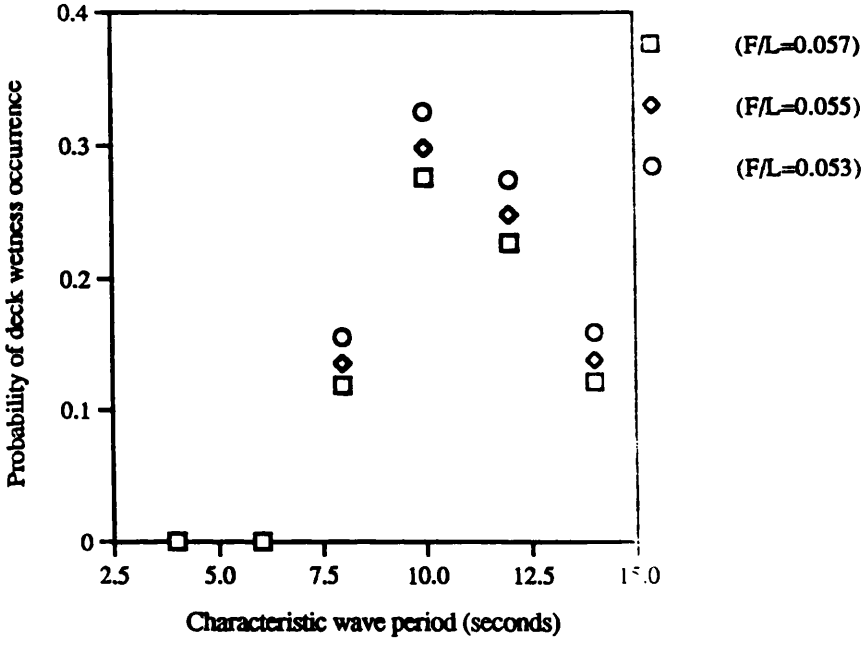

Fig. 6.41 Probability of deck wetness occurrence for Fr=0.278 and H=12 metres

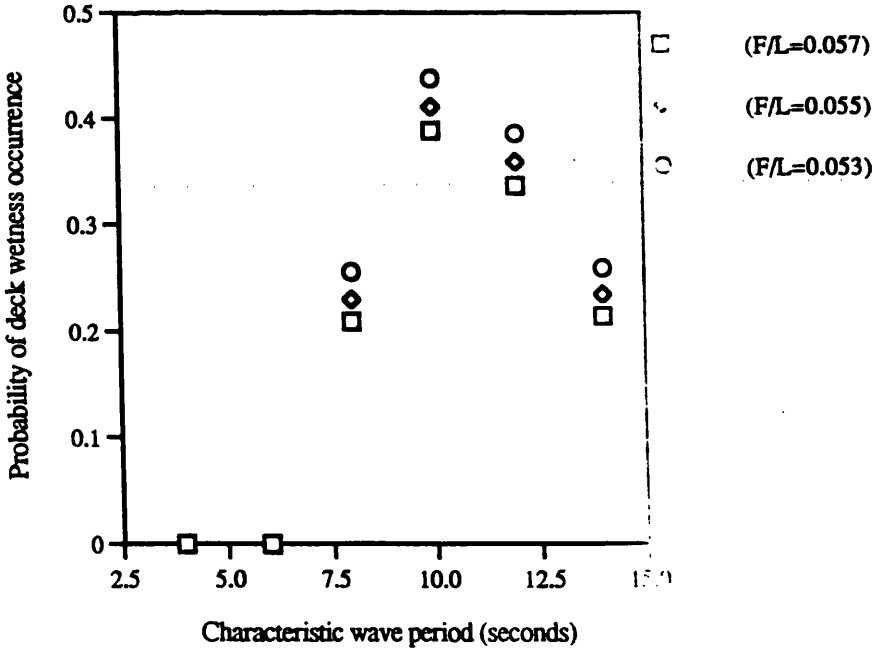

Fig. 6.42 Probability of deck wetness occurrence for Fr=0.278 and H=14 metres

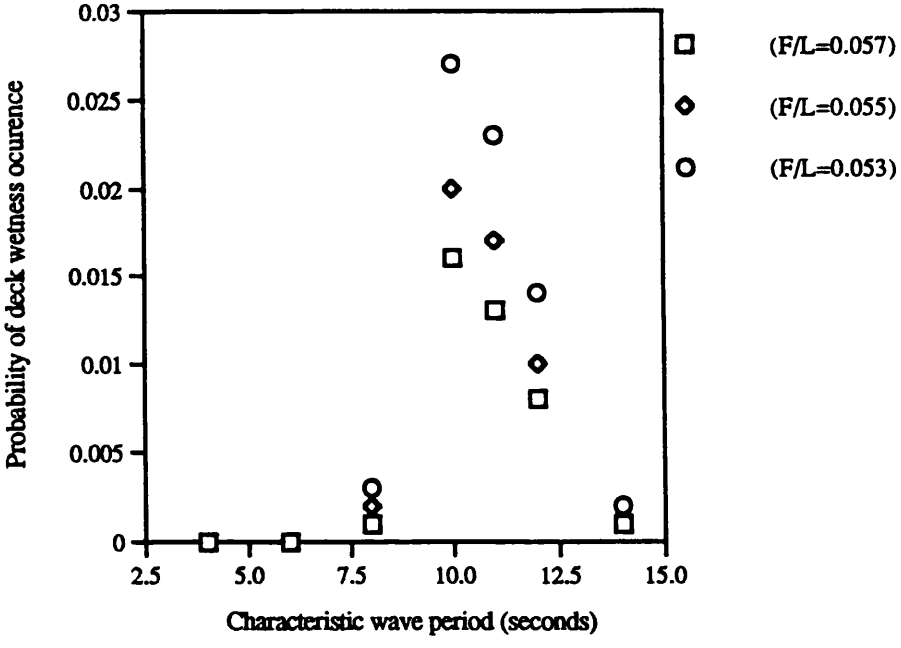

Fig. 6.43 Probability of deck wetness occurrence for Fr=0.3 and H=6 metres

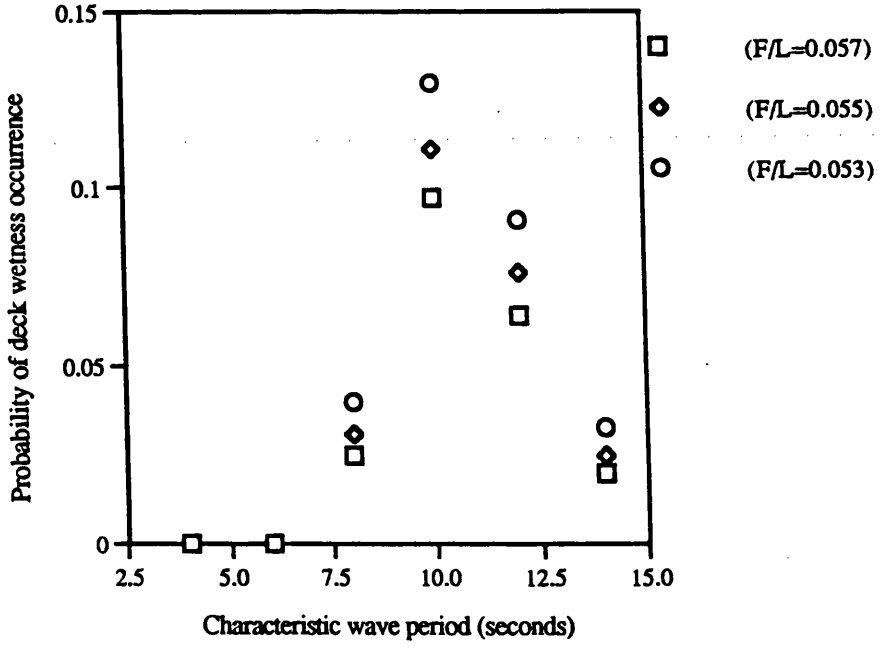

Fig. 6.44 Probability of deck wetness occurrence for Fr=0.3 and H=8 metres

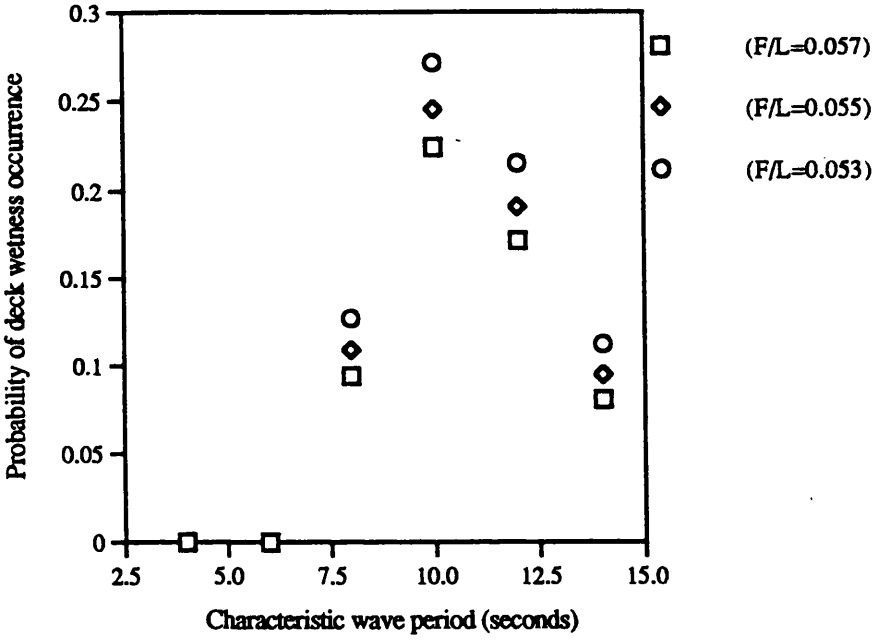

Fig. 6.45 Probability of deck wetnes occurrence for Fr=0.3 and H=10 metres

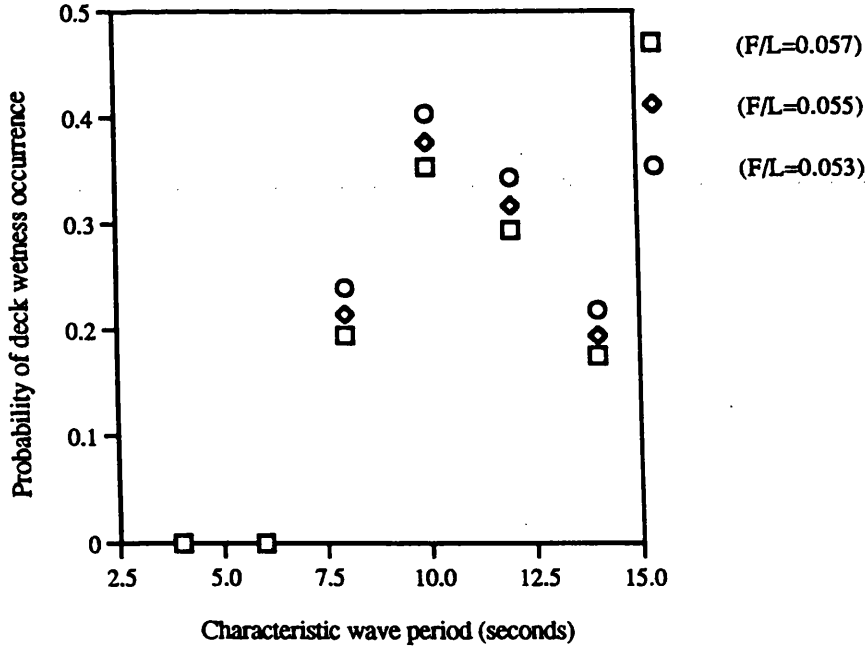

Fig. 6.46 Probability of deck wetness occurrence for Fr=0.3 and H=12 metres

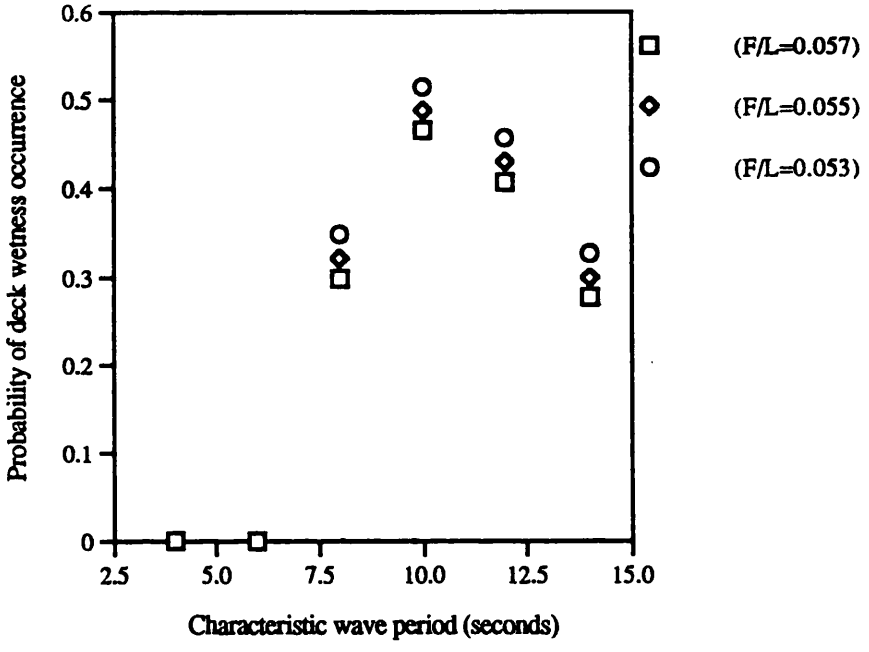

Fig. 6.47 Probability of deck wetness occurrence for Fr=0.3 and H=14 metres

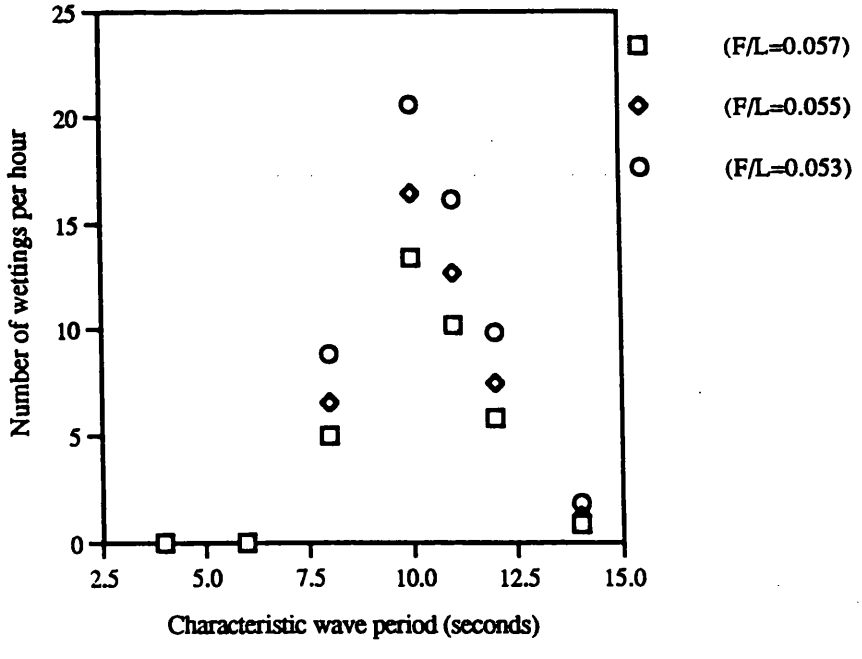

Fig. 6.48 Number of wettings per hour for Fr=0.1 and H=6 metres

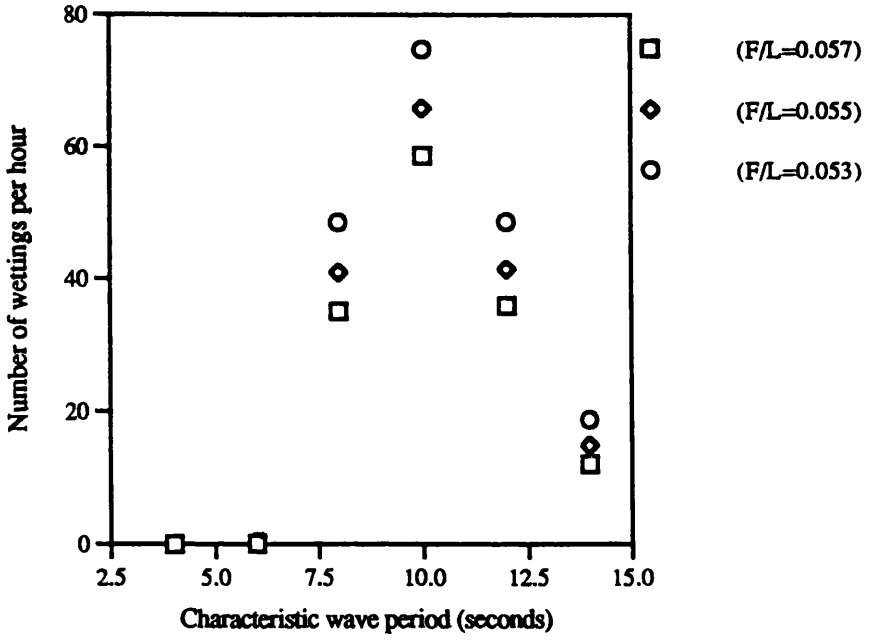

Fig. 6.49 Number of wettings per hour for Fr=0.1 and H=8 metres

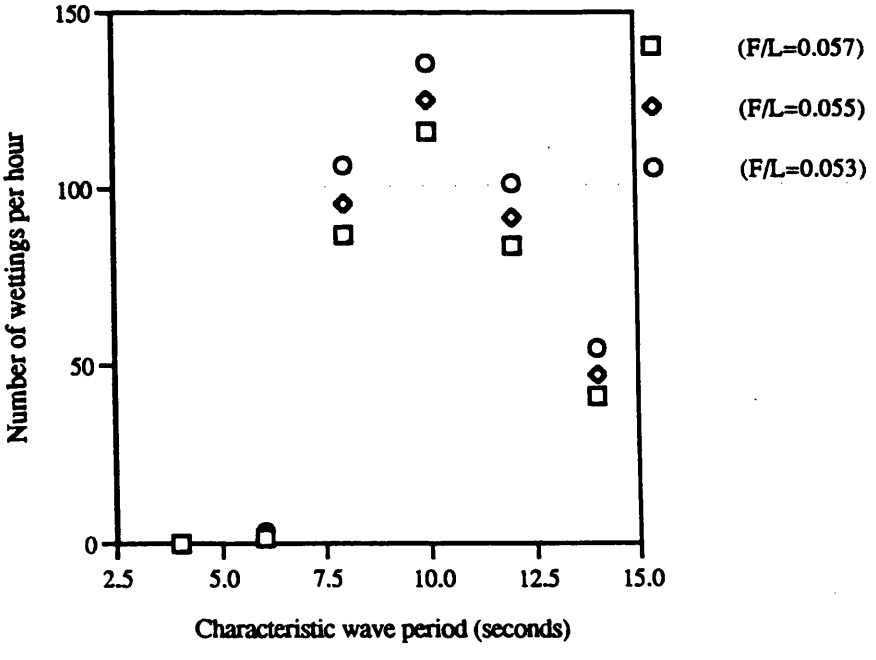

Fig. 6.50 Number of wetings per hour for Fr=0.1 and H=10 metres

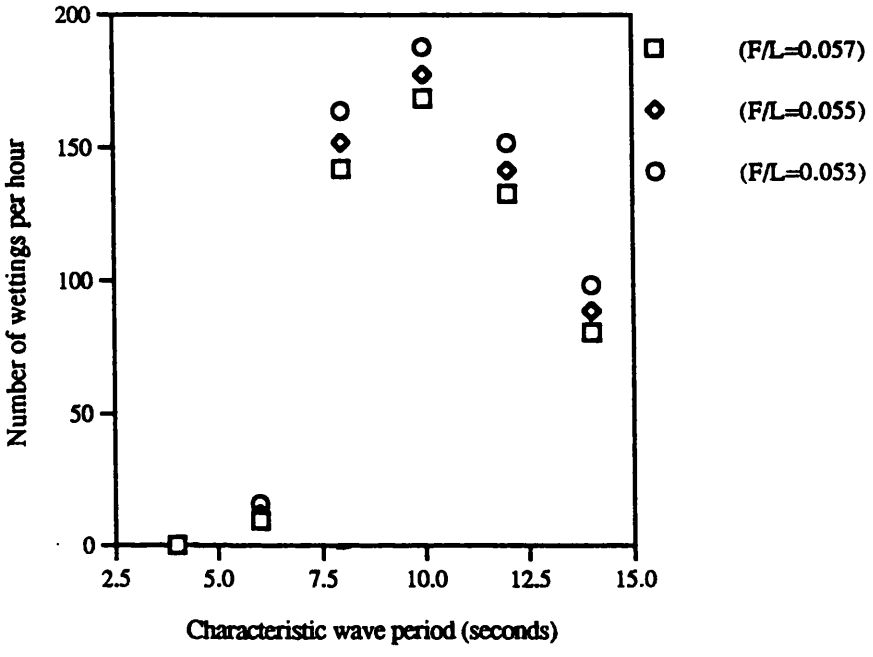

Fig. 6.51 Number of wettings per hour for Fr=0.1 and H=12 metres

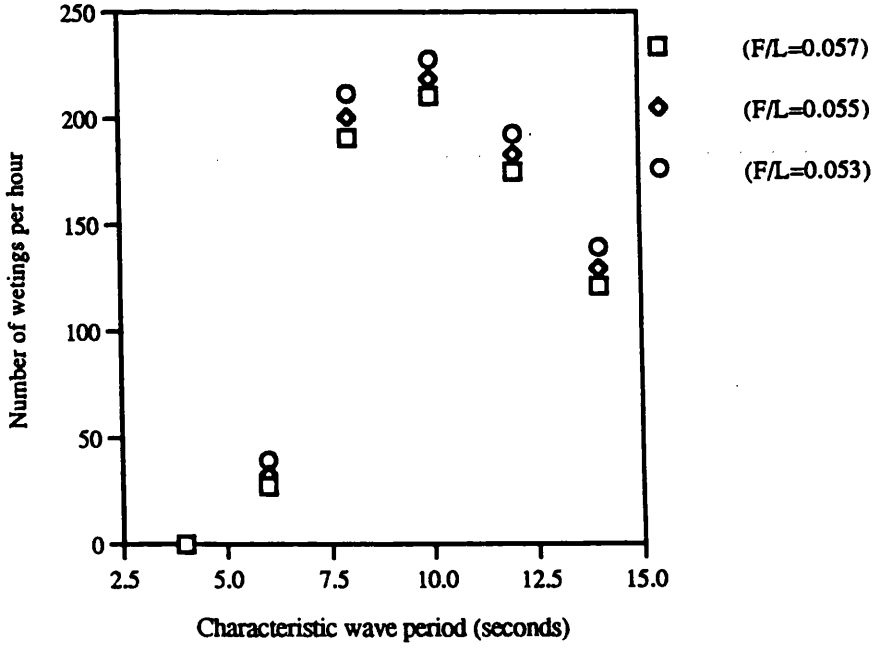

Fig. 6.52 Number of wettings per hour for Fr=0.1 and H=14 metres

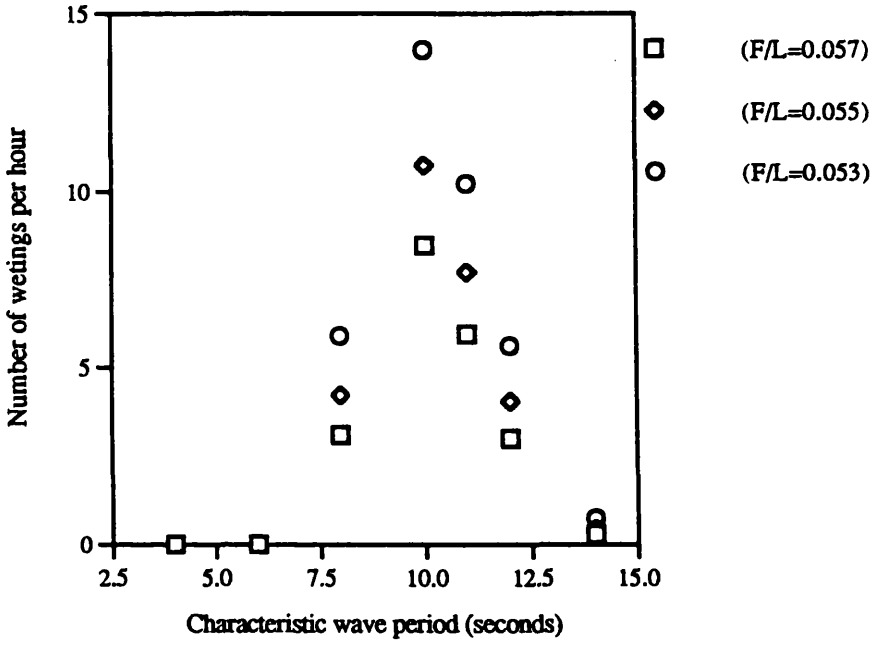

Fig. 6.53 Number of wettings per hour
for Fr=0.15 and H=6 metres

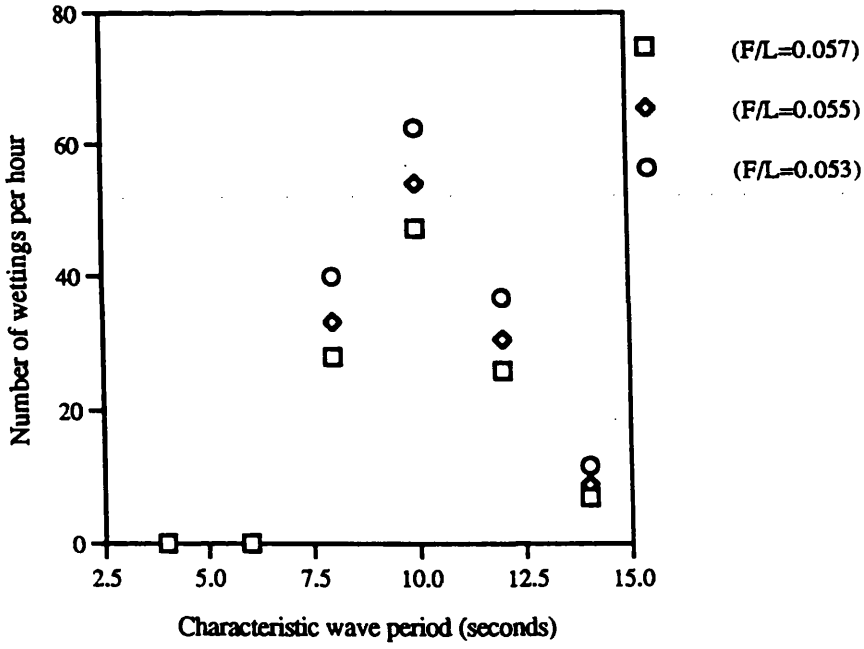

Fig. 6.54 Number of wettings per hour for
Fr=0.15 and H=8 metres

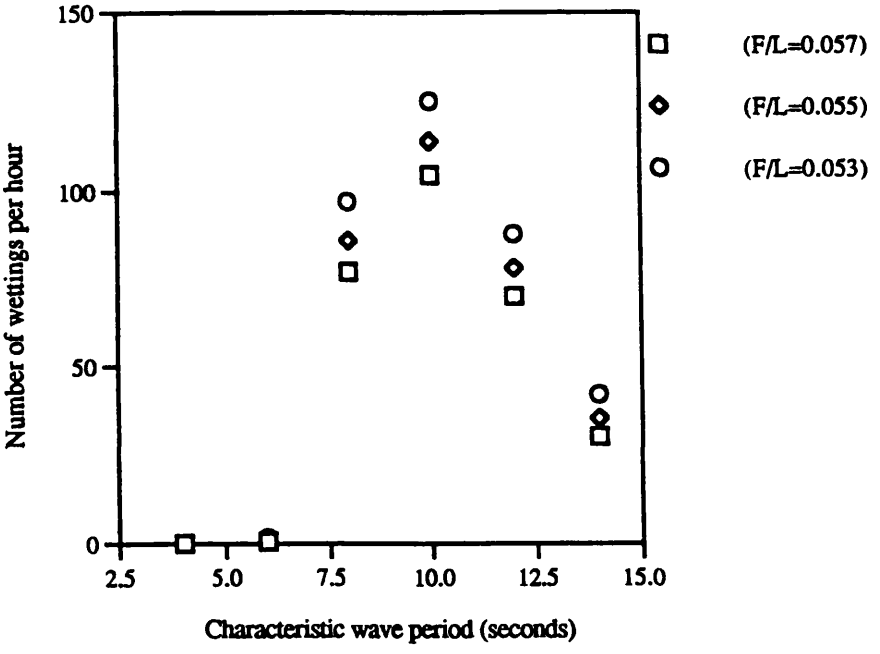

Fig. 6.55 Number of wettings per hour
for Fr=0.15 and H=10 metres

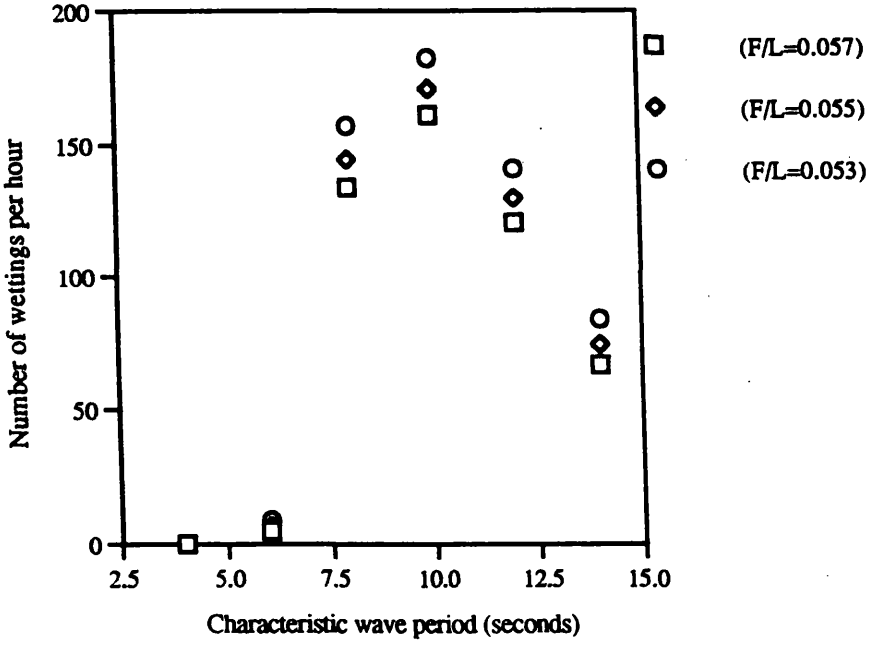

Fig. 6.56 Number of wettings per hour
for Fr=0.15 and H=12 metres

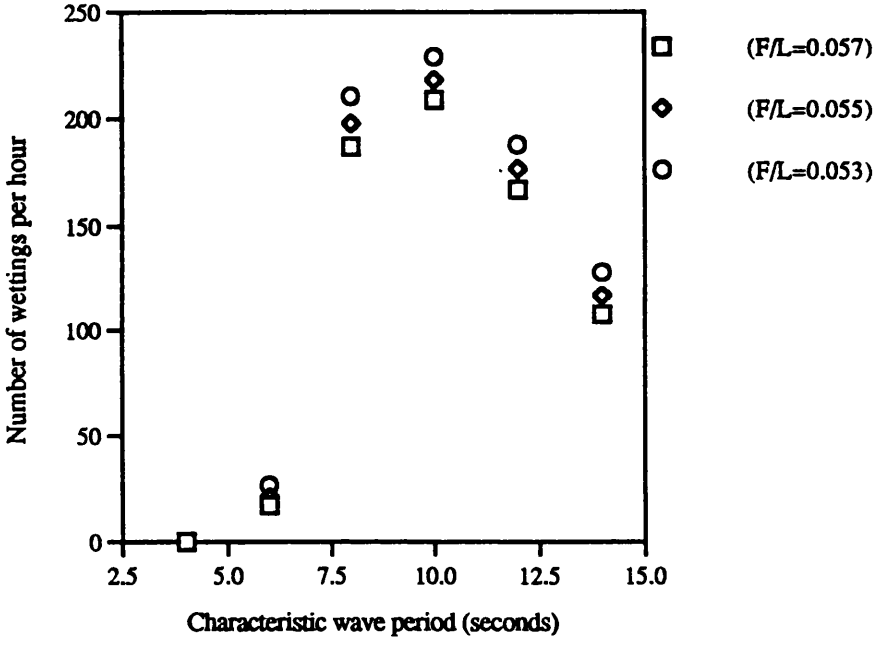

Fig. 6.57 Number of wettings per hour
for Fr=0.15 and H=14 metres

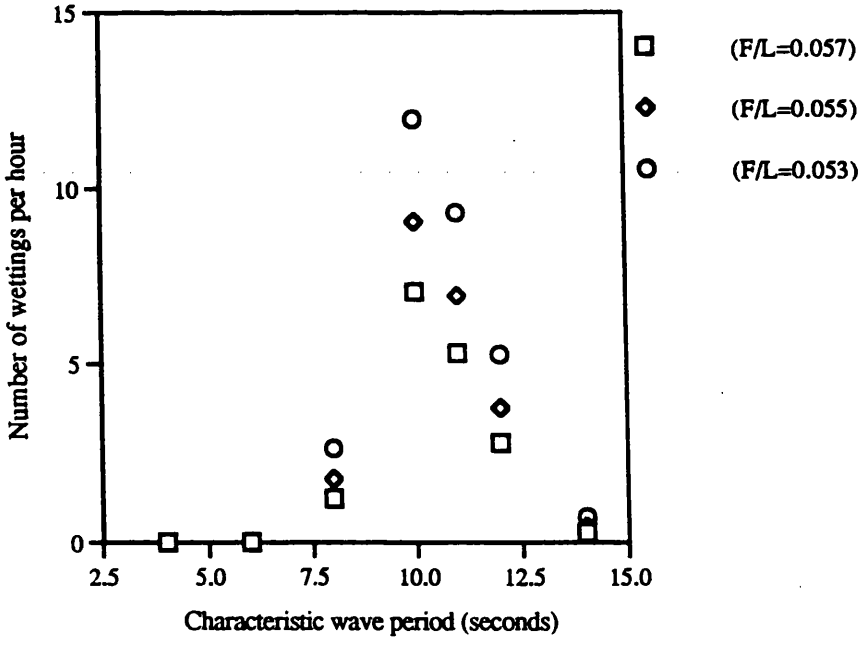

Fig. 6.58 Number of wettings per hour
for Fr=0.2 and H=6 metres

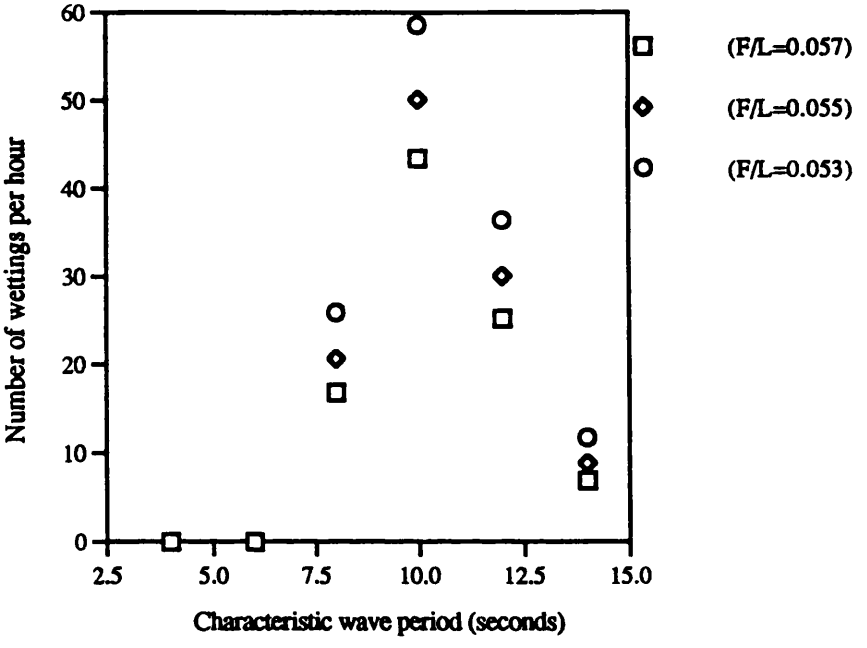

Fig. 6.59 Number of wettings per hour
for Fr=0.2 and H=8 metres

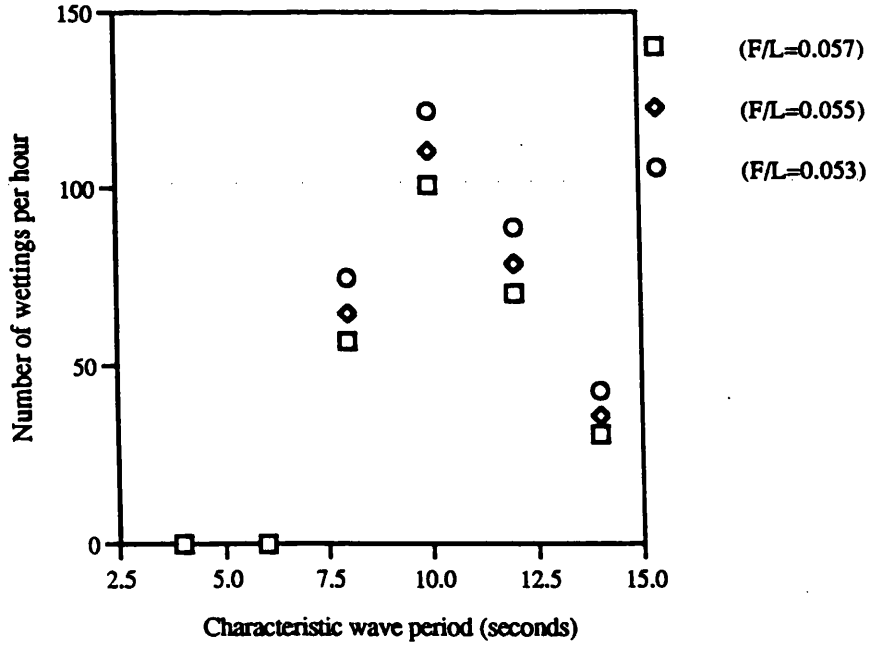

Fig. 6.60 Number of wettings per hour
for Fr=0.2 and H=10 metres

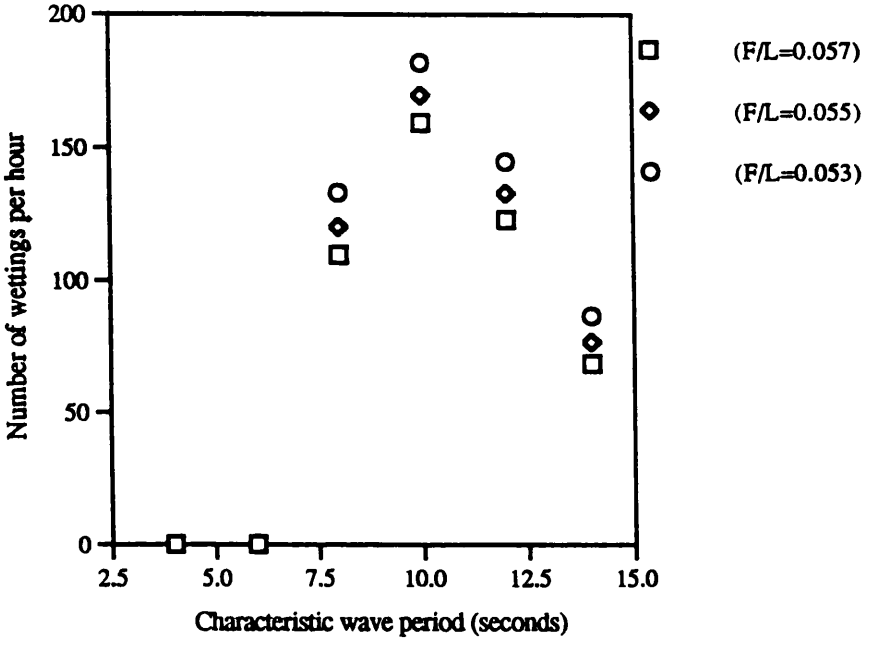

Fig. 6.61 Number of wettings per hour
for Fr=0.2 and H=12 metres

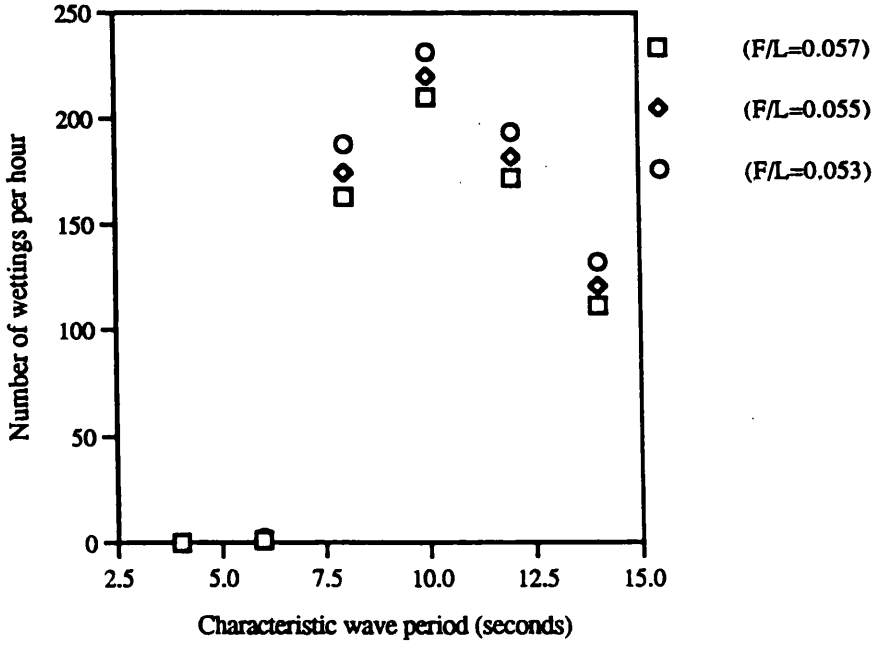

Fig. 6.62 Number of wettings per hour
for Fr=0.2 and H=14 metres

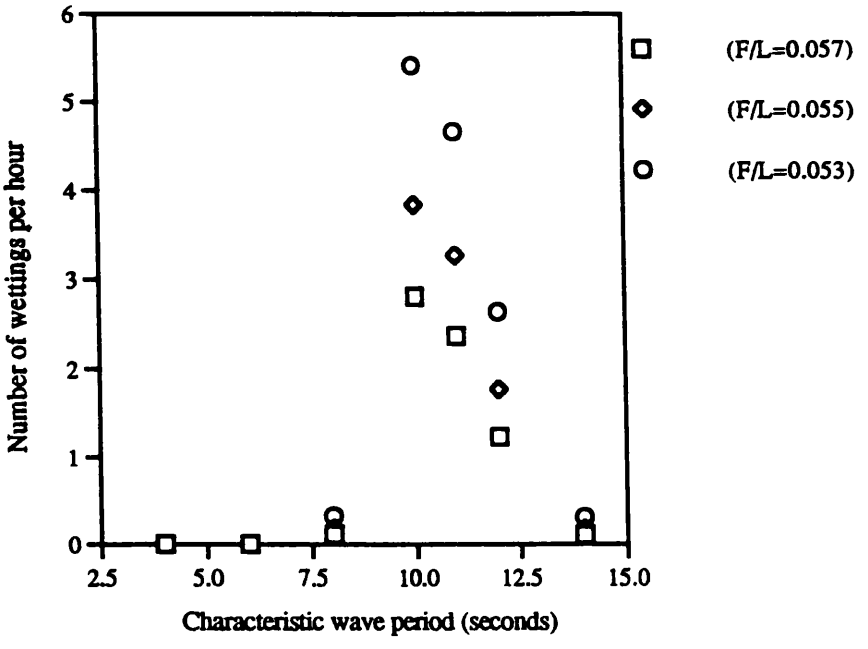

Fig. 6.63 Number of wettings per hour
for Fr=0.278 and H=6 metres

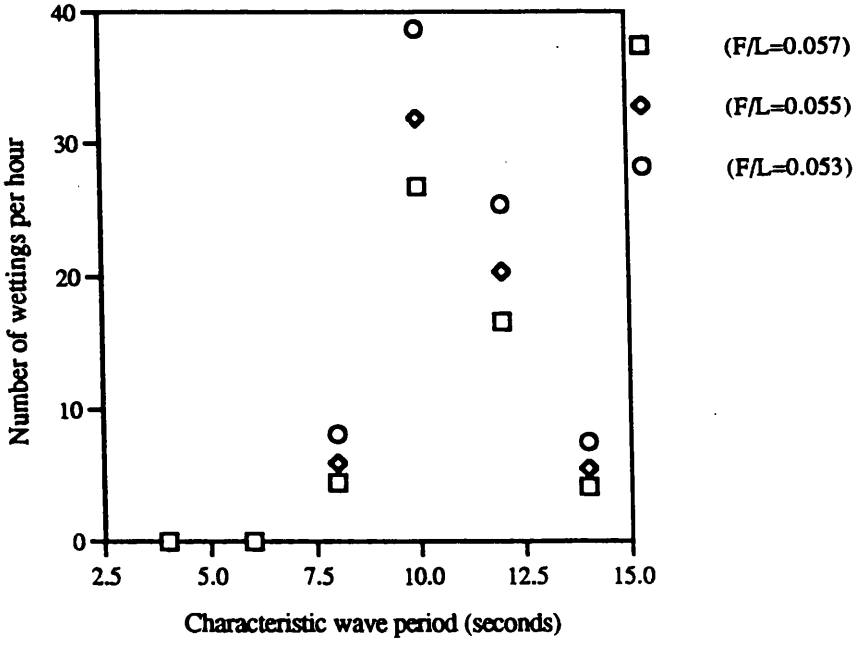

Fig. 6.64 Number of wettings per hour
for Fr=0.278 and H=8 metres

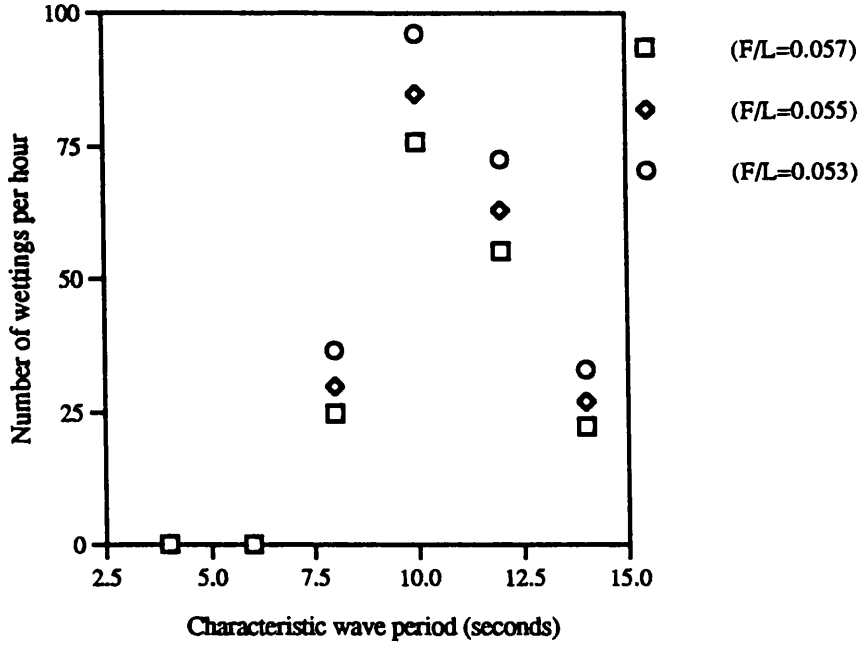

Fig. 6.65 Number of wettings per hour
for Fr=0.278 and H=10 metres

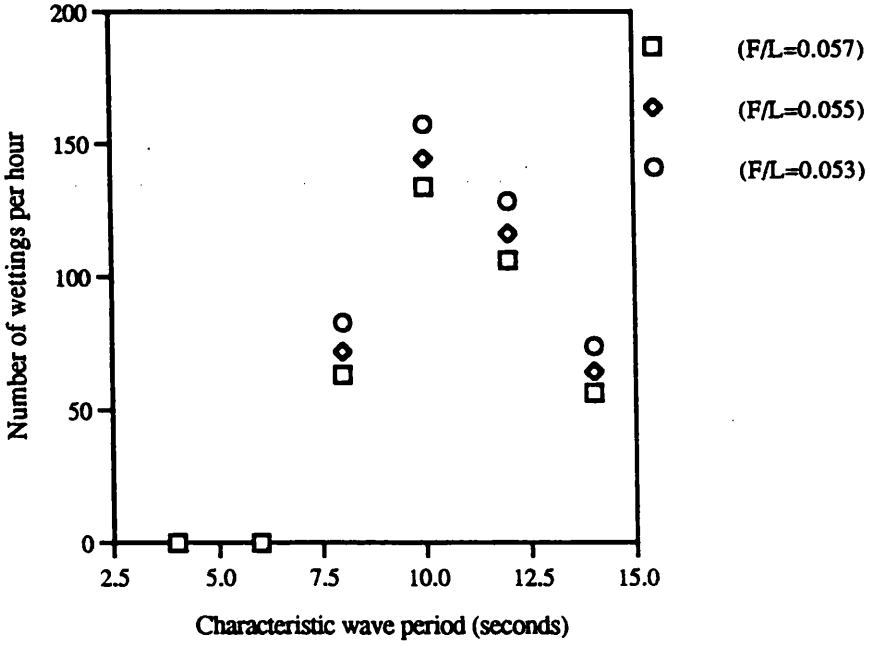

Fig. 6.66 Number of wettings per hour
for Fr=0.278 and H=12 metres

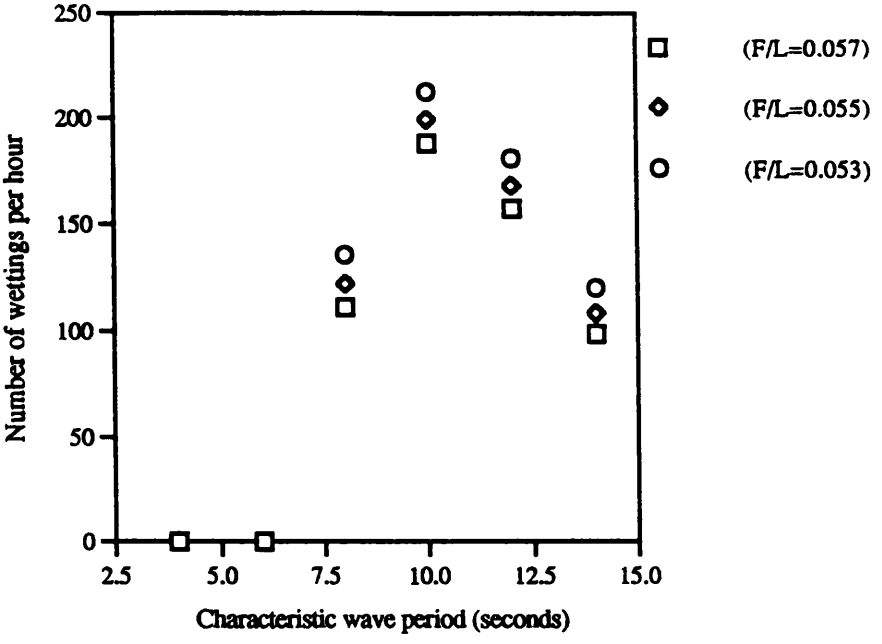

Fig. 6.67 Number of wettings per hour
for Fr=0.278 and H=14 metres

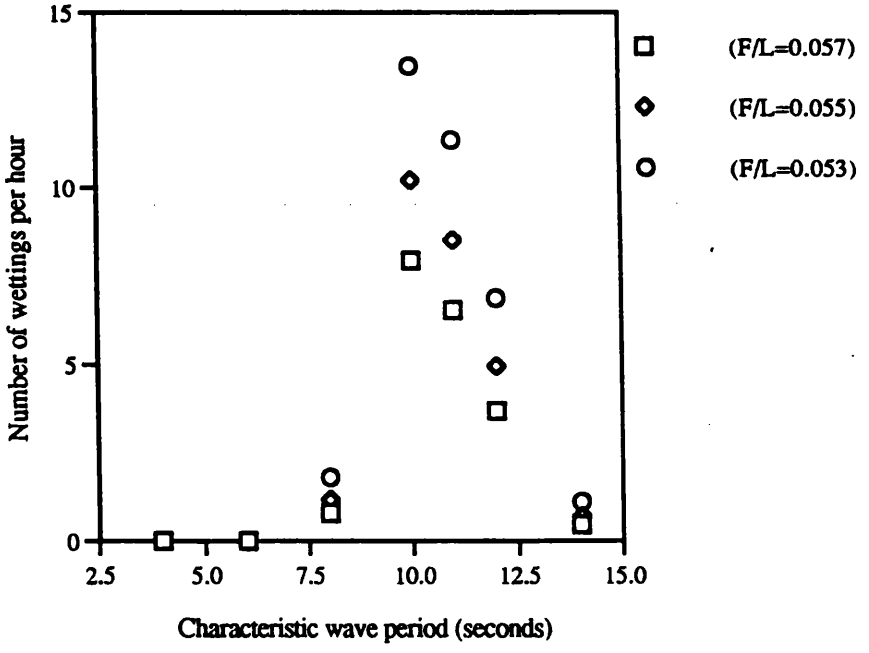

Fig. 6.68 Number of wettings per hour
for Fr=0.3 and H=6 metres

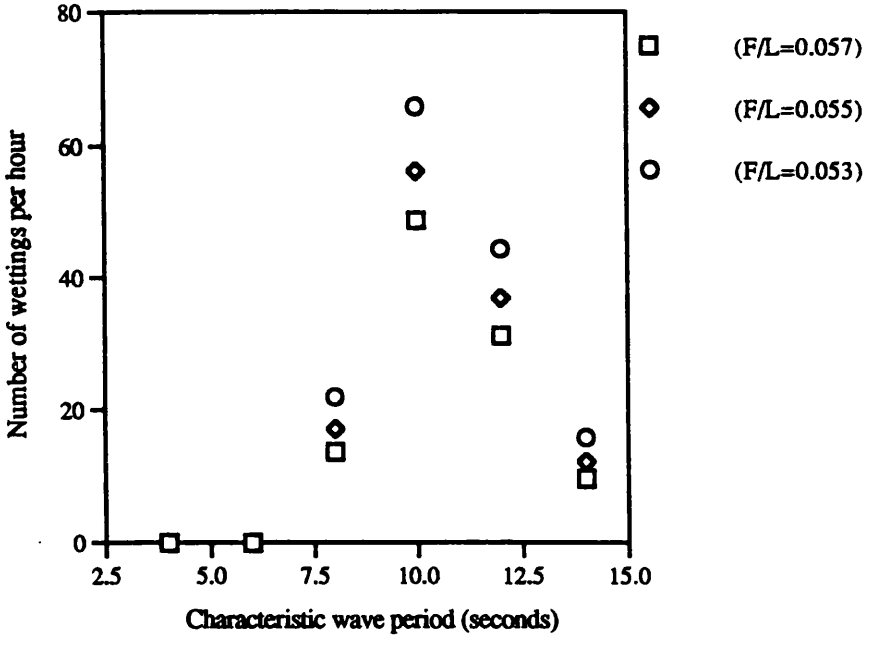

Fig. 6.69 Number of wettings per hour
for Fr=0.3 and H=8 metres

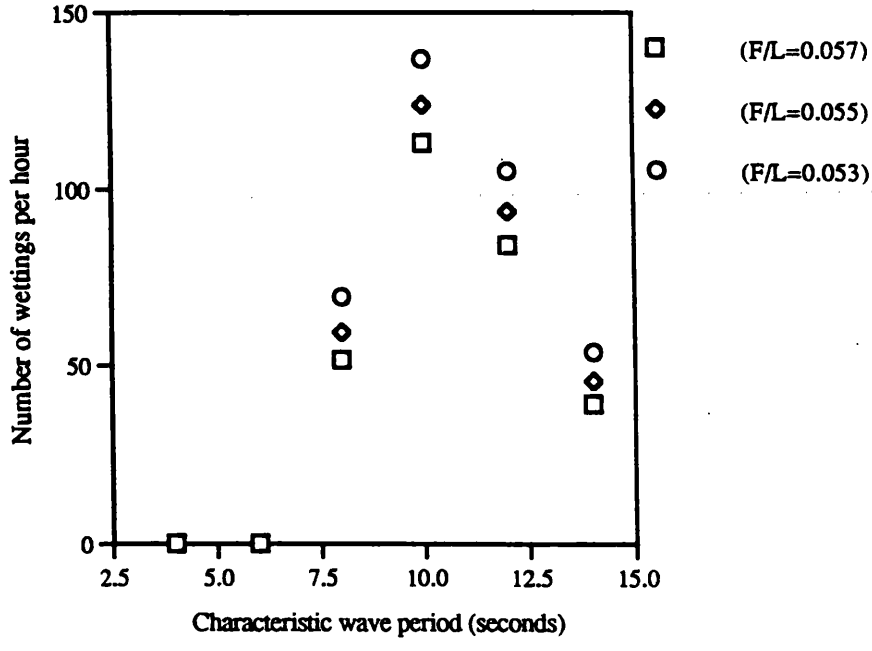

Fig. 6.70 Number of wettings per hour
for Fr=0.3 and H=10 metres

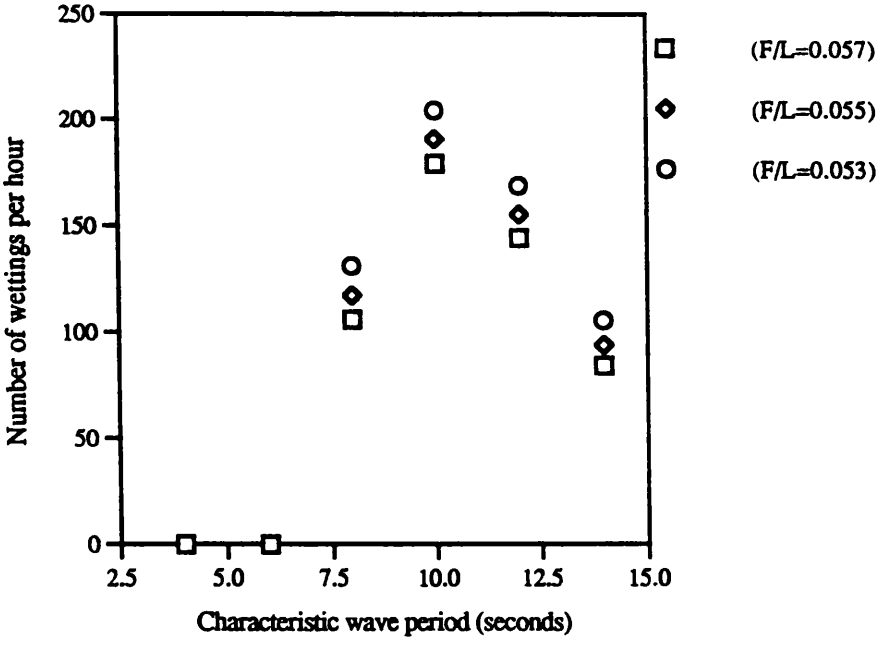

Fig. 6.71 Number of wettings per hour
for Fr=0.3 and H=12 metres

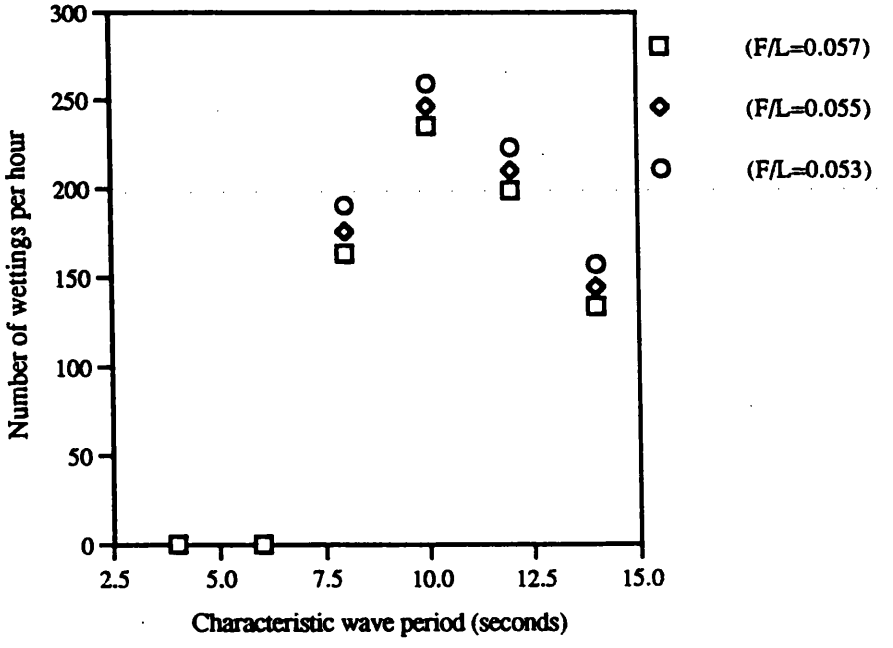

Fig. 6.72 Number of wettings per hour
for Fr=0.3 and H=14 metres

CHAPTER 7
CONCLUSIONS AND RECOMMENDATIONS

CHAPTER 7

CONCLUSIONS AND RECOMMENDATIONS

7.1 CONCLUSIONS

Theoretical and experimental investigations on bottom slamming and deck wetness were the aims of this research.

The hydrodynamic coefficients were calculated by using the conformal mapping parameter in the multipole expansion method. To get reasonable and accurate predictions of the hydrodynamic coefficients for input into the equations of motions, it is usual to truncate the mapped section to two parameters only from the point of numerical accuracy. The end effect terms play an important role in the prediction of ship motions.

For accurate numerical prediction of the coefficients a least square method is adopted and these results are compared with those of Tasai (1959) and Bishop and Price (1979). For nearly the same conditions, the present method and Tasai's method match very well as for example in Fig. 2.21. However, the differences in the free surface coefficient of added mass as shown in Fig. 2.24 are due to the differences in input conditions.

The results of the motions obtained by the present method, the New Strip Method, and by the SHIPMO package are as in Figs. 2.42 to 2.43 and Figs. 2.46 and 2.47. For the lower frequency range one can notice the shift in the peak and an increase in the magnitude of the heave motion which results in large motions of the ship and which in turn may cause slamming and/or deck wetness.

Prediction of pressure due to bottom slamming is given. The momentum theory or von Karman theory, is adequate for describing flare slamming, and bottom slamming is investigated by using Wagner's impact theory.

The pressure due to bottom slamming is proportional to the square of the vertical relative velocity and the constant of proportionality is determined from the pressure coefficient or factor of ship hull which depends mainly on the shape of the bottom portion of the section under consideration.

The pressure coefficient can be determined by several methods, such as conformal mapping (two or three parameter prediction techniques), prediction based on deadrise angle, impact angle, breadth and draught (at one tenth of the design draught) and experimental methods. Comparison of the pressure coefficient by different methods is given and good correlation is found between these methods. For example, the pressure coefficient predicted by the three parameter technique using an iteration program is 15.1 for station 8 1/2 for the S175 container ship and 15.35 using Ochi's (1971) prediction technique. Predicting the pressure coefficient by two parameters does not fully agree with that from three parameters, but it gives reliable results, and for the same station the pressure coefficient is found to be 11.46, the variation is 24% when compared with the three parameters mapping technique.

Though various methods have been discussed for determining the pressure coefficient, emphasis has been placed on obtaining it by conformal mapping and breadth and draught formulae. Depending on the amount of input data available one may need to adopt either of these methods. There is also good agreement with the experimental pressure coefficient at station 8 1/2 obtained by Kawakami et al (1980).

There are hardly any open literature references which give a detailed procedure for calculating the third parameter a_5 as even Kawakami et al (1980) used the relation that a_1 equals 10 times a_3 and a_1 also equals 20 times a_5 for their calculations of the slamming pressure coefficient. The present prediction technique, which incorporates the third parameter a_5 arising from additional information of the centre of gravity of the station under consideration, will benefit designers to obtain a more accurate pressure coefficient without having to make approximations.

The distribution of pressure due bottom slamming over the girth is given and is a maximum at the centre of the girth and zero at one tenth of the design draught. Hence if the maximum impact pressure is obtained through experiments or calculations, the distribution can be obtained.

The trapped air plays an important role in reducing the pressure due bottom slamming. But air entrapment is not included in the scaling laws and may cause errors when extrapolating model results of initial impact pressure to full scale.

The interpretation of the threshold velocity is still vague as not enough investigations have been carried out to interpret its physical meaning. Hence wide use of Ochi's (1964) postulation for the threshold velocity is employed.

A model of the S175 container ship was used in the present study. Characteristics associated with slamming phenomenon were also investigated by taking measurements from model tests for different conditions, such as draught, forward speed and wave frequency.

The vertical relative motion was measured and its differentiation with respect to time was taken, in order to obtain vertical relative velocity. Using this the impact pressure was calculated. The measurement of impact pressure was first made by using pressure transducers located at station 8 and 8 1/2 on the bottom of the model. These measurements were repeated three times in order to gather a bigger population of scatter.

The pressures recorded at ballast draught are much higher, and sometimes twice that of the loaded draught cases.

The vertical relative velocity and vertical acceleration at which slamming was observed are lower than Ochi's threshold values. The magnitude of the slamming pressure and its occurrence are different for the three tests. This difference is believed to be due to some nonlinearities which are ignored during the investigation, such as compressibility of water and air and the cushioning effect of air (air boundary layer, depression of the water surface just before impact) and due to the limitations of the degrees of freedom and also due to the errors resulted from experiment. The maximum measured magnitude of the impact pressure due to bottom slamming is found to be 3.476 kN/m2 for the S175 container ship model, this corresponds to a vertical relative velocity of 0.724 m/sec and a vertical acceleration of 0.63g for loaded draught and for Fr=0.275. The maximum impact pressure calculated by the three parameter method is 7.42 kN/m2 and by two parameter it is 5.53 kN/m2, these pressures correspond to vertical relative velocity of 0.84 m/sec. The equivalent full scale pressures would be 23.62 times as great. This scaling factor is determined by applying Allen and Jones method for the ship and model.

As the measured impact values are lower than the calculated values, three repetitive tests were conducted for the same set of conditions. However when the calculated pressures were compared with the measured pressures for the three test cases, it is noticed that though there is consistency with the calculated data, in the case of the

measured values there is not much consistency. From this one can conclude that it is more appropriate to use the theoretical three parameter prediction method, due to consistency of the results.

The calculated pressure coefficient for station 81/2 is 15.1, using conformal mapping (three parameter), but some measured values for the same relative velocity at the instant of impact, are approximately 4 times higher than the calculated values and this is attributed to nonlinearities, possible errors of calibration and errors from experiment and also interaction between the wave and the model.

The average time interval of an impact is found to be 5.5 milliseconds for the 2.5 metre length model of the S175 container ship. This is in good agreement with the experimental measurements of Verhagen (1967).

The present results will be useful for developing further studies on ship slamming for high speed marine vehicles. Setting up a data bank, of the measured results will be useful in future to enhance the present method.

It must also be noted that in towing tanks, conditions of rough weather cannot be satisfied because of the following reasons:

- motions are limited by the set up of the equipments (guides),
- avoid damage of the equipment,
- slam may not occur during the very limited time of the run length, which is 12 seconds on an average.

The probability of occurrence of slamming events depends mainly on motion response of the ship and the sea environment. The highest probability of occurrence of slamming for Fr=0.275 and a significant wave height of 4 m and characteristic wave period of 10 seconds is 0.188. For a characteristic wave period of 10 seconds and significant wave height of 10 m the probability of occurrence is 0.005 for loaded draught and 0.213 for ballast draught conditions.

The number of slamming impacts depend on the probability of occurrence and ship operation time. The highest value for the probability of occurrence occurs with the longest navigation time and results in a large number of impacts as given in Table 5.2.

The extreme pressure depends mainly on the probability of occurrence, the number of impacts and the ship operation time. The extreme pressure (with probability of occurrence 0.025) exceeds 1540 kPa. This extreme pressure is predicted when the significant wave height is 12.0 metres and the characteristic period is 10.0 seconds.

The design pressure by the Allen and Jones method for the model of the S175 container ship is found to be 1.285 psi (8.865 kN/m^2). The maximum pressure measured for the S175 container ship model is 0.503 psi (3.476 kN/m^2) for loaded draught condition and Fr=0.275 when the model was underway in a head sea condition and the corresponding maximum impact pressures calculated by the three and two parameter conformal mapping techniques are 1.075 psi (7.42 kN/m^2) and 0.801 psi (5.53 kN/m^2) respectively. One may conclude that the design pressures calculated by the Allen and Jones method for the model and the maximum impact pressure calculated by three parameter, for loaded draught condition and for Fr=0.278, are in a good agreement.

The second part of this research has been experimental work to investigate deck wetness. A set of experiments were carried out in ballast and loaded draught conditions in regular waves. A model of the container ship S175 was equipped with plates mounted on load cells in order to measure the impact pressure due to the force in the longitudinal direction. This investigation leads to some conclusions, as described bellow.

Deck wetness occurs when the relative motions exceed the freeboard. Also, there is no occurrence of deck wetness at the ballast draught condition except for some sprays, but for the loaded draught condition the phenomenon was very violent. Hence this event depends mainly on the freeboard.

The forward speed of the vessel plays an important role. At high speed (for example Fr=0.3) deck wetness becomes more violent. The force in the longitudinal direction (impact pressures) follows the same trend as the vertical relative motions.

The impact pressures on the bottom row of plates are higher than the top row of plates. For example, when the model was underway in the head sea condition at Fr=0.2 and for the frequency $\omega\sqrt{\frac{L}{g}}=2.5$, plate 5 which is in the centre of the bottom row recorded 1.945 kN/m^2 (corresponding to 136 kN/m^2 full scale). For the same conditions plate 2 which is in the centre of the upper row recorded 0.418 kN/m^2 (29.4 kN/m^2 full scale), this load acting on plate 2 is not far from the design load given by Lloyd's Register

of Shipping (1982), which is about 24 kN/m^2(full scale). However the load acting on plate 5 is more than 5.5 times higher than the design load which is due to the severeness of the event.

The mass of water shipped on deck mainly depends on the forward speed of the vessel and the relative motion exceeding the freeboard. For example, at Fr=0.3 the highest mass of water is more than 40 kg. The trend of the curve of mass of water collected is the same as the relative motion curve.

This thesis presents an approximate method to predict load in the longitudinal direction on a vertical superstructure or deck mounted equipment due to green water shipped on the deck of floating bodies (ship, platforms) with or without forward speed.

The force in the longitudinal direction presented has only recently been formulated and it is inversely proportional to the distance at which the vertical wall is positioned from where the water is shipped.

The measured load is always lower than the calculated load, and that is why the dispersion factor always lies in the range of 0.0 and 1.0. This is also clear from the fact that not all the mass of water collected, did hit the load cells wall, for example at Fr=0.3 the collected mass of water is more than 40 Kg. In other words, a certain quantity of water comes from other directions, such as the sides and from above the wall. The histogram of the mass of water shipped on the deck of the container ship model, serves good design data for the dispersion factor. The minimum value of the dispersion factor calculated in the present research is 0.13 and the maximum value is around 0.94.

The probability of deck wetness occurring and the number of wettings depends mainly on the freeboard parameter. There are also other parameter, such forward speed, significant wave height and characteristic wave period. The number of wettings resulting from this investigation differs from that of Lloyd et al (1982) due to the different models and set up. The maximum number of wettings obtained from the present investigation, for the ratio of freeboard to ship length of 0.05, Fr=0.1, significant wave height of 6 m and characteristic wave period of 11 seconds, is about 11 wettings per hour.

The results of significant loads compared with those of Lloyd et al (1982) are not far from each other but there is some difference and this may be due to the different conditions satisfied during the test.

The difference in the result obtained in the present research and that of the Lloyd et al (1982) investigation can be explained by one statement, i.e results of one type of ship are not applicable to another type of ship. In other words a data bank should be prepared for different high speed vessels, so that future researchers can make use of these data for investigating loads on deck mounted equipment.

7.2 RECOMMENDATIONS

Due to the extensive time required to tackle a large number of experimental conditions for predicting slamming and deck wetness some recommendations are made for future work.

In the first part of the research on bottom slamming, more theoretical and experimental investigations need to be carried out. Theoretically, one has to look carefully at complicated nonlinearities, such as effect of air which reduces the impact pressure. Experimentally, the model under investigation needs to be free from other degrees of freedom (such as roll motion) and not just pitch and heave. More pressure transducers need to be placed at the fore end (station 9, 9 1/2 and FP) and on different levels around the girths. Furthermore, one has to know all the properties of the pressure transducer used during the test, such as how fast a pressure transducer responds to an impact.

Due to the limited length of the towing tank, it is a difficult to satisfy the conditions for slamming to occur. If the length of a run is short sometimes slamming may not take place. Hence investigation of bottom slamming in longer tanks is recommended.

The second part of this investigation provides data on the deck wetness phenomenon and present new method to predict load in the longitudinal direction. Though the present set of data recorded are adequate from the point of view of preliminary design, more data collected is also needed.

The load cell wall has to be placed at different stations in the fore end in order to gather more data about shipping of water on deck. The relative motion also needs to be measured at the fore station for comparison with the freeboard.

The dispersion factor has to be looked into, because the present research places emphasis on a particular type of vehicle navigating under certain conditions. However, this dispersion factor may be used as a first guide for design purposes.

It is also recommended that the mass of water shipped on deck needs more investigation of its geometric, kinematic and dynamic properties to enhance the new method for the prediction of the force in the longitudinal direction. To achieve this, more theoretical work validated by experiments needs to be carried out.

REFERENCES

REFERENCES

REFERENCES FOR CHAPTER 1

Bales, K., (1979), "Minimum Freeboard Requirements for Dry Foredeck", SNAME, *Symp*..

Belik, O., Bishop, R.E.D. and Price, W.G., (1979), "On the Slamming Response of Ships to Regular Head Waves", RINA.

Belik, O., Bishop, R.E.D. and Price, W.G., (1982), "A Simulation of Ship Responses due to Slamming in Irregular Head Waves", RINA.

Bishop, R.E.D. and Price, W.C., (1979), "Hydroelasticity of Ships", Cambridge University Press.

Chuang, S.L., (1966), "Experiments on Flat-Bottom Slamming", *Journal of Ship Research*, Vol. 10 No. 1, March.

Chuang, S.L., (1967), "Experiments on Slamming of Wedge-Shaped Bodies", *Journal of Ship Research.*

Chuang, S.L., (1969), "Theoretical Investigation on Slamming of Cone- Shaped Bodies", *Journal of Ship Research*, Vol. 13, No. 4, Dec.

Chuang, S.L., (1970), "Investigation of Impact of Rigid and Elastic Bodies with Water", *NSRDC*, Report 3248.

Chuang, S.L., (1973), "Slamming Tests of Three-Dimensional Models in Calm Water and Waves", *NSRDC*, Report 4095.

Chu, W-H. and Abramson, H.N., (1961), "Hydrodynamic Theories of Ship Slamming - Review and Extension", *Journal of Ship Research.*

Edward, J. and Todd, F.H., (1938-39), "Steam Drifters: Tank and Sea Tests", IESS, Vol. 82.

Fang, M-C., Lee, M-L. and Lee, C-K., (1993), "Time Simulation of Water Shipping Advancing in Large Longitudinal Waves", *Journal of Ship Research*, Vol. 37, No. 2, pp. 126-137.

Faulkner, D., Das, P.K. and Djatmiko, E.B., (1993), "Some Aspects of Structural Design of Fast Multi-Hull Ships", *Proc.* IOS-5, Glasgow, U.K.

Ferro, G. and Mansour, A.E., (1985), "Probabilistic Analysis of the Combined Slamming and Wave-Induced Responses", *Journal of Ship Research*, Vol.29 No. 3.

Goda, K., Miyamoto, T. and Yamamoto, Y., (1978), "A Study of Shipping Water Pressure on Deck by Two-dimensional Ship Model Test", JSNA, Japan, Vol. 143.

Goodrich, G.J., (1964), "The Influence of Freeboard on Wetness", *5th. Symp. on Naval Hydrodynamics*, Bergen.

Hamoudi, B. and Varyani, K.S., (1993), "Experimental Aspect of Bottom Slamming on a Container Ship: Design Stage', *IMAM Conf.*, Varna, Bulgaria.

Khattab, O., (1986), "Slamming Prediction", *British Maritime Technology*, Report 14011.

Lewison, G., (1970 a), "On the Reduction of Slamming Pressures", *RINA Trans.*, Vol. II2.

Lewison, G.R.G., (1970 b), "Slamming", *National Physical Laboratory*, Ship Report 138, Mar.

Lloyd, A.R.J.M. and Hammond, M.A., (1982), "The Effect of Bow Shape on Ship Motions and Deck Wetness", Report AMTE(H) R82012, Unclassified.

Lloyd, A.R.J.M., (1983), "Deck Wetness Experiments", *Proc. 20th* ATTC, Vol. 2, Hoboken, New Jersey.

Lloyd, A.R.J.M., Salsish, J.O. and Zseleczky, J.J., (1986), "The Effect of Bow Shape on Deck Wetness in Head Seas", *Proc.* RINA, Vol. 128.

Lloyd, A.R.J.M., (1989), "Seakeeping: Ship Behaviour in Rough Weather", Ellis Horwood Ltd.

Mansour, A.E. and d'Oliviera, J.G., (1975), "Hull Bending Moment due to Bottom Slamming in Regular Waves", *Journal of Ship Research*, Vol. 19 No. 2.

Miyamoto,T., Tanizawa, K., (1985), "A Study of the Impact Load on Ship Bow", 2nd Report, *JSNA*, Japan, Vol. 158.

Mizoguchi, S., (1988), "Analysis of Shipping Water with the Experiments and the Numerical Calculations", *JSNA*, Japan, Vol. 163.

Nagai, T., Chuang, L.S., (1977), "Review of Structural Response Aspect of Slamming', *Journal of Ship Research.*

Newton, R.N., (1960), "Wetness Related to Freeboard and Flare", RINA, Vol. 102.

Ochi, K., (1958), "Model Experiments on Ship Strength and Slamming in Regular Waves", SNAME. Trans., Vol. 66.

O'Dea, J.F. and Walden, D.A., (1984), "The Effect of Bow Shape and Nonlinearities on the Prediction of Large Amplitude Motions and Deck Wetness", *Office of Naval Research Symp.*, Humburg.

Oliver, J.C., (1981), "Analytical Methods to Predict Transient Loads on Floating Platforms", IOS Conf.

Radev, D. and Beukelman, W., (1992), "Slamming on Forced Oscillating Wedges at Forward Speed Part 1-Test Results", *Int Shipbuilding Progress.*, Vol 39, no. 420 pp. 399-422.

Stavovy, A.B. and Chuang, S.L., (1976), "Analytical Determination of Slamming Pressures for High-Speed Vehicles in Waves", *Journal of Ship Research.*

Swaan, W.A. and Vossers, G., (1961), "The effect of Forebody Shape on Ship Behaviour in Waves", RINA, Vol. 103.

Tasai, F., (1969), "On the Deck Wetness and Slamming of Full Ship Forms", 12th ITTC, Rome.

Tick, L.J., (1958), "Certain Probabilities Associated with Bow Submergence and Ship Slamming in Irregular Seas", *Journal of Ship Research*, Vol. 2.

Ulbright, H., (1985), "Loading on the Ship's Hull due to Slamming", Schiffbauforschung 24 (3).

Verhagen, J.H.G., (1967), "The Impact of Flat Plate on a Water Surface", *Journal Ship Research.*

Yamamoto, Y., Ohtsubo, H. and Kohno, Y., (1984), "Water Impact of Wedge Model", *JSNA*, Japan, Vol. 155.

Watanabe, I., (1987), "Effect of the Three-Dimensionality of the Ship Hull on the Wave Impact Pressure", *JSNA*, Japan.

Watanabe, I., Ueno, M. and Sawada, H., (1989), "Effects of Bow Flare to the Wave Loads of Container Ship", *JSNA*, Japan.

REFERENCES FOR CHAPTER 2

Bishop, R.E.D. and Price, W.G., (1974). "The Dynamics of Marine Vehicles and Structures in Waves", Paper 27, *Mechanical Engineering Publications Ltd.*, London.

Bishop, R.E.D. and Price, W.C., (1979), "Hydroelasticity of Ships", Cambridge University Press.

Chan, H.S., (1990), "A Three-Dimensional Technique for Predicting First and Second Order Hydrodynamic Forces on Marine Vehicle Advancing in Waves", *PhD Thesis*, University of Glasgow.

De Jong, B., (1973), "Computation of the Hydrodynamic Coefficients of Oscillating Cylinders", Netherland Ship Research Centre TNO, Report No. 145 S.

Djatmiko, E.B., (1992), "Hydro-Structural Studies on Swath Type Vessels", *PhD. Thesis*, University of Glasgow.

Hamoudi, B. and Varyani, K.S., (1992), "On the Prediction of Impact Slamming for High Speed Vehicles", *Dept. Report*, NAOE-92-19, University of Glasgow.

Kent, J.L., (1948-49), "The Causes and Prevention of Slamming on Ships in a Seaway", *Trans.*, NECIES, Vol. 65.

Kent, J.L., (1949-50), "The Design of Seakindly Ships", *Trans.*, NECIES, Vol. 66.

Korvin-Kroukovsky, B.V., (1955), "Investigation of Ship Motions in Regular Waves", SNAME, Vol. 63.

Lloyd, A.R.J.M. and Crossland, P., (1989 a), "Motions of Steered Model Warship in Oblique Waves", RINA.

Lloyd, A.R.J.M., (1989 b), "Seakeeping: Ship Behaviour in Rough Weather", Ellis Horwood Ltd.

Ochi, M.K. and Motter, L., (1973), "Prediction of Slamming Characteristics and Hull Responses for Ship Design", Trans. SNAME, Vol. 81.

Price, W.G. and Bishop, R.E.D., (1974), "Probabilistic Theory of Ship Dynamics", Chapman and Hall Ltd., London.

Salvesen, N., Tuck, E.O. and Faltinsen, O., (1970), "Ship Motions and Sea Loads", SNAME, Trans. Vol. 78, pp.250-287.

Seakeeping Symposium, (1969), Society of Naval Architects of Japan, (in Japanese).

'Software for Seakeeping Prediction', (1992), SHIPMO-PC, Version 1.22, Sable Maritime Ltd., Canada.

Tasai, F., (1959), "On the Damping Force and Added Mass of Ships Heaving and Pitching", *Reports of Research Institute for Applied Mechanics*, Vol. VII, No.

26.

Ulbright, H., (1985), "Loading on the Ship's Hull due to Slamming", Schiffbauforschung 24 (3).

REFERENCES FOR CHAPTER 3

Aertssen, G., (1969), "Laboring of Ships in Rough Seas", SNAME, Vol. 77.

Aertssen, G., (1978), "DISCUSSION on the paper: On the Dynamic of Slamming", RINA.

Allen, R.G. and Jones, R.R., (1977), "Consideration on the Structural Design of High Performance Marine Vehicles", prepared for the presentation at the New York Metropolitan Section of SNAME.

Belik, O., Bishop, R.E.D. and Price, W.G., (1979), "On the Slamming Response of Ships to Regular Head Waves", RINA.

Belik, O., Bishop, R.E.D. and Price, W.G., (1987), "Influence of Bottom and Flare Slamming on Structural Responses", RINA.

Bishop, R.E.D., Price, W.G. and Tam, P.K.Y., (1978), "On the Dynamic of Slamming", RINA.

Chan, H.S., Djatmiko, E.B., Miller, A.F. and Blyth, L., (1992), "Aspect of Structural Loading in the Design of SWATH Ships", PRADS *Conf.*, Newcastle, U.K.

Chuang, S-L., (1965), "Experimental Investigation of Rigid Flat-Bottom Body Slamming", *David Taylor Model Basin, Report* 2041.

Chuang, S-L., (1966), "Experiments on Flat-Bottom Slamming", *Journal of Ship Research*, Vol. 10.

Chuang, S-L., (1967), "Experiments on Slamming of Wedge-Shaped Bodies", *Journal of Ship Research.*

Chuang, S-L., (1970), "Investigation of Impact of Rigid and Elastic Bodies with Water", *Naval Ship Research and Development Centre, Report* 3248, Washington.

Chuang, S-L., (1973), "Slamming Tests of Three-Dimensional Models in Calm Water and Waves", *Naval Ship Research and Development Centre, Report* 4095, Bethesda, Maryland.

Faltinsen, O.M., (1990), "Sea Loads on Ships and Offshore Structures", Cambridge University Press.

Fukasawa, T. and Yamamoto, Y., (1980), "Some Consideration on Bow and Handling of Fast Cargo/Container Ships from the Viewpoint of Slamming", *JSNA*, Japan, Vol. 148.

Hamoudi, B. and Varyani, K.S., (1992 a), "On the Prediction of Impact Pressure due to Bottom Slamming for Container Ship", CADMO *Conf.*, Spain.

Hamoudi, B. and Varyani, K.S., (1992 b), "On the Prediction of Impact Pressure due to Bottom Slamming for High Speed Vehicles", *Dept. Report*, NAOE-92-19,

University of Glasgow.

Hamoudi, B. and Varyani, K.S., (1993), "Experimental Aspect of Bottom Slamming on a Container Ship: Design Stage", *International Maritime Association of the Mediterranean* (IMAM), Vol. 1, Varna, Bulgaria.

Hwang, J.H., Kim, Y.J., Min, K.S. and Ahn, S.I., (1983), "Prediction of Bow Flare Impact Pressure by Momentum Slamming Theory", *Proc. International Workshop on Ship and Platform Motions*, University of California, Berkeley.

Jones, N., (1976), "Plastic Behaviour of Ship Structure", SNAME, Vol. 84.

Kawakami, M., Tanaka, K., Michimoto, J-I, Nitta, S. and Kanazawa, M., (1980), "On the Whipping due to Slamming of General Cargo Ship", *Tran. The West- Japan Society of Naval Architects*, No. 60.

Lloyd, A.R.J.M., (1989), "Seakeeping: Ship Behaviour in Rough Weather", Halsted Press, John Wiley & Sons.

Lewison, G.R.G. and Maclean, W.M., (1968), "On the Cushioning of Water Impact by Entrapped Air", *Journal of Ship Research*, Vol. 12.

Lewison, G.R.G., (1970 a), "On the Reduction of Slamming Pressures", *Trans.* RINA , Vol. II2.

Lewison, G.R.G., (1970 b), "Slamming", *National Physical Laboratory, Ship Report* 138.

Ochi, M.K., (1964), "Extreme Behaviour of a Ship in Rough Seas-Slamming and Shipping of Green Water", SNAME, Vol. 72.

Ochi, M.K. and Motter, L.E., (1971), "A Method to Estimate Slamming Characteristics for Ship Design", *Marine Technology*, No. 8.

Ochi, M.K. and Motter, L.E., (1973), "Prediction of Slamming Characteristics and Hull Responses for Ship Design", *Trans.* SNAME, Vol. 81.

Price, W.G. and Bishop, R.E.D., (1974), "Probabilistic Theory of Ship Dynamics", Chapman and Hall Ltd.

Stavovy, A.B. and Chuang, S-L., (1976), "Analytical Determination of Slamming Pressures for High Speed Vehicles in Waves", *Journal of Ship Research*, Vol. 20, No. 4, pp. 190-198.

Sellars, F.H., (1976), "Water Impact Loads", *Marine Technology*, Vol. 13, No.1.

"Transient Dynamic Loading and Response", (1985), *Proc. 9th International Ship Structure Congress* (ISSC), Committee II.3, Vol. 1, Geneva.

Umeda, N., Yamakoshi, Y. and Suzuki, S., (1993), "Bottom Plating Strength of High Speed Fishing Craft", FAST'93, Vol. 2, Japan.

von Karman, Th., (1929), "The Impact on Seaplane Floats During Landing", *National Advisory Committee for Aeronautics, Technical Note* No. 321, Washington.

Wilson, P.A. Discussion on Hamoudi, B. and Varyani, K.S., (1992), "On the Prediction of Impact Pressure due to Bottom Slamming on Container Ship", CADMO *Conf.*, El-Pardo, Spain.

REFERENCES FOR CHAPTER 4

Belik, O, Bishop, R.E.D. and Price, W.G., (1982), "A Simulation of Ship Responses Due to Slamming in Irregular Head Waves", RINA.

Blok, J.J. and Huisman, J., (1983),"Relative Motions and Swell-Up for a Frigate Bow", RINA.

Boylston, J.W., De Koff, D.J. and Muntjewert, J.J., (1974), "SL-7 Container Ships: Design, Construction, and Operational Experience", *Trans.* SNAME, Vol. 82.

Chatterjee, A.K., (1982), "Economic Design of Container Ship", *PhD Thesis*, University of Glasgow.

Elbatouti, A.M.T. and Jan, H-Y., (1976), "Structural Analysis of a Container Ship Steel Model and Comparison with Test Results", *Trans.* SNAME, Vol. 84.

Fang, C.C., (1994), "Experimental Investigation of Large Amplitude Motions of Catamaran in Waves", *Dept. Report*, NAOE-94-15, University of Glasgow.

Faulkner, D., (1994), "Ocean Engineering Challenges and Opportunities", Public Lecture, Dept. NAOE, University of Glasgow.

Fukasawa, T. and Yamamoto, Y., (1980), "Some Consideration on Bow Form and Handling of Fast Cargo/Container Ships from the Viewpoint of Slamming", *JSNA*, Japan, Vol. 148.

Fukuda, J. and Shinkai, A., (1983), "Speed Loss of a Container Ship on the Different Routes in the North Pacific Ocean in Winter", *International Symposium on Ship Hydrodynamics and Energy Saving*, Spain.

Gatzer, H.G, Varyani, K.S. and Hamoudi, B. (1992), Private Communication.

Hamoudi, B., (1991), "Dynamic Response of Hull due to Bottom Slamming and Deck Wetness", *Annual Report*, Dept. NAOE, University of Glasgow.

Hamoudi, B., (1992 a), "Effect of Speed and Draught on the Bottom Slamming and Deck Wetness in Regular Waves", *Dept. Report*, NAOE-92-18, University of Glasgow.

Hamoudi, B. and Varyani, K.S., (1992 b), "On the Prediction of Impact Pressure due to Bottom Slamming for High Speed Vehicles", *Dept. Report*, NAOE-92-19, University of Glasgow.

Hamoudi, B., (1993 a), "Dynamic Response of Hull due to Bottom Slamming and Deck Wetness: Review and Extension", *Dept. Report*, NAOE-93-18, University of Glasgow.

Hamoudi, B. and Varyani, K.S., (1993 b), "Experimental Aspect of Bottom Slamming on Container Ship: Design Stage", IMAM, VI Congress, Vol.1, Varna, Bulgaria.

Lewison, G.R.G., (1970), "Slamming", *National Physical Laboratory, Ship Report* 138.

Lloyd, A.R.J.M., (1989), "Seakeeping: Ship Behaviour in Rough Weather", Ellis Horwood Ltd.

Murdey, D.C., (1978), "Specification for a Comparative Study of Computed Ship Motions in Six Degrees of Freedom", *NRC, Marine Dynamics and Ship Laboratory, Report* LTR-SH- 228, Canada.

Nakamura, T., (1980), "On the Character of a Container Ship", *Proc. Naval Architecture and Ocean Engineering*, Vol. 18 pp-187-202.

Ochi, K., (1958), "Model Experiments on Ship Strength and Slamming in Regular Waves", *Trans.* SNAME, Vol. 66.

Ochi, M.K. and Motter, L.E., (1973), "Prediction of Slamming Characteristics and Hull Responses for Ship Design", SNAME, Vol. 81.

"Performance Committee", (1978), *Proc.* 15th ITTC, Vol.1, The Hague, Netherlands.

Principles of Naval Architecture, (1988), Vol. 1, Stability and Strength.

Radev, D., (1990), "Investigation of Seakeeping Qualities and Bottom Slamming of a Container Ship in Irregular Waves", Proc. 5th Congress IMAEM, Athens.

"Seakeeping Committee", (1978), Proc. 15th ITTC, Vol.1, The Hague, The Netherlands.

"The Selspot System", (1977), Technical Manual, Selective Electronic Company, Sweden.

Stiansen, S.G., Jan, H-Y. and Liu, D., (1979), "Dynamic Stress Correlation for the SL-7 Container Ship", *Trans.* SNAME, Vol. 87.

Son, K-H. and Nomoto, K., (1981), "On the Coupled Motion of Steering and Rolling of High Speed Container Ship", *JSNA*, Japan, Vol. 150.

Verhagen, J.H.G., (1967), "The Impact of Flat Plate on a Water Surface", *Journal of Ship Research.*

Watanabe, I., (1987), "Effect of the Three-Dimensionality of the Ship Hull on the Wave Impact Pressure", *JSNA*, Japan.

Yoshifumi, T., Yoshino, T., Takagi, M. and Saito, K., (1971), "On the Motions of a High Speed Container Ship with a Single Screw in Oblique Waves", *JSNA*, Japan, Vol. 129.

REFERENCES FOR CHAPTER 5

Bledsoe, M., Bussemaker, O. and Cummins, W.E., (1960), "Seakeeping Trails on Three Dutch Destroyers", Trans. SNAME, Vol.68, pp 39-137.

DET NORSKE VERITAS, (1978), Classification and Registry of Shipping, "Ships' Load and Strength Manual".

Djatmiko, E.B., (1992), "Hydro-Structural Studies on Swath Type Vessels", *PhD. Thesis*, Glasgow University.

Hamoudi, B., (1994), "Probability Approach on Bottom Slamming : a Tool for an Optimum Design", *Proc.* BLACK SEA'94, Varna, Bulgaria.

Lewison, G.R.G., (1970), "On the Reduction of Slamming Pressures", *Trans.* RINA , Vol. II2.

Ochi, M.K. and Motter, L.E., (1973), "Prediction of Slamming Characteristics and Hull Responses for Ship Design", SNAME, Vol. 81, pp. 144-176.

Ohkusu, M. and Hamoudi, B., (1993), Private Discussion, IMAM'93, Varna, Bulgaria.

PANEL HS-2 (Impact Loading and Response), (1993), "Notes on Ship Slamming", *Technical and Research Bulletin* 2-30, SNAME.

Technical Decisions and Recommendations, (1969), *Proc.* 12th I.T.T.C., Rome.

REFERENCES FOR CHAPTER 6

Bales, N.K., (1979), 'Minimum Freeboard Requirements for Dry Deck Foredecks: A Design Procedure' SNAME/STAR *Symp.*, Texas.

Edward, J. and Todd, F.H., (1938-39), 'Steam Drifters: Tank and Sea tests', I.E.S.S, Vol. 82.

Fukuda, J. and Shinhai, A., (1983), 'Speed Loss of a Container Ship on the Different Routes in the North Pacific Ocean in Winter', ISSHES-83, El Pardo, Spain.

Hamoudi, B., (1992 a), 'Effect of Speed and Draught on the Bottom Slamming and Deck Wetness in Regular Waves', *Dept. Report*, NAOE-92-18, University of Glasgow, Glasgow.

Hamoudi, B. and Varyani, K.S., (1992 b), 'On the Prediction of Impact Pressure due to Bottom Slamming on a Container Ship', *Proc.* CADMO, Madrid, Spain.

Hamoudi, B., (1993 a), "Experimental Investigation of Deck Wetness for Container Ship", *4th Congress*, IMAM'93, Vol. 2, Varna, Bulgaria.

Hamoudi, B., Varyani, K.S, Incecik, A. and Chang, H.S., (26th March 1993 b), 'Private Discussion', HLPM&RP Meeting, Glasgow University.

Hamoudi, B. and Varyani, K.S., (1994), "Load Prediction due to Green Water on Deck Mounted Equipment for Floating Bodies", CADMO, Southampton, U.K.

Lloyd, A.R.J.M. and Hammond, M.A., (1982), 'The Effect of Bow Shape on Ship Motions and Deck Wetness', *Report AMTE(H)* R82012, Unclassified.

Lloyd, A.R.J.M., (1983), 'Deck Wetness Experiments', 20th ATTC, Vol.2, New Jersey.

Lloyd, A.R.J.M., Salsich, J.O. and Zseleczky, J.J.; (1985), 'The Effect of Bow Shape on Deck Wetness in Head Seas', RINA.

Lloyd's Register of Shipping, (1982), Rules and Regulations for the Classification of Ships.

Mizoguchi, S., (1988), 'Analysis of Shipping water with the Experiments and the Numerical Calculations', *JSNA*, Japan, Vol. 163.

Murdey, D.C., (1978), 'Specification for a Comparative Study of Computed Ship Motions in Six Degrees of Freedom', *NRC, Marine Dynamics and Ship Laboratory, Report* LTR-SH-228, Division of Mechanical Engineering, Canada.

Oliver, J.C., (1981), 'Analytical Methods to Predict Transient Loads on Floating Platforms', IOS Conference.

Price, W.G. and Bishop, R.E.D., (1974), "Probabilistic Theory of Ship Dynamics", Chapman and Hall Ltd.

Seakeeping Committee, (1978), 15th ITTC, The Hague, The Netherland.

APPENDIX

APPENDIX

METHOD OF DETERMINING THE COEFFICIENTS OF ADDED MASS K_4 AND AMPLITUDE RATIO $\overline{A}_H$

It was Ursell (1949) who first analysed the hydrodynamic forces on 2D circular cylinder. Conformal mapping is the process of transforming an arbitrary section shape to a unit semi circle. It was professor Tasai of Kyushu University who first expanded Ursell's method and referred to as Ursell-Tasai method. The mapping function of conformal mapping is as in Fig. A.2.1 and for ease of calculation we use the same symbols

If we consider port and starboard symmetry we then have as follows:

$$Z = M[\varsigma + \sum_{n=1}^{N} a_{2n-1}\varsigma^{-(2n-1)}] \qquad \text{(A2.1)}$$

and

$$x = M[r\sin\theta + \sum_{n=1}^{N}(-1)^{n+1} a_{2n-1}\frac{\sin(2n-1)\theta}{r^{2n-1}}] \qquad \text{(A2.2.a)}$$

$$y = M[r\cos\theta + \sum_{n=1}^{N}(-1)^{n} a_{2n-1}\frac{\cos(2n-1)\theta}{r^{2n-1}}] \qquad \text{(A2.2.b)}$$

Here 'M' is a contraction factor. The coefficient a_{2n-1} can be obtained by suitable methods. If $N = 2$ it is referred to as Lewis Form.

The x and y of equation (A2.2.a) and (A2.2.b) are introduced in equation (2.4) and (2.5) in chapter 2 with different orientation of the angle. The waveless potential part only is considered essential. The basis of Ursell-Tasai method is the use of the waveless potential.

4.3. Waveless Velocity Potential

Since we are considering the waveless velocity potential which satisfies the free surface condition, equation of continuity (Laplace equation), it is sufficient to consider the linearised free surface condition. The Laplace equation in $[L]_\varsigma$ plane is:

$$\frac{\partial^2\phi}{\partial\xi^2}+\frac{\partial^2\phi}{\partial\eta^2}=0 \tag{A2.3}$$

Therefore the physical representation is by using arbitrary constant, we have as:

$$\phi=\sum_{k=1}^{\infty}\frac{1}{r^k}\{A_k\cos k\theta+B_k\sin k\theta\} \tag{A2.4}$$

Next let us consider about the free surface conditions in the Z plane and on $y=0$

$$\frac{\partial\phi}{\partial y}+K\phi=0 \tag{A2.5}$$

and converting to ς plane it is exactly as follows and from equation (A2.2.a) and (A2.2.b) we have:

$$\frac{\partial x}{\partial r}=M[\sin\theta-\sum_{n=1}^{N}(-1)^{n+1}a_{2n-1}(2n-1)\frac{\sin(2n-1)\theta}{r^{2n}}]=MA \tag{A2.6.a}$$

$$\frac{\partial y}{\partial r}=M[\cos\theta-\sum_{n=1}^{N}(-1)^{n}a_{2n-1}(2n-1)\frac{\cos(2n-1)\theta}{r^{2n}}]=MB \tag{A2.6.b}$$

$$\frac{\partial x}{\partial\theta}=M[r\cos\theta+\sum_{n=1}^{N}(-1)^{n+1}a_{2n-1}(2n-1)\frac{\cos(2n-1)\theta}{r^{2n-1}}]=MC \tag{A2.6.c}$$

$$\frac{\partial y}{\partial\theta}=M[-r\sin\theta-\sum_{n=1}^{N}(-1)^{n}a_{2n-1}(2n-1)\frac{\sin(2n-1)\theta}{r^{2n-1}}]=MD \tag{A2.6.d}$$

Hence

$$\frac{\partial\phi}{\partial r}=\frac{\partial\phi}{\partial x}\frac{\partial x}{\partial r}+\frac{\partial\phi}{\partial y}\frac{\partial y}{\partial r},\quad \frac{\partial\phi}{\partial\theta}=\frac{\partial\phi}{\partial x}\frac{\partial x}{\partial\theta}+\frac{\partial\phi}{\partial y}\frac{\partial y}{\partial\theta}$$

and from which

$$\begin{vmatrix} \frac{\partial x}{\partial r} & \frac{\partial y}{\partial r} \\ \frac{\partial x}{\partial \theta} & \frac{\partial y}{\partial \theta} \end{vmatrix} \begin{vmatrix} \frac{\partial \phi}{\partial x} \\ \frac{\partial \phi}{\partial y} \end{vmatrix} = \begin{vmatrix} \frac{\partial \phi}{\partial r} \\ \frac{\partial \phi}{\partial \theta} \end{vmatrix}$$

therefore

$$\frac{\partial \phi}{\partial y} = \frac{A\frac{\partial \phi}{\partial \theta} - C\frac{\partial \phi}{\partial r}}{M(AD - BC)} \qquad \text{(A2.7)}$$

For $y = 0$ corresponds to $\theta = \pm\frac{\pi}{2}$ in equation (4.56). When $\theta = \pm\frac{\pi}{2}$ let us investigate A to D and from equation (A2.6.a) and (A2.6.d), B and C become zero and from equation (A2.6.b) and (A2.6.c) for $y = 0$ we have as:

$$\left.\frac{\partial \phi}{\partial y}\right|_{y=0} = \frac{\partial \phi}{\partial \theta} / M[\pm r \pm \sum_{n=1}^{N}(2n-1)\frac{a_{2n-1}}{r^{2n-1}}] \text{ at } \theta = \pm\frac{\pi}{2} \qquad \text{(A2.8)}$$

If we introduce this in equation (A2.5) the free surface equation in the mapped plane (ς plane) at $\theta = \pm\frac{\pi}{2}$ is as follows:

$$\mp\frac{\partial \phi}{\partial \theta} + \phi KM[r - \sum_{n=1}^{N}(2n-1)\frac{a_{2n-1}}{r^{2n-1}}] = 0 \qquad \text{(A2.9)}$$

From above if we establish a relation of the coefficients such that equation (A2.4) satisfies the equation of the free surface (A2.9). If we take the flow field as symmetrical flow, from Fig. A.2.1 it is clear that it is sufficient to consider even function of θ i.e $\cos k\theta$ (using θ of Fig. A.2.1). Generally let us introduce equation (A2.4) in equation (A2.9).

$$\sum_{k=1}^{\infty}[KM\{r - \sum_{n=1}^{N}(2n-1)\frac{a_{2n-1}}{r^{2n-1}}\}\frac{A_k}{r^k} \pm k\frac{B_k}{r^k}]\cos k\theta$$
$$+ \sum_{k=1}^{\infty}[KM\{r - \sum_{n=1}^{N}(2n-1)\frac{a_{2n-1}}{r^{2n-1}}\}\frac{B_k}{r^k} \pm k\frac{A_k}{r^k}]\sin k\theta = 0$$

$$\theta = \pm\frac{\pi}{2}$$

$$\sum_{m=1}^{\infty}[KM\{r-\sum_{n=1}^{N}(2n-1)\frac{a_{2n-1}}{r^{2n-1}}\}\frac{A_{2m}}{r^{2m}} \pm 2m\frac{B_{2m}}{r^{2m}}](-1)^m$$
$$\pm\sum_{p=1}^{\infty}[KM\{r-\sum_{n=1}^{N}(2n-1)\frac{a_{2n-1}}{r^{2n-1}}\}\frac{B_{2p-1}}{r^{2p-1}} \pm (2p-1)\frac{A_{2p-1}}{r^{2p-1}}](-1)^{p+1} = 0$$

Hence for $\theta = \frac{\pi}{2}$ we have in details as follows:

$$KM\{r-\sum_{n=1}^{N}(2n-1)\frac{a_{2n-1}}{r^{2n-1}}\}\frac{B_1}{r}+\frac{A_1}{r}-KM\{r-\sum_{n=1}^{N}(2n-1)\frac{a_{2n-1}}{r^{2n-1}}\}\frac{A_2}{r^2}+2\frac{B_2}{r^2}$$
$$-KM\{r-\sum_{n=1}^{N}(2n-1)\frac{a_{2n-1}}{r^{2n-1}}\}\frac{B_3}{r^3}-3\frac{A_3}{r^3}+KM\{r-\sum_{n=1}^{N}(2n-1)\frac{a_{2n-1}}{r^{2n-1}}\}\frac{A_4}{r^4}-4\frac{B_4}{r^4}+.....=0$$

if we arrange in terms of $\frac{1}{r}$, it becomes as follows:

$$KMB_1+\frac{1}{r}(A_1-KMA_2)+\frac{1}{r^2}(-KMa_1B_1+2B_2-KMB_3)$$
$$+\frac{1}{r^3}(-KMa_1A_2-3A_3+KMA_4)+\frac{1}{r^4}(-KM3a_3B_1+KMa_1B_3-4B_4+KMB_5)+.....=0 \qquad (A2.10)$$

similarly for $\theta = -\frac{\pi}{2}$ the above corresponding equation becomes:

$$-KMB_1+\frac{1}{r}(A_1-KMA_2)-\frac{1}{r^2}(-KMa_1B_1+2B_2-KMB_3)$$
$$+\frac{1}{r^3}(KMa_1A_2-3A_3+KMA_4)-\frac{1}{r^4}(-KM3a_3B_1+KMa_1B_3-4B_4+KMB_5)+.....=0 \qquad (A2.11)$$

therefore, if we arrange the free surface condition we must simultaneously arrange equation (A2.10) and (A2.2.a) and(A2.2.b):

$$B_1 = 0$$

$$-pA_p+KM[A_{p+1}-\sum_{n=1}^{\frac{p}{2}}(2n-1)(-1)^n a_{2n-1}A_{p+1-2n}]=0 \qquad (A2.12.a)$$

$$-mB_m + KM[B_{m+1} - \sum_{n=1}^{\frac{m}{2}}(2n-1)(-1)^n a_{2n-1}B_{m+1-2n}] = 0 \qquad \text{(A2.12.b)}$$

(p: odd number, m: even number)

Such a relation is important. As obvious from the above equation there is no relation between A_k and B_k. It only demonstrates that $\cos k\theta$ corresponds to symmetrical flow field and $\sin k\theta$ terms corresponds to unsymmetrical flow field terms. But A_k and B_k respectively follow equation (A2.12.a) and (A2.12.b). Next if we write the waveless velocity potential from symmetrical flow field in detail we have from equation (A2.4) as:

$$\phi_A = \sum_{k=1}^{\infty}\frac{A_k}{r^k}\cos k\theta = \sum_{l=1}^{\infty}\frac{A_{2l-1}}{r^{2l-1}}\cos(2l-1)\theta + \sum_{m=1}^{\infty}\frac{A_{2m}}{r^{2m}}\cos 2m\theta$$

From (A2.12.a) and (A2.12.b) we have

$A_{2l-1} = \frac{KM}{2l-1}[A_{2l} - \sum_{n=1}^{l-1}(2n-1)(-1)^n a_{2n-1}A_{2l-2n}]$, and if we introduce this in the above equation, we have

$$\phi_A = \sum_{m=1}^{\infty}\frac{A_{2m}}{r^{2m}}\cos 2m\theta + KM\sum_{l=1}^{\infty}\frac{1}{2l-1}\frac{A_{2l}}{r^{2l-1}}\cos(2l-1)\theta$$
$$- KM\sum_{l=1}^{\infty}\frac{\cos(2l-1)\theta}{(2l-1)r^{2l-1}}\sum_{n=1}^{l-1}(2n-1)(-1)^n a_{2n-1}A_{2l-2n}] \qquad \text{(A2.13)}$$

The third term is:

$$= -KM\{\frac{\cos(2l-1)\theta}{(2l-1)r^{2l-1}}\}_{l=2}(-a_1A_2)$$
$$-KM\{\frac{\cos(2l-1)\theta}{(2l-1)r^{2l-1}}\}_{l=3}(-a_1A_4 + 3a_3A_2)$$
$$-KM\{\frac{\cos(2l-1)\theta}{(2l-1)r^{2l-1}}\}_{l=4}(-a_1A_6 + 3a_3A_4 - 5a_5A_2) - \ldots.$$

$$= KM\sum_{l=2}\frac{\cos(2l-1)\theta}{(2l-1)r^{2l-1}}a_1A_{2(l-1)} - KM\sum_{l=3}\frac{\cos(2l-1)\theta}{(2l-1)r^{2l-1}}3a_3A_{2(l-2)}$$
$$+ KM\sum_{l=4}\frac{\cos(2l-1)\theta}{(2l-1)r^{2l-1}}5a_5A_{2(l-3)} - + \ldots..$$

$$= KM\sum_{k=1}\frac{\cos(2k+1)\theta}{(2k+1)r^{2k+1}}a_1A_{2k} - KM\sum_{k=1}\frac{\cos(2k+3)\theta}{(2k+3)r^{2k+3}}3a_3A_{2k}+....$$

$$= KM\sum_{k=1}A_{2k}\sum_{n=1}^{N}(-1)^{n+1}\frac{(2n-1)a_{2n-1}\cos(2k+2n-1)\theta}{(2k+2n-1)r^{2k+2n-1}}$$

we can rewrite like this and if we introduce in equation (A2.13) and rearrange we have as:

$$\phi_A = \sum_{m=1}^{\infty}A_{2m}[\frac{\cos 2m\theta}{r^{2m}} + KM\{\frac{\cos(2m-1)\theta}{(2m-1)r^{2m-1}} + \sum_{n=1}^{N}(-1)^{n+1}\frac{(2n-1)a_{2n-1}\cos(2m+2n-1)\theta}{(2m+2n-1)r^{2m+2n-1}}\}] \tag{A2.14}$$

This the waveless potential in the ς plane. It is the varied form of the waveless velocity potential in the Z plane of the earlier section (only one has to be careful about the notation of r).

In similar way if we consider the unsymmetrical field for the waveless potential we have from equation (A2.4):

$$\phi_B = \sum_{k=1}^{\infty}\frac{B_k}{r^k}\sin k\theta = \sum_{m=1}^{\infty}\frac{B_{2m}}{r^{2m}}\sin 2m\theta + \sum_{l=1}^{\infty}\frac{B_{2l+1}}{r^{2l+1}}\sin(2l+1)\theta \tag{A2.15}$$

when $B_1 = 0$ of equation (4.66) was considered, and from equation (4.66) we have the following relation

$$B_{2m} = \frac{KM}{2m}[B_{2m+1} - \sum_{n=1}^{m}(2n-1)(-1)^n a_{2n-1}B_{2m+1-2n}]$$

and if we introduce in equation (A2.15) we have the following:

$$\phi_B = \sum_{l=1}^{\infty}\frac{B_{2l+1}}{r^{2l+1}}\sin(2l+1)\theta + KM\sum_{m=1}^{\infty}\frac{B_{2m+1}}{2mr^{2m}}\sin 2m\theta$$
$$- KM\sum_{m=1}^{\infty}\frac{\sin 2m\theta}{2mr^{2m}}\sum_{n=1}^{m}(2n-1)(-1)^n a_{2n-1}B_{2m+1-2n} \tag{A2.16}$$

Here we ought to be careful of $B_1 = 0$ and if we vary the 3rd term we have:

$$= -KM\{\frac{\sin 2m\theta}{2mr^{2m}}\}_{m=2}(-a_1B_3)$$
$$-KM\{\frac{\sin 2m\theta}{2mr^{2m}}\}_{m=3}(-a_1B_5+3a_3B_3)$$
$$-KM\{\frac{\sin 2m\theta}{2mr^{2m}}\}_{m=4}(-a_1B_7+3a_3B_5-5a_5B_3)-.....$$

$$= KM\sum_{m=2}\frac{\sin 2m\theta}{2mr^{2m}}a_1B_{2m-1} - KM\sum_{m=3}\frac{\sin 2m\theta}{2mr^{2m}}3a_3B_{2m-3}$$
$$+KM\sum_{m=4}\frac{\sin 2m\theta}{2mr^{2m}}5a_5B_{2m-5} -+.....$$

$$= KM\sum_{m=1}\frac{\sin 2(m+1)\theta}{2(m+1)r^{2(m+1)}}a_1B_{2m+1} - KM\sum_{m=1}\frac{\sin 2(m+2)\theta}{2(m+2)r^{2(m+2)}}3a_3B_{2m+1}+.....$$

$$= KM\sum_{m=1}B_{2m+1}\sum_{n=1}^{N}(-1)^{n+1}\frac{(2n-1)a_{2n-1}\sin 2(m+n)\theta}{2(m+n)r^{2(m+n)}}$$

If we introduce this in equation (A2.16) the waveless velocity potential for unsymmetrical flow field becomes:

$$\phi_B = \sum_{m=1}^{\infty}B_{2m+1}[\frac{\sin(2m+1)\theta}{r^{2m+1}} + KM\{\frac{\sin 2m\theta}{2mr^{2m}} + \sum_{n=1}^{N}(-1)^{n+1}\frac{(2n-1)a_{2n-1}\sin 2(m+n)\theta}{2(m+n)r^{2(m+n)}}\}] \quad \text{(A2.17)}$$

If we then write using the angle θ as:

$$\varsigma = \xi + i\eta$$

$$(\xi = r\cos\theta',\ \eta = r\sin\theta')$$

when we consider these coordinates for calculation purpose and use the relation $\theta = \frac{\pi}{2} - \theta'$, we introduce this in equation (A2.14) and (A2.17) we arrive at the following equation:

$$\phi_A = \sum_{m=1}^{\infty}A_{2m}[\frac{\cos 2m\theta'}{r^{2m}} - KM\{\frac{\sin(2m-1)\theta'}{(2m-1)r^{2m-1}} - \sum_{n=1}^{N}\frac{(2n-1)a_{2n-1}\sin(2m+2n-1)\theta'}{(2m+2n-1)r^{2m+2n-1}}\}] \quad \text{(A2.18)}$$

$$\phi_B = \sum_{m=1}^{\infty} B_{2m+1}[\frac{\cos(2m+1)\theta}{r^{2m+1}} - KM\{\frac{\sin 2m\theta}{2mr^{2m}} - \sum_{n=1}^{N}\frac{(2n-1)a_{2n-1}\sin 2(m+n)\theta}{2(m+n)r^{2(m+n)}}\}] \quad (A2.19)$$

These equations also match with the equations in the Seakeeping Symposium (1969).

4.4. Ursell-Tasai Method

In connection with multipole expansion method let us analyse Ursell-Tasai method. Just as in the case of the integral equation method, we will explain only for the case of symmetric motion. In the case of unsymmetric motion the method is the same. The waveless potential terms are as in the previous section and it is appropriate if we replace it with equation (A2.14).

The unknown coefficients as explained in the integral equation method are to be considered as complex numbers. The added mass and damping forces are ofcourse in terms of the progressive wave coefficient $\overline{A}_H$ the phase due to body motion ε_H (i.e Kochin Function). It is convenient if the physical importance of the unknown coefficients is established from the beginning. To fulfil this purpose first let us investigate the velocity potential at far infinity. If we introduce $N = 2$ this corresponds to Lewis form section in the waveless potential equation we then have:

$$\varphi = A_0[\phi_{co} + \phi_{so}] + \sum_{m=1}^{\infty} A_{2m}\phi_{2m} \quad (A2.20)$$

Here

$$\phi_{co} + i\phi_{so} = \lim_{\mu\to 0}\int_0^{\infty}\frac{e^{-ky}\cos kx}{k-K+i\mu}dk$$

$$= \int_0^{\infty}\frac{k\cos ky - K\sin ky}{k^2+K^2}e^{-k|x|}dk - i\pi e^{-Ky-iK|x|}$$

$$\phi_{2m} = \frac{\cos 2m\theta}{r^{2m}} + KM\{\frac{\cos(2m-1)\theta}{(2m-1)r^{2m-1}} + \frac{a_1\cos(2m+1)\theta}{(2m+1)r^{2m+1}} - \frac{3a_3\cos(2m+3)\theta}{(2m+3)r^{2m+3}}\}$$

The contraction value % M when $\theta = \frac{\pi}{2}$ is introduced in equation (A2.2) becomes:

$$K(\frac{B}{2}) = \frac{\omega^2}{g}(\frac{B}{2}) = \xi_B = KM(1 + a_1 + a_3) \tag{A2.21}$$

The behaviour of equation (A2.20) at far infinity is harmonic as:

$$\varphi \approx A_o[-i\pi e^{-Ky - iK|x|}] \equiv iH_z^{\pm}(K)e^{-Ky - iK|x|}$$

it then becomes

$$A_o = -\frac{1}{\pi}H_z^{\pm}(K) = -\frac{i}{\pi K}\overline{A}_H e^{i\varepsilon_H} \tag{A2.22}$$

If the unknown coefficients are represented as above, $\overline{A}_H$ and ε_H can be obtained from numerical solution. Once again if we introduce equation (A2.22) into (A2.20) we can then write as follows:

$$\varphi = \frac{\overline{A}_H}{\pi K}e^{i(\varepsilon_H - \frac{\pi}{2})}[\phi_\infty + i\phi_{so} + \sum_{m=1}^{\infty}(p_{2m} + iq_{2m})\phi_{2m}] \tag{A2.23}$$

The velocity potential is normalised by unit velocity and it is done so that the body boundary condition is satisfied.

$$\frac{\partial \varphi}{\partial \eta} = \frac{\partial y}{\partial \eta}\text{, z-plane}$$

$$\frac{\partial \varphi}{\partial r} = \frac{\partial x}{\partial \theta}\bigg|_{r=1} = M\{(1 + a_1)\cos\theta - 3a_3\cos 3\theta\},\ \varsigma\text{-plane} \tag{A2.24}$$

we arrive at solving the unknown coefficients $\overline{A}_H$, ε_H, p_{2m} and q_{2m}. When solving the integral equation and when performing the normal derivative the accuracy will become bad. Generally using the stream function and in such way that it satisfies the body boundary condition and the stream function corresponding to equation (A2.23) is:

$$\psi = \frac{\overline{A}_H}{\pi K}e^{i(\varepsilon_H - \frac{\pi}{2})}[\psi_\infty + i\psi_{so} + \sum_{m=1}^{\infty}(p_{2m} + iq_{2m})\psi_{2m}] \tag{A2.25}$$

here

$$\psi_{co} + i\psi_{so} = \lim_{\mu \to 0} \int_0^{\infty} \frac{e^{-ky} \sin kx}{k - K + i\mu} dk$$

$$= \pm \int_0^{\infty} \frac{k \sin ky + K \cos ky}{k^2 + K^2} e^{-k|x|} dk \pm \pi e^{-Ky - iK|x|}$$

$$\psi_{2m} = \frac{\sin 2m\theta}{r^{2m}} + KM\{\frac{\sin(2m-1)\theta}{(2m-1)r^{2m-1}} + \frac{a_1 \sin(2m+1)\theta}{(2m+1)r^{2m+1}} - \frac{3a_3 \sin(2m+3)\theta}{(2m+3)r^{2m+3}}\}$$

The body boundary condition in ς is as follows:

$$\psi|_{r=1} = -x|_{r=1} = -M\{(1 + a_1)\sin\theta - a_3 \sin 3\theta\} \qquad \text{(A2.26)}$$

and from equation (A2.25) and (A2.26) we have

$$\psi_{co} + i\psi_{so} + \sum_{m=1}^{\infty} (p_{2m} + iq_{2m})\psi_{2m} = \frac{\pi}{\overline{A}_H} e^{-i(\varepsilon_H + \frac{\pi}{2})} \xi_B f_o(\theta) \equiv (p_o + iq_o) f_o(\theta) \qquad \text{(A2.27)}$$

where

$$f_o(\theta) = \frac{(1 + a_1)\sin\theta - a_3 \sin 3\theta}{1 + a_1 + a_3}$$

$$\xi_B = KM(1 + a_1 + a_3)$$

from equation (A2.27)

$$\left.\begin{aligned} \overline{A}_H &= \frac{\pi \xi_B}{\sqrt{p_o^2 + q_o^2}} \\ \varepsilon_H &= -\frac{\pi}{2} - \tan^{-1} \frac{q_o}{p_o} \end{aligned}\right\} \qquad \text{(A2.28)}$$

and from equation (A2.27) the algebraic equation that we have to solve are:

$$\left.\begin{aligned}\psi_{\infty} &= \sum_{m=0}^{\infty} p_{2m} f_{2m}(\theta) \\ \psi_{\infty} &= \sum_{m=0}^{\infty} q_{2m} f_{2m}(\theta)\end{aligned}\right\} \qquad \text{(A2.29)}$$

here

$$f_{2m}(\theta) = \begin{cases} \dfrac{(1+a_1)\sin\theta - a_3 \sin 3\theta}{1+a_1+a_3} & (m=0) \\ -\psi_{2m}\big|_{r=1} & (m \neq 0) \end{cases}$$

How to go about solving the linear equation (A2.29) is a matter of numerical analysis. In wave theory the method mostly used is the least square method. We will now procced to solve the first equation of (A2.29):

$$E \equiv \sum_{i=1}^{N} [\sum_{m=0}^{M} p_{2m} f_{2m}(\theta_i) - \psi_{\infty}(\theta_i)]^2 \qquad \text{(A2.30)}$$

if we put $\dfrac{\partial E}{\partial p_{2n}} = 0$ $\quad (n = 0,1,2,.....M)$ we arrive at the following equation:

$$\sum_{m=0}^{M} p_{2m} \{\sum_{i=1}^{N} f_{2m}(\theta_i) f_{2n}(\theta_i)\} = \sum_{i=1}^{N} \psi_{\infty}(\theta_i) f_{2n}(\theta_i) \qquad \text{(A2.31)}$$

for $n = 0,1,2,.....M$

Here M is Coefficient of p_{2m} and N is the number of points which satisfy the body boundary equation. We should take N greater than M and from equation (A2.31) if we solve for p_{2m}, even in terms of accuracy it is sufficient.

In this way we can establish p_{2m} and q_{2m}, then using them we go about solving the added mass and damping forces, as follows:

The velocity potential normalised by unit velocity is obtained from equation (A2.23) and from equation (A2.27) as:

$$\frac{\overline{A}_H}{\pi K} e^{i(\varepsilon_H - \frac{\pi}{2})} = -\frac{B}{2}\frac{p_o - iq_o}{p_o^2 + q_o^2} \tag{A2.32}$$

Making use of the following relation

$$\left.\begin{aligned} \phi_c &= \phi_{co} + \sum_{m=1}^{M} p_{2m}\phi_{2m} \\ \phi_s &= \phi_{so} + \sum_{m=1}^{M} q_{2m}\phi_{2m} \end{aligned}\right\}$$

and from equation (A2.23) we have

$$\varphi = -\frac{B}{2}\frac{p_o - iq_o}{p_o^2 + q_o^2}(\phi_c + i\phi_s) = \varphi_c + i\varphi_s$$

that is

$$\left.\begin{aligned} \varphi_c &= -\frac{B}{2}\frac{p_o\phi_c + q_o\phi_s}{p_o^2 + q_o^2} \\ \varphi_s &= -\frac{B}{2}\frac{p_o\phi_s - q_o\phi_c}{p_o^2 + q_o^2} \end{aligned}\right\} \tag{A2.33}$$

Let us do the calculation in detail. First the added mass using φ_c

$$M_H = -\rho\int_{SH}\varphi_c\frac{\partial y}{\partial n}ds = -2\rho\int_0^{\frac{\pi}{2}}\varphi_c\frac{\partial x}{\partial\theta}\Big|_{r=1}d\theta \tag{A2.34}$$

is as above. Here if we introduce $\frac{\partial x}{\partial\theta}$ of equation (A2.6.c) and if we use the contraction M and equation (A2.21) on the body $r = 1$, we have as:

$$\frac{\partial x}{\partial\theta} = \frac{(\frac{B}{2})}{1 + a_1 + a_3}\{(1 + a_1)\cos\theta - 3a_3\cos 3\theta\} \tag{A2.35.a}$$

if we then introduce equation (A2.33) and (A2.35.a) into equation (A2.34) we have as follows:

$$M_H = 2\rho \frac{(\frac{B}{2})^2}{1+a_1+a_3} \frac{1}{p_o^2+q_o^2} [p_o \int_0^{\frac{\pi}{2}} \phi_c \{(1+a_1)\cos\theta - 3a_3\cos 3\theta\} d\theta$$
$$+ q_o \int_0^{\frac{\pi}{2}} \phi_s \{(1+a_1)\cos\theta - 3a_3\cos 3\theta\} d\theta] \qquad \text{(A2.35.b)}$$

here

$$\begin{cases} \phi_c = \phi_{co}|_{r=1} + \sum_{m=1}^{M} p_{2m} \phi_{2m}|_{r=1} \\ \phi_s = \phi_{so}|_{r=1} + \sum_{m=1}^{M} q_{2m} \phi_{2m}|_{r=1} \\ \phi_{2m}|_{r=1} = \cos 2m\theta + \frac{\xi_B}{1+a_1+a_3} \{\frac{\cos(2m-1)\theta}{2m-1} + \frac{a_1\cos(2m+1)\theta}{2m+1} - \frac{3a_3\cos(2m+3)\theta}{2m+3}\} \end{cases}$$
(A2.36)

if we introduce in equation (A2.34) and if we perform the integration with respect to θ we define the following symbols:

$$(1+a_1+a_3)M_0 = \int_0^{\frac{\pi}{2}} \phi_{co}|_{r=1} \{(1+a_1)\cos\theta - 3a_3\cos 3\theta\} d\theta$$
$$+ \sum_{m=1}^{M} p_{2m} \int_0^{\frac{\pi}{2}} \phi_{2m}|_{r=1} \{(1+a_1)\cos\theta - 3a_3\cos 3\theta\} d\theta \qquad \text{(A2.37)}$$

$$(1+a_1+a_3)N_0 = \int_0^{\frac{\pi}{2}} \phi_{so}|_{r=1} \{(1+a_1)\cos\theta - 3a_3\cos 3\theta\} d\theta$$
$$+ \sum_{m=1}^{M} q_{2m} \int_0^{\frac{\pi}{2}} \phi_{2m}|_{r=1} \{(1+a_1)\cos\theta - 3a_3\cos 3\theta\} d\theta \qquad \text{(A2.38)}$$

here

$$\int_0^{\frac{\pi}{2}} \cos 2m\theta \cos\theta d\theta = \frac{(-1)^{m-1}}{4m^2-1}$$

$$\int_0^{\frac{\pi}{2}} \cos 2m\theta \cos 3\theta d\theta = \frac{3(-1)^{m}}{4m^2-9}$$

$$\left.\begin{aligned} \sum_{m=1}^{M} \frac{p_{2m}}{2m-1} \int_0^{\frac{\pi}{2}} \cos(2m-1)\theta \cos\theta d\theta &= p_2(\frac{\pi}{4}) \\ \sum_{m=1}^{M} \frac{p_{2m}}{2m-1} \int_0^{\frac{\pi}{2}} \cos(2m-1)\theta \cos 3\theta d\theta &= \frac{p_4}{3}(\frac{\pi}{4}) \end{aligned}\right\} \quad \text{(A2.39.a)}$$

using the integral equation and solving the second term of equation (A2.37) and (A2.38) we have as follows:

$$(1+a_1+a_3)M_0 = \int_0^{\frac{\pi}{2}} \phi_{co}|_{r=1} \{(1+a_1)\cos\theta - 3a_3\cos 3\theta\} d\theta + \sum_{m=1}^{M} p_{2m}(-1)^{m-1}(\frac{1+a_1}{4m^2-1} + \frac{9a_3}{4m^2-9}) + \frac{\xi_B}{1+a_1+a_3}\frac{\pi}{4}\{(1+a_1-a_1a_3)p_2 - a_3p_4\} \quad \text{(A2.39.b)}$$

$$(1+a_1+a_3)N_0 = \int_0^{\frac{\pi}{2}} \phi_{so}|_{r=1} \{(1+a_1)\cos\theta - 3a_3\cos 3\theta\} d\theta + \sum_{m=1}^{M} q_{2m}(-1)^{m-1}(\frac{1+a_1}{4m^2-1} + \frac{9a_3}{4m^2-9}) + \frac{\xi_B}{1+a_1+a_3}\frac{\pi}{4}\{(1+a_1-a_1a_3)q_2 - a_3q_4\} \quad \text{(A2.39.c)}$$

if we introduce the above results result in equation (A2.35.b) the added mass is written as follows:

$$M_H = 2\rho(\frac{B}{2})^2 \frac{p_o M_o + q_o N_o}{p_o^2 + q_o^2} \quad \text{(A2.40)}$$

If we rearrange this equation with K_4 of free surface coefficient, it becomes convenient

$$\left.\begin{aligned} M_H &= \frac{1}{2}\rho\pi(\frac{B}{2})^2 C_0 K_4 \\ C_0 &= \frac{(1+a_1)^2+3a_3^2}{(1+a_1+a_3)^2} \\ K_4 &= \frac{4}{\pi}\frac{p_o M_o + q_o N_o}{p_o^2+q_o^2}\frac{(1+a_1+a_3)^2}{(1+a_1)^2+3a_3^2} \end{aligned}\right\} \qquad \text{(A2.41)}$$

Here C_0 is the added mass coefficient that is obtained when $\omega \to \infty$.

Next when we consider calculating the damping force the methodology is the same and using φ_s of equation (A2.33) we can write

$$\begin{aligned} N_H &= \rho\omega\int_{SH}\varphi_s\frac{\partial y}{\partial n}ds = 2\rho\omega\int_0^{\frac{\pi}{2}}\varphi_s\frac{\partial x}{\partial\theta}d\theta \\ &= 2\rho\omega\frac{(\frac{B}{2})^2}{(1+a_1+a_3)(p_o^2+q_o^2)}\{q_o\int_0^{\frac{\pi}{2}}\phi_c\{(1+a_1)\cos\theta-3a_3\cos3\theta\}d\theta \\ &\quad -p_o\int_0^{\frac{\pi}{2}}\phi_s\{(1+a_1)\cos\theta-3a_3\cos3\theta\}d\theta \end{aligned}$$

we can write as above and using M_0 and N_0 we can write as follows:

$$N_H = 2\rho\omega(\frac{B}{2})^2\frac{q_o M_o - p_o N_o}{p_o^2+q_o^2} \qquad \text{(A2.42)}$$

Also as explained in the integral equation method the damping force is obtained using the progressive wave coefficient $\bar{A}_H$ and using energy principals we can represent as below, and from equation (A2.28) we have

$$N_H = \frac{\rho g^2}{\omega^3}\bar{A}_H^2 = \frac{\rho g^2}{\omega^3}\frac{\pi^2}{p_o^2+q_o^2}(\frac{\omega^2}{g})^2(\frac{B}{2})^2 = 2\rho\omega(\frac{B}{2})^2\frac{\frac{\pi^2}{2}}{p_o^2+q_o^2} \qquad \text{(A2.43)}$$

from equation (A2.42) and (A2.43) the calculation accuracy check is done by the following relation:

$$q_o M_o - p_o N_o = \frac{\pi^2}{2} = 4.9348... \qquad \text{(A2.44)}$$

In this way even with multipole expansion method we can obtain similar calculation as with integral equation method. We can say that the 2D steady motion theory is established.

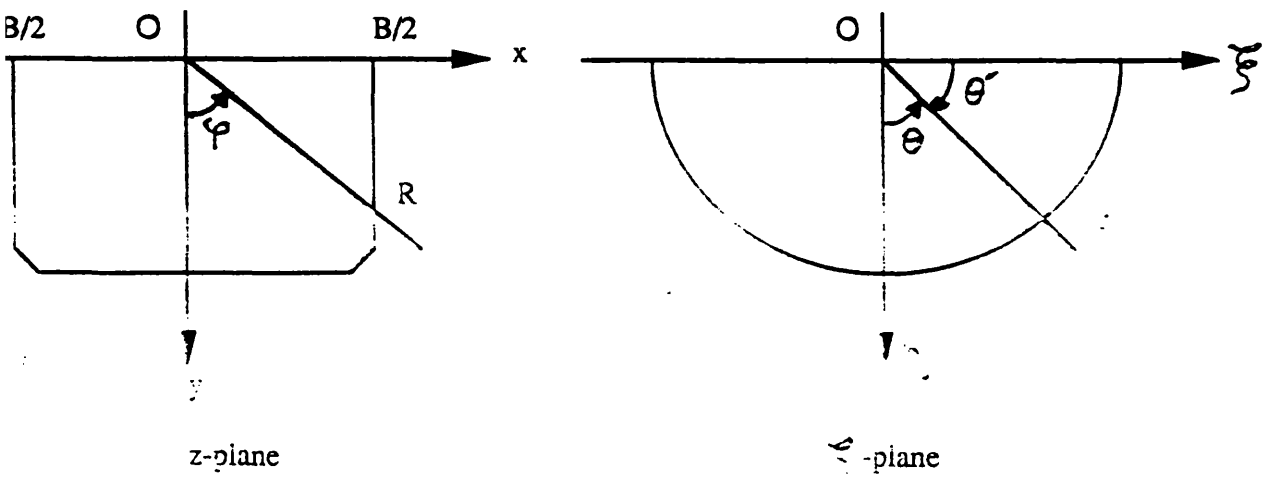

Fig. A.2.1 Mapped ship section to semi circle by two parameter

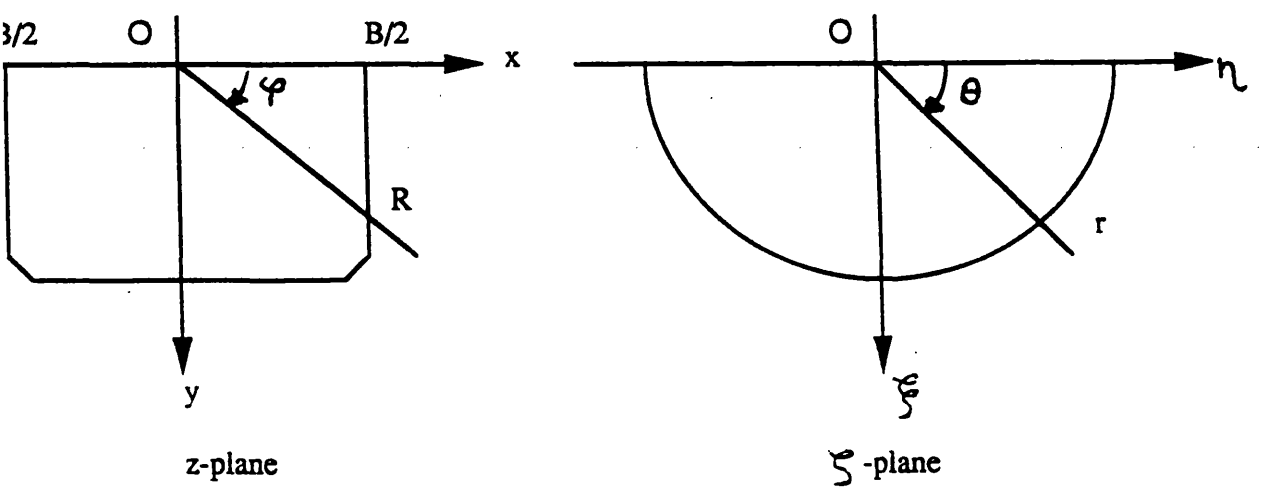

Fig. A.2..2 Mapped ship section to semi circle by three parameter

REFERENCES FOR APPENDIX

Seakeeping Symposium, (1969), Society of Naval Architect of Japan, (in Japanese).

Ursell, F., (1949), "On the Heaving Motion of a Circular Cylinder on the Free Surface of a Fluid", Journal of Mechanics and Applied Mathematics, 2-3.